

The mammalian EMC in membrane protein biogenesis

Norbert Volkmar

A thesis submitted for the degree of

Doctor of Philosophy

St. Cross College

Ludwig Institute for Cancer Research

Nuffield Department of Medicine

University of Oxford

Trinity 2016

Supervisor: Dr. John C. Christianson

Declaration

I hereby declare that this thesis has only been submitted to the University of Oxford and never to any other institution, either in partial or full form. The thesis and the data presented herein are entirely my own work, except where otherwise indicated. The use of public data, where applicable, is clearly stated. All paraphrased material has been indicated with appropriate references. Any assistance I have received from persons other than my supervisor has been acknowledged. I have not copied from work of any other candidate or source. I have not made use of services of any agency providing ghostwritten or model work in the preparation of this thesis. The work described in this thesis was performed during my time as a DPhil student of the University of Oxford at the Ludwig Institute for Cancer Research under supervision of Dr. John Christianson.

Approximate word count (excluding Figure legends, diagrams, tables and bibliography): **44.000**

Norbert Volkmar, 03.10.2016

Abstract

The mammalian Endoplasmic Reticulum Membrane protein Complex (mEMC) has previously been implicated in a range of cellular activities, including the biogenesis of oligomeric plasma membrane receptors, endoplasmic reticulum (ER)-mitochondrial phospholipid transfer, and as a host factor modulating viral pathogenicity. Despite its evolutionary conservation in all eukaryotes, the biological functions and molecular mechanism of the EMC remain poorly understood. Here, the requirement of the mEMC for integral membrane protein biogenesis is investigated. It is reported that the mEMC is involved in the biogenesis of squalene synthase (SQS), an integral ER-resident cholesterogenic enzyme with tail-anchor protein topology. The mEMC is assembled from 10 subunits (EMC1 - 10). Quantitative proteomics on mEMC-deficient ΔEMC5 and ΔEMC6 U2OS Flp-In cells revealed reduced steady-state levels of select cell surface and intracellular proteins. In particular, both EMC5 and EMC6 knockout cells exhibited substantial co-depletion of SQS. The enzyme was significantly destabilized and rapidly degraded by the ubiquitin/proteasome system (UPS) in ΔEMC6 cells. Cells lacking the mEMC were viable under replete media conditions, but were prone to enhanced cell death upon acute cholesterol depletion. Sensitivity to cholesterol loss in EMC6 knockout cells was reproduced by direct deletion or pharmacological inhibition of SQS. mEMC depletion also caused imbalances in the mevalonate pathway, likely leading to increased shunting of the farnesyl pyrophosphate precursor into the isoprenoid pathway, increasing the detection of prenylated proteins. It is proposed that the mEMC is a maturation factor for SQS, and potentially other transmembrane proteins sharing critical molecular features with the biogenesis of this enzyme.

Acknowledgements

For the last four years, I have had the privilege to pursue my studies as a DPhil student of the University of Oxford at the Ludwig Institute for Cancer Research. I would like to express my sincere gratitude to those who enabled this valuable opportunity. First and foremost, I thank my supervisor Dr. John C. Christianson for accepting me as member of his research group and his immediate supervision, and Prof. Xin Lu for her co-supervision during the first year of my PhD work. Throughout the course of my work here at the Ludwig Institute both John and Xin have been supportive and constructive and have helped me greatly developing the many key skills necessary for scientific enquiry. John has reinforced in me a sense of appreciation for fully committing to an aim, and to actively create the conceivably best conditions to pursue it, while always diligently testing the premises that guide the way. I am grateful for his trust in my ability and for his unrelenting encouragement along this at times difficult and uncertain journey.

My everyday experience in the lab was primarily influenced by interaction with the current and past members of the lab. I am grateful to Federica Lari, Emma Fenech, Dr. Donem Acvi, and Dr. Sebastien Lacroix-Desmazes for the many valuable discussions and mutual support. In this regard, I am also particulary thankful for the jovial and motivating atmosphere within and outside the lab, without which my time here would have undoubtedly been less rich. I also owe gratitude to past members of lab, including Dr. Jasmin Schulz, Dr. Markus Queisser and Dr. Stephanie Jones. It was always a pleasure and great help having you around and learning from you all.

Dr. Rodrigo Ribeiro played a special role both as a friend and source of inspiration. It was Rodrigo's work as a visiting PhD student to the lab that encouraged me to make the mEMC the focal point of my research during the last three years here in Oxford.

I was honored to stand on the shoulders of giants, who were always willing to lend a helping hand, guide, and inspire me to be creative and pursue my goals. Among them,

I am particularly indebted to Prof. Benedikt Kessler and members of his group. It was a pleasure to work with Marie-Laetitia Thezenas and Dr. Roman Fischer, who helped me with the initial SILAC-PMP screen, and with Dr. Zhanru Yu, who introduced me to the world of lipidomics. My thinking was greatly influenced by the prospering collaboration with Dr. Ramanujan Hegde and Dr. Liz Miller. It was their enthusiasm and genuine interest in the mEMC that encouraged and enabled me to expand my view and I am looking forward to a continuing and fruitful collaboration. Prof. Ineke Braakman and members of her lab, in particular Anna Chatsisvili, were of great help testing the effects of mEMC-deficiency on a panel of classical ERAD substrates. Even though insight gained from their work are not presented in this study, I am confident that these data will be incorporated into work on the mEMC in the near future.

Without the expertise and technical support of staff and scientists within and beyond Oxford, this study would certainly have taken on a different shape. Dr. Mark Shipman was and continues to be invaluable in assisting with rich knowledge, diligence, and technical skill in any aspect related to microscopy, including the design of algorithms for the computational quantification of micrographs presented in this study. Dr. Andrew Bassett was instrumental in helping to establish the CRISPR/Cas9 system in our lab and his advice and care in choosing and creating the gRNA vectors used in this study made it possible to establish the knockout cell lines which have become the backbone of this study. I would also like to thank Prof. David Beeson, Prof. Franz-Ulrich Hartl, and Enilza Espreafico for providing essential reagents. Dr. Allan Hayle enabled access to facilities at the Weatherall Institute of Molecular Medicine. Dr. Thomasz Konopka contributed crucial advice on the bioinformatics analysis of mEMC expression. I have also learned a lot from Dr. Matous Hrdinka and Dr. Rasmus Freter who patiently advised me on technical issues and also provided reagents. Dr. Leonid Nikitenko taught me patience, gratitude, perseverance, and contributed much-appreciated advice in a number of occasions. My time here at the Institute was marked by a constant atmosphere of mutual understanding and fruitful collaboration.

I am deeply grateful to my patient proofreaders Dr. Donem Avci, Andreas Harst, and Dr. Rodrigo Ribeiro, who were willing to peruse earlier versions of this manuscript.

Most importantly, I consider myself blessed with the life-long support of a wonderful family and loving wife, who have always patiently and selflessly stood by my side both in times of difficulty and mirth. Without them, I would undoubtedly be a different, less fortunate man. I dedicate this thesis is dedicated to them.

Contents

I Introduction **19**

1 The endoplasmic reticulum (ER) **20**

1.1 Structure of the ER 20

1.2 Functions of the ER 20

1.3 Protein biogenesis at the ER 21

1.3.1 Co-translational protein targeting and insertion *via* the signal recognition particle (SRP)-dependent pathway 21

1.3.2 Post-translational membrane protein targeting and insertion 22

1.4 Mislocalized proteins: recognition, extraction, and degradation 26

2 Chaperoning, folding, and modification of polytopic TM proteins **27**

2.1 ER-resident molecular chaperones 27

2.2 Chaperoning of TM proteins 28

2.3 Assembly of TM protein complexes 30

2.4 Post-translational modifications in the ER 32

2.5 ERAD 32

2.5.1 Step 1: substrate recognition 32

2.5.2 Step 2: retrotranslocation and polyubiquitination 34

2.5.3 Step 3: dislocation and degradation 34

3 Lipid metabolism at the ER **36**

3.1 The ER is a hub for *de novo* membrane lipid biosynthesis 36

3.1.1 Biosynthesis of glycerophospholipids 36

3.1.2 Sphingolipid biosynthesis 37

3.1.3 Sterol biosynthesis 38

3.1.4 Protein prenylation at the ER 40

3.2 Translational regulation of cholesterol homeostasis 42

3.3 Post-translational regulation of cholesterol synthesis 43

3.4 LDL-mediated cholesterol import 44

4 The ER membrane protein complex (EMC) **46**

4.1 Structure of the EMC 46

4.1.1 mEMC subunits 47

4.2 Evolution of the EMC . . . 50
4.3 Subcellular localization of the EMC . . . 50
4.4 The EMC in protein folding, trafficking, and degradation . . . 51
4.4.1 The EMC in ERAD . . . 51
4.4.2 The EMC in the biogenesis and trafficking of membrane proteins . . . 52
4.5 Involvement of the EMC in lipid metabolic pathways . . . 54
4.6 Implications of EMC involvement in multiple cellular functions . . . 54
4.7 Cellular stress pathways and the EMC . . . 55
4.8 The mEMC in human pathologies . . . 56
4.8.1 Role of the mEMC in human cancers . . . 56
4.8.2 Other mEMC-associated pathologies . . . 57
4.9 Aim of this study . . . 58

II Results 59

5 EMC1 - EMC10 are members of an ER-localized protein complex in mammalian cells 60
5.1 EMC1 - EMC10 are ubiquitously expressed in a range of human tissues and cell lines . . . 60
5.2 EMC1 - EMC10 form a protein complex . . . 63

6 The stability of mEMC subunits is interdependent and regulates complex formation 65
6.1 Loss of certain mEMC subunits disrupts the mEMC . . . 65
6.1.1 EMC1 - 3 and EMC5/6 are essential for mEMC biogenesis . . . 65
6.1.2 Interdependence of mEMC subunit stability . . . 69
6.1.3 mEMC biogenesis is mildly affected upon depletion of EMC7 - EMC10 . . . 71
6.2 Isolation of an EMC5/6 sub-complex . . . 74
6.3 Depletion of EMC8 upregulates its close homologue EMC9 . . . 77

7 Disruption of the mEMC does not impair ER protein homeostasis 80
7.1 Loss of EMC5 or EMC6 does not trigger the unfolded protein response *per se* 81
7.2 ER and mitochondrial morphology in mEMC-deficient cells . . . 82
7.3 Loss of the mEMC does not impair the degradation and maturation of an endogenous *bona fide* ERAD substrate . . . 85
7.4 Loss of the mEMC does not inhibit cell migration or cell proliferation in a scratch assay . . . 87

8 The mEMC regulates the abundance of integral membrane proteins 89
8.1 Proteomic PM profiling . . . 90
8.2 SILAC-based PMP (SILAC-PMP) in mEMC-depleted cells . . . 93

8.2.1 Constitutive mEMC-deficiency correlates with co-depletion of a set of cell surface proteins . . . 93
8.2.2 The mEMC is necessary for the expression of a set of intracellular proteins 97

9 The mEMC affects cholesterol biosynthesis of U2OS cells 101
9.1 The mEMC is essential for the biogenesis of SQS in U2OS cells . . . 101
9.1.1 Steady-state levels of SQS are significantly reduced upon loss of the mEMC . . . 102
9.1.2 EMC5 and EMC6 are necessary but not sufficient for SQS biogenesis . 105
9.2 Depletion of the mEMC perturbs the cholesterol biosynthesis pathway . . . 109
9.2.1 EMC6 knockout cells are sensitized to cholesterol depletion by MBCD 109
9.2.2 The transcriptional regulation of select SREBP2 target genes remains intact in EMC6 knockout cells . . . 114
9.2.3 Prenylation of Rap1a is increased in EMC6 knockout cells . . . 117
9.2.4 Lack of the mEMC correlates with increased levels of squalene monooxygenase (SM) . . . 120

10 Newly synthesized SQS is destabilized in mEMC-deficient cells 122
10.1 Post-transcriptional downregulation of SQS upon mEMC deficiency . . . 122
10.1.1 *De novo*-synthesized SQS is destabilized in EMC6 knockout cells . . . 123
10.2 SQS is an ER-localized membrane protein . . . 126
10.3 SQS biogenesis is sensitive to disruption of components of the GET/TRC40 pathway . . . 128
10.4 The mEMC and SQS do not form a stable complex . . . 131
10.5 mEMC-deficient cells do not accumulate SQS cleavage intermediates . . . 132

11 Conclusions and working model 134

III Discussion and Perspective 137

11.1 Architecture, biogenesis, and stability of the mEMC . . . 138
11.1.1 Examples for co-dependent expression of protein complex subunits . . 141
11.2 mEMC involvement in SQS biogenesis . . . 143
11.2.1 Model A - The mEMC as a putative membrane insertion factor for SQS 145
11.2.2 Model B - The mEMC operating at a post-insertion step . . . 148
11.2.3 The GET/TRC40 pathway in SQS biogenesis . . . 149
11.3 Metabolic flux through the mevalonate/cholesterol biosynthesis pathways in mEMC-deficient cells . . . 150
11.4 Sensitization of mEMC-deficient cells to cholesterol depletion . . . 152
11.4.1 The mEMC and SQS in the context of mevalonate/cholesterol biosynthesis and virus propagation . . . 153
11.5 SQS and cell viability . . . 154
11.6 Changes to the cell-surface glycoproteome in mEMC-deficient cells . . . 155

11.7 Conclusion 156

IV Materials and Methods 157

12 Materials 158

13 Methods in Molecular Biology 171

13.1 Polymerase chain reaction (PCR) 171
13.2 Purification of PCR products 171
13.3 Restriction endonuclease digestion 171
13.4 DNA ligation 172
13.5 Bacterial transformation 172
13.6 DNA preparation 172
13.7 RNA isolation, reverse transcription, and qPCR 172

14 Methods in Cell Biology 174

14.1 Cell culture 174
14.2 Cryopreservation of cells 174
14.3 Transfection of plasmids 175
14.4 siRNA-mediated knockdown 175
14.5 Genome editing 176
14.5.1 gRNAs 176
14.5.2 Transfection and selection 176
14.5.3 Establishment of single cell clones 176
14.6 Gene knockdown using lentiviruses 176
14.6.1 Production of lentivirus 176
14.6.2 Transduction and selection 177
14.7 Generation of stable cell lines using the Flp-In system 177
14.8 Cholesterol depletion 177
14.9 Crystal violet-staining 178
14.10 Imaging-based quantification of crystal violet-staining 178
14.11 Lipid extraction from cells and cholesterol quantification 178
14.12 Scratch assay 179

15 Methods in protein biochemistry 180

15.1 Preparation of whole-cell protein lysates 180
15.2 Determination of protein concentration 180
15.3 SDS-PAGE 181
15.4 Immunoblotting and detection 181
15.5 Densitometry 182
15.6 SILAC-PMP 182
15.6.1 SILAC labelling and cell surface biotinylation 182

15.6.2 Sample preparation for MS/MS . . . 182
15.6.3 Peptide analysis by UHPLC-coupled mass spectrometry . . . 184
15.6.4 Data processing . . . 184
15.7 ^{35}S-methionine/cysteine pulse-chase . . . 185
15.8 Velocity gradient sedimentation . . . 185
15.8.1 Molecular weight markers . . . 186
15.9 Membrane fractionation . . . 186
15.10 Protein precipitation with TCA . . . 186
15.11 Affinity purification and co-immunoprecipitation . . . 187
15.11.1 Affinity purification of epitope-tagged proteins . . . 187
15.11.2 Affinity purification of epitope-tagged proteins from sucrose gradient fractions . . . 187
15.12 Solubilization of RIPA-insoluble protein fractions . . . 187

16 Purification and quantification of lipids **189**
16.1 Lipid extraction, derivatization, and quantification . . . 189
16.1.1 Quantification of cholesterol . . . 190

17 Microscopy **191**
17.1 Confocal microscopy . . . 191

18 Bioinformatics **192**
18.1 Gene Ontology (GO) analysis . . . 192
18.2 Domain and motif annotation . . . 192
18.3 Helical wheel prediction . . . 192
18.4 Multiple sequence alignment . . . 192
18.5 Expression profiling . . . 193

V Supplemental Data **194**

Bibliography **213**

List of Figures

3.1 Cholesterol biosynthesis 40

4.1 Primary structure of mammalian EMC proteins. 48

5.1 The mEMC is ubiquitously expressed. 63
5.2 EMC proteins form a complex of approximately 300 - 400 kDa 64

6.1 EMC1 - 3 and EMC5/6 are essential for mEMC biogenesis 69
6.2 Depletion or loss of EMC5/6 causes posttranslational attenuation of the mEMC 71
6.3 Depletion of the 'secondary subunits' EMC7 - 10 only mildly affects incorporation of remaining EMCs into the mEMC 73
6.4 EMC5 and EMC6 can form a sub-complex without participation of other EMC proteins 77
6.5 Depletion of EMC8 upregulates its close homologue EMC9 79

7.1 Loss of EMC5, or EMC6 did not trigger the unfolded protein response . . . 82
7.2 ER and mitochondrial morphology in mEMC-deficient cells. 84
7.3 Loss of the mEMC does not impair the degradation of an endogenous *bona fide* ERAD substrate 86
7.4 mEMC-deficiency did not inhibit cell migration or cell proliferation in a scratch assay 88

8.1 PMP of U2OS Flp-In cells. 93
8.2 mEMC depletion affects the expression of cell surface proteins. 97
8.3 Depletion of the mEMC affects the abundance of intracellular proteins. . . . 100

9.1 SQS is decreased in mEMC-depleted cells. 105
9.2 EMC5 and EMC6 are necessary but not sufficient for SQS biogenesis 109
9.3 EMC6 knockout cells are sensitised to cholesterol depletion by MBCD . . . 112
9.4 SQS inhibition sensitized U2OS Flp-In cells to MBCD 113
9.5 The transcriptional regulation of select SREBP2 target genes remains intact in EMC6 knockout cells 116
9.6 Prenylation of Rap1a is increased in EMC6 knockout cells 119
9.7 SM is increased in mEMC-deficient cells. 121

10.1 *De novo* synthesized SQS was destabilized in EMC6 knockout cells 126
10.2 SQS is an ER-localized TM protein 127
10.3 SQS biogenesis was affected by depleting components of the GET pathway . 130
10.4 SQS and the mEMC did not form a stable complex 131
10.5 mEMC-deficient cells did not accumulate SQS cleavage intermediates 133

11.1 Working model 136
11.2 Insertase model 145
11.3 The mEMC acting at a post-insertion step 148

18.1 Velocity gradient sedimentation in 1% Triton X-100 195
18.2 Velocity gradient sedimentation of gel filtration markers 196
18.3 Exogenous expression of EMC subunits 197
18.4 Co-dependent EMC depletion in multiple mammalian cell lines 198
18.5 EMC proteins do not form RIPA-insoluble aggregates. 199
18.6 Isolation of an mEMC assembly intermediate 200
18.7 Sucrose gradient sedimentation of mEMC subunits from EMC2-depleted cells 201
18.8 EMC7/9 knockdown efficiency as determined by qPCR 202
18.9 Specificity of PM protein enrichment 203
18.11 Proteins downregulated both, in ΔEMC5, and ΔEMC6 cells 205
18.10 GO annotation of cell surface fraction 205
18.12 Cell surface proteins downregulated only in ΔEMC5 and ΔEMC6 cells . . . 206
18.13 SQS is decreased in ΔEMC6 cells. 207
18.14 The velocity gradient sedimentation pattern of SQS is not affected by EMC RNAi. 208
18.15 Velocity gradient centrifugation in the presence of 1% Triton-X 100 209
18.16 SQS is destabilised in ΔEMC5 cells 210
18.17 SQS contains a predicted hydrophilic TMD 211
18.18 Predicted topology of EMC3 212
18.19 Conservation of EMC6 primary structure 213

List of Tables

1.1 TMD hydrophobicity of selected TA proteins 25

12.1 qPCR primers 158
12.2 Compounds 159
12.3 Antibodies 160
12.4 Plasmids 161
12.5 Primers for cloning 162
12.6 CRISPR/Cas9 plasmids 163
12.7 siRNAs and shRNA plasmids 164
12.8 Beads for affinity purification 165
12.9 Antibiotics 165
12.10 Antibiotics 166
12.11 Buffers and solutions 167
12.12 Buffers and solutions (continued) 168
12.13 Buffers and solutions (continued) 169
12.14 Miscellaneous materials 170

List of Abbreviations

aa	Amino acid
AAA+	ATPases associated with diverse cellular activities
ABCA1	ATP binding cassette subfamily A member 1
ABCG1	ATP binding cassette subfamily G member 1
AChR	Acetylcholine receptor
AOB	Aminooxy-biotin
AP	Affinity purification
ApoE	Apolipoprotein E
ATF4	Activating transcription factor 4
ATP	Adenosine triphosphate
ATPase	Adenosine triphosphatase
BafA1	Bafilomycin A1
Bag6	BCL2-associated athanogene 6
BAP29	B-cell receptor (BCR)-associated proteins 29
BAP31	B-cell receptor (BCR)-associated proteins 31
bHLH	Basic helix-loop-helix
BiP	Binding immunoglobulin protein
CAML	Calcium modulating cyclophilin ligand
CCp	LCCL (Limulus coagulation factor C, cochlear protein Coch-5b2, and late gestation lung protein Lgl1) domain-containing protein
CDP	Cytidine diphosphate
CD	Cluster of differentiation
CF	Cystic fibrosis
CFTR	Cystic fibrosis transmembrane conductance regulator
CHOP	CCAAT-enhancer-binding protein homologous protein
CHX	Cycloheximide
CL	Cardiolipin
CMV	Cytomegalovirus
CNX	Calnexin
COPII	Coat protein complex II
COX	Cytochrome c oxidase
CRISPR	Clustered regularly interspaced short palindromic repeats

CTL	Choline transporter-like protein
CTP	Cytidine triphosphate
CUE domain	Coupling of ubiquitin to ER degradation domain
CYB5A	Cytochrome B5 type A
DAG	Diacylglycerol
DAmP	Decreased abundance by mRNA peturbation
Der	Derlin
DMAPP	Dimethyl-allyl diphosphate
DMEM	Dulbecco's Modified Eagle Medium
DMSO	Dimethyl sulfoxide
DNA	Deoxyribonucleic acid
DNV	Dengue virus
Dox	Doxycycline
DTT	Dithiotreitol
DUF	Domain of unknown function
e.v.	Empty vector (pcDNA^{TM}/5/FRT/TO)
EDEM	ER degradation-enhancing alpha-mannosidase-like protein
eIF2α	Eukaryotic initiation factor 2α
EMC	Endoplasmic reticulum membrane protein complex
ER	Endoplasmic reticulum
ERAD	ER-associated degradation
ERdj protein	ER DnaJ protein
FCS	Foetal calf serum
FDPS	Farnesyl-diphosphate synthase
FDFT1	Farnesyl-diphosphate farnesyltransferase 1
FKBP	FK506 binding protein
FPKM	Fragments per kilobase of exon per million fragments mapped
FPP	Farnesyl diphosphate
FTase	Farnesyl transferase
GABA	Gamma aminobutyric acid
GC-MS/MS	Gas chromatography tandem mass spectrometry
GET	Guided entry of TA proteins
GFP	Green fluorescent protein
GGPP	Geranylgeranyl diphosphate
GGTase-I	Geranylgeranyl transferase-I
GlcNAc	*N*-acetylglucosamine
GO	Gene ontology
GOI	Gene of interest
GPI	Glycosylphosphatidylinositol
GPT	GlcNAc phosphotransferase

GTEx	Genome-based tissue expression
GTP	Guanosine triphosphate
H	Amino acid isotopes R10 and K8
HAC1	Homologous to Atf/Creb1
HDL	High-density lipoprotein
HEK	Human embryonic kidney
hERG	Human ether-a-go-go-related gene
HERP	Homocysteine-induced ER protein
HMG-CoA	3-hydroxy-3-methylglutaryl-Coenzyme A
HMGCR	Hydroxymethylglutaryl-CoA reductase
HO-1	Haem oxygenase-1
HOP	Hsp90 organizing protein
Hrd1	HMG-CoA reductase degradation 1 homologue
HRP	Horseradish peroxidase
Hsc70	Heat shock cognate 71 kDa protein
HSM1	Haematopoietic signal peptide-containing membrane domain-containing 1
Hsp40	Heat shock 40 kDa protein
Hsp70	Heat shock 70 kDa protein
Hsp90	Heat shock 90 kDa protein
HSS1	Haematopoietic signal peptide-containing secreted 1
HTN	Harringtonin
ICMT	Isoprenylcysteine carboxylmethyltransferase
IDOL	Inducible degrader of LDLR
Ig	Immunoglobulin
Insig1/2	Insulin-induced gene protein 1/2
IPP	Isopentenyl-diphosphate
IRE1	Inositol-requiring enzyme 1
L	Amino acid isotopes R0 and K0 (unlabelled)
L-AChR	Levamisole-sensitive acetylcholine receptor
LAP	LCCL-lectin adhesive-like protein
LDL	Low-density lipoprotein
LDLR	Low density lipoprotein receptor
LMNG	Lauryl maltose neopentyl glycol
LPDS	Lipoprotein-deficient serum
LTN1	Listerin E3 ubiquitin protein ligase 1
LXR	Liver X receptor
M	Amino acid isotopes R6 and K4
MAM	Mitochondria-associated membrane
MARCH6	Membrane-associated RING-CH finger protein 6
MBCD	Methyl-β-cyclodextrin

mEMC	Mammalian endoplasmic reticulum membrane protein complex
MICOS	Mitochondrial contact site and cristae organizing system
MMGT1/2	Membrane magnesium transporter 1/2
mRNA	Messenger RNA
MS	Mass spectrometry
mTOR	Mechanistic target of rapamycin
n.a.	Not applicable
nAChR	Nicotinic acetylcholine receptor
NBD	Nucleotide binding domain
NinaA	Neither inactivation or afterpotential A
Npl4	Nuclear protein localization homologue 4
NTC	Non-targeting control
OS-9	Osteosarcoma amplified 9
OST	Oligosaccharyltransferase
PAM	Plasma membrane-associated membrane
PC	Phosphatidylcholines
PDI	Protein disulphide isomerase
PE	Phosphatidylethanolamine
PEMT	Phosphatidylethanolamine *N*-methyltransferase
PI	Phosphatidylinositol
PI3K	Phosphoinositide 3-kinase
PM	Plasma membrane
PMP	Plasma membrane profiling
PNGase F	Peptide:*N*-glycosidase F
pob	Partial optokinetic response b
PPIase	Peptidyl-prolyl *Cis-trans* isomerase
PQQ	Pyrroloquinoline quinone
PrP	Prion protein
PS	Phosphatidylserine
PTM	Post-translational modification
PTP-1B	Protein-tyrosine phosphatase 1B
qPCR	Quantitative polymerase chain reaction
RAMP-4	Ribosome-attached membrane protein 4
RCE1	Ras-converting CAAX endopeptidase 1
Rh	Rhodopsin
RING	Really interesting new gene
Rh1/3/4	Rhodopsin 1/3/4
RIC-3	Resistant to inhibitors of cholinesterase-3
RNAi	RNA interference
RNC	Ribosome-nascent chain complex

RNF126	Ring finger protein 126
RNAi	RNA interference
S1P	Sphingosine-1-phosphate
SCAP	SREBP cleavage-activating protein
SCRB-1/2	Scavenger type B receptor 1/2
S.D.	Standard deviation
Sec61β	Translocon β subunit
sgRNA	Single guide RNA
SGTA	Small glutamine rich tetratricopeptide repeat containing α
shRNA	Short hairpin RNA
SILAC	Stable isotope labelling with amino acids in cell culture
siRNA	Small interfering RNA
SLC	Solute carrier
SM	Squalene monooxygenase
SNARE	Soluble *N*-ethylmaleimide-sensitive factor (NSF) attachment protein receptor
SPP	Signal peptidase
SPT	Serine palmitoyl transferase
SQS	Squalene synthase
SR	SRP receptor
SRE	Sterol regulatory element
SREBP1/2	Sterol regulatory element binding protein 1/2
SRP	Signal recognition particle
SS	Signal sequence
Strep-HRP	Streptavidin-horseradish peroxidase
SURF1	Surfeit 1
Syb2	Synaptobrevin 2
TA protein	Tail-anchored protein
TCA	Trichloroacetic acid
TCR	T-cell receptor
TFA	Trifluoroacetic acid
TLA1	Truncated light-harvesting chlorophyll antenna size
Tm	Tunicamycin
TM	Transmembrane
TMD	Transmembrane domain
TMEM111	Transmembrane protein 111
TPR	Tandem tetratricopeptide repeat
TRAM	Translocating chain associated membrane protein
TRAP	Translocon-associated protein
TRC8	Translocation in renal carcinoma on chromosome 8 protein
TRC35	Transmembrane domain recognition complex subunit of 35 kDa

TRC40	Transmembrane domain recognition complex subunit of 40 kDa
tRNA	Transfer RNA
TRP	Transient receptor potential
TX-100	Triton X-100
UBA domain	Ubiquitin-associated domain
UBAC2	UBA domain containing 2
UBE2G2	Ubiquitin conjugating enzyme E2 G2
UBE2j1	Ubiquitin conjugating enzyme E2 j1
UBQLN	Ubiquilin
Ufd1	Ubiquitin fusion degradation 1
UGGT	UDP-glucose/glycoprotein glucosyl transferase
UBIAD1	UbiA prenyltransferase domain-containing protein 1
UBL4A	Ubiquitin like 4A
UPR	Unfolded protein response
UPS	Ubiquitin/proteasome system
VCP	Valosin containing protein
VLDL	Very low-density lipoprotein
WNV	West Nile virus
WRB	Tryptophan rich basic protein
wt	Wild type
X	Any physiological amino acid
XBP1	X-box binding protein 1
YNV	Yellow fever virus
ZA	Zaragozic acid A

Part I

Introduction

Chapter 1

The endoplasmic reticulum (ER)

1.1 Structure of the ER

The ER is an extensive intracellular, continuous membrane network [1] with structurally and functionally distinct domains [2], [3]. The two principal domains of the ER are the nuclear envelope and the peripheral ER [4]. The latter exhibits complex architectures with flat cisternal 'sheets' and reticulated 'tubules' [3], [5], which likely allow functional compartmentalization [4]. Due to recent advances in imaging technology, the 'sheet-like' subcompartments of the ER have recently been observed to consist of densely clustered tubular junctions, forming 'matrices' [6]. These distinct morphologies are maintained by a set of ER-resident membrane proteins [7]. The peripheral ER forms promiscuous and dynamic contacts with virtually all cellular organelles, the most prominent being mitochondria-associated membranes (MAMs) [8], and plasma membrane (PM) associated membranes (PAMs) [9].

1.2 Functions of the ER

The cellular functions of the ER are multifarious. Principal biochemical processes localized to, or associated with the ER encompass lipid homeostasis (biosynthesis [10] and trafficking [11]), calcium storage and signalling [12], organelle biogenesis [13], and carbohydrate metabolism [14]. Importantly, the ER is the entry point of the secretory pathway and therefore governs major aspects of proteostasis, such as protein synthesis, maturation (folding, post-translational modification, and oligomerization), quality control (ER-associated degradation (ERAD)) [15], [16], [17], and protein trafficking to a multitude of cellular subcompartments [18].

1.3 Protein biogenesis at the ER

Protein biogenesis encompasses all processes involved in attaining a polypeptide's native conformation, including biosynthesis of the polypeptide chain, its subcellular co- or post-translational translocation and subsequent modification and/or assembly into larger complexes [18]. Polypeptides synthesized at the ER include secretory proteins, proteins of the Golgi apparatus, lysosomes, components of the nuclear envelope, and integral membrane proteins embedded in ER-derived membranes [19]. The ER is also increasingly being acknowledged as an important compartment for the biosynthesis of cytosolic proteins. In this regard, ER-localized messenger RNA (mRNA)-receptors such as p180 can enrich mRNAs at the cytoplasmic face of the ER [20], [21].

1.3.1 Co-translational protein targeting and insertion *via* the signal recognition particle (SRP)-dependent pathway

Many mammalian secretory proteins are co-translationally targeted to the ER [22]. Delivery to the ER is determined by an approximately 20 amino acid long N-terminal signal sequence (SS)/leader peptide, or the presence of one or more transmembrane (TM) domains (TMDs) in integral membrane proteins [23], [24], [25]. Leader peptides vary in their primary sequence, but share an N-terminal short, positively charged region, a hydrophobic core, and a polar C-terminal stretch [26]. As the SS of a nascent secretory protein emerges from the ribosomal polypeptide exit tunnel, it is recognized by the SRP, a cytoplasmic heptameric (six proteins and one RNA molecule) nucleoprotein complex [27], [28]. Once the SRP engages a ribosome-nascent chain complex (RNC), the ribosomal peptide elongation rate falls, allowing the RNC to be targeted to the ER membrane [29]. At the cytoplasmic face of the ER, the SRP is then recognized by the SRP receptor (SR) [30], [31], [32], [33], [34], which is associated with the Sec61 protein translocation channel [35]. The SR and the SRP subunit SRP54, which directly binds the SS, are members of the GTPase superfamily [36], [37]. GTPase cycling controls the release of SRP from the SRP-RNC and transfer of the RNC to the Sec61 translocon [38], [39], [36], [40]. The evolutionarily conserved Sec61 translocon is composed of Sec61$\alpha/\beta/\gamma$ and forms an aqueous pore in the ER membrane through which the nascent ribosome-bound polypeptide enters the ER lumen [41], [42], [43], [44]. Soluble, lumenal ER proteins or the hydrophilic domains of TM proteins pass through this polypeptide-conducting channel into the ER lumen, whereas TM segments are inserted into the ER lipid bilayer by exiting through a temporary lateral opening of the Sec61 translocon [45]. The details of Sec61-mediated TMD insertion into

the lipid bilayer are under intense investigation, and several competing hypotheses are being explored [46]. The translocon associates with a range of accessory factors and post-translational processing complexes [47]. These include the oligosaccharyltransferase (OST), the signal peptidase complex (SPC), the chaperone BiP, the translocating chain-associating membrane protein (TRAM), and the translocon-associated protein (TRAP) complex [47]. Once in the ER lumen, the SS is proteolytically removed by the SPC. The OST catalyses *N*-linked glycosylation at N-X-T sequons [48]. TRAM acts in the early translocation process, potentially chaperoning TMDs that leave the translocon through its lateral gate [49], [50]. TRAP is suggested to be involved in TM protein topogenesis [51].

1.3.2 Post-translational membrane protein targeting and insertion

Membrane proteins constitute approximately 20-30% of the human proteome [52]. Due to their propensity to aggregate in aqueous environments, the presence of hydrophobic sequences, such as TMDs, poses a significant challenge to the cellular protein synthesis and chaperoning machineries [53]. Using the conventional SRP pathway (**Section 1.3.2.2**), nascent integral membrane proteins can be co-translationally targeted and integrated into the ER lipid bilayer *via* the Sec61 translocon [19]. However, approximately 5% of membrane proteins are anchored to the membrane by a single C-terminal TMD, and are therefore classified as tail-anchored (TA) proteins [54], [55]. TA proteins perform a plethora of functions and include components of the vesicle fusion machinery (i.e. soluble *N*-ethylmaleimide-sensitive factor (NSF) attachment protein receptors (SNAREs)) [56], a subunit of the ER-resident Sec61 protein translocation channel (i.e. Sec61β) [57], and important metabolic enzymes (i.e. haem oxygenase-1) [58], [59], [54]. Several parallel pathways of post-translational TM protein targeting and insertion have been described in the literature (**Table 1.1**, page 30) [60]. The presence of multiple pathways might reflect client-specific constraints (e.g. TMD hydrophobicity) or, in the case of overlapping specificity, a mechanism to increase robustness of protein targeting.

1.3.2.1 SRP-dependent post-translational pathway

The role of the SRP in co-translational protein targeting is well established (**Section 1.3.1**). In contrast, a post-translational function of the SRP in TA protein delivery to the ER membrane has emerged only recently [61]. Clearly distinct from the conventional co-translational pathway of TMD targeting/insertion, SRP can form a ribosome-free complex with TA proteins containing relatively hydrophobic TMDs (e.g. synaptobrevin 2 (Syb2) and Sec61β; **Table 1.1**) [61]. Capture of the C-terminal TMD might be facilitated by SRP recruitment to translating

ribosomes before the TMD leaves the ribosome exit tunnel [62]. Similar to the co-translational pathway, integration of SRP-bound TA proteins into the ER lipid bilayer requires the SRP receptor and is guanosine triphosphate (GTP)-dependent; however, the exact mechanism of membrane integration remains unclear [61]. Since the SRP receptor is involved and synaptobrevin seems in close proximity to Sec61 subunits [63], translocon-mediated insertion is a possibility. Of note, the fact that Sec61β and Syb2 are predominantly targeted by the Guided Entry of TA proteins (GET)/ transmembrane domain recognition complex subunit of 40 kDa (TRC40) pathway [57] (**Section 1.3.2.4**) clearly highlights overlapping specificities and a hierarchy of several post-translational targeting machineries.

1.3.2.2 SRP-independent post-translational protein targeting and insertion

1.3.2.3 Sec62/63-complex mediated protein targeting

In yeast, proteins containing SSs of moderate hydrophobicity that are not efficiently recognized by the SRP can be post-translationally targeted to the dedicated ER-resident Sec62/Sec63 membrane protein complex [64], [65], [66]. In contrast, mammalian cells predominantly use the co-translational targeting pathway, but also express orthologues of Sec62p, and Sec63p [67]. The function of the mammalian Sec62/Sec63 complex is not fully understood [67], [68]. In an ATP-dependent process, the newly synthesized protein is bound by cytosolic chaperones of the Heat shock cognate 71 kDa protein (Hsc70) family and handed over to the SEC complex, a heptameric TM protein complex composed of the Sec62/Sec63 sub-complex (Sec62p/63p/66p/72p) and a Sec61 complex [66]. The Sec62/63 complex cooperates with the ER-lumenal Kar2p (Binding immunoglobulin protein (BiP) in mammals), which binds to the J-domain of Sec63p [69], and provides the driving force for the Sec61-assisted translocation of the polypeptide across the lipid bilayer [70].

1.3.2.4 The GET/TRC40 pathway

Early studies showed that, during polypeptide biosynthesis, the ribosome exit channel occludes up to 30-40 amino acids of nascent proteins [71], [72]. Consequently, TMDs at the extreme C-terminus of a polypeptide would be prevented from associating with chaperones prior to the termination of mRNA translation. This necessitates a dedicated chaperoning pathway that both retains the solubility of TA proteins in the cytosol and mediates their correct targeting and membrane insertion [73]. These functions are performed by an evolutionarily conserved

chaperone cascade termed the GET/TRC40 pathway [57], [74], [75], [76]. Once the TMD of a TA protein is released from the ribosome, it is recognized and bound by the hetero-oligomeric BCL2-associated athanogene 6 (Bag6) pre-targeting complex [77]. Central to this complex is the molecular chaperone Bag6, which also acts a scaffold for the co-chaperones small glutamine-rich tetratricopeptide repeat-containing protein α (SGTA), Ubiquitin like 4A (UBL4A) and transmembrane domain recognition complex 35 kDa subunit (TRC35) [77]. Bag6 contains a series of domains essential for its participation in multiple pathways: The N-terminal ubiquitin-like (UBL) domain can interact either with the E3 ligase gp78 in ER-associated degradation (ERAD) [78] or SGTA [79], [80]. C-terminal binding surfaces independently recruit UBL4A and TRC35 [81], [82], whereas the central region of Bag6 binds the TMD of TA proteins directly [79]. A C-terminal BAG domain can interact with Hsp70 chaperones [83]. The exact role of SGTA and UBL4A in TA protein targeting is not entirely clear, but recent work paints an emerging picture where UBL4A could be an adaptor for SGTA, which, in turn, might recruit hydrophobic substrates to the Bag6 complex [79]. According to this model, the N-terminal dimerization domain of SGTA [80] binds to the N-terminal UBL domain of UBL4A [79], while its C-terminal glutamine-rich domain binds short hydrophobic sequences [84]. Therefore, it is conceivable that the glutamine-rich domain of SGTA could associate with the TMD of TA proteins. The UBL domain of Bag6 appears to be dispensable for chaperoning TA proteins [79]. Since the central region of Bag6 was sufficient for TA protein binding in an *in vitro* assay, accessory proteins such as SGTA and UBL4A likely modulate the different functions of Bag6 (e.g. ERAD [85], clearance of mislocalized proteins [53], or defective polypeptides [86]), depending on the substrate. It is thought that in the pre-targeting complex, Bag6 directly associates with the translating ribosome, to facilitate capture of TA client proteins [77], [87], [53]. Once bound to the pre-targeting complex, the client is transferred to the homodimeric cytosolic adenosine triphosphatase (ATPase) TRC40 (Get3 in yeast) [88]. It is likely that TRC40 associates with the pre-targeting complex *via* TRC35 [89], since the yeast homologue of TRC35 (Get4) interacts with Get3 [90], [91], [92]. ATP binding to Get3 drives formation of a 'closed', high-affinity state of the Get3 dimer with a large hydrophobic groove at the dimer interface that accepts a TA client from the Get4-Get5 complex [93], [88], [94]. TRC40 hands off its cargo to the ER membrane-embedded hetero-oligomeric tryptophan-rich basic protein (WRB)/Calcium modulating cyclophilin ligand (CAML) insertase complex, which is homologous to the Get3-receptor Get1/2 in yeast (Get1 is the homologue of WRB, however, Get2 does not possess a structural homologue in mammals) [95], [74], [96], [97], [98]. In yeast, ATP bound to the Get3-TA complex is hydrolysed and interaction of the cargo-loaded Get3

dimer with the cytosolic domain of Get1 promotes the structural rearrangement of Get3, TA protein release and integration into the phospholipid bilayer [99], [100]. ATP exchange releases Get3 from the receptor complex for the next round of TA protein binding [99]. In mammals, the presence of the WRB/CAML complex is sufficient to mediate TRC40-dependent TA protein insertion [101]. The detailed mechanism of this insertion step remains to be worked out.

1.3.2.5 The Hsc70/Hsp40-dependent pathway

The chaperone Hsc70 and its co-chaperone Hsp40 can mediate the insertion of a subset of TA proteins in an *in vitro* reconstitution system even in the presence of TRC40, implying the existence of multiple, independent targeting pathways [102], [103]. The specificity of a TA protein for a particular pathway (SRP-/TRC40- or Hsc70/Hsp40-mediated) appears to be generally dictated by the hydrophobicity index of its TMD [102]. TA proteins containing a relatively hydrophilic TMD are predominantly targeted by the Hsc70/Hsp40 chaperone system, whereas more hydrophobic TMDs convey specificity for the conventional GET pathway [102], (**Table 1.1**). A caveat of this model is the (hitherto) unidentified membrane receptor/insertase for the Hsc70/Hsp40/cargo complex. That said, receptors for cytosolic chaperones have been identified in mitochondria and chloroplasts [104], [105]. Therefore, it is conceivable that an ER-resident chaperone receptor accepting client proteins from Hsc70/Hsp40 remains to be descried. Alternatively, Hsc70/Hsp40 might merely sequester the TMD of TA proteins in the cytosol and maintain them in an insertion-competent conformation. This model is consistent with the observation that cytochrome b5a (CYB5A) can be chaperoned by Hsc70/Hsp40, but is able to efficiently integrate into protein-free membranes [106]. It should be emphasized that the Hsc70/Hsp40-dependent pathway has so far only been demonstrated in an *in vitro* reconstitution system. Therefore, its physiological role remains to be shown.

Protein	**TMD**	**Hydrophobicity [54]**	**Pathway**	**Reference**
Syb 2	MMIILGVICAIILIIIIVYF	64.2	TRC40; SRP	[61]
Sec61β	PVLVMSLLFIASVFMLHIWG	47.1	TRC40; SRP; Hsp40/Hsc70	[61], [103], [102]
RAMP-4	GPWLLALFIFVVCGSAIFQII	41.2	TRC40	[102]
PTP-1B	FLVNMCVATVLTAGAYLCYRF	29.6	Hsp40/Hsc70	[102]
CYB5A	WWTNWVIPAISAVAVALMYRLYM	24.8	Hsp40/Hsc70; unassisted	[102], [106]
SQS	PIYLSFVMLLAALSWQYLTTL	23.7	unknown	

Table 1.1: TMD hydrophobicity of selected TA proteins as calculated by Kalbfleisch *et al.* (2007) [54]. CYB5A, cytochrome b5a; PTP-1B, protein-tyrosine phosphatase 1B; RAMP-4, ribosome-attached membrane protein 4; SQS, squalene synthase; Syb 2, synaptobrevin 2.

1.4 Mislocalized proteins: recognition, extraction, and degradation

Targeting of TA proteins to the ER is an error-prone process [107]. Consequently, mechanisms have evolved to ameliorate mistargeting [107], [53]. Membrane proteins that fail to reach their destination are recognized by cytosolic factors and targeted for degradation. In an elegant *in vitro* model system, translocation-deficient prion protein (PrP), Hessa *et al.* (2011) showed that non-translocated (and therefore mislocalized) PrP was efficiently ubiquitinated and degraded in a Bag6-dependent manner [53]. Ubiquitination was strictly dependent on the presence of exposed hydrophobic sequences [53]. A subsequent study showed that Bag6 recruits the E3 ligase ring finger protein 126 (RNF126) to promote the ubiquitination of Bag6-associated substrates [108].

The presence of a dedicated protein complex to sequester and degrade mislocalized ER-targeted proteins spurred the search for a similar system for mitochondrial membrane proteins that fail to reach their destination and are aberrantly retained in the cytoplasm. Such a complex has long remained elusive; however, a recent study reports that the ubiquilin (UBQLN) protein family performs a triage function reminiscent of Bag6 [109]. Interestingly, client protein specificities of the UBQLN family and of the Bag6 complex overlap and UBQLN4 was found to target mislocalized ER membrane proteins for proteasomal degradation [110]. UBQLNs can act as bridging complexes between a substrate, an E3 ligase, and the proteasome [109]. They exhibit an evolutionarily conserved domain architecture with an N-terminal UBL domain, a methionine-rich M-domain (in the middle region of the protein), and a C-terminal ubiquitin-associated (UBA) domain [111], [109]. The UBL domain can associate with the proteasome, while UBQLN is concomittantly bound to the ubiquitinated substrate [109]. The free TMD of its ubiqutinated client binds to the M-domain, while the UBA domain recruits an E3 ligase and recognizes ubiquitin itself [109]. In situations where the GET/TRC40 pathway is compromised, a subset of TA proteins is often found to be mislocalized to mitochondria [74], [95]. To prevent the detrimental consequences of erroneous accumulation of mistargeted TA proteins in the outer mitochondrial membrane, the AAA+ (ATPases associated with diverse cellular activities) protein ATAD1 (Msp1 in yeast) has been suggested to unfold and/or extract mislocalized TA proteins from the outer mitochondrial membrane [107].

Chapter 2

Chaperoning, folding, and modification of polytopic TM proteins

2.1 ER-resident molecular chaperones

TMD exposure to hydrophilic surroundings (e.g. the cytoplasm or ER lumen) is energetically unfavourable and can lead to protein aggregation, disrupting vital cellular processes [46]. Consequently, nascent TMDs either require chaperoning and/or strict mechanistic and functional coupling of their biogenesis and membrane insertion (e.g. co-translational insertion) to limit prolonged exposure to lipid-free environments.

Molecular chaperones are proteins that bind unfolded, or partially folded, polypeptides (termed 'clients') and assist in attaining their native conformation without being incorporated into the final structure [112]. Chaperones can possess ATPase activity, which enables them to induce conformational changes in their client proteins [113]. An important feature of molecular chaperones is their dual role in protein folding and degradation [114]. In this respect, chaperones assist nascent proteins to reach their native fold, but at the same time can also recognize and divert terminally misfolded proteins or orphan subunits into degradation pathways [113]. The spectrum of client proteins can be broad for promiscuous chaperones (i.e. BiP) or more restricted for chaperones such as GRP94, and is modulated by co-chaperones [115], [116].

In the ER, BiP/GRP78 and GRP94/gp96 are by far the most abundant molecular chaperones [117]. BiP is an Hsp70-like ATPase, binding to non-native proteins and maintaining them in a folding-competent state [118]. Substrate binding is mediated by its C-terminal do-

main, while the N-terminal region of BiP contains a nucleotide-binding domain [119], [120]. At the Sec62/Sec63 translocon, BiP functions as an ATP-dependent molecular ratchet, providing the driving force for protein translocation [70], [121]. Substrate binding is facilitated by ATP hydrolysis, and the ATPase cycle of BiP is regulated by the nucleotide exchange factors GRP170 and Sil1 [122]. BiP is able to bind a plethora of client proteins and relies on a host of co-chaperones (ERdj proteins) for directing its activity [116]. ER DnaJ (ERdj) proteins stimulate ATP hydrolysis of BiP and, therefore, substrate binding [116]. Whereas all ERdj proteins contain a J domain for BiP interaction, a subset also features substrate binding domains through which BiP is recruited to client proteins [123], [124], [125].

The Hsp90-like chaperone GRP94 acts on a more restricted set of client proteins than BiP [126], [117]. The chaperoning activity of GRP94 is ATP-dependent [127], but the nucleotide cycle of GRP94 differs in several aspects from that of Hsp90 [126]. Nonetheless, GRP94 can adopt conformations similar to that of Hsp90, likely facilitating its activity [128]. Which accessory factors are involved in the ATPase cycling of GRP94 is currently unknown [129]. GRP94 binds to immunoglobulins [130], Toll-like receptors [131], [132], low density lipoprotein receptor (LDLR) family proteins [133], integrins [134], insulin-like growth factors [135], and procollagen [136]. The structural and functional heterogeneity of GRP94 clients complicates the identification of features responsible for this high degree of selectivity [115]. Recently, proteins of the Canopy family have been implicated as GRP94 co-chaperones mediating specific interactions with select clients [137], [138]. GRP94 also plays a role in ERAD and collaborates with the lectin Osteosarcoma Amplified 9 (OS-9) in the targeting of misfolded proteins to membrane-embedded E3 ligases [139].

ER-resident chaperones can cooperate and form transient complexes to direct protein folding. BiP and GRP94 can cooperate in the maturation of particular substrates such as immunoglobulin light chain intermediates, which associate first with BiP and later with GRP94, suggesting a form of division of labour between both chaperones [140]. This paradigm is similar to cytoplasmic Hsp70/Hsp90 chaperone networks, where co-chaperone-mediated client handover from Hsp70 to Hsp90 chaperones is common [141].

2.2 Chaperoning of TM proteins

TM proteins of the ER are in direct contact with three cellular compartments: the ER lumen, the lipid bilayer, and the cytoplasm. Therefore, different sets of chaperones and co-chaperones are implicated in the folding of lumenal, cytoplasmic, and, potentially, TMDs [117]. Perhaps

the most extensively studied folding pathway of a TM protein is that of the cystic fibrosis transmembrane conductance regulator (CFTR) [142]. CFTR is a polytopic chloride channel present in the apical PM of epithelial cells where it regulates electrolyte transport [143]. Pathogenic point mutations within the CFTR gene can lead to inefficient folding, intracellular retention, and degradation of CFTR, resulting in the channelopathy cystic fibrosis (CF) [144]. A hallmark of CF is the accumulation of viscous mucus in the lungs of affected individuals, resulting from defective ion and water transport [145]. CFTR has two membrane-spanning domains (MSD1/2), each comprising six α-helical TMDs. MSD1 and MSD2 are connected *via* a cytoplasmic loop composed of the nucleotide binding domain 1 (NBD1) and a regulatory domain (R). The C-terminus of the protein folds into a second cytoplasmic NBD (NBD2). The synthesis of a single CFTR molecule takes approximately 9 minutes and its native state can only be attained after translation has been completed [146], [143]. Therefore, during co-translational integration of CFTR, its cytosolic and lumenal loops are retained in a folding-competent state by binding to the molecular chaperones Hsp90/Hsp70/Hsc70 and calnexin (CNX), respectively [143], [142], [147]. Reminiscent of the concept of 'template-assisted folding' (**Section 2.3**), fully synthesized domains mutually stabilize one another and displace bound chaperones from their binding interfaces [143], [148]. Hsp70 and Hsc70 chaperones act in concert with DNAJ co-chaperones (DNAJB1, and DNAJA1, respectively) in folding the cytoplasmic NBD1 of wild-type or ΔF508 CFTR [148], [149]. CFTR folding is inefficient and misfolded variants are degraded by the ubiquitin/proteasome system (UPS) [144]. The Hsp70/Hsc70 and Hsp90 chaperone systems are also involved in targeting misfolded CFTR for degradation. Binding of the Hsc70 co-chaperone and the E3 ligase CHIP to immature CFTR results in its degradation by the UPS [150].

The translocating chain associated membrane protein (TRAM) cooperates with the Sec61 translocon in protein translocation and has a stimulatory effect on the membrane integration of certain TM proteins [151], [152], [44]. TRAM possesses eight TMDs, some of which show relatively low hydrophobicity [50]. Even though the precise role of TRAM in TM protein chaperoning remains to be determined, several studies show that TRAM is in close apposition with hydrophobic sequences such as short signal sequences [153], [152] and moderately hydrophobic TMDs [154], [155] of nascent translocating polypeptides. The presence of charged residues in several TMDs of TRAM has therefore been interpreted to favour the sequestration of hydrophilic client TMDs and present an amphiphathic environment assisting their controlled partitioning into the lipid bilayer [50]. Hsp70/Hsc70 and their co-chaperones DNAJA1, DNAJA2, and DNAJA4 have also been observed to play a role in chaperoning the imma-

ture subunits of the voltage-gated potassium channel hERG (human ether-a-go-go-related gene/Kv11.1) [156]. In this case, the abundance of DNAJs appears to decide over the balance of folding and degradation, as their overexpression leads to the destabilization of hERG [156]. These findings exemplify the dual functions of chaperones in the maturation process of transmembrane proteins.

A number of chaperones specific for one or a narrow range of client TM proteins have been described. The evolutionarily conserved resistant to inhibitors of cholinesterase-3 (RIC-3) chaperone family is required for the correct folding/assembly and trafficking of acetylcholine receptor (AChR) subtypes [157], [158], [159], [160], [161]. RIC-3 proteins are ER-resident maturation factors whose binding to AChR subunits appears to stabilize assembly intermediates or mature receptors, but the exact mechanism is still elusive. RIC-3 proteins have two TMDs, connected by a proline-rich spacer region [162]. The C-terminal part of RIC-3 proteins contains one or more cytoplasmic coiled-coil domains [162]. Intriguingly, the second TMD of RIC-3 is remarkably well conserved across species, implying a functional role beyond that of a membrane anchor [158]. Given that RIC-3 client proteins also exhibit significant TMD conservation, the RIC-3 TMD has been speculated to mediate receptor subunit assembly by intramembrane interaction with TMDs of individual AChR subunits [158]. Accordingly, the two RIC-3 TMDs and a proline-rich spacer are sufficient to promote AChR maturation[163]. Thus, both the TM segments and a predicted lumenal region of RIC-3 could serve as potential scaffolds for AChR subunit assembly, but the mechanistic details underlying RIC-3 function in AChR maturation remain to be clarified.

PAT-10 is an enigmatic 10-kDa protein which as been found to associate with specific nascent TMDs of the hepta-helical opsin receptor [164], [165]. Its cooperation with the Sec61 translocon and its prolonged interaction with nascent opsin TMD1 and TMD5 suggest a chaperoning/holdase function, and/or an accessory role in regulating TMD exit from the translocon and subsequent membrane integration [164], [165]. No doubt, future studies will elucidate the exact function of PAT-10 and other putative membrane-embedded chaperones in TMD protein biogenesis.

2.3 Assembly of TM protein complexes

Knowledge of the assembly parameters of multi-protein complexes in the ER is still very limited [166]. Nonetheless, the study of a few important TM protein complexes has contributed immensely to the understanding of a number of central principles governing their folding and

assembly.

Complex assembly (and folding) can be promoted by accessory factors that are present in assembly intermediates but excluded from the mature complex. In this regard, chaperones with holdase function such as BiP stabilize otherwise labile assembly intermediates. These accessory factors can perform similar functions in the assembly of a range of protein complexes (e.g. BiP), or be more specific to particular complexes or subunits.

An important principle derived from the maturation of immunoglobulin (Ig) heavy and light chains is 'template-assisted folding'. Ig light chains are fully translocated before assembling with heavy chains [167]. As the heavy chain is co-translationally translocated across the ER membrane, BiP binds to the CH1 domain and prevents its folding [168]. Chaperoning by BiP promotes ER retention of the unassembled heavy chain and therefore forestalls premature export or aggregation [167]. Only in the presence of the light chain is BiP displaced from the CH1 domain, which then attains its native fold [168], [169]. Thus, complex assembly can concomitantly assist folding of its individual subunits by displacement of a holdase. Another example of template-assisted folding is the formation of the oligomeric T-cell receptor (TCR). In this case, both, α and β subunits achieve their native fold only upon dimerization [170]. It should be noted that by far not all TM proteins follow the principle of template-assisted folding. For example, the α subunit of nicotinic acetylcholine receptors (nAChRs) acquires its native fold in the absence of the remaining subunits [171].

The overall amount of a mature complex can be limited by the abundance of one of its subunits: Complexes following this principle include the TCR [172] and the oligosaccharyltransferase (OST) complex [173]. Underlying mechanisms leading to the loss of the complex in the absence of individual subunits include regulated degradation of unassembled subunits. A case in point is the $\alpha\beta$TCR. Its single-pass α subunit contains a weak TMD due to the presence of a central lysine residue [174]. In the absence of sufficient amounts of assembly partners (CD3δ and CD3ε), the α subunit mislocalizes to the ER lumen where it is rapidly degraded [175]. Hence, in the $\alpha\beta$TCR, complex assembly and membrane integration are intimately linked. By showing that the weak TMDs of single-span subunits of other complexes can also mislocalize and be degraded, Feige *et al.* (2013) suggest that this might be a general principle controlling the amount of unassembled subunits [175].

In conclusion, the processes of protein folding and complex assembly can be interdependent, and involve ER-resident chaperones such as BiP that act as holdases.

2.4 Post-translational modifications in the ER

A host of ER-resident enzymes facilitate and direct the correct folding of newly synthesized proteins. Folding enzymes include peptidyl-prolyl *cis-trans* isomerases (PPIases), and protein disulphide isomerases (PDIs). PPIases catalyse the kinetically unfavourable *cis-trans* isomerization of proline, which can be a prerequisite for the introduction of disulphide bonds [176]. The ER contains three classes of PPIases (FK506 binding proteins (FKBPs), cyclophilins, and parvulins), which might, in complex with other protein maturation factors, exhibit substrate specificity [117]. PDIs assist in the co- and post-translational formation of cysteine disulphide bonds. Depending on the oxidation status of their active site CXXC motif, these enzymes can oxidize or reduce substrate disulphide bonds, and thereby engage in disulphide bond isomerization in repeated oxidation/reduction cycles [177]. PDIs are embedded in ER chaperone networks; a complex of CNX, or CRT and the PDI ERp57 couples oxidative folding with the *N*-linked glycosylation machinery [178], [179]. The addition of *N*-linked glycan chains to N-X-S/T consensus motifs ('sequons') within nascent polypeptides promotes folding, i.e. by enabling association with lectins such as CNX and calreticulin (CRT) (**Section 2.5.1**) [180]. Other post-translational modifications (PTMs) within the ER include the covalent conjugation of glycosylphosphatidylinositol (GPI) anchors [181], proline and lysine hydroxylation of procollagen [182], [183], [184], and the limited proteolysis of signal sequences by signal peptidase I in the ER lumen [185].

2.5 ERAD

ERAD is a protein quality control mechanism that mediates the recognition, retrotranslocation, and degradation of misfolded or damaged ER-lumenal and TM proteins [186], [16]. This process is part of a general cellular strategy to recognize and eliminate potentially cytotoxic protein species by means of dedicated quality control machineries in the cytoplasm [53], and other cellular sub-compartments such as the mitochondria [187], the inner nuclear membrane [17], the Golgi apparatus [188], and the ER [189]. The following sections summarize the principal steps involved in ERAD.

2.5.1 Step 1: substrate recognition

Recognition of glycoproteins with misfolded lumenal domains

Proteins that fail to reach their native conformation, for instance due to mutations (i.e.

CFTRΔF508 [190]), or fail to correctly assemble into higher-order complexes (i.e. subunits of the AChR [191], [192], [193] and CD147 [194]), need to be removed from the ER to prevent their accumulation and interference with vital cellular functions. ERAD also serves in metabolic adaptation by adjusting enzyme levels (i.e. hydroxymethylglutaryl-CoA reductase (HMGCR) [195] and squalene monooxygenase [196]) to metabolic demands (see also **Section 3.3**). Glycoprotein folding in the ER and degradation are functionally coupled through the modification (trimming and extension) of *N*-linked core-glycans ($Glc_3Man_9GlcNAc_2$) [197], transferred from the carrier dolichol pyrophosphate to sequons by the OST complex [48]. The glycosylation status of a protein determines the repeated association with lectins (CNX and CRT) [197], [198], which recruit the oxidoreductase Erp57 [199]. Erp57 catalyses the formation and, in particular, the reshuffling of disulphide bonds; rate-limiting steps of protein folding in the ER [200]. The number of successive folding cycles is controlled by sequential removal of the terminal three glucose residues by glucosidases I and II (promoting release from CNX/CRT), and re-glucosylation of non-native glycoproteins by uridine diphosphate (UDP)-glucose/glycoprotein glucosyl transferase (UGGT) [201]. Terminally misfolded proteins, e.g. proteins unable to attain their native conformations after repeated folding attempts, are extracted from the CNX/CRT folding cycle *via* demannosylation by ER-resident mannosidases (ERManI [202], [203], EDEM1 [204], EDEM3 [205], and Man1C1 [206]). Removal of mannose residues prevents re-glucosylation by UGGT and enables recognition of the trimmed glycan tree by mannose-specific lectins (e.g. OS-9 and XTP3-B) [139].

Recognition of aberrant TMDs

Lesions within the TMDs of ER-membrane proteins would not be accessible for quality control by ER-lumenal or cytosolic chaperone systems. Instead, aberrations in the TMD segments indicative of misfolding such as exposed hydrophilic residues within the plane of the membrane, can be recognized by the TMDs of ERAD E3 ligases such as Hrd1 (HMG-CoA reductase degradation 1 homologue) [207]. This recognition is mediated by several charged residues within the TMD segments of ERAD E3 ligases (i.e. Hrd1) [207]. Subsequent retrotranslocation of membrane proteins containing TMD defects appears to require the ubiquitination of lysine side chains within their cytoplasmic domain [208]. Derlin-1 (Der1) has been found to promote the degradation of a CFTR TMD mutant (G85E), and might be another recognition factor for aberrant TMDs [209]. Furthermore, the ER-resident proteins B-cell receptor (BCR)-associated proteins 29/31 (BAP29/BAP31) form a complex that plays a role in recognizing unstable TMDs of a range of substrates [210], [211], [212].

2.5.2 Step 2: retrotranslocation and polyubiquitination

Once bound by the lectins OS-9 and XTP3-B (see 'Step 1'), terminally misfolded glycoproteins need to be retrotranslocated across the ER membrane into the cytoplasm to be targeted to the 26S proteasome for degradation [213]. Although a retrotranslocon still remains to be unequivocally identified, the latter appears to be either closely associated with a membrane embedded E3 ligase [213] or has been suggested to be the E3 ligase Hrd1 itself [214], [215]. Other candidates with proposed retrotranslocon acitivty include Sec61 [216], [217], and Der1 [218], [219]. Sel1L, an integral component of the Hrd1 ligase complex [189], is a TM adaptor protein that binds to substrate-loaded OS-9/XTP3-B [139], [220], [221]. Erlin-1/2 appear to have a similar adaptor function and can associate with multiple ER-resident E3 ligases [222], [223], [189]. A third class of adaptors are Insig-1/2, whose role in steroid biogenesis will be discussed in **Section 3.3**. ERAD substrates are polyubiquitinated by E3 ligases, most likely while emerging from the retrotranslocon. The driving force for retrotranslocation of polypeptides across the ER lipid bilayer is thought to be provided by the AAA+ ATPase valosin containing protein (VCP)/p97 on the cytoplasmic face of the ER membrane (see below) [224], [225], [226].

Polyubiquitination is a prerequisite for degradation by the 26S proteasome. ERAD substrates are ubiquitinated by a range of integral ER-resident Really Interesting New Gene (RING) finger domain E3 ligases. Mammalian cells contain genes encoding approximately 25 RING finger domain-containing, ER-resident integral membrane proteins [227], [228], [229], [16].

2.5.3 Step 3: dislocation and degradation

After passage through the retrotranslocon and ubiquitination by E3 ligases, ERAD substrates are dislocated into the cytosol and transferred to the 26S proteasome for degradation. VCP/p97 receives ubiquitinated cargo from the retrotranslocon and is proposed to promote ATP-dependent extraction from the E3 ligase/retrotranslocon complexes [226]. It also forms a scaffold for a variety of accessory factors involved in ubiquitin editing of ERAD substrates (deubiquitinases and E3 ligases) [230]. The adaptor complex Ufd1-Npl4 mediates substrate binding of VCP by concomitant association with both, polyubiquitin (*via* a zinc-finger motif in Npl4), and VCP [231]. VCP complexes then transfer cargo either directly to the proteasome or hand them over to the shuttling factors Rad23 or Dsk2, which direct substrates to the proteasome [232]. VCP has also been suggested to participate in partial unfolding of cytosolic

substrates at the proteasome [233].

Retrotranslocated proteins with hydrophobic segments (i.e. TMDs) are prevented from aggregating and retained in a degradation-competent conformation by cytosolic chaperones. One of these chaperones, the Bag6-UBL4A-SGTA/TRC35 chaperone complex, captures cargo destined for degradation from gp78, an ERAD E3 ligase [234], [85]. Transfer of retrotranslocated cargo is coordinated by binding of the ubiquitin-like (UBL) domain of Bag6 to the CUE (coupling of ubiquitin to ER degradation) domain of gp78, and concomitant association of Bag6 with its co-factor UBL4A [85]. SGTA is recruited by the non-canonoical UBL domain of UBL4A and mediates sampling of retrotranslocated cargo containing hydrophobic patches, thus cooperating with Bag6 in substrate capture [85].

Chapter 3

Lipid metabolism at the ER

Lipid catabolic and anabolic pathways are highly compartmentalized in human cells. The following section will outline the role of the ER in cellular lipid metabolism.

3.1 The ER is a hub for *de novo* membrane lipid biosynthesis

The ER is the major organelle of lipid biosynthesis in eukaryotic cells. The three main classes of lipids synthesized in the ER can be classified as glycerophospholipids, sphingolipids, and sterols [235], [11]. While the ER accommodates many of the enzymatic activities involved in lipid metabolism, lipid intermediates are trafficked to other subcellular compartments where they are further modified, returned to the ER, or incorporated into cellular sub-compartments [10].

3.1.1 Biosynthesis of glycerophospholipids

Glycerophospholipids include phosphatidylserine (PS), phosphatidylethanolamine (PE), phosphatidylcholine (PC), phophatidylinositol (PI), and cardiolipin (CL). They are the most abundant structural lipids (>50%) and dominate the composition of eukaryotic cellular membranes [236], [235]. Among glycerophospholipids, PC is the most abundant membrane lipid and is synthesized by two pathways localized across subcellular compartments (ER, Golgi and mitochondria) [11], [237]: In the cytidine diphosphate (CDP)-choline pathway, also termed the 'Kennedy Pathway', PC is produced by the condensation of CDP-choline and diacylglycerol (DAG) [236]. Whereas the final step occurs in the Golgi apparatus, CDP-choline is synthesized in the ER from cytidine triphosphate (CTP) and phosphocholine by two sequential enzy-

matic reactions. The alternative 'methylation pathway' is localized to mitochondria-associated membranes (MAMs) and utilizes the enzyme phosphatidylethanolamine *N*-methyltransferase (PEMT) for the sequential methylation of PE to PC [238]. The CDP-choline pathway is active in all cells, whereas the methylation pathway is specific to hepatocytes [235]. PE, the second most abundant glycerophospholipid after PC, is produced in the ER in a second branch of the Kennedy Pathway, constituting an analogous reaction to the CDP-choline pathway, with CDP-ethanolamine taking the place of CDP-choline [236]. Alternatively, PE can be formed by decarboxylation of PS at the inner mitochondrial membrane [239]. This so-called decarboxylation pathway accounts for the bulk synthesis of PE [11]. PS synthesis occurs *via* the replacement of choline (in PC) or ethanolamine (in PE) by L-serine [240]. The reaction is restricted to MAMs, facilitating the import of PS into mitochondria and further conversion to PE (see above). PI synthesis is catalysed at the ER and potentially at the PM from CDP-DAG and *myo*-inositol [241], [242], [11].

3.1.2 Sphingolipid biosynthesis

Sphingolipids play important roles in signalling pathways and are a structural component of cholesterol-rich sub-domains of the PM [243]. An example of a well-characterized sphingolipid is sphingosine-1-phosphate (S1P), the interaction of which with specific S1P receptors controls multiple physiological processes, including the modulation of immune cell activity and chemotaxis [244]. As a constituent of the PM, the structurally diverse head groups of sphingolipids in the outer membrane leaflet face the extracellular space and can thereby interact with proteins in a cell's surroundings. This is particularly evident in the nervous system, where gangliosides (sialic acid-containing glycosphingolipids) function as a receptor facilitating myelin-axon association [245].

Sphingolipid biosynthesis involves both the ER and the Golgi compartment [246]. Ceramide, the precursor of complex sphingolipids, is synthesized in the ER from L-serine, palmitoyl-CoA, and long-chain fatty acids [247]. The ER-resident polytopic TM protein serine palmitoyl transferase (SPT) catalyses the Claisen-like decarboxylative condensation of cytoplasmic L-serine and palmitoyl-CoA to 3-ketodihydrosphingosine, which is subsequently reduced to sphinganine. *N*-acylation and a second reduction then yields ceramide [248]. Compared to glycerolipids, a distinctive feature of the fatty acid side chain of ceramide is its increased average length, due to the concerted action of chain elongase complexes in the ER membrane [249]. Ceramides are trafficked to the Golgi apparatus along vesicular and non-vesicular pathways, where their head groups are further modified [10]. This modification gives rise to different

complex sphingolipids, which can be further trafficked to the PM [247], [250].

3.1.3 Sterol biosynthesis

Sterols are tetracyclic triterpenoids derived from the C-30 isoprenoid squalene. They are involved in a number of signalling functions and impart important biophysical properties to cell membranes (e.g. regulation of membrane fluidity and permeability) [251], [252]. Sterols are present in all kingdoms of life except bacteria (which contain hopanoids instead) and archaea [253]. In vertebrates, the major steroid is cholesterol, which can be further metabolized to bile acids [254], vitamin D [255], steroid hormones (progesterone, estradiol, testosterone, cortisol, and aldosterone), [256], or oxysterols (i.e. 25-hydroxycholesterol), [257]. Insects produce ecdysteroids and nematodes the so-called dauer steroids [258]. In plants, the steroid backbone is found in phytosterols and their derivatives: saponins, glycoalkaloids, brassinosteroids, and withanolides [258]. Fungi, such as *Saccharomyces cerevisiae*, produce ergosterol [259].

In mammals, *de novo* biosynthesis of cholesterol is accomplished by a reaction sequence involving more than 20 enzymes [260], [261]. A concise overview of the reaction sequence is given in **Figure 3.1**. The sterol biosynthesis pathway can be envisaged to proceed in four steps. The first step, mevalonate synthesis, begins with the condensation of acetyl-CoA and acetoacetyl-CoA to 3-hydroxy-3-methylglutaryl-CoA (HMG-CoA) by HMG-CoA synthase [258]. HMG-CoA is then reduced to mevalonate by the ER-resident tetrameric integral membrane protein HMG-CoA reductase (HMGCR) [262]. HMGCR is considered to be the rate-limiting enzyme of the sterol biosynthesis pathway [263], [264]. The second step encompasses six enzymes leading to the triterpene squalene, and is localized to peroxisomes and the ER [265]. In peroxisomes, mevalonate is activated by sequential phosphorylation to mevalonate-5-phosphate (mevalonate-5-P) and mevalonate-5-diphosphate (mevalonate-5-PP), followed by decarboxylation and dehydration to isopentenyl-diphosphate (IPP). IPP is inter-convertible with its isomer dimethylallyl-diphosphate (DMAPP). The reaction sequence from (aceto-)acetyl-CoA to IPP/DMAPP is also commonly called the 'Mevalonate/Isoprenoid Pathway'. Head-to-tail condensation of two IPPs with DMAPP by farnesyl diphosphate (FPP) synthase (FDPS) produces the terpene FPP. Squalene synthase/FPP farnesyltransferase 1 (SQS/FDFT1), a TA protein in the ER membrane, then catalyses the head-to-head condensation of two FPP molecules to presqualene-PP, and a subsequent nicotinamide adenine dinucleotide phosphate (NADPH)-dependent reduction to squalene [266]. SQS is uniquely situated to regulate the metabolic flux of FPP, since it catalyses the first committed step of the cholesterol biosynthesis pathway; whereas squalene can only be metabolized to sterol intermediates and eventually to cholesterol,

FPP can alternatively serve as a precursor for dolichol, haem a, ubiquinone, or be used for protein farnesylation [267]. Condensation of FPP with IPP gives rise to geranylgeranyl-PP (GGPP), which can be used for protein geranylgeranylation [268]. Therefore, SQS has been considered a 'gatekeeper' enzyme of the sterol biosynthesis pathway [269], [270]. In the third step, squalene is further metabolized to cholesterol. Squalene monooxygenase (SM) epoxidates squalene to squalene-2,3-epoxide [271], which is subsequently converted to lanosterol in a cyclization reaction catalysed by oxidosqualene cyclase (lanosterol synthase) [272], [273]. Lanosterol is the first intermediate with a sterol core and is further modified to cholesterol by a series of demethylation, oxidation, and reduction events [258]. Step four encompasses all reactions in which cholesterol serves as a precursor for a variety of steroids produced through the action of dedicated enzymes in different tissues [256].

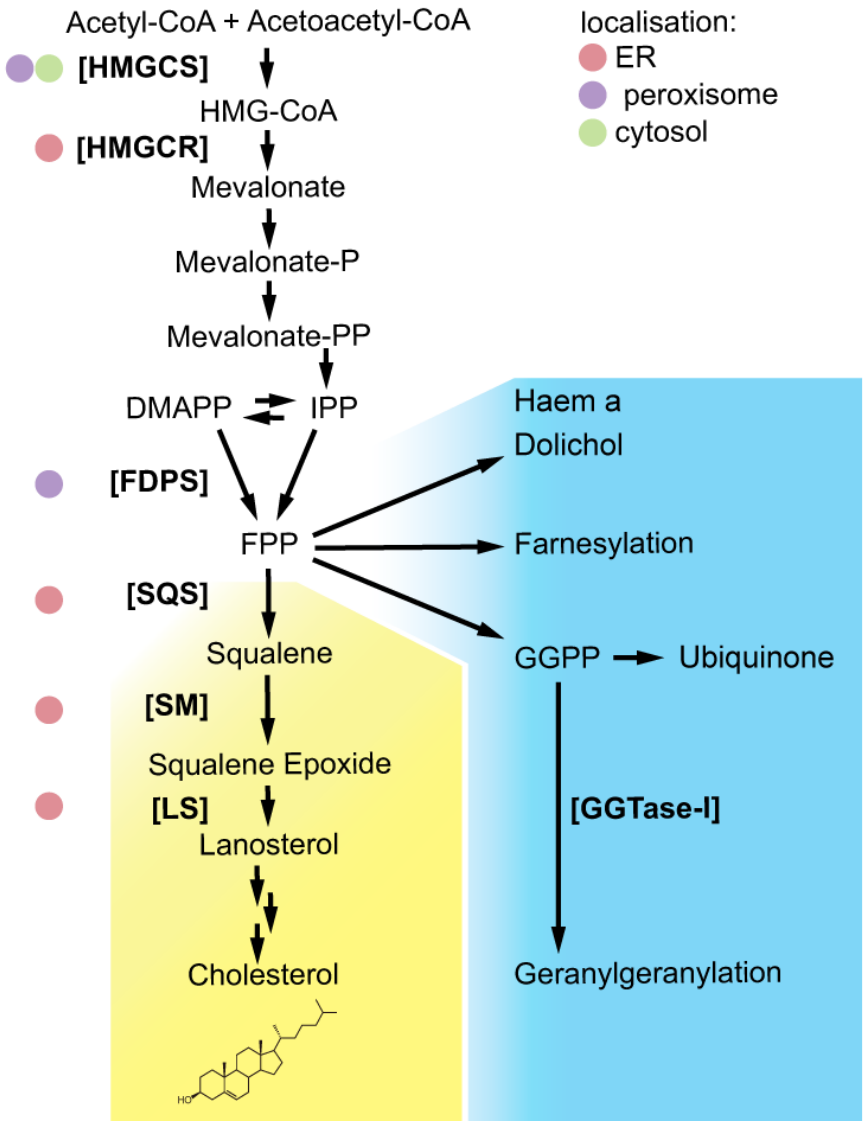


Figure 3.1: ***De novo*** **formation of cholesterol and non-sterol isoprenoids.** Scheme representing the metabolite flux of cholesterol (yellow) and non-sterol isoprenoid pathways (blue). The subcellular localisation of individual enzymes involved in cholesterol biosynthesis is indicated in coloured circles (ER (red), peroxysome (lilac), cytosol (green)). Enzymes from top to bottom: HMGCS, HMG-CoA synthase; HMGCR, HMG-CoA reductase; FDPS, FPP synthase; SQS, squalene synthase; SM, squalene monooxygenase; LS, lanosterol synthase; GGTase-I, geranylgeranyl transferase-I.

3.1.4 Protein prenylation at the ER

Intermediates of the mevalonate/isoprenoid pathway serve vital functions beyond being precursors for cholesterol (**Figure 3.1**). IPP-derived isoprenoids are essential for the biosynthesis of prosthetic groups such as haem a, the production of the polysaccharide carrier dolichol, the redox cofactor ubiquinone (coenzyme Q10), or isopentyladenine in some transfer RNAs (tRNAs) [274]. FPP and GGPP are used for the covalent and irreversible modification of proteins in a reaction termed (iso)prenylation [275]. Prenylation increases the hydrophobicity of the target protein and can be a prerequisite for membrane association [276]. Prenylated proteins

are involved in a plethora of cellular processes including cell signalling, growth, proliferation (e.g. Ras GTPases), and subcellular protein trafficking (e.g. Rab GTPases) [268]. The conventional signal for isoprenoid attachment is the presence of a C-terminal CaaX motif, wherein 'a' represents an aliphatic amino acid and 'X' defines the specificity for one of two prenyltransferases, farnesyl transferase (FTase), and gernaylgeranyl transferase-I (GGTase-I) [277], [278]. Formation of the thioether linkage between FPP or GGPP and the cysteine residue within the CaaX motif occurs in the cytoplasm [275]. The thus prenylated protein is then further processed by polytopic ER membrane proteins: Ras-converting CAAX endopeptidase 1 (RCE1) [279] cleaves the prenylated protein directly after the modified cysteine residue, and the new C-terminal carboxyl group is then methylated by isoprenylcysteine carboxylmethyltransferase (ICMT) [280], [281], [282].

Since isoprenoids serve a dual function as intermediates in sterol biosynthesis and for protein prenylation (**Figure 3.1**), their flux along both metabolic pathways must be highly coordinated. Excess amounts of cholesterol, as well as inhibition of isoprenoid synthesis, are cytotoxic [283]. In this regard, the activity of the mevalonate pathway must balance the production of cholesterol and related sterols as well as other isoprenoid compounds without leading to over- or underproduction of either end product. Adequate distribution of mevalonate pathway intermediates between both metabolic branches is precisely regulated on at least three different levels. Firstly, the higher affinity of enzymes involved in the non-steroid pathway for mevalonate-derived intermediates over enzymes of the steroid branch allows for a considerable reduction of cholesterol production without affecting isoprenoid shunting [274]. In fact, saturation of intracellular cholesterol stores has been shown to inhibit HMGCR activity by up to 98% [283]. However, under these conditions, suppression never reaches 100%, as low HMGCR activity is required to generate mevalonate for the non-steroid pathway. SQS has a relatively low Km value for FPP of 2 μM, whereas that of GGPP synthase (converting FPP into GGPP) is 1 μM and the Km of FTase was determined to be 5 nM [284]. Consequently, when FPP becomes limiting (due to downregulation of HMGCR), sterol biosynthesis would be affected first, and FPP is instead diverted into the non-sterol branch. Secondly, the presence of excess cholesterol leads to the transcriptional and post-transcriptional downregulation of enzymes distal to HMGCR (i.e. SQS or SM). This limits the incorporation of isoprenoids into cholesterol intermediates, re-directing their flux into pathways such as ubiquinone synthesis [283]. Thirdly, HMGCR is subject to 'multivalent feedback regulation' [283]. As is common for branched metabolic pathways, complete shutdown of HMGCR activity can only occur when the products of both branches are present in excess. Therefore, efficient HMGCR repres-

sion can only be achieved in the presence of both cholesterol and the non-steroid mevalonate derivative GGPP [283], [285], [286], [287] (**Section 3.3**).

3.2 Translational regulation of cholesterol homeostasis

Cholesterol homeostasis is achieved by balancing *de novo* synthesis with cholesterol uptake and efflux [261]. The major regulators of lipogenesis are the sterol regulatory element binding proteins 1/2 (SREBP1/2) and the liver X receptors α/β (LXRα/β) [288], [289], [290]. In vertebrates and invertebrates, lipid biosynthesis is under stringent transcriptional control by the SREBP pathway [291]. Mammals express three SREBPs belonging to the basic helix-loop-helix (bHLH) transcription factor family. SREBP1a/c predominantly control fatty acid biosynthesis, whereas SREBP2 target genes are primarily involved in sterol production [292]. Transcriptional regulation is exerted by binding of SREBPs to sterol regulatory elements (SREs) in the promoter regions of their target genes [293]. SREBP activation is proteolytically controlled [294]. When inactive, SREBPs are ER-resident TM proteins with two TMDs, and N- and C-terminal cytoplasmic domains [290]. Lipid deficiency stimulates the translocation of SREBPs from the ER to the Golgi complex [295]. Regulated intramembrane proteolysis (by S1P and S2P in the Golgi apparatus) then releases the N-terminal bHLH activity-containing domain into the cytoplasm, where it is free to translocate into the nucleus and bind to SRE-containing promoters [294]. The initial ER-to-Golgi translocation event of SREBP2 is regulated by two SREBP-binding proteins, Insig-1/2 and SREBP cleavage-activating protein (SCAP) [290]. SCAP constitutively binds to the C-terminal, regulatory SREBP domain [296]. As soon as ER-cholesterol levels fall below 5% of total ER lipids, SCAP mediates the sequestration of SREBP in coat protein complex II (COPII) vesicles for transport to the Golgi, where activation occurs [295]. However, if the cellular demand of cholesterol is met, cholesterol binds to the sterol-sensing domain of SCAP, leading to a conformational change [297] that increases the affinity of SCAP to Insig-1/2 [298]. Once bound to SCAP-SREBP2, Insig-1/2 are stabilized and prevent packaging of the SREBP2-SCAP complex into COPII vesicles [298].

As opposed to SREBPs, which are activated by cholesterol depletion, another transcription factor family, the LXRs, is induced by surplus cellular cholesterol [288]. LXRα and LXRβ activity promotes cholesterol efflux and post-translational repression of the receptor-mediated cholesterol import pathway [288]. Oxysterols (i.e. 24(S),25-epoxycholesterol and 27-hydroxycholesterol) have been recognized as endogenous LXR ligands [299], [300]. LXRs can block LDLR-mediated cholesterol import by facilitating the expression of inducible de-

grader of LDLR (IDOL), a RING E3 ligase that targets the LDLR for degradation by the proteasome [301]. Concomitantly, cholesterol efflux is promoted by LXR-induced transcriptional upregulation of the cholesterol efflux pumps ATP binding cassette subfamily A member 1 (ABCA1) [302], [303] and ABCG1 [304], [305], [306]. In conclusion, the transcriptional regulation of enzymes involved in cholesterol *de novo* biosynthesis, as well as of factors controlling cholesterol uptake and efflux mechanisms, enables efficient adaptation to changing cellular cholesterol demands.

3.3 Post-translational regulation of cholesterol synthesis

Post-translational feed-forward and feedback regulation of SREBP and its binding partners in the ER is well documented [290], [263], [261]. SREBP2 activity is controlled by 'convergent feedback inhibition' [307], [290], meaning that two parameters need to be met to preclude SREBP2 trafficking to the Golgi apparatus. Firstly, intracellular cholesterol levels must be sufficiently high to bind to SCAP [307]. Secondly, the constitutively degraded Insig-1 needs to be present at adequate amounts to associate with SCAP and retain the SCAP-SREBP2 complex in the ER [307], [290]. Insig-1 is rapidly ubiquitinated and degraded by the proteasome when not bound to SCAP [307]. The E3 ligases TRC8 (translocation in renal carcinoma on chromosome 8 protein) and gp78 have been implicated in the binding to, and degradation of, Insig-1 [308], [309]. Insig-1 degradation allows SREBP2 maturation and activation in the Golgi apparatus. Importantly, Insig-1 is among the many target genes of SREBP2 [310]. Therefore, increased Insig-1 transcription sets the stage for feedback inhibition. As soon as cholesterol homeostasis has been restored and cholesterol levels have risen to, or above, 5% of overall ER lipids, the binding of cholesterol to the SCAP-SREBP2 complex triggers a conformational change that allows Insig-1 binding to SCAP, leading to Insig-1 stabilization and SREBP2 retention [295]. The fully processed forms of SREBPs themselves are targeted for degradation after binding to their target DNA sequences (SREs) [311], [312]. This mechanism of decreased SREBP stability when fully active has also been termed 'destruction by activation' [261].

Besides modulating the regulatory circuits of sterol biosynthesis, the UPS also exerts control over the main rate-limiting steroidogenic enzymes HMGCR and SM. HMGCR can be targeted for degradation by ER-resident E3 ligases, both in a sterol-independent and -dependent manner [313], [314], [315]. For efficient degradation of HMGCR, GGPP has to be present in addition to sterols [285]. GGPP interferes with the protective sequestration of a subpopulation of HMGCR by the UbiA prenyltransferase domain-containing protein 1 (UBIAD1) [287]. This

requirement for GGPP might ensure that low levels of HMGCR are maintained for isoprenoid synthesis even in the presence of excess cholesterol. When overexpressed in NIH-3T3 cells, the E3 ligase Hrd1 was observed to mediate turnover of mammalian HMGCR under steady-state conditions [195]. The role of endogenous Hrd1 in the regulation of basal HMGCR remains to be demonstrated. The proposed involvement of another two E3 ligases, gp78 [316] and TRC8 [317], in sterol-regulated degradation of HMGCR has been disproved as HMGCR was not stabilized in gp78 (-/-) mouse embryonic fibroblasts (or gp78-depleted SV-589 cells) and upon RNAi of TRC8 [318].

Downstream of HMGCR, SM constitutes the second major control point for the regulation of metabolic flux through the sterol pathway. SM protein levels are modulated by MARCH6 through sterol-dependent ERAD [319]. Enhanced degradation of SM is strongly stimulated by cholesterol, as opposed to HMGCR degradation, where oxysterols rather than cholesterol facilitate its turnover (see above) [320]. The presence of increased levels of cholesterol in the ER membrane is likely to induce a conformational change within a region encompassing the first 100 amino acids of SM, eventually leading to its degradation [321]. The mechanistic details remain to be defined, but the conformational change of SM and an altered lipid composition of the ER membrane appear to facilitate the recognition of SM as a misfolded ERAD substrate [321].

3.4 LDL-mediated cholesterol import

Cholesterol import is mainly achieved by receptor-mediated endocytosis of lipid-loaded lipoprotein particles [322]. Different classes of lipoproteins, such as chylomicrons, high-density lipoprotein (HDL), intermediate-density lipoprotein (IDL), low-density lipoprotein (LDL), or very low-density lipoprotein (VLDL), contain characteristic ratios of phospholipids, triacylglycerides, cholesterol, and cholesterol esters [323], [324]. A major distinguishing feature is the presence of large apolipoproteins embedded in the lipid cargo, mediating their recognition, and subsequent internalization by the target cell. As lipids are progressively transferred to cells, lipoproteins can interconvert, i.e. transfer of triacylgycerides from VLDL and exchange of the apolipoprotein E (ApoE) for ApoB100, converts VLDL into the cholesterol-rich LDL [324].Recognition and endocytosis of lipoprotein particles is achieved by two groups of cell surface receptors. Scavenger type B receptors (SCRB-1/2) and CD37 facilitate lipid transfer from lipoprotein particles without internalization of the apolipoprotein itself [322]. The ancient family of LDLRs, on the other hand, mediates endocytosis of entire lipoproteins and

targets them for degradation and lipid release in lysosomal compartments [325]. Defects in this process can lead to the metabolic syndrome of familial hyperlipidemia, a genetic condition characterized by pathologically increased levels of lipids and lipoprotein particles in the blood stream [326], [327], [328].

Chapter 4

The ER membrane protein complex (EMC)

4.1 Structure of the EMC

In a systematic unfolded protein response (UPR)-based screen of approximately 4500 yeast deletion strains, Jonikas *et al.* (2009) characterized genes involved in protein folding in the ER [95], leading to the identification of a hitherto unrecognized hetero-oligomeric membrane protein complex, the EMC. Affinity capture of an epitope-tagged variant of EMC3 co-purified additional EMC subunits EMC1/2 and EMC4-6, and the TM proteins SOP4, and YDR056C, which were later re-classified as EMC7 and EMC10, respectively [95], [329]. Three years later, in a mass spectrometry-based exploration of the ERAD interaction network, Christianson *et al.* (2012) confirmed the presence of a mammalian EMC orthologue, the mEMC [189]. Importantly, despite being evolutionarily remarkably conserved, the mEMC contains two additional vertebrate-specific subunits, EMC8 and EMC9, both of which apparently lack TMDs [189], [329]. The ability to affinity-purify the mEMC in the presence of 1% Triton X-100, a strong non-ionic detergent, suggests that EMC1 - 10 form a complex of high stability in mammalian cells [189].

Information on the overall architecture of the EMC and the structure of its subunits is scarce. Based on silver staining of affinity-purified yeast EMC, roughly stoichiometric subunit ratios were observed [95]. This finding was further supported by work from the Weissman lab in 2014, observing proportional synthesis of EMC1 - 6 in yeast, and therefore arguing for a 1:1 interaction stoichiometry [330]. Finally, green fluorescent protein (GFP)-tagged variants of EMC1 - 6 under the control of their endogenous promoters were expressed at comparable

ratios in *S. cerevisiae* [331]. Label-free MS-aided quantification of the absolute abundance of a subset of individual EMC subunits implies a similar scenario in mammalian cells [332]. In this respect, Hein *et al.* (2015) found that HeLa cells express comparable amounts of each subunit [332]. Roughly equal subunit ratios were also maintained when the complex was purified via affinity-capture of GFP-tagged EMC variants [332]. Collectively, these data indicate that the majority of EMC proteins are assembled into the larger oligomeric mEMC at any time, and are unlikely to perform additional, mEMC-independent functions under steady-state conditions.

Even though the structure of the mEMC, or any of its constituents, has not been resolved, topology prediction of its individual subunits can give valuable insights into a putative, coarse-grained organization of this complex. Seven out of ten subunits are predicted to contain at least one, and up to three, TMDs [333], [334], [335], [336]. Therefore, these subunits are embedded in the lipid bilayer of the ER [337]. Additionally, N-terminal signal sequences in EMC1, EMC5, EMC7, and EMC10 support the notion of a type I topology [338], [339]. Interestingly, computational structure prediction (TOPCONS [340], http://topcons.net/) suggests that the remaining three subunits of the mEMC (EMC2, EMC8, and EMC9) possess no apparent TMDs or leader sequences. Hence, EMC2/8/9 are most likely engaged with the cytoplasmically exposed sections of one or several integral mEMC subunits. EMC1 and EMC10 are *N*-glycosylated at Asn913 and Asn182, respectively, [341], [338], [339] (**Figure 4.1**). Additionally, EMC1 might also carry glycans at the predicted *bona fide* sequons including Asn370 and Asn818 [339]. Since glycosylation occurs in the lumenal compartment of the ER, the N-terminus of both subunits may be exposed to the ER lumen.

4.1.1 mEMC subunits

A compounding factor in the functional characterization of the mEMC is the relative paucity of functionally annotated domains and motifs (**Figure 4.1**). Besides the aforementioned signal sequences, glycosylation consensus sites, and TMDs, only EMC1 and EMC2 contain well characterized domains. EMC1 is the largest component of the mEMC and exhibits Pyrroloquinoline quinone (PQQ)-like repeats (aa 21-252) and a C-terminal domain of unknown function (DUF1620, aa 787 - 992) that also spans the TMD [339]. PQQ repeats typically form a β-propeller structure and are commonly found in quinoproteins, such as bacterial dehydrogenases [342], [343]. The function of the PQQ-like domain in EMC1 is currently unknown. Ninagawa *et al.* (2015) demonstrated that the deletion of a large proportion (Δ35 - 220) of the PQQ-like domain induces partial unfolding, but did not lead to increased destabilization of EMC1 [339].

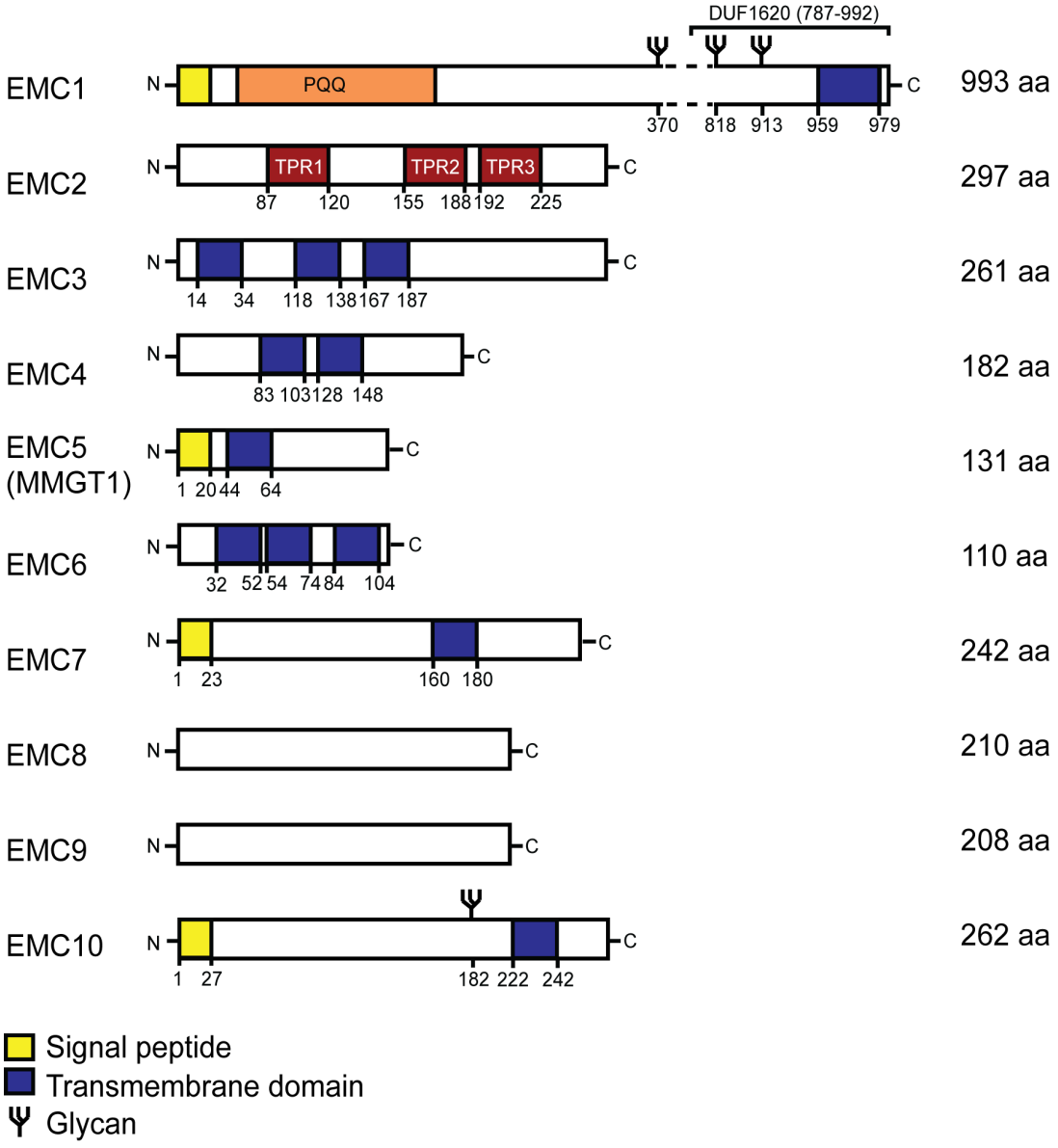


Figure 4.1: Primary structure of mammalian EMC proteins. The primary structures of EMC1 - 10 are depicted with predicted domains indicated by colour (signal peptide, yellow; TMD, blue). The amino acid positions of domain boundaries and of predicted glycosylation sites are shown. 'N' and 'C' designate the N- and C-termini. EMC5 is also known as MMGT1. aa, amino acid; DUF1620, domain of unknown function 1620; PQQ, pyrroloquinoline quinone repeat; TPR1/2/3, tetratricopeptide repeat 1/2/3.

EMC2 features three tandem tetratricopeptide repeats (TPRs) [344]. TPRs are degenerate sequences of 34 amino acids, and are associated with a variety of proteins with diverse cellular functions [345]. A single TPR consists of two amphipathic α helices that are in anti-parallel arrangement, and subsequent TPRs are arranged in parallel [346], [347]. This allows tandem-TPRs to form a large amphipathic groove that can accommodate complementary polypeptide sequences [346]. A unifying feature of TPR-containing proteins is their participation in protein complexes, and the TPR domain has been proposed to serve scaffolding functions [348], [347]. Accordingly, the TPRs of EMC2 might be involved in either docking this cytoplasmic subunit to the rest of the mEMC, or in mediating interactions with potential mEMC client proteins. TPRs are also commonly found in a class of co-chaperones (i.e. CHIP and HOP (Hsp90 organizing protein)) catering to Hsp70 and Hsp90 [141], and might therefore allow EMC2 to recruit molecular chaperones to the mEMC.

EMC3 bears similarity to the archaeal DUF106 protein family (Pfam [349], http://pfam.xfam.org/), members of which share a common fold with the YidC/Oxa1/Alb3 insertase families [350], [351]. EMC6 contains a poorly defined Rab5-interacting domain (aa 25 - 104), which might be implicated in the formation of autophagosome precursor structures [335]. EMC9 is a homologue of EMC8 and is thought to have arisen by gene duplication [329].

Sequence alignment of human EMC8 and EMC9 shows significant sequence identity (44.72% according to ClustalO [352] (https://www.ebi.ac.uk/Tools/msa/clustalo/)). EMC8/9 are classified as proteins of the UPF0172 family (Pfam [349]). A member of this family (truncated light-harvesting chlorophyll antenna size (TLA1)) regulates chlorophyll-a antenna size in *Chlamydomonas reinhardtii*, and shares 28.79% and 28.57% sequence identity (Clustal O [352], https://www.ebi.ac.uk/Tools/msa/clustalo/) with EMC8 and EMC9, respectively. TLA1 associates with thylakoid membranes [353]. The underlying molecular mechanism of TLA1 activity remains to be determined, but it has been surmised to promote the assembly of chlorophyll-a antennae [353]. Interestingly, its close homologue in *Arabidopsis thaliana* (AT5G55940) apparently localizes to the ER [354]. Whether EMC8/9, TLA1, and its homologue AT5G55940 participate in functionally related processes is unknown. EMC10 is expressed as two splice variants in haematopoietic stem cells. The shorter of these two variants, haematopoietic signal peptide-containing secreted 1 (HSS1), is secreted, whereas the larger haematopoietic signal peptide-containing membrane domain-containing 1 (HSM1) has a TMD [338]. Both variants arise by differential splicing of the last exon [338]. The authors further report that EMC10 does not share sequence homology with other known proteins, and,

based on structure prediction, propose a globular fold of α helices and β-sheets shared with an artificial protein designed to withstand extreme temperature and pH conditions [338], [355]. Moreover, HSS is both *N*-, and *O*-glycosylated when expressed in HEK293T cells [338]. The observation of a secreted form of EMC10 could indicate a dedicated function of this particular splice variant outside the mEMC.

4.2 Evolution of the EMC

The EMC is an evolutionarily ancient protein complex, likely reaching back to the last eukaryotic common ancestor (LECA) [329]. Despite the predominantly ubiquitous presence of the EMC, phylogenetic analysis has confirmed that the complex, or several of its subunits, has been lost in some lineages. For example, the *Ascomycetes* have lost EMC8, and some microsporidians (e.g. *Nosema ceranae*, *Encephalitozoon cuniculi*) appear to have lost the EMC entirely [329]. The absence of individual subunits might indicate that the EMC is in the process of being gradually lost in some lineages or that certain functionalities of these components have been delegated to other proteins or pathways. In summary, these observations imply that the EMC was present before the diversification of the kingdoms of life. Moreover, the EMC, or some of its subunits, likely continue to play a physiologically relevant role in eukaryotes [329].

4.3 Subcellular localization of the EMC

ER localization of the EMC, or at least one of its subunits, has been confirmed in multiple model systems [337], [189], [356], [339], [336], [335], [331], [357]. The mEMC appears to be almost exclusively restricted to the rough ER (rER), as EMC1 - 6 were predominantly found in rat liver microsomes isolated from rER, but not in smooth ER (sER) [337]. However, despite overwhelming consensus, an early report describes localization of epitope-tagged membrane magnesium transporter 1 (MMGT1/EMC5) in Golgi and post-Golgi compartments of COS-7 cells [333]. Similarly, the gene product of partial optokinetic response b (pob), the zebrafish orthologue of EMC3, was observed in both the ER and the trans-Golgi [358]. It is not known whether individual subunits of the EMC, or even the mature complex, can be targeted to organelles different to the ER in a species-specific manner. Corroborating this notion, a soluble splice variant of EMC10 (HSS1) has been shown to be secreted into the extracellular space in haematopoietic stem cells and HEK293T cells [338]. Dreger *et al.* (2001) found EMC2 in the inner nuclear membrane of mouse neuroblastoma N2a cells [359]. This finding indicates that EMC2 could have distinct molecular functions at different intracellular sites or in different

tissues/cell types.

4.4 The EMC in protein folding, trafficking, and degradation

Several studies have implicated the EMC, or at least one of its subunits, in protein folding, trafficking, or degradation pathways. In the following section, evidence brought forward in favour of each of the aforementioned processes will be reviewed.

4.4.1 The EMC in ERAD

Proteostasis in the ER involves the degradation of excess, damaged, misfolded, or aged proteins by ERAD [360]. The EMC has been repeatedly implicated in ERAD. In an integrated mass spectrometry (MS)-based screen to identify the protein interaction network orchestrating ERAD in HEK293 cells, Christianson *et al.* (2012) revealed a novel link between components of the ERAD machinery and the mEMC [189]. In detail, UBA domain containing 2 (UBAC2) forms complexes with EMC1, EMC2, and EMC3. In addition, Der1 interacts with EMC1, whereas Der2 binds to both EMC1 and EMC3. Derlins are involved in preemptive translocon-associated quality control [361], and/or could be part of a retrotranslocon complex [218]. CNX complexes with EMC1 [189], an observation that was later confirmed for the EMC1 orthologue in *Drosophila melanogaster* [357]. Since EMC1 is glycosylated, association with CNX is likely to occur during EMC1 maturation *via* the CNX/CRT cycle, but this remains to be conclusively demonstrated.

The nAChR is an endogenous ERAD substrate [193]. Depletion of the EMC in *Caenorhabditis elegans* leads to a substantial decrease in AChR levels in muscle cells [336]. This observation provides another link between ERAD and the EMC, even though direct involvement of the EMC in ERAD oversight of unassembled AChR subunits remains to be unequivocally demonstrated. Furthermore, RNA interference (RNAi)-mediated depletion of EMC1/2 or EMC7/8 led to the accumulation of multiple lumenal ERAD model substrates, attesting to a functional role of the mEMC in ER quality control [189]. In this context, it is worth noting that the mEMC itself is likely to be a substrate of ERAD, since the degradation of EMC1 was delayed in EDEM (ER degradation-enhancing alpha-mannosidase-like protein) 1 - 3 triple knockout cells [339].

Multiple studies, which were conducted in various model systems, identified the EMC as a subset of ER quality control-related genes that play a role in modulating the cytotoxicity of a

range of stressors including antifungal compounds, viruses, and toxic protein species. Jonikas *et al.* (2009) originally identified the EMC on the basis of the similar genetic interaction profiles of its subunits EMC1 - 6 in a large-scale screen for genes involved in protein folding [95]. Perturbation of the ERAD machinery has been shown to be closely linked to induction of the UPR [362], [363]. The UPR increases the folding capacity in the ER when ERAD substrates accumulate [363]. Accordingly, loss of EMC3, as well as conventional ERAD genes (e.g. Sel1, Hrd1 and Ubc7), was accompanied by UPR activation [95]. In a chemical toxicity screen of haploid deletion mutants and haploid DAmP (decreased abundance by mRNA peturbation) strains, several EMC subunits (EMC1 - 6) contributed to increased resistance against a novel antifungal compound (sr7575) that caused cytotoxicity, presumably by interfering with ERAD [364]. Similarly, EMC1 - 4 were found to facilitate ERAD of a mutated form of the uracil permease YlFur4p in *Yarrowia lipolytica*, leading to enhanced 5-fluorouracil resistance [365]. A genome-wide screen for host factors mediating the pathogenicity of West Nile virus (WNV) revealed increased resistance to WNV-induced cell death upon depletion of a subset of ERAD components (Hrd1, Sel1L, UBE2J1, UBE2G2, and DER2) and EMC subunits (EMC2/3) [366]. Flaviviruses such as WNV, harness the ER for replication, inducing ER membrane proliferation and alterations in ER lipid homeostasis [367]. Consequently, WNV infection can cause ER stress and induction of the UPR [368]. Why the loss of core components of the ERAD machinery should play a cytoprotective role in WNV pathogenicity is not clear and mechanistic details of this process await further study. Nonetheless, the findings of Ma *et al.* (2015) [366] emphasize the close functional link between proteostasis networks in the ER and the EMC, which had been observed in a number of model systems [95], [189], [369], [336], [357].

4.4.2 The EMC in the biogenesis and trafficking of membrane proteins

Membrane proteins are predicted to represent 20 - 30% of the cellular proteome [370]. An emerging theme in EMC biology over the last years is its apparent involvement in the biogenesis, maintenance, or trafficking of polytopic membrane proteins [369], [371], [336], [357], [372]. The current understanding of multipass protein biogenesis is fragmentary. PM proteins are co-translationally inserted into the ER membrane as the entry point into the secretory pathway. While further maturing, they are transported to the Golgi apparatus where they are packaged into transport vesicles for PM integration.

Using a combination of optokinetic response and electroretinogram assays in *Danio rerio*,

Brockerhoff *et al.* (1997) correlated a mutation of the pob gene, a close homologue of human EMC3, with degeneration of red-opsin expressing cones [373], [358]. Based on these findings, the authors suggested that pob might be involved in protein sorting or protein trafficking [373]. These early observations were extended to *D. melanogaster* by Satoh *et al.* in 2015 [357]. Analogous to its function in zebrafish, the authors found that loss of the *D. melanogaster* homologue of Pob (dPob) causes rhabdomere degeneration. Moreover, dPob mediated the biogenesis of membrane proteins such as rhodopsins 1, 3, and 4 in photoreceptor cells [357]. Rhodopsins (Rhs) are heptameric photoreceptors in the plasma membrane [374]. The loss of dPob function, or knockout of the fly homologues for EMC1 and EMC8/9, selectively affected the abundance of polytopic, but not of single-pass, TM proteins (e.g. the polytopic Rh1/3/4, and TRP, the α subunit of Na^+/K^+-ATPase were all reduced) [357]. Furthermore, the authors report that a double mutant of dPob and NinaA (neither inactivation or afterpotential A), a Rh1-specific peptidyl-prolyl-cis-trans isomerase, showed that dPob acted upstream of NinaA. Intriguingly, dPob deletion mutants were lethal early in development, suggesting additional vital functions of this EMC subunit in flies.

A genetic screen for proteins involved in the biogenesis of Yor1-ΔF670, a yeast model for the disease-causing point mutant of CFTR (CFTR-ΔF508), identified EMC1 - 7 as maturation factors [369]. Interestingly, only loss of EMC7 caused decreased translation of this mutated ABC transporter, suggesting a distinct role of EMC7 [369]. Knockdown of EMC2 in HeLa cells caused a significant decrease in CFTR-ΔF508 levels [369]. Previously, EMC2 had been demonstrated to bind to CFTR-ΔF508 in human cells (Supplemental data of [375]).

In *C. elegans*, Richard *et al.* (2013) demonstrated that the EMC is required for the correct synthesis of members of the Cys-loop receptor family, such as the levamisole-sensitive acetylcholine receptors (L-AChRs), the nAChR and the gamma-aminobutyric acid (GABA) receptor [336]. In nematodes carrying an inactivating EMC6 mutation, the total amounts of L-AChRs at neuromuscular junctions, and of unassembled, ER-resident subunits of the L-AChR were decreased [336]. Consequently, it is plausible that the EMC carries out a (co-)chaperoning function in the maturation of Cys-loop receptors.

EMC proteins might affect the trafficking of certain integral membrane proteins along the secretory pathway. Using gene co-expression networks derived from immortalized human B cells, Nayak and colleagues (2009) report that EMC3 (TMEM111) is confined to a sub-network containing genes whose expression patterns are intercorrelated [376]. These genes are involved in Golgi vesicle-mediated transport, or the secretory pathway in general [376]. In a trafficking assay using the non-essential deletion mutant array in yeast, loss of EMC1 - EMC6 resulted in

an ER/Golgi-retention of a normally PM-localized model substrate (Mrh1-GFP) [377]. This implies that the EMC might act in the early anterograde or retrograde secretory pathway.

Over the last decade, the pro-biogenesis effect of the EMC on polytopic TM proteins, often in homo- or hetero-oligomeric assemblies, has emerged as a unifying functional aspect of the evolutionarily conserved EMC in a range of different organisms. Therefore, it has been generally assumed that the EMC exhibits client-specific (co-)chaperone activity. This is in line with the complicated process of TM protein biosynthesis, which often requires a specialized chaperoning environment for correct folding and assembly. In some cases, the EMC has been shown to interact physically with membrane proteins (e.g. EMC2 binding to CFTR-ΔF508 [375]). Nonetheless, the exact mechanism of how the EMC affects the abundance of TM proteins still remains enigmatic.

4.5 Involvement of the EMC in lipid metabolic pathways

The ER is one of the principal sites of cellular lipid biosynthesis [237]. In a synthetic genetic array screen for factors that aggravate the loss of the PE methyltransferase CHO2 in yeast, the EMC was found to promote PS/PE trafficking between the ER and mitochondria [331]. The authors report that cells lacking five EMC subunits (EMC1 - 3 and EMC5/6) showed severely reduced rates of PE synthesis [331]. EMC4 features in a synthetic lethality screen in work published by Willingham *et al.* [378]. Deletion of the EMC4 gene (YGL231c) resulted in increased lethality in cells expressing α-synuclein, a protein involved in Parkinson's disease [378]. Gene ontology (GO) analysis reveals that a large proportion of genes whose deletion led to synthetic lethality in this context are also involved in lipid metabolic pathways and in vesicle trafficking [378]. In conclusion, evidence in favour of the EMC regulating lipid metabolism is scarce and can be most likely attributed to pleiotropic knock-on effects of interfering with the primary function of the EMC.

4.6 Implications of EMC involvement in multiple cellular functions

A number of independent observations suggest hitherto unrecognized and potentially unrelated activities of the EMC. In 2012, Cui *et al.* performed subcellular fractionation experiments to enrich for proteins associated with ER-localized polysomes [20]. Their dataset implies that EMC5 associates with ER-localized mRNA. However, EMC5 lacks positively charged motifs,

which are commonly found in RNA receptors such as p180, and the biological significance of this observation remains to be assessed [20]. The first comprehensive attempt to characterize EMC5 biochemically was undertaken by Goytain and colleagues in 2008 [333]. Based on microarray data derived from magnesium-starved cells, the authors identified two transcripts (MMGT1/2) to be upregulated upon magnesium depletion. When overexpressed in *Xenopus laevis* oocytes, EMC5 (MMGT1) localized to the cell surface, and magnesium was able to readily enter the cytoplasm. As transport was substrate-specific and subject to inhibition, both MMGT1 (EMC5), and MMGT2 were classified as magnesium transporters. Since EMC5 possesses only two predicted TMDs (one of which is a predicted SS), the authors argue for homo- or hetero-oligomerization to perform magnesium transport across the cell membrane. However, since the EMC is normally restricted to the ER (despite some reports observing Golgi localization (**Section 4.3**)), the role of the EMC as a cell-surface magnesium transporter is highly improbable. Consistent with a putative role of the EMC in the maturation of polytopic membrane proteins, an alternative hypothesis is suggested here in which EMC5, and possibly by extension the EMC, is instrumental for the biogenesis of a magnesium transporter. EMC6 has recently been classified as a Rab5A- and Beclin1-interacting protein in mammalian cells and was suggested to promote autophagosome formation [335]. In summary, several reports suggest involvement of the EMC in diverse cellular processes. Whether these are related to a single, unifying function of the EMC remains to be shown.

4.7 Cellular stress pathways and the EMC

As a putative complex involved in protein folding or trafficking, the EMC might prevent cellular stress arising from otherwise misfiolded or mislocalized proteins. Ring *et al.* (2008) reported that a C-terminally shortened splice variant of human EMC4 acts as an anti-apoptotic factor when expressed in yeast in the presence of the pro-apoptotic stimulus H_2O_2 [334]. The molecular mechanisms of this phenotype remain to be addressed. Loss of individual EMC proteins has been found to induce ER stress in *S. cerevisiae* [95], *D. melanogaster* [357], and *C. elegans* [336]. However, several publications have challenged these observations. In contrast to Jonikas *et al.* (2009), Lahiri and colleagues (2014) did not detect UPR activation in *S. cerevisiae* lacking five EMC subunits (EMC1 - 3 and EMC5/6) [331], and another group observed no genetic interaction between EMC proteins and the UPR components HAC1 (homologous to Atf/Creb1) or IRE1 (inositol-requiring enzyme 1) [377]. Nonetheless, loss of EMC1 or of EMC3 - 5 in ΔHAC1/ΔIRE1 double mutants sensitized cells to tunicamycin-induced ER

stress [377]. Human glioblastoma cell lines either depleted of, or overexpressing, EMC6 did not exhibit any obvious signs of ER stress [379]. Therefore, further research into the potentially cell type- or organism-specific parameters responsible for these conflicting observations will be needed.

4.8 The mEMC in human pathologies

The expression or mutation status of individual mEMC subunits has repeatedly been correlated with a variety of human pathologies. The following sections aim to describe recent advances in this growing field of research.

4.8.0.1 The mEMC as a host factor in viral infections

Viruses have evolved a variety of means to exploit cellular protein biosynthesis, maturation, and secretion pathways for their own replication. ERAD components, and the mEMC, have repeatedly been shown to play a role in the pathogenicity of *flaviviridae* such as WNV, Yellow fever virus (YFV), dengue virus (DV) or Zika virus (ZV) [380], [381], [382]. In a systematic genome-wide screen for host factors determining WNV pathogenicity, Ma *et al.* (2015) identified EMC2 and EMC3, alongside proteins of the ERAD machinery (i.e. Hrd1, Sel1L and Der2) as factors contributing to WNV-induced cell death [366]. Specifically, genetic deletion of EMC2 or EMC3 protected HEK293 FT cells from WNV cytotoxicity but did not prevent replication of the virus [366]. Additionally, the authors reported that the loss of EMC2 or EMC3 also protected from Saint Louis Encephalitis Virus-induced cell death. Similarly, EMC3 is required for YFV replication (Supplemental data of [381]). As opposed to WNV, where the mEMC did not affect viral replication, in YFV, DV, and different ZV strains, the mEMC plays a role in the early viral replication cycle [383]. In this respect, HeLa cells transiently depleted of EMC1 - EMC6 show lower infection rates for YFV, DV, and ZV [383]. Therefore, it is likely that the mEMC supervises the biogenesis of one or more cell surface or intracellular proteins required for viral entry and replication.

4.8.1 Role of the mEMC in human cancers

Two groups have implicated EMC proteins in modulating the proliferation and migration capacity of glioblastoma cells. Junes-Gill *et al.* (2011, 2014) reported anti-proliferative and anti-tumourigenic properties of a secreted splice variant of EMC10 (hHSS1) in multiple glioblastoma cell lines [338], [384]. A subsequent study linked increased glioblastoma tumourigenicity to a

pro-proliferative autophagy defect in cells with decreased levels of EMC6 [379]. Accordingly, overexpression of EMC6 leads to increased autophagic flux due to impaired phosphoinositide 3-kinase (PI3K)/protein kinase B (AKT)/mechanistic target of rapamycin (mTOR)-signalling and facilitates the clearance of cytosolic protein aggregates, while inhibiting glioblastoma cell proliferation [379].

4.8.2 Other mEMC-associated pathologies

A case study of seven individuals from four families correlates the presence of four potentially pathogenic mutations within the EMC1 gene to a severe neurodegenerative disorder marked by cerebellar atrophy, developmental delay, scoliosis, and hypotonia [385]. 75% (3/4) of mutations were mapped to either the PQQ2 domain (c.245C>T;p.Thr82Met) or the DUF (c.2602G>A; p.Gly868Arg / c.2619_2622delTCCT;p.Pro874Argfs*21). Deletion of the PQQ2 domain has been shown to promote ERAD of EMC1 [339]. Whether these mutations have a similar effect on the stability of EMC1 remains to be seen. The fourth mutation was found in the central region of EMC1 (c.1411G>C;p.Gly471Arg). The majority of patients also showed abnormal electroretinograms, and one individual exhibited retinal atrophy [385]. These findings are consistent with another case study describing a missense mutation (c.430G>A; p.Ala144Thr) within the PQQ domain of EMC1 as a potential causative factor for retinal dystrophy [386]. Moreover, in *D. rerio*, deletion of EMC3 leads to retinal dystrophy [357]. Consequently, it is possible that mutations within the EMC1 gene might impair the function of the mEMC on the whole. Tissue-specific effects of EMC dysfunction could convey different EMC-dependencies of certain tissues.

4.9 Aim of this study

The EMC is evolutionarily conserved in all eukaryotic kingdoms of life [329], where it is likely to be involved in protein biogenesis/maturation [95], [336], [357], [189]. Nevertheless, the molecular function of the complex and its fundamental biological features remain enigmatic. This study aims to address these aspects by following an integrative approach. The basic properties of the mEMC, including its assembly parameters and general architecture, are delineated by a combination of genomic editing and functional reconstitution assays. The insights thus gained are leveraged to further define its molecular function. Depletion of the mEMC by targeted disruption of critical steps of its assembly in combination with quantitative proteomics then enables its role in protein biogenesis to be assessed, and novel putative mEMC clients to be identified. Clustered regularly interspaced short palindromic repeats (CRISPR)/Cas9-mediated knockout and recombinase-directed reconstitution models of the complex allow the effect of the mEMC on its newly identified clients to be dissected, and its putative function as a protein maturation factor to be investigated in considerable detail.

Part II

Results

Chapter 5

EMC1 - EMC10 are members of an ER-localized protein complex in mammalian cells

5.1 EMC1 - EMC10 are ubiquitously expressed in a range of human tissues and cell lines

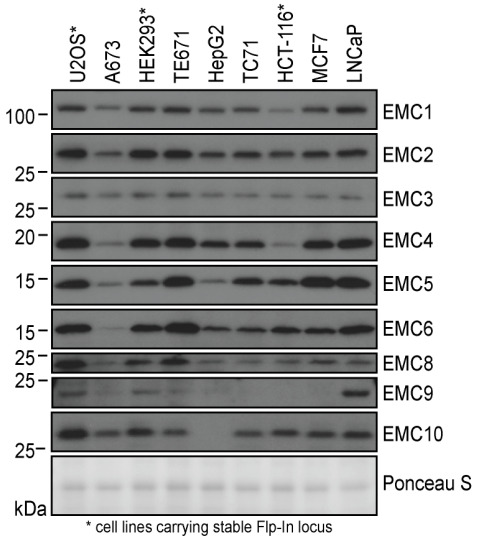
The vertebrate genome contains 10 genes encoding single subunits of the hetero-oligomeric EMC [329], [189]. **Figure 4.1** summarizes the predicted topological features of each complex member. Seven subunits (EMC1, EMC3 - 7, and EMC10) are predicted to contain one or more TMDs, whereas the remaining three (EMC2/8/9) are not integral membrane proteins. Excluding signal peptide sequences and TMDs, only EMC1 and EMC2 harbour *bona fide* functional motifs as identified by the Pfam database [349]. EMC1 was predicted to contain a β propeller PQQ (Pyrrolo-Quinoline Quinone) motif [339]. The function of this domain within EMC1 is currently unknown. EMC2 contains three TPRs (TPR1 - 3) [344]. TPRs are often found in co-chaperones and mediate protein-protein interaction [348], [347]. The role of TPR1 - 3 in EMC2 biology remains to be investigated. EMC1 and EMC10 are complex glycosylated proteins [341], [338], [339].

To determine the protein expression of the endogenous mEMC, lysates from nine human cell lines of diverse tissue origin were probed for individual subunits of the complex. Conditions for detecting endogenous EMC proteins were optimised using a set of antibodies specific for each individual subunit. Antibody specificity is evidenced by (1) signal attenuation or loss upon transient (i.e. **Figure 6.1 A**) or stable depletion/knockout (i.e. **Figure 6.1 B-D**

and immunoblotting, **Figure 6.5 D**) of the respective subunit, (2) the ability to detect the subunit from affinity-purified mEMC (i.e. **Figure 5.2 B**, **Figure 18.3 C**), or upon exogenous expression of the EMC protein itself (i.e. **Figure 6.1 F-G**), and (3) recognition of the target protein in velocity gradient sedimentation fractions corresponding to the mEMC (i.e. **Figure 5.2 A**). EMC7 protein levels were not tested due to the lack of a reliable anti-EMC7 antibody, but exogenous expression of an S-tagged variant of EMC7 (EMC7-S) and subsequent affinity capture demonstrates that EMC7 is part of the mEMC in U2OS Flp-In cells (**Figure 18.3 C**).

Indeed, EMC1 - 6, EMC8, and EMC10 were co-expressed in most cell lines (**Figure 5.1 A**). The only exception were HepG2 cells, which apparently lacked EMC10. EMC9 proved difficult to detect in most cell lines tested. The ubiquitous nature of mEMC expression is also reflected in tissue-wide gene expression data, publicly available through the genome-based tissue expression (GTEx) consortium [387]. The abundance of EMC1 - 10 transcripts in 30 different tissues is shown in **Figure 5.1 B** [387]. The relative transcript levels of EMC1 - EMC10 vary widely within most tissue types, but are predominantly comparable for the same gene across different tissues. Notably, transcript levels of EMC1, EMC5, and EMC6 are consistently low compared to other subunits. This observation indicates that the mEMC is transcriptionally co-regulated.

A



B

tissue:	EMC1	EMC2	EMC3	EMC4	EMC5	EMC6	EMC7	EMC8	EMC9	EMC10
adipose	4.93	23.59	22.85	29.31	12.04	3.02	31.15	9.73	6.18	28.06
adrenal	4.88	23.65	21.5	32.49	5.02	7.79	48.11	9.94	21.57	69.03
artery	4.93	22.59	12.83	28.81	15.23	2.69	30.09	7.68	9.27	60.17
bladder	4.58	20.76	18.5	27.66	11.02	3.72	24.21	8.68	8.34	39.5
blood	1.08	4.48	21.85	13.61	5.42	2.48	18.92	5.34	3.37	25.84
brain (cerebellum)	6.92	17.24	11.58	30.9	7.28	4.02	21.74	7.25	18.04	28.18
brain (cerebrum)	4.06	27.02	14.28	33.22	7.11	2.92	31.32	7.84	8.25	41.84
breast	5.17	23.04	15.38	29.99	9.58	3.16	27.46	9.98	8.67	39.34
cervix	5.46	21.36	12.24	32.42	11.65	2.74	27.08	9.46	9.47	47.09
colon	4.82	18.36	14.97	24.16	9.36	5.19	25.83	10.4	10.87	51.91
esophagus	4.23	19.82	17.26	28.48	6.56	5	20.61	8.34	8.3	34.49
fallopian tube	5.67	19.77	13.07	31.22	12.07	3.5	29.34	9.28	8.58	45.18
heart	3.89	17.57	17.58	21.92	7.49	5.09	24.48	8.65	6.21	36.95
kidney	3.32	18.97	11.91	22.52	5.66	5.66	25.51	9.3	12.46	68.88
liver	2.96	12.13	11.4	16.74	2.58	5.36	21.19	5.93	10.2	47.43
lung	5.4	22.93	15.64	27.99	10.7	3.91	30.43	8.82	6.98	45.13
nerve	5.48	27.16	12.8	31.44	11.78	2.66	34.16	9.74	8.38	43.59
ovary	5.75	18.06	10.03	31.01	8.8	3.2	24.05	7.46	10.31	67.45
pancreas	2.56	14.6	8.67	16.81	5.26	3.24	18.78	4.98	8.94	35.64
pituitary	5.2	22.97	11.73	31.81	8.44	5.49	34.22	10.93	26.66	175.92
prostate	4.91	18.33	12.89	25.86	7.62	4.55	24.44	10.7	14.24	56.17
skeletal muscle	4.62	16.68	33.02	29.55	8.18	11.58	23.67	7.67	10.34	16.91
skin	4.5	16.54	17.57	26.51	8.53	2.81	28.98	8.7	10.57	37.78
small intestine	4.26	16.9	12.55	23.2	8.1	4.85	23.06	9.35	11.53	47.04
spleen	4.36	16.68	12.48	24.5	6.42	6.31	23.87	10.58	13.52	44.24
stomach	4.1	18.86	15.55	27.5	8.89	4.95	28.25	8.51	8.46	49.76
testis	6.01	31.55	28.28	31.61	2.77	9.61	46.02	17.8	16.6	93.81
thyroid	5.1	21.4	18.73	28.7	10.05	3.12	29.13	10.12	10.92	88.6
uterus	5.82	17.48	11.91	32.86	10.92	4.05	26.98	10.16	9.28	48.45
vagina	5.58	20.11	12.61	31.87	8.53	3.56	24.59	8.28	9.81	40.49

See next page for Figure legend.

5.2 EMC1 - EMC10 form a protein complex

In yeast, EMC1 - EMC6 are synthesized at equimolar ratios and form a complex with a 1:1 stoichiometry [330]. However, there is little evidence indicating the size, structure, and dynamics of both the yeast orthologue and the related mEMC. Here, determination of the approximate molecular weight was sought, alongside the characterization of the molecular organization of the endogenous mEMC using sucrose gradient velocity centrifugation. The intact mEMC was isolated from U2OS Flp-In cells under mild lysis conditions in the presence of 1% lauryl maltose neopentyl glycol (LMNG). Compared to a more stringent Triton X-100 lysis buffer, LMNG allowed enhanced resolution on shallow (5 - 15%) sucrose gradients (compare **Figure 5.2 A** and **Supplemental Figure 18.1**). Subunits of the endogenous mEMC co-sedimented in fractions 7 - 10 (**Figure 5.2 A**). Based on the sedimentation behaviour of the gel filtration markers β-amylase and apoferritin (**Supplemental Figure 18.2**), this was reminiscent of a complex of approximately 300 - 400 kDa. The finding is consistent with each subunit being present at equimolar ratios, as EMC1 - 10 amount to a combined predicted molecular weight of 315.3 kDa, not including PTMs. EMC1 and EMC10 were also detectable in lower fractions (4 - 6), **Figure 5.2 A**, potentially representing unassembled forms or assembly intermediates. Alternatively, some portion of the mEMC might have partially fragmented during cell lysis or subsequent sample processing. To determine whether all co-sedimenting EMCs were indeed part of a single complex, FLAG:HA-tagged EMC6 was stably expressed in U2OS Flp-In cells at levels below that of the endogenous subunit (**Supplemental Figure 18.3 B**), isolating complexes from each sucrose gradient fraction by affinity capture. Of note, exogenous expression of FLAG:HA:EMC6 led to concomitantly decreased steady-state levels of endogenous EMC6, indicative of functional replacement by the epitope-tagged variant (**Supplemental Figure 18.3 A/B**). **Figure 5.2 B** shows that the majority of FLAG:HA:EMC6 co-sedimented, and interacted with the remaining EMC proteins. Hence, subunits in fractions 7 - 10 are likely to be representative of the mature mEMC with a molecular weight exceeding 300 kDa. In most cases, EMC7 could not be consistently detected at endogenous levels. To show that EMC7 is a *bona fide* subunit of the mEMC in U2OS Flp-In cells, affinity purification of transiently

Figure 5.1 ***(previous page)*****: Expression of the mEMC in mammalian cells. A.** EMC1-6/8-10 are expressed in a panel of nine different human cell lines. Immunoblot analysis of whole-cell lysates shows endogenous EMC subunits at steady-state. Cell lines carrying the genomic Flp-In locus are indicated by an asterisk (*). **B.** Bioinformatic analysis of the expression pattern of individual EMCs from human tissue. Publically available RNAseq data was obtained from the genome-based tissue expression (GTEx) consortium as listed in [387]. FPKM (fragments per kilobase of exon per million fragments mapped) values are shown and colour-coded red (low) to green (high).

expressed S-tagged EMC7 (EMC7-S) was performed. As expected, EMC7-S interacted with other EMCs (**Supplemental Figure 18.3 C**).

Here, I have confirmed that the endogenous mEMC consists of 10 subunits (EMC1 - 10). Isolation of native mEMC, and resolution on sucrose gradients, indicate that EMC1 - 10 are incorporated into a single complex of approximately 300 - 400 kDa. Considering that a predicted 1:1 stoichiometry predominates in the fungal homologue of the EmMC [330], a similar subunit balance for the mEMC would be a reasonable conclusion.

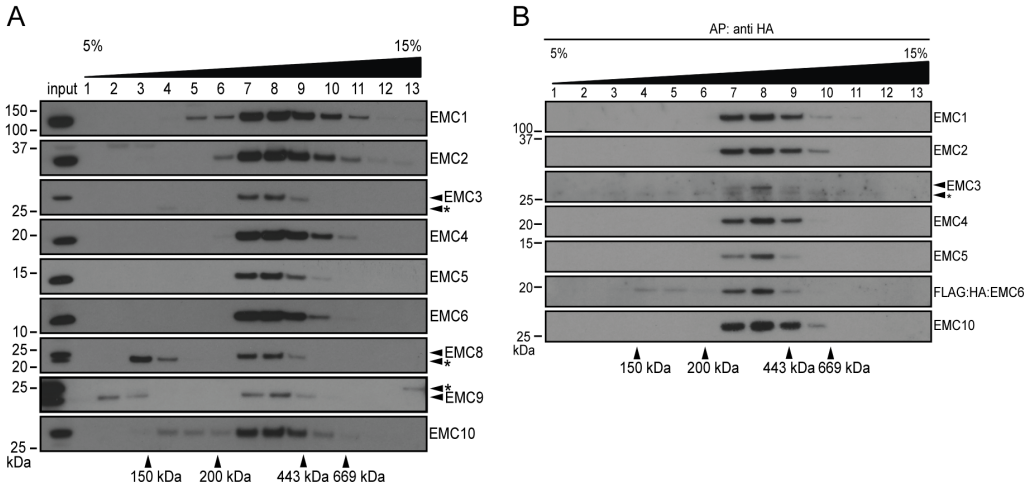


Figure 5.2: EMC proteins form a complex of approximately 300 - 400 kDa. A. EMC proteins co-sediment. Whole-cell lysate from U2OS Flp-In cells was separated on a 5 - 15% sucrose gradient and thirteen fractions were collected. Endogenous mEMC subunits were detected by immunoblotting. Fraction numbers are indicated. Asterisks (*) denote unspecific bands. The corresponding molecular weights of native protein complexes are indicated for individual fractions. **B.** The mature mEMC migrates in fractions 7 - 9. FLAG:HA:EMC6 was stably introduced into U2OS Flp-In cells using the Flp-In recombinase system. Expression of the transgene was induced by adding 1 ng/ml doxycycline for 18 hours. Protein lysates were subjected to velocity sucrose gradient centrifugation as described in (A) and FLAG:HA:EMC6-associated proteins were captured from each fraction by affinity purification (AP) using a monoclonal anti-HA agarose-conjugated antibody. Interacting proteins were detected by immunoblotting.

Chapter 6

The stability of mEMC subunits is interdependent and regulates complex formation

6.1 Loss of certain mEMC subunits disrupts the mEMC

The assembly of oligomeric protein complexes generally follows a highly coordinated sequence of folding factors and assembly intermediates [166], [388], [389]. In the case of the mEMC, it is intriguing how 10 subunits whose genes are distributed across different loci and chromosomes are transcribed, translated, targeted, and assembled at a rate that allows controlled complex formation. However, the mechanisms that drive the concerted formation of the mEMC still remain elusive. One possibility is that the assembly of the mature mEMC is monitored by several checkpoints, such as the relative abundance of its constituents. Accordingly, it was hypothesized that the mEMC biogenesis is partially controlled by the relative abundance of its individual subunits. This would allow efficient control over the assembly process by altering the steady-state levels of one or more subunits.

6.1.1 EMC1 - 3 and EMC5/6 are essential for mEMC biogenesis

To test whether mEMC subunits were essential for complex biogenesis, EMC1 - EMC10 were systematically depleted by RNAi-mediated knockdown while the steady-state levels of the remaining subunits were monitored. To this end, U2OS Flp-In cells were transfected with a pool of four small interfering RNAs (siRNAs) for each EMC and the endogenous levels of mEMC constituents were monitored by immunoblotting. **Figure 6.1 A** shows that depletion

of multiple subunits differentially affected the steady-state protein levels of the remaining components. Depletion of EMC5 or EMC6 caused pronounced disruption of the entire complex, as evidenced by a marked reduction of the remaining subunits (**Figure 6.1 A**, lanes 6 and 7). A similar phenomenon was observed when EMC2, and to a lesser extent EMC1 and EMC3, were knocked down (**Figure 6.1 A**, lanes 2 - 4). A more selective co-depletion was evident in cells depleted of EMC8 - EMC10. Here, EMC5 and EMC6 were diminished, but still readily detectable (**Figure 6.1 A**, lanes 9 - 11).

To better study mEMC function, architecture, and the interrelationships of its subunits, the knowledge of the strict interdependence between EMC proteins was used to guide the creation of multiple EMC knockout cell lines. Accordingly, EMC2, EMC5, and EMC6 were deleted by CRISPR/Cas9-mediated genomic editing to obtain cell lines that were unable to fully form the mature mEMC. Multiple ΔEMC2, ΔEMC5, and ΔEMC6 single cell clones were tested for mEMC subunit expression (**Figure 6.1 B - D**). Despite some variation between ΔEMC2 clonal lines, the remaining mEMC subunits were notably reduced in ΔEMC5, ΔEMC6, and ΔEMC2 cells when compared to wild type. All EMC2 'knockout' clonal lines tested still retained trace amounts of EMC2 as determined by immunoblotting (**Supplemental Figure 18.7 B**). Therefore, ΔEMC2 cells should instead be considered severely depleted of EMC2. The failure to obtain EMC2 knockout cells could reflect decreased viability or growth inhibition if EMC2 is completely lost. EMC2 knockout clones appeared to exhibit slower growth or increased cell death when maintained in culture. However, further experiments are needed to substantiate this observation. Nonetheless, these data strongly suggest that EMC2, EMC5, and EMC6 act *via* a similar mechanism, and/or at the same stage of mEMC biogenesis.

Next, I assessed whether or not the loss of the mEMC was reversible. To this end, the Flp-In recombinase system was used, which allows targeted, single-site genomic integration of a transgene downstream of a doxycycline (Dox)-inducible cytomegalovirus (CMV) promoter. ΔEMC5 cells were reconstituted with the complete cDNA sequence of EMC5. EMC5 expression was then induced by addition of 1 ng/ml Dox for 24 hours. **Figure 6.1 E** depicts that accumulating levels of EMC5 are closely tracked by the remaining EMC subunits, indicating the restoration of the mEMC. For the remainder of this document, the relative abundances of EMC2, EMC4, EMC5, and EMC6 will be used to reflect the integrity of the mature mEMC. Several findings justify this approach. Firstly, EMC4 was among the subunits most strongly affected by the depletion of other mEMC components (**Figure 6.1**), and therefore constitutes a sensitive readout for the integrity of the complex. Secondly, EMC2 is one of the few subunits that are predicted to be cytoplasmic. Monitoring EMC2 levels partially reduces the risk of

introducing a bias by TMDs. Finally, EMC2, EMC5, and EMC6 are essential for mEMC biogenesis; the absence of any of these subunits precludes maturation (**Figure 6.1 A**).

Since loss of either EMC5 or EMC6 resulted in pronounced mEMC depletion from the cell, I investigated whether EMC5 and EMC6 were required in the same manner for mEMC biogenesis. If both proteins are functionally equivalent, EMC5 may be able to rescue mEMC expression in ΔEMC6 cells and *vice versa*. To test this hypothesis, ΔEMC5 and ΔEMC6 cells were complemented with the missing subunit or its putative counterpart. Expression of each subunit in its respective knockout line resulted in restoration of mEMC biogenesis (**Figure 6.1 F and G**, compare lanes 2 and 3). In contrast, EMC5 and EMC6 were not able to functionally replace one another (**Figure 6.1 F, G**, compare lanes 3 and 4). In fact, while EMC6 returned to wild type levels in ΔEMC5 cells, EMC1 - 4 did not increase. Exogenous EMC5 could not be expressed at near-wild type levels in ΔEMC6 cells (**Figure 6.1 G**, lane 4) due to its increased proteasome-dependent degradation in the absence of EMC6 (**Section 6.1.2**, and **Figure 6.2**). Consequently, it was concluded that EMC5 and EMC6 are not functionally redundant for the formation of the mEMC.

In summary, this section demonstrates strict mEMC subunit interdependence. Depletion of individual components of the mEMC impacted steady-state levels and assembly of the remaining subunits. Loss of EMC5 and EMC6 caused notable disruption of the entire complex. This was reproduced to a lesser extent by depletion of EMC2, EMC3, and EMC1 (in descending order of magnitude). It is conceivable that EMC5 and EMC6 are needed in the early steps of mEMC assembly. In this respect, interference with EMC5/6 expression could negatively affect the ordered incorporation of other subunits into a mature mEMC. The fate of most EMC subunits in the absence of EMC5 or EMC6 remains to be shown. However, the proteasome-dependent destabilization of individual subunits suggests increased turnover by the UPS when EMC5/6 are not present. Furthermore, mEMC depletion can be reversed by restoring the missing subunit (EMC5 in ΔEMC5 cells), offering a valuable means to artificially manipulate mEMC abundance. Finally, both EMC5 and EMC6 are necessary but not sufficient for mEMC biogenesis. These observations suggest that the assembly and maintenance of the mEMC is a highly controlled and ordered process.

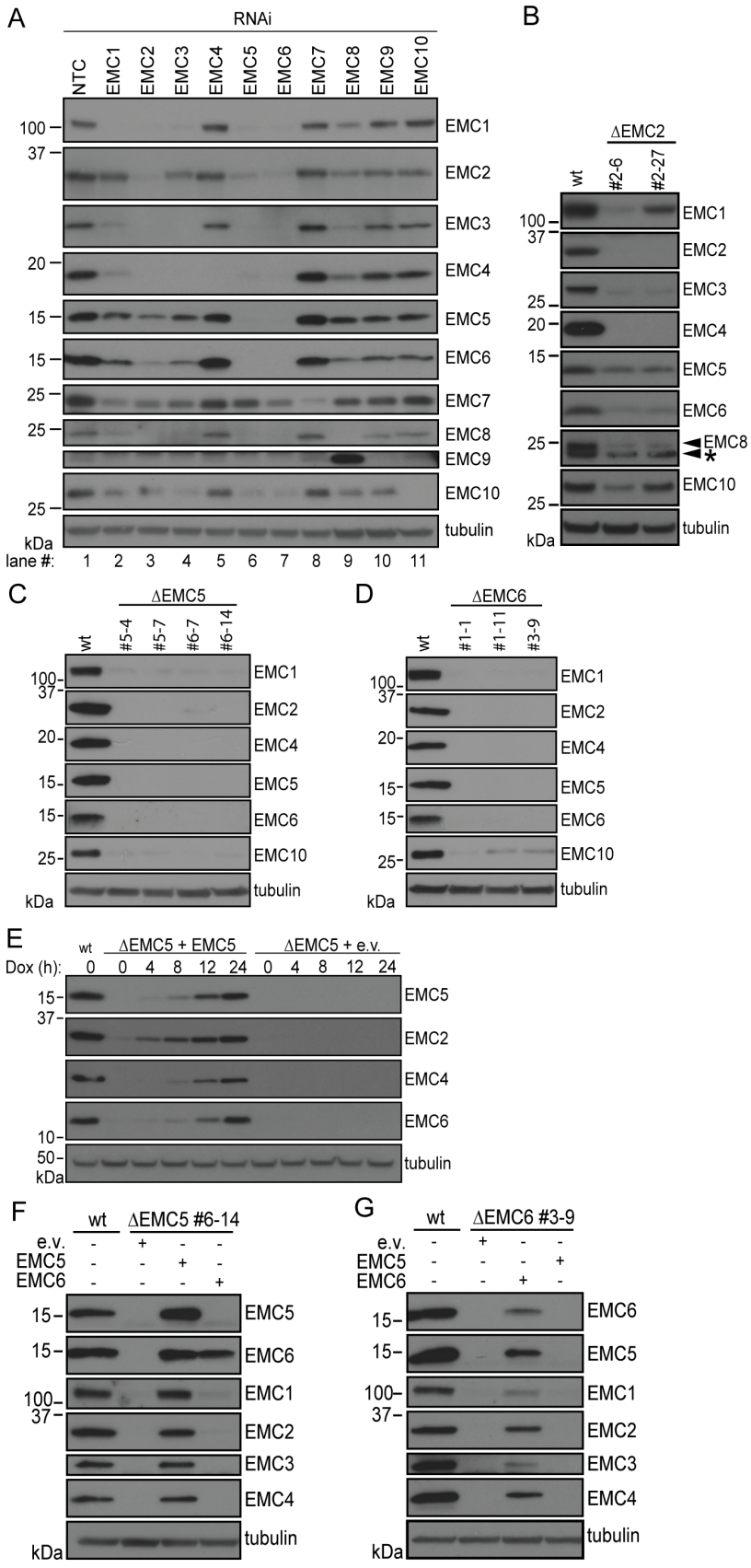


Figure legend on next page.

Figure 6.1 ***(previous page)*****: EMC1 - 3 and EMC5/6 are essential for mEMC biogenesis.** **A.** Co-dependent expression of distinct mEMC subunits. Immunoblot of whole-cell lysate from cells transfected with siRNAs specific for EMC1 - EMC10. U2OS Flp-In cells were transfected with a set of four siRNAs for each gene, and collected after 72 hours. **B.** EMC2 depletion affects the abundance other mEMC subunits. Whole-cell lysates of U2OS Flp-In wild-type (wt) cells and of two single cell clones stably depleted of EMC2 (#2-6 and #2-27) were subjected to immunoblotting. The asterisk symbolizes an unspecific band. **C.** mEMC depletion in CRISPR/Cas9-derived ΔEMC5 cells. ΔEMC5 clones (#5-4, #5-7, #6-7, and #6-14) were derived by CRISPR/Cas9-mediated knockout in U2OS Flp-In cells. Whole-cell lysates were separated on a gel and immunoblotting was performed for mEMC subunits. **D.** ΔEMC6 cells show perturbed mEMC biogenesis. Three EMC6 knockout cell lines (#1-1, #1-11, #3-9) were generated by gene editing and whole-cell lysates were subjected to immunoblotting for mEMC components. **E.** mEMC depletion is reversible. ΔEMC5 U2OS Flp-In cells (#6-14) were reconstituted with EMC5 or empty vector (e.v.) control (pcDNA^{TM}/5/FRT/TO). EMC5 expression was induced by supplementation with 1 ng/ml Dox and cells were collected at the indicated times after Dox addition. **F.** EMC6 expression is not sufficient to reverse mEMC loss in ΔEMC5 cells. EMC5 knockout cells were stably reconstituted with an empty vector (e.v.) control, EMC5, or EMC6, using the Flp-In recombinase system. Expression of the gene of interest was induced with 1 ng/ml Dox for 72 hours. Whole-cell lysates were monitored for the levels of select mEMC subunits by immunoblotting. **G.** EMC6 is necessary to maintain EMC5 expression. ΔEMC6 U2OS Flp-In cells were stably complemented with an empty vector (e.v.) control, EMC6, or EMC5, and treated as in (F). e.v., empty vector (pcDNA^{TM}/5/FRT/TO); Dox, doxycycline; NTC, non-targeting control.

6.1.2 Interdependence of mEMC subunit stability

To assess whether the loss of mEMC subunits was caused by translational attenuation, quantitative polymerase chain reaction (qPCR) was performed on mEMC subunit transcripts. mRNA was isolated from U2OS Flp-In cells that were transiently depleted of EMC6 by RNAi for 72 hours. Following reverse transcription, the mRNA abundance of EMC1-10 was determined by the $\Delta\Delta Ct$ method. As shown in **Figure 6.2 A**, mRNA levels were comparable to those of cells transfected with a non-targeting siRNA pool. The lack of a detectable transcriptional change suggested subunit loss was attributable to a post-translational mechanism. One possibility is increased proteasomal turnover of subunits that fail to assemble due to the lack of EMC5 or EMC6. I have shown previously that EMC6 was necessary for the expression of exogenously introduced EMC5 (**Figure 6.1 G**). Lack of exogenous EMC5 expression in EMC6 knockout cells suggested rapid degradation. To address this question, EMC5 expression was induced for 24 hours in ΔEMC6 + EMC5 cells, followed by proteasome inhibition with 5 μg/ml MG-132 for an additional 8 hours (**Figure 6.2 B**). In this context, EMC5 expression was potently restored, indicating that (exogenous) EMC5 is efficiently targeted for degradation by the proteasome in ΔEMC6 cells (**Figure 6.2 B**, compare lanes 6 and 8). For reasons that are not clear, endogenous subunit levels could not be restored by MG-132 treatment (**Figure 6.2 B**, compare lanes 5 and 6 for EMC4/5). Further evidence for destabilization of the mEMC can be derived from the low steady-state levels of EMC2 in ΔEMC5 and ΔEMC6 cells. To determine the relative stability of EMC2 in these cells, translation was blocked by the ribosome inhibitor

cycloheximide (CHX) for 2 - 8 hours. Residual EMC2 in ΔEMC5 and ΔEMC6 cells was rapidly lost and was barely detectable after 8 hours (**Figure 6.2 C**), but could be restored by adding MG-132. In contrast, in wild-type cells EMC2 remained remarkably stable over the entire treatment period, reflecting a long half-life for the mEMC. Even though these observations imply increased turnover of EMC proteins in the absence of EMC6, expression to wild-type levels could not be fully restored by proteasome inhibition. One possible explanation could be that polyubiquitination alters their migration pattern. Alternatively, individual subunits might be removed by proteasome-independent degradation pathways. Autophagy can efficiently remove cellular organelles (macroautophagy) and individual protein species (microautophagy) without proteasome involvement [390]. To investigate a possible role of autophagy in EMC protein loss, EMC5 and EMC6 knockout cells were treated with the autophagy inhibitor Bafilomycin A1 (BafA1) and the mEMC was monitored [391]. Treatment with 100 nM BafA1 for 0 - 8 hours did not restore the mEMC in ΔEMC5/6 cells (**Supplemental Figure 18.5**). Next, it was determined whether the missing mEMC subunits were retained in a RIPA-insoluble post-lysis fraction. Extraction of proteins from the RIPA-insoluble fraction of ΔEMC6 cells did not recover a considerable amount of EMC proteins (**Supplemental Figure 18.5 A**). Therefore, it is unlikely that EMC proteins form insoluble aggregates in the absence of EMC6.

In this section, the fate of mEMC subunits when mEMC assembly is disrupted was investigated. Residual EMC2 in EMC6-deficient cells was destabilized in a proteasome-dependent manner. Similarly, exogenously expressed EMC5 was rapidly degraded by the proteasome when EMC6 was absent. These findings indicate that mEMC subunits might be post-translationally degraded. However, failure to fully rescue mEMC subunits by proteasome inhibition does not rule out a co-translational degradation route.

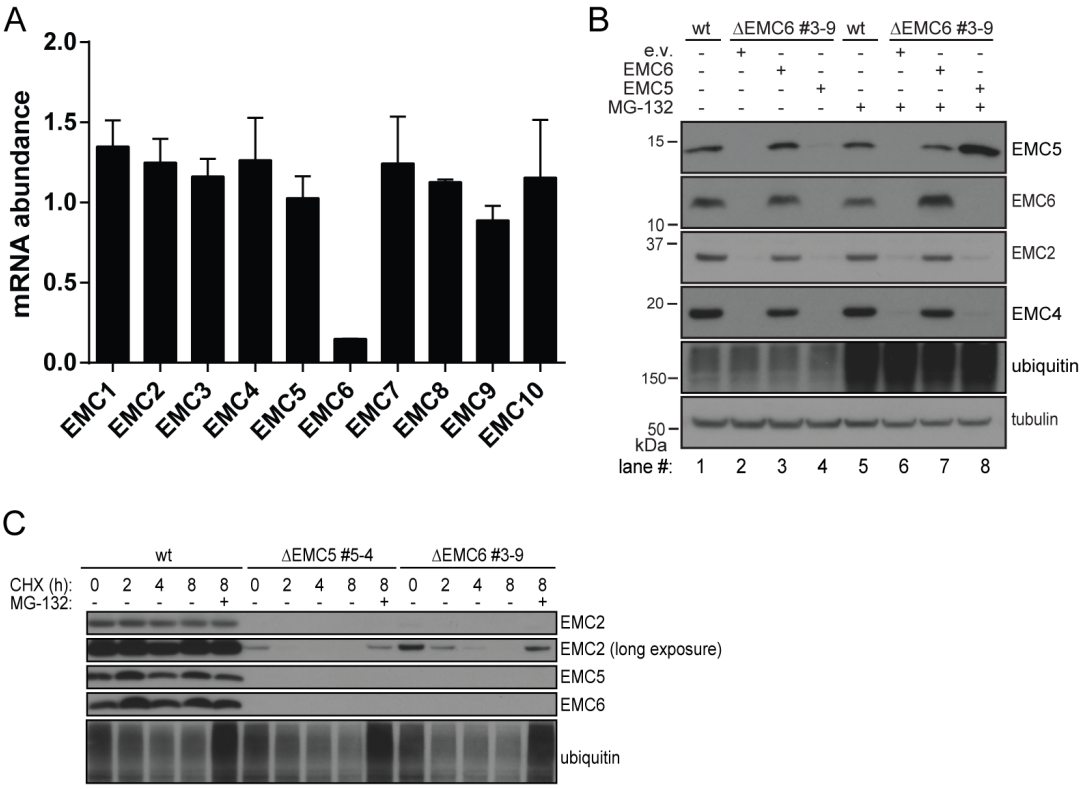


Figure 6.2: Depletion or loss of EMC5/6 causes posttranslational attenuation of the mEMC. A. mEMC subunits were not transcriptionally attenuated upon knockdown of EMC6. U2OS Flp-In cells were transfected with a pool of four siRNAs targeting EMC6 or a pool of non-targeting siRNAs (NTC). After 72 hours, qRT-PCR was performed. mRNA abundances were calculated using the $\Delta\Delta Ct$ method and normalized to mRNA levels in NTC cells. Mean values of three independent experiments and standard deviations (S.D.) are shown. **B.** In the absence of EMC6, EMC5 was degraded in a proteasome-dependent manner. Using the Flp-In recombinase system, ΔEMC6 cells were stably transfected with EMC5, EMC6, or an empty vector control (e.v.). Expression of the transgene was induced by addition of 1 ng/ml Dox for 72 hours, after which 5 μg/ml MG-132 was added for an additional 8 hours. Whole-cell lysates were subjected to immunoblotting. Ponceau S staining served as a loading control. **C.** Residual amounts of EMC2 were destabilized in ΔEMC5 and ΔEMC6 cells. Cells were treated with 100 ng/ml cycloheximide for the indicated time in the presence or absence of 5 μg/ml MG-132. Immunoblotting of whole-cell lysates was performed for EMC2/5/6 and ubiquitin. CHX, cycloheximide; Dox, doxycycline; e.v., empty vector (pcDNA^{TM}/5/FRT/TO).

6.1.3 mEMC biogenesis is mildly affected upon depletion of EMC7 - EMC10

Having shown that depletion of individual EMC proteins differentially impacted the stability of the remaining subunits in cells, EMC1 - 10 were classified based on their contribution to mEMC biogenesis. In this paradigm, 'primary subunits' (EMC1 - 3/5/6) play an important role in mEMC biogenesis or in maintaining the steady-state levels of the mature mEMC. In contrast, 'secondary subunits' (EMC4/7 - 10), when depleted, only moderately affected the steady-state amounts of the remaining EMC subunits (**Figure 6.1 A**). This implies that secondary subunits are dispensable for the ordered biogenesis of the complex.

To ascertain the impact on mEMC formation in the absence of these 'secondary' sub-

units, complex integrity was assessed using sucrose gradient sedimentation. U2OS Flp-In cells were transiently depleted of EMC4 and EMC7 - 10 by RNAi for 72 hours, and the sedimentation pattern of the mEMC was evaluated. The knockdown efficiency was monitored by immunoblotting (**Figure 6.3 B**). **Figure 6.3 A** shows that the majority of the mEMC subunits co-sedimented in fractions 7 - 10, reminiscent of the mEMC in control (siNTC) cells. Nonetheless, several subunits exhibited clear deviations from their normal migration patterns. The loss of EMC4 caused all remaining subunits to shift by one or more fractions, indicative of a complex of lower hydrodynamic radius. EMC10 exhibited a marked shift to fractions 4 - 7, thereby indicating that EMC10 might bind to the rest of the complex *via* EMC4 (**Figure 6.3 A (g)**). This phenomenon is mirrored in EMC3-depleted cells, where the complex appeared to undergo a more pronounced disruption. Depletion of EMC7 had a similar impact on EMC10 as EMC4 knockdown, whereas the remaining subunits were unaltered, suggesting that EMC7 is peripherally located within the mEMC (**Figure 6.3 A (g)**). Knockdown of EMC8 led to the marked loss of EMC5 and EMC6 (**Figure 6.3 A (d)/(e)**), with little effect on the sedimentation pattern of the remaining mEMC components.

In contrast to the loss of the 'secondary' subunits, depletion of 'primary' subunits, such as EMC1 and EMC3, caused the complex to disintegrate as other subunits were concomitantly destabilized. The abundance of EMC2 remained largely unaffected in cells knocked down for either EMC1, or EMC3, but its shift from fractions 7 - 10 into lower fractions (3 - 6) reflects its failure to assemble into larger complexes (**Figure 6.3 A (d)/(e)**). ΔEMC2 cells maintained moderate levels of EMC5, EMC6, and EMC10 while apparently losing other subunits. However, as is the case for EMC2 in EMC1- and EMC3-depleted cells, EMC5/6, and EMC10 were markedly shifted into lighter fractions (4 - 5) (**Figure 6.4 B**).

Here, I have demonstrated that the loss of individual subunits differentially affects the composition of the mEMC, reflected in the altered hydrodynamic radii of its subunits in sucrose sedimentation assays. Both EMC4 and EMC7 appear to be required for the incorporation of EMC10 into the complex. Nonetheless, the sedimentation pattern of most subunits resembles that of the mature mEMC in cells transiently depleted of EMC4 and EMC7 - 10. These findings support the notion that the 'secondary subunits' (EMC4/7 - 10) might be incorporated into the mEMC after the 'primary subunits' (EMC1 - 3/5/6), and are therefore not as instrumental for the recruitment of other EMC proteins (with the exception of EMC10) to the complex.

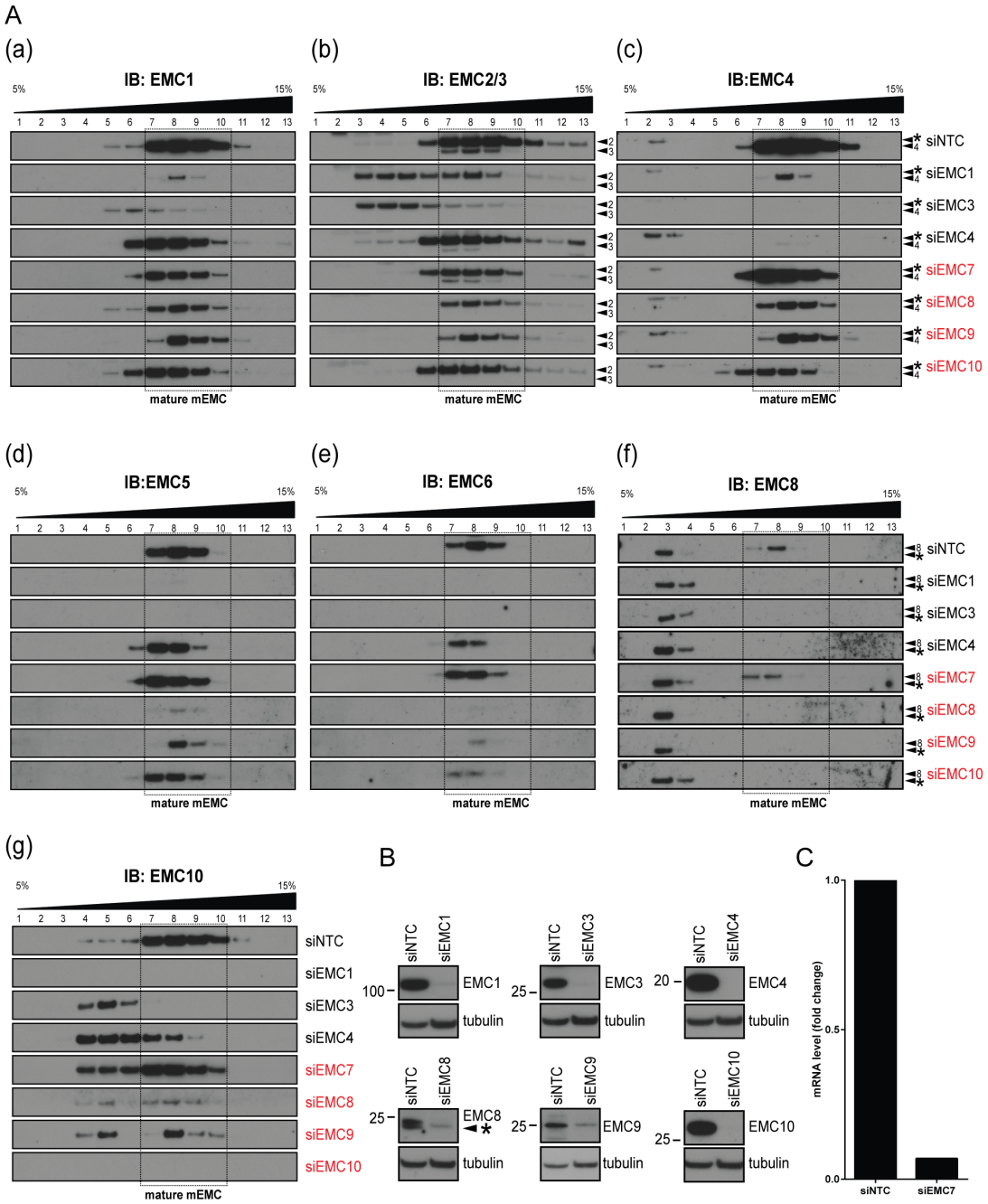


Figure 6.3: Depletion of the 'secondary subunits' EMC7 - 10 only mildly affects incorporation of remaining EMCs into the mEMC. A. (a - g). Depletion of the 'secondary subunits' EMC7 - 10 (red) only mildly affects incorporation of remaining EMCs into the mEMC. U2OS Flp-In cells were depleted of EMC1/3/4/7 - 10 by siRNA-mediated knockdown for 72 hours. A pool of non-targeting siRNAs served as a control (siNTC). Whole-cell lysates were applied to velocity gradient sedimentation on a 5-15% sucrose gradient. Thirteen fractions were collected for immunoblotting. Fraction numbers are indicated. Boxed areas demarcate fractions comprising the mature mEMC in siNTC-transfected cells. Asterisks (*) designate unspecific bands. **B.** Knockdown efficiencies. Immunoblotting of whole-cell lysates from (A). **C.** EMC7 mRNA levels in EMC7-depleted cells. The relative amount of EMC7 mRNA was determined by qPCR from RNA samples corresponding to EMC7-knockdown cells shown in (A). IB, immunoblot; siNTC, non-targeting control siRNA.

6.2 Isolation of an EMC5/6 sub-complex

To better define the subunit organization and assembly process of the mEMC, potential stable assembly intermediates were investigated. EMC2 is one of the 'primary' subunits, meaning that its depletion interferes strongly with the overall abundance of the remaining mEMC components (**Figure 6.1 B**). Unexpectedly, EMC5 and EM10 were only moderately decreased. EMC6 levels were markedly affected and showed greater variation between experiments, but were still detectable by immunoblotting. The (partial) preservation of EMC5, EMC6, and EMC10, even upon depletion of a 'primary subunit' (EMC2), posed a unique opportunity to interrogate their interrelationship among each other and with EMC2.

To address the hypothesis of EMC5/6/10 forming sub-complexes that reflect stable, 'dead-end' assembly intermediates in EMC2-depleted cells, FLAG:HA:EMC6 was affinity-captured from sucrose gradient fractions **Figure 6.4 A**. **Figure 6.4 B** illustrates pronounced co-sedimentation of EMC5, EMC6, and EMC10 in lower fractions (4 and 5) of EMC2-depleted cells. This unusual sedimentation pattern is not a consequence of FLAG:HA:EMC6 expression, as mEMC subunits co-sedimented in fractions 7 - 9 in the parental cell line expressing FLAG:HA:EMC6 (**Figure 6.4 B**). Moreover, sedimentation of EMC5 or EMC10 was similar in EMC2-depleted cells carrying an empty vector control (e.v.) (**Supplemental Figure 18.7**). Affinity purification of EMC6 from fractions 3 - 9 revealed binding of EMC6 to EMC5 in fractions 4 and 5 (**Figure 6.4 C**). However, EMC10 did not participate in this sub-complex. Hence, EMC2 was dispensable for EMC5-EMC6 interaction. Association of the EMC5-EMC6 sub-complex with EMC10, on the other hand, appears to require EMC2. These findings were recapitulated when epitope-tagged EMC6 was affinity purified from whole-cell lysate prior to sucrose gradient sedimentation, thereby ruling out loss of EMC5/6-binding to EMC10 during velocity gradient sedimentation (**Supplemental Figure 18.6 A**). In the absence of EMC2, EMC10 might be present as monomeric subunits or associate with other (non-EMC) proteins.

Next, attempts were made to dissect EMC6 connectivity with the rest of the mEMC subunits. Using a combination of RNAi and affinity purification, I assessed which subunits modulated the binding capacity of EMC6 to the remaining complex. Since depletion of 'primary subunits' led to the co-depletion of other remaining EMCs, the 'secondary' subunits (EMC4/7 - 10) were the primary focus. FLAG:HA:EMC6 was expressed in HEK293 Flp-In cells, and EMC1/4 and EMC7 - 10 were depleted for 72 hours. EMC6-containing complexes were then captured by affinity purification with a monoclonal anti-HA agarose-conjugated antibody. EMC6-associated proteins were visualized by immunoblotting, with EMC7, and EMC9

knockdown verified by qPCR (**Supplemental Figure 18.8**). Binding of FLAG:HA:EMC6 to EMC10 was consistently found to be markedly diminished in EMC4-depleted cells (**Figure 6.4 D**, compare EMC10 in lanes 9 and 11). Likewise, depletion of EMC4 or EMC10 lead to decreased binding of EMC6 to EMC1, but this observation could not be consistently reproduced. Intriguingly, RNAi of EMC10 also notably reduced the binding of EMC6 to EMC4, implying that both subunits are mutually dependent on one another to contact EMC6 (**Figure 6.4 D**, compare EMC4 in lanes 9 and 15). Additionally, EMC4 depletion in U2OS Flp-In cells resulted in the loss of EMC10 from mature mEMCs sedimented on sucrose gradients (**Figure 6.4 E**), whereas EMC2 was only mildly affected (**Figure 6.3 A (b)**).

Experiments detailed in this section reflect preliminary attempts to define the inter-subunit connectivity of the mEMC. Depletion of several 'secondary subunits' affected the composition of EMC6 sub-complexes. In particular, EMC4 was required for EMC6 to bind EMC10, implying that EMC4 is the bridge for EMC6-EMC10 interaction. Future work will aim to create a detailed interaction map by using *in vivo* cross-linking and mass spectrometry (MS)/MS-based identification of interaction surfaces between mEMC subunits.

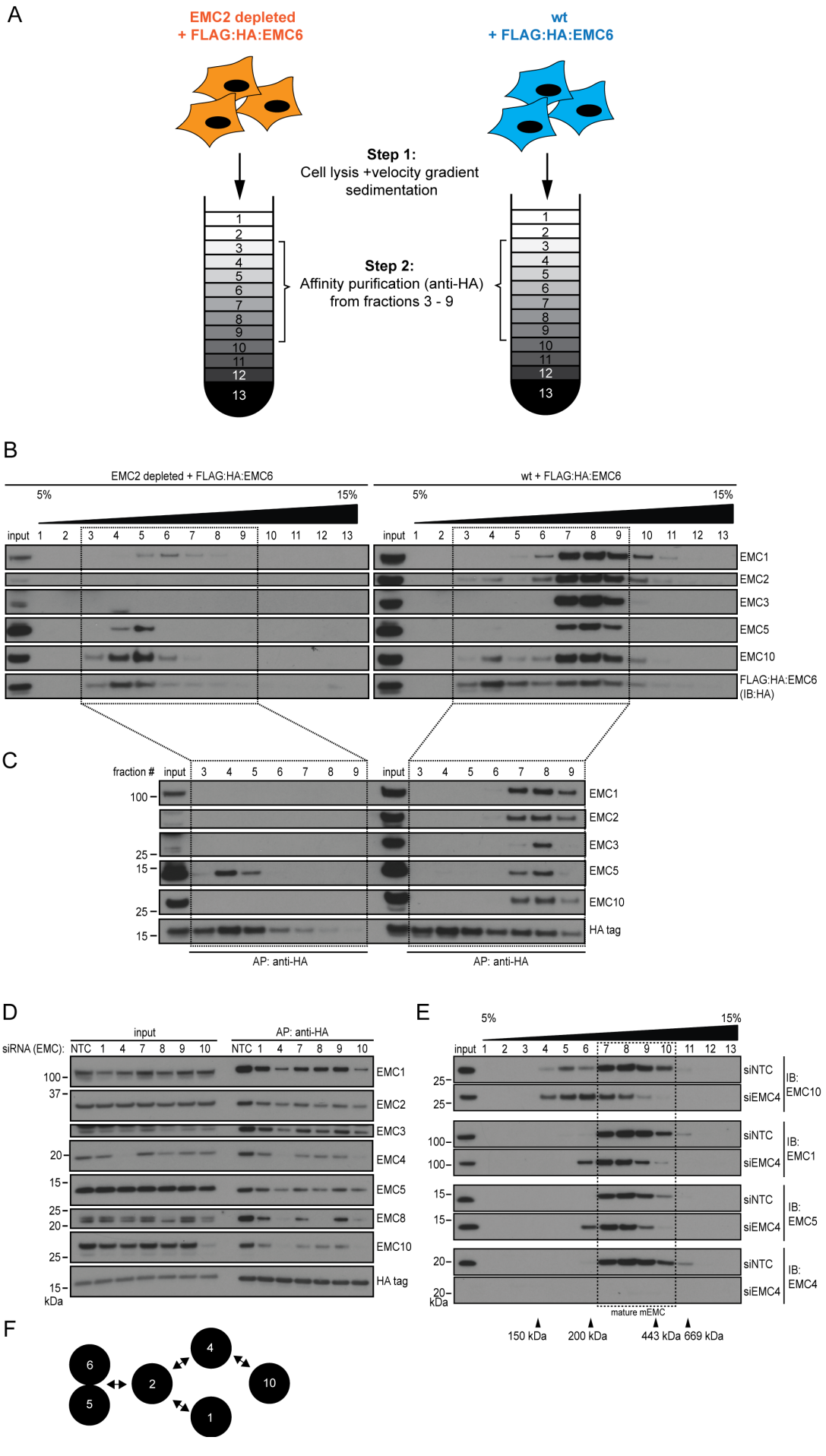


Figure legend on next page.

6.3 Depletion of EMC8 upregulates its close homologue EMC9

EMC8 and EMC9 are the only two subunits within the mEMC that exhibit significant sequence identity (44.72% sequence identity between human EMC8 and EMC9, **Figure 6.5 A**). Accordingly, EMC9 is thought to have arisen from a duplication event of the EMC8 gene [329]. However, it remains unknown whether both subunits are functionally and structurally interchangeable. Though speculative, the evolutionary conservation of EMC9 [357] suggests a specialized function, which could replace or complement EMC8 under certain conditions. Here, a potential regulatory mechanism in which the abundance of EMC8 determines the amount of EMC9 being incorporated into the mEMC is described.

When performing systematic RNAi-mediated depletion of EMC1 - EMC10 in U2OS Flp-In cells to determine which subunits were essential for the biogenesis of the mEMC, an increase of EMC9 protein levels was observed in EMC8-depleted cells (**Figure 6.5 B**). Whereas EMC9 was difficult to detect by immunoblotting under steady-state conditions, the depletion of EMC8 greatly facilitated its detection. To rule out a cell line-specific phenomenon, the experiment was repeated in HEK293 Flp-In cells, observing a similar upregulation of EMC9 (**Figure 6.5 C**). To address potential pleiotropic effects of the EMC8 siRNA pool used, U2OS Flp-In cells were stably depleted of EMC8 by lentiviral transduction with four individual EMC8-specific short hairpin RNAs (shRNAs). **Figure 6.5 D** (lanes 2 and 3) demonstrates that in two out of four EMC8 knockdown cell lines, each derived with a different shRNA (456, 745), EMC9 was

Figure 6.4 ***(previous page)*****: EMC5 and EMC6 can form a sub-complex without participation of other EMC proteins. A.** Sample preparation scheme for experiments shown in panel **B** and **C**. An epitope-tagged variant of EMC6 (FLAG:HA:EMC6) was stably introduced into ΔEMC2 ('EMC2 depleted') cells and the parental U2OS Flp-In cells using the Flp-In recombination system. FLAG:HA:EMC6 expression was induced with 10 ng/ml doxycycline for 18 hours, and cell extracts were separated on a 5 - 15% sucrose gradient. Thirteen fractions per gradient were collected and complexes associated with FLAG:HA:EMC6 were affinity-captured from fractions 3 - 9 by an anti-HA antibody. Fraction numbers are indicated. **B.** Step 1 (see (**A**)): Depletion of EMC2 changes the sedimentation pattern of EMC5, EMC6, and EMC10. **C.** Step 2 (see (**A**)): EMC5, but not EMC10, binds to EMC6 in EMC2-depleted cells. FLAG:HA:EMC6 was affinity purified from fractions 3 - 9 shown in (A) using a monoclonal anti-HA agarose-conjugated antibody. 50% of each fraction was used for affinity purification (AP). **D.** Association of EMC6 with EMC10 depends on EMC4 in HEK293 Flp-In cells. FLAG:HA:EMC6 expression in HEK293 FLAG:HA:EMC6 Flp-In cells was induced with 1 ng/ml doxycycline 24 hours before transfection with SMARTpool siRNAs for EMC1/4/7 - 10, or a non-targeting siRNA control (NTC) pool. The cells were collected 72 hours after transfection, proteins were extracted in 1% Triton-100 lysis buffer and FLAG:HA:EMC6 and associated factors captured by affinity purification (AP) *via* the HA-tag. **E.** Knockdown of EMC4 affects the hydrodynamic radius of EMC10. EMC4 was depleted from U2OS Flp-In cells by siRNA-mediated knockdown for 72 hours and whole-cell lysates were subjected to velocity gradient centrifugation on a 5 - 15% sucrose gradient. Fraction numbers are shown. **F.** Proposed interaction map. The interaction map was derived from data presented in (A) - (D) and in Figure 6.3. siNTC/NTC, non-targeting control siRNA.

readily detectable. In contrast, EMC9 levels in cells carrying a non-targeting control (NTC) shRNA were below the detection limit (**Figure 6.5 D**, lane 1). Of note, the remaining two EMC8-specific shRNAs, which did not cause a marked increase in EMC9 levels (835, 1669), also had reduced EMC8 knockdown efficiencies, as reflected by higher levels of residual EMC8 (**Figure 6.5 D**, lanes 4 - 5). The effect was not reciprocal: depletion of EMC9 did not lead to elevated EMC8 levels. It can therefore be speculated that the amount of EMC9 participating in the mEMC is partly determined by the abundance of its close ancestral homologue, but not *vice versa*. To address whether the additional EMC9 was incorporated into the mature mEMC, or instead performed mEMC-independent functions, complexes containing EMC9 in siEMC8 U2OS Flp-In cells were monitored by sucrose sedimentation. Consistent with a role of EMC9 in the mEMC, the majority of EMC9 co-sedimented with the remaining mEMC subunits (**Figure 6.5 E**).

The EMC9 gene has originated from a duplication event of the gene encoding EMC8 [329]. Accordingly, both subunits exhibit significant sequence identity. Hence, it is likely that EMC8 and EMC9 share similar interaction interfaces with the remaining EMCs and can functionally substitute for each other. Here, EMC9 was demonstrated to be strongly affected by the abundance of EMC8 in different cell lines. Furthermore, the additional EMC9 appears to be incorporated into the mature mEMC. Whether or not both subunits are in fact equivalent and EMC9 can functionally and structurally replace EMC8 remains to be shown.

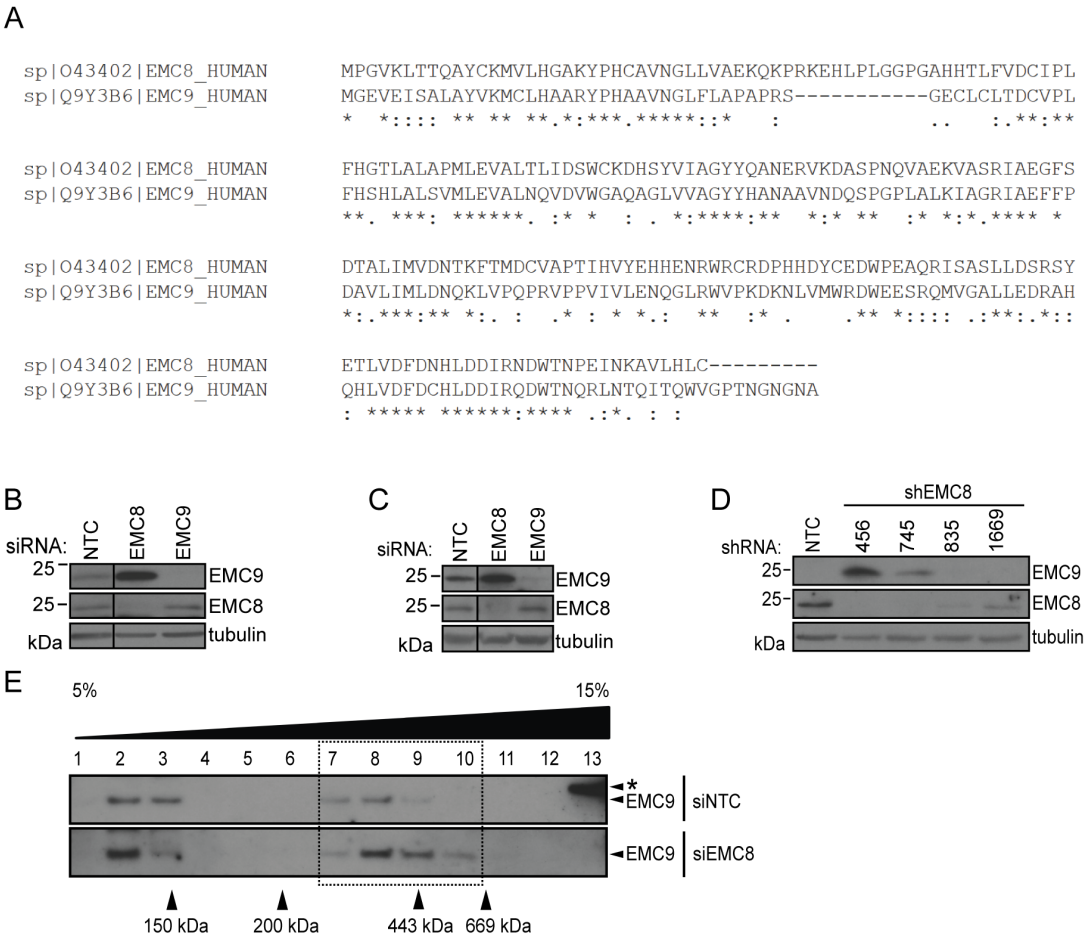


Figure 6.5: Depletion of EMC8 upregulates its close homologue EMC9. A. EMC8 and EMC9 share 44.72% sequence identity. Alignment of human EMC8 and EMC9 in ClustalO 1.2.1. Asterisks (*) signify conservation, whereas (:) denote conservative and (.) semi-conservative mutations, respectively. **B.** EMC9 levels are increased upon RNAi of EMC8 in U2OS Flp-In cells. U2OS Flp-In cells were depleted of EMC9 by siRNA-mediated knockdown for 72 hours. Whole-cell lysates were separated on a gel and endogenous EMC8/9 was detected by immunoblotting. **C.** EMC9 is increased upon depletion of EMC8 in HEK293 Flp-In cells. HEK293 Flp-In cells were treated as in (B) and EMC8/9 was visualized by immunoblotting of whole-cell lysate. **D.** Upregulation of EMC9 by constitutive depletion of EMC8. U2OS Flp-In cells stably expressing four different EMC9-specific shRNAs (456, 745, 835 and 1669) or a scrambled control sequence (NTC) were tested for EMC9 expression. Immunoblots of whole-cell lysates are shown. **E** Additional EMC9 is incorporated into the mEMC. U2OS Flp-In cells were depleted of EMC8 as described in (B). Protein lysates were then subjected to sucrose gradient sedimentation. Fraction numbers (1 - 13) are indicated. Unspecific bands are marked by an asterisk (*). NTC, non-targeting control.

Chapter 7

Disruption of the mEMC does not impair ER protein homeostasis

The ER is a major hub for protein synthesis, folding, and modification. ER homeostasis is maintained as long as the folding capacity of the ER does not exceed the import of nascent polypeptides [392]. This balance can be perturbed by a range of external (e.g. heat shock or oxidative stress) or internal factors (e.g. mutations) favouring protein misfolding. The resulting accumulation of unfolded, or misfolded, potentially proteotoxic polypeptides is remedied by activation of the UPR [393]. As a result of UPR engagement, the folding capacity of the ER is enhanced by transcriptional induction of ER-resident chaperones (i.e. BiP and GRP94), as well as factors involved in protein maturation, degradation, and lipid biosynthesis [362], [363], [393].

In 2009, the EMC was first described in a systematic UPR screen in yeast in an effort to characterize the genes necessary for the maintenance of an appropriate protein folding and maturation environment in the ER [95]. The authors reported potent activation of a UPR reporter (UPRE-GFP) upon deletion of several EMC subunits. A subsequent study in *C. elegans* has demonstrated activation of the UPR upon depletion of EMC1 - 6, as measured by GFP expression under control of an hsp-4 promoter [336]. Similarly, dPob (EMC3) deficiency in photoreceptor cells of *D. melanogaster* correlated with expression of the UPR reporter X-box binding protein 1 (XBP1)-GFP and eukaryotic initiation factor 2α (eIF2α) phosphorylation. These observations imply a broader, homeostatic function of the EMC in the ER. Therefore, I addressed whether or not mEMC deficiency would lead to cellular stress in human cells or

impair essential functions of the ER.

7.1 Loss of EMC5 or EMC6 does not trigger the unfolded protein response *per se*

To monitor constitutive ER stress, ΔEMC5 and ΔEMC6 cells were collected at steady-state, and the expression of a select set of ER stress markers was assessed by immunoblotting. Cells lacking EMC5 or EMC6, and by extension, a mature mEMC, did not exhibit increased expression of the ER-resident chaperone BiP, the highly stress-regulated protein HERP (homocysteine-induced ER protein) or the UPR response genes CHOP (CCAAT-enhancer-binding protein homologous protein) and ATF4 (activating transcription factor 4) (**Figure 7.1 A**). These data suggest that mEMC-depletion does not perturb protein homeostasis in the ER under steady-state conditions. Next, I asked whether the mEMC might be needed to resolve or abate ER stress. To test this hypothesis, ER stress was induced by treatment of ΔEMC5 and ΔEMC6 cells with 2 μg/ml of the *N*-acetylglucosamine phosphotransferase (GPT) inhibitor tunicamycin (Tm) over a period of 2 - 8 hours, and UPR activation was monitored. As shown in **Figure 7.1 B**, wild-type and mEMC-deficient cells responded similarly when exposed to Tm. ATF4, phospho-eIF2α, HERP, and BiP were upregulated when exposed to Tm, demonstrating that the UPR remained intact and functional in ΔEMC5 and ΔEMC6 cells. These findings suggest that mEMC loss does not grossly affect protein homeostasis in the mammalian ER.

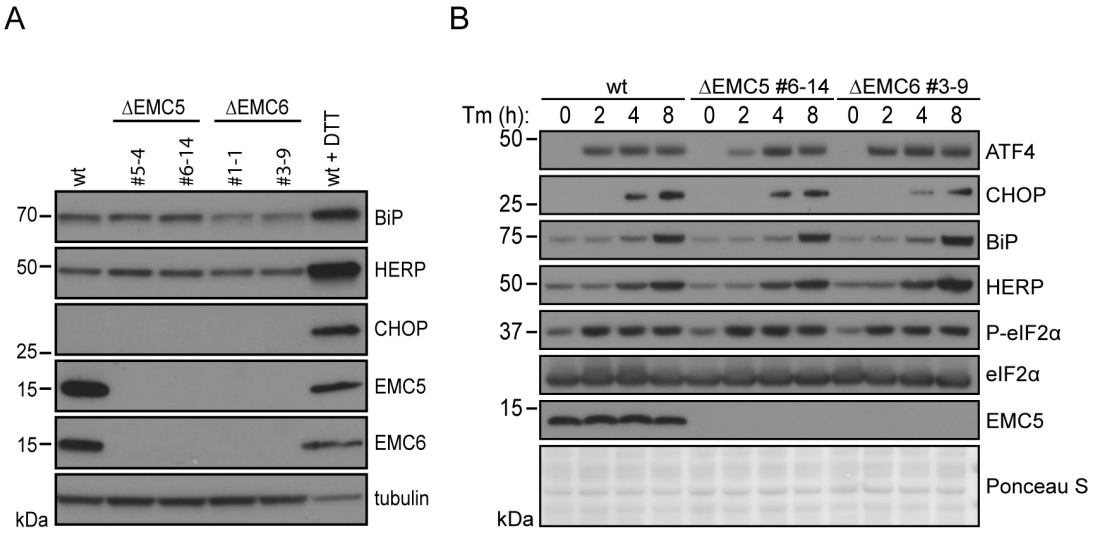


Figure 7.1: Loss of EMC5, or EMC6 did not trigger the unfolded protein response. A. mEMC-deficient U2OS Flp-In cells did not exhibit ER stress under steady-state conditions. Wild-type (wt), ΔEMC5 (#5-4 and #6-14), and ΔEMC6 (#1-1 and #3-9) cells were collected and whole-cell lysates were subjected to immunoblotting. As positive control, parental wt cells were treated with 1 mM dithiothreitol (DTT) for 4 hours. **B.** ΔEMC5, and ΔEMC6 cells were not sensitized to tunicamycin (Tm)-induced ER stress. 0.5×10^6 cells were seeded to 6 cm tissue culture plates, and after 48 hours, treated with 2 μg/ml Tm or dimethyl sulfoxide (DMSO) (vehicle control) for the indicated time. Whole-cell lysates were analysed by immunoblotting. DMSO, dimethyl sulfoxide; DTT, dithiothreitol; Tm, tunicamycin.

7.2 ER and mitochondrial morphology in mEMC-deficient cells

The ER is a dynamic subcellular compartment that is subject to constant remodelling of its overall structure, and of its contact sites with other organelles [394] [395]. Moreover, ER function is closely linked to its morphology [394], [396], [397].

Loss of individual EMC subunits has been associated with the induction of ER stress in *S. cerevisiae* [95] and is accompanied by increased KDEL expression and ER expansion in the photoreceptor cells of *D. melanogaster* [357]. In 2014, Lahiri and colleagues suggested an ER-mitochondrial tethering function of the EMC in yeast and facilitating PS transfer from the ER to mitochondria [331]. Finally, a recent report has found that the mEMC associates with the mitochondrial outer membrane metabolite carrier protein SLC25A46 (Solute Carrier Family 25 Member 46) [372]. The authors reported that a mutated variant of SLC25A46 leads to mitochondrial hyperfusion and severe morphological alterations of the ER. However, it is worth mentioning that their work did not show a direct involvement of the mEMC in these phenotypes.

Due to the multiple links of the mEMC to ER proteostasis, structure, and mitochondrial

function, ER and mitochondrial morphology was monitored in mEMC-deficient U2OS Flp-In cells by confocal microscopy. In **Figure 7.2**, ER morphology of two ΔEMC5 and two ΔEMC6 cell lines was visualized by indirect immunofluorescence using anti-KDEL (ER) and Mito-Tracker Red CMXRos (mitochondria). When compared to wild-type cells, mEMC-deficient cells exhibited a comparable ER and mitochondrial pattern (**Figure 7.2**). No alterations in mitochondrial content or architecture were apparent (**Figure 7.2**).

In summary, these data indicate that mEMC deficiency does not grossly alter ER or mitochondrial structure. However, the current approach does have technical limitations that might be overcome by using transmission electron super-resolution microscopy to detect ultrastructural changes of the ER or mitochondria. Similarly, the number, structure, and distribution of ER-mitochondrial contact sites has not been addressed; therefore alterations to inter-organelle contact sites cannot be ruled out.

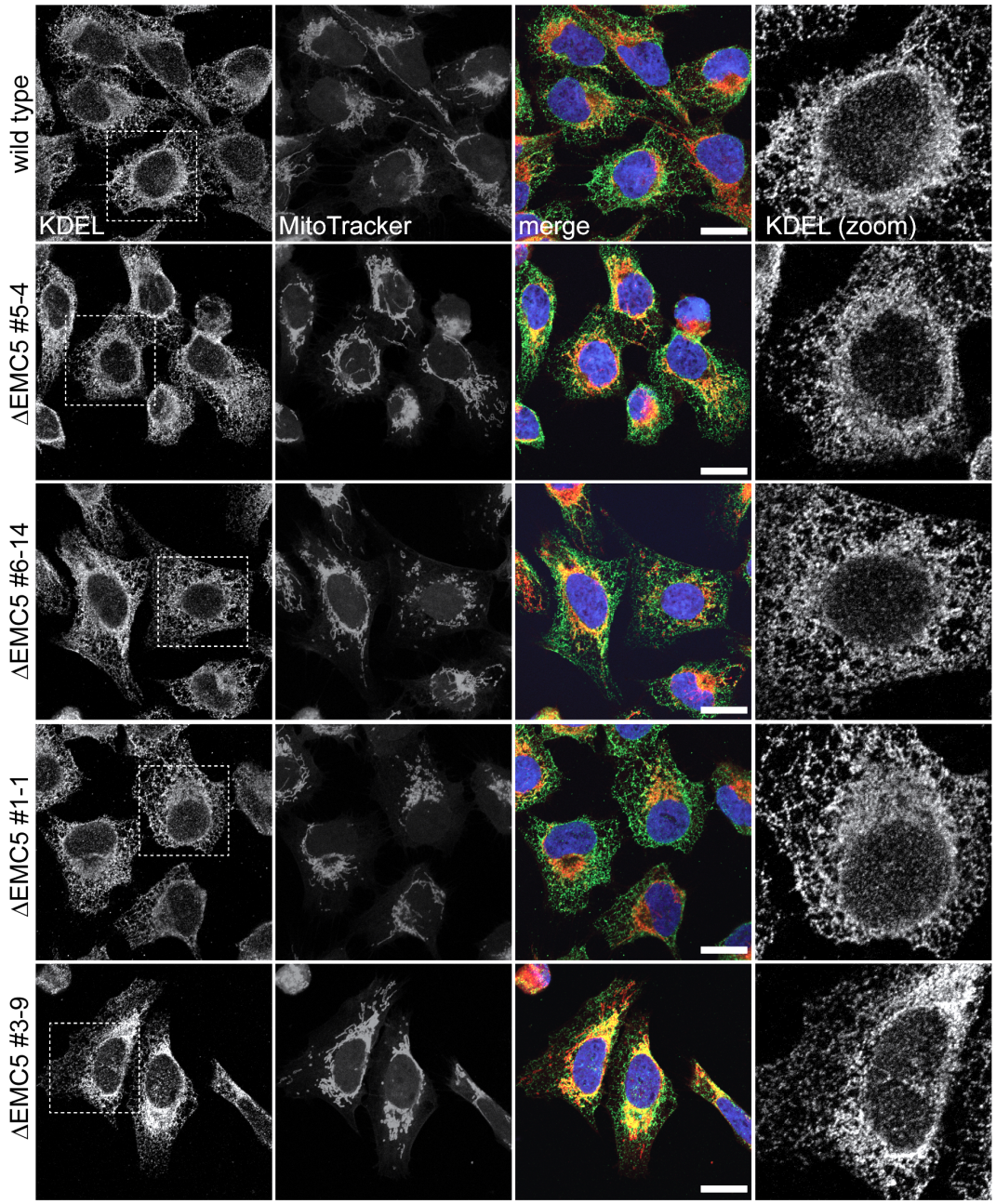


Figure 7.2: ER and mitochondrial morphology in mEMC-deficient cells. The morphology of the ER and mitochondria in mEMC-deficient cells was examined by confocal microscopy. ΔEMC5 and ΔEMC6 U2OS Flp-In cells were grown on glass cover slips, and mitochondria were stained using MitoTracker Red CMXRos (Fisher) for 45 minutes. Cells were then fixed and KDEL was visualized by a specific anti-KDEL antibody. Immunofluorescence signals were converted to greyscale. Dashed boxes indicate magnified areas. Scale bar = 10 μm.

7.3 Loss of the mEMC does not impair the degradation and maturation of an endogenous *bona fide* ERAD substrate

In 2012, Christianson *et al.* published a comprehensive interaction map of the ERAD network in HEK293 cells [189]. This seminal work shows that multiple mEMC subunits physically interact with several ERAD components, most notably, UBAC2, and, derlin-2 (Der2). Moreover, the authors reported impaired degradation of several model substrates in HEK293 cells depleted of EMC1/2/7/8. Therefore, the consequence of EMC5 or EMC6 deletion for the degradation and maturation of the endogenous, *bona fide* ERAD substrate CD147 [194] was assessed. CD147/Basigin is an assembly factor for monocarboxylate transporters and endogenous, unassembled CD147 is degraded in a Hrd1-dependent fashion [194]. To monitor the CD147 turnover and stability, ΔEMC5 and ΔEMC6 cells were exposed to the translation inhibitor CHX for 2 - 8 hours. Loss of EMC5 or EMC6 did not noticeably impair the degradation or maturation of endogenous CD147, as was evidenced by the rapid depletion of the ER-resident form of CD147 (**Figure 7.3**). The core and complex glycosylated form(s) of CD147 (see also **Section 8.1**) had low turnover rates both in wild-type and mEMC-depleted cells, implying that ERAD is not affected by mEMC deficiency (**Figure 7.3**). However, to arrive at a comprehensive statement on the integrity of ERAD in these cells, it is advisable to corroborate this finding with substrates of different topologies, especially those targeted by gp78 (e.g. CD3δ [398]), which has been shown to interact with EMC1/2/3 *via* UBAC2 [189]. Of note, the biological function of mEMC-UBAC2 binding is unclear.

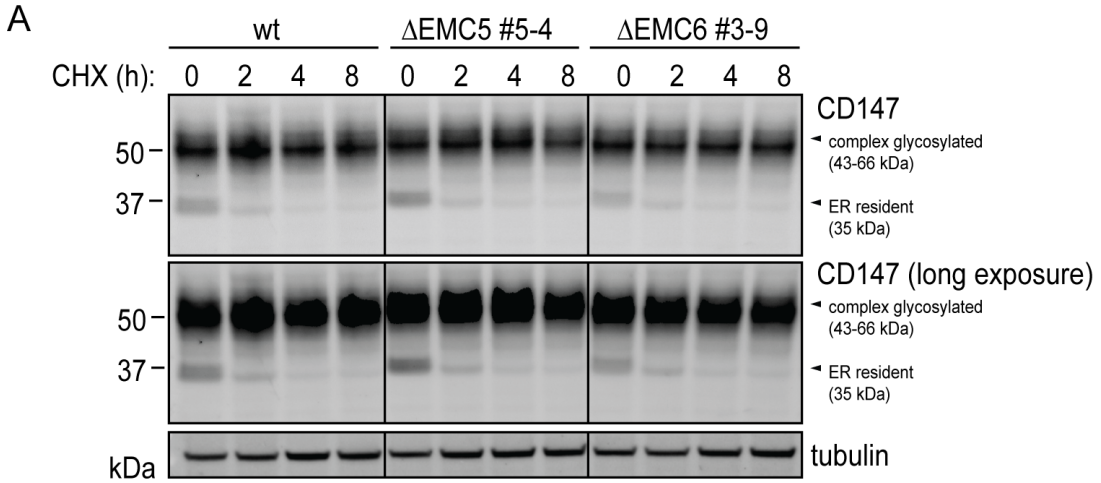


Figure 7.3: Loss of the mEMC does not impair the degradation of an endogenous *bona fide* ERAD substrate. A. CD147 degradation kinetics were not affected by the loss of EMC5 or EMC6. Clonal EMC6, and EMC5 knockout cell lines (ΔEMC5 #5-4 and ΔEMC6 #3-9) or wild-type cells (wt), were treated with 100 ng/ml cycloheximide (CHX) for the indicated period of time. Endogenous CD147 (ER-resident and complex glycosylated) was detected from whole-cell extracts by immunoblotting. Two different exposures are shown. Areas where lanes have been cropped out are represented by black lines. CHX, cycloheximide.

7.4 Loss of the mEMC does not inhibit cell migration or cell proliferation in a scratch assay

Orthologues of the mEMC in *C. elegans* and *D. melanogaster* have previously been implicated in the maturation of plasma membrane proteins in the ER [336], [357], [377]. Potential changes in the cell-surface proteome of mEMC-deficient cells might be reflected in altered cell-substratum interactions affecting cell adhesion and migration. To test this hypothesis, scratch assays were performed evaluating the migration and proliferation capacity of mEMC-deficient cells. Equal numbers of ΔEMC5 and ΔEMC6 cells were seeded and the cell monolayer was locally disrupted using a P10 micro pipette tip, creating an artificial 'wound' or cell exclusion area. Cell migration into the cell exclusion area was then followed by live cell imaging. **Figure 7.4 A** conveys the elapsed time to 50% wound closure in three independent experiments. The time elapsed for the 'wound' to close is a function of both cell migration and cell proliferation at the leading edge. In the parental cell line, a 50% reduction of the cell exclusion area was observed after 347.52 minutes on average. EMC5 knockout cells covered the same area after 343.85 minutes (ΔEMC5 #5-4) and 342.10 minutes (ΔEMC5 #5-4). These results were closely mirrored by EMC6-deficient cells with 329.83 minutes (ΔEMC6 #1-1) and 352.45 minutes (ΔEMC6 #3-9). Four representative micrographs for each cell line at different time points are shown in **Figure 7.4 B**. In conclusion, the mEMC is not essential for cell migration or proliferation under steady-state conditions.

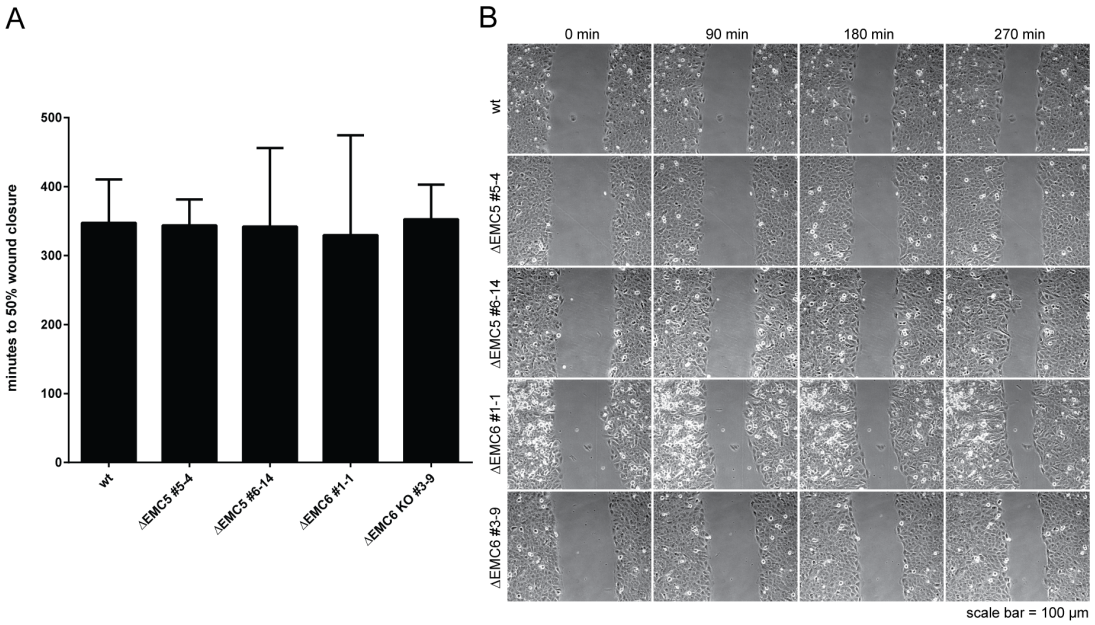


Figure 7.4: mEMC-deficiency did not inhibit cell migration or cell proliferation in a scratch assay. A. Proliferation and migration are comparable between wild-type (wt) and mEMC-deficient cells. A confluent monolayer of cells was locally removed by mechanical disruption ('scratching') using a P10 micro pipette tip. Immediately after scratching, detached cells were removed by a washing step, and cell migration and proliferation were immediately monitored by live-cell imaging over a period of 18 - 24 hours. The time it took to reduce the scratch area by 50% was computationally evaluated. Three independent experiments (n = 3) are shown. Error bars repesent the S.D.. **B.** Micrographs. A representative sub-set of micrographs that were used for evaluation in (A) is shown. Four time points are shown at a 10x magnification. Brightness and contrast of the image were adjusted.

Chapter 8

The mEMC regulates the abundance of integral membrane proteins

The ER is the entry point for the conventional secretory pathway. Cell surface and secreted proteins are co-translationally delivered to the ER by SRP-dependent or -independent targeting pathways [89]. TM proteins are inserted co-translationally into the ER lipid bilayer and mature with assistance from ER-lumenal and membrane-embedded chaperone complexes [46], [22]. PTMs such as disulphide bond formation and *N*-linked glycosylation promote correct folding and guide the assembly of oligomeric protein complexes [117]. Once these proteins have obtained an export-competent conformation, they are packaged into COPII vesicles and shuttled to the Golgi apparatus, where they can be modified further (e.g. by *O*-glycosylation, *N*-glycan modification, or limited proteolysis) [18]. The biogenesis and assembly of oligomeric protein complexes in the ER is highly regulated and requires coordination between a range of different proteins involved in folding (chaperones and co-chaperones), modification (saccharyl transferases, deglycosylases, and lectins) and degradation (E3 ligase complexes) [117], [399].

The EMC has been shown previously to regulate the abundance of a range of integral, polytopic plasma-membrane proteins in different model organisms [369], [336], [357], [377]. However, the molecular mechanisms underlying this activity have hitherto been enigmatic and several questions remain outstanding. Firstly, it is not clear what role the mEMC plays in the secretory pathway and, more specifically, how it mechanistically influences the biogenesis of TMD-containing proteins. Several groups have independently demonstrated that disrupting the EMC impacts the expression of distinct classes of cell surface proteins, most likely during

their maturation in the ER [357], [336]. Secondly, it is unclear whether the loss of individual EMC subunits affects putative 'client proteins' directly or indirectly modulates the secretory pathway. Thirdly, it is not known whether any functions of the mEMC are evolutionarily conserved. Several studies have investigated EMC orthologues in a variety of model organisms and observed effects that were often specific to a particular cell type (e.g. co-depletion of nAChRs in muscle cells of *C. elegans* [336] or loss of rhodopsin expression in *D. melanogaster* [357]). Nonetheless, the significant sequence conservation of EMC subunits across the animal and plant kingdoms suggests an evolutionarily conserved function [329]. This further implies that the EMC performs an important cellular function/s and stresses the scarcity of information on functional data concerning its mammalian homologue. The consequences of mEMC loss for proteins in the secretory pathway have not been systematically addressed. Since an impairment of the EMC has been shown to disrupt aspects of integral membrane protein biosynthesis [369], [336], [357], in this study, changes of the cell surface and intracellular proteomes of mEMC-deficient cells were investigated.

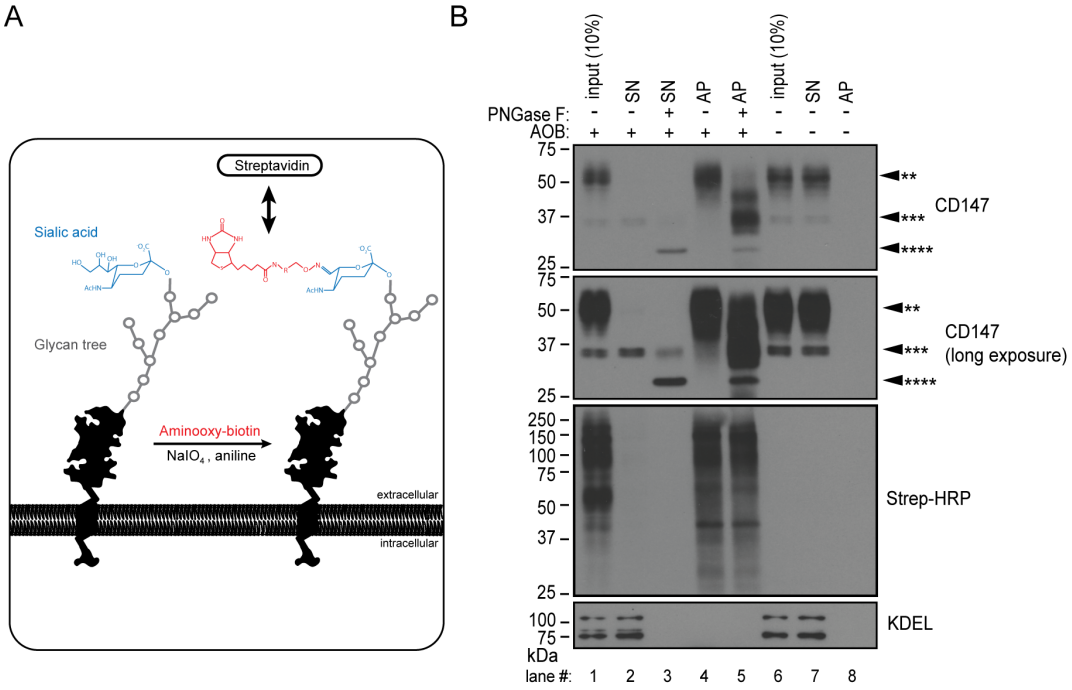
8.1 Proteomic PM profiling

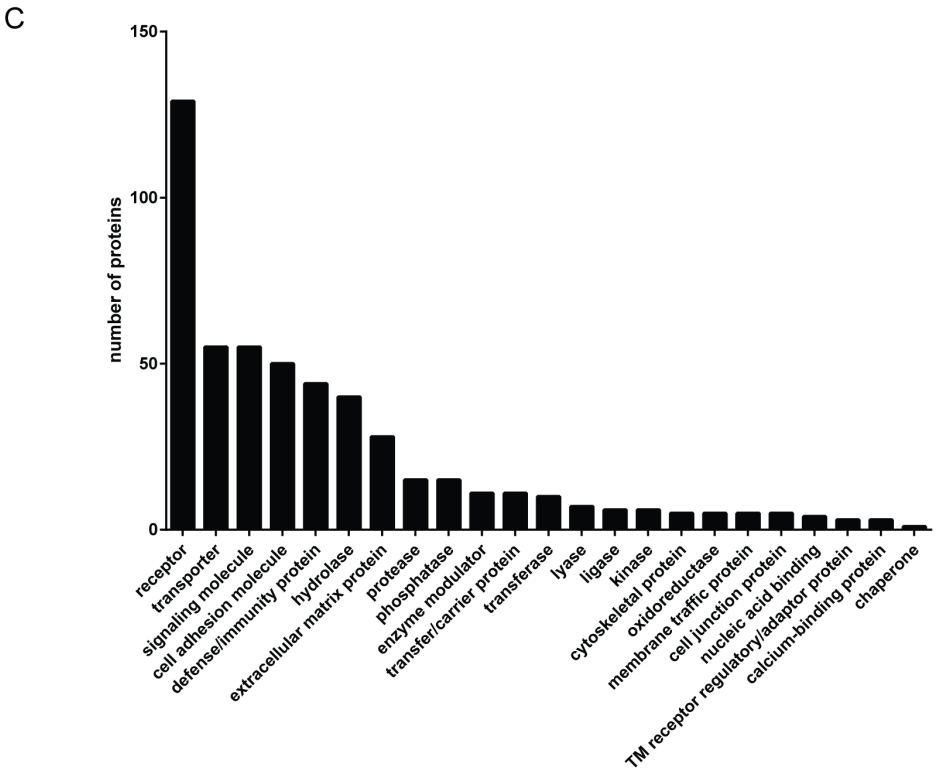
Identification of cell surface proteins by mass spectroscopy is hampered by their comparatively low abundance in complex whole-cell protein mixtures [400]. This is compounded by the hydrophobicity of integral membrane proteins and their derived peptides [401]. To identify and quantify the cell surface proteome from whole-cell lysates, it is necessary to remove high-abundance cytoplasmic, nuclear, and cytoskeletal proteins. The extracellular domains of PM proteins are often extensively glycosylated [402]. In vertebrates, the presence of terminal sialic acids in complex glycans is a common feature of glycosylated cell surface proteins [403]. This feature was harnessed to purify, identify and quantify the cell surface glycoproteome of U2OS Flp-In cells by proteomic PM profiling (PMP) [404], [405], [133].

The free 1,2-diol of a terminal sialic acid group can be specifically oxidized to an aldehyde by sodium metaperiodate, which, in the presence of the catalyst aniline, is covalently conjugated to aminooxy-biotin (AOB). Biotinylated proteins are then purified by streptavidin and further processed for tandem mass spectrometry (**Figure 8.1 A**). PMP and analogous techniques have been used in a number of cell lines to identify cell surface glycoproteins [133], [404], [406], [407], [408]. To interrogate the selectivity of PMP for cell surface proteins in U2OS Flp-In cells, the biotinylation profile of the abundant oligomannosidic carbohydrate receptor CD147 (basigin) was monitored [409]. CD147 is a type I TM protein whose two

extracellular immunoglobulin domains are highly *N*-glycosylated [410]. Additionally, 5A11, the chicken orthologue of CD147, has been demonstrated to be sialylated [411]. Due to the vectorial nature of the secretory pathway, the glycosylation status of CD147 correlates with its subcellular localization. Whereas the complex glycosylated, mature PM form of CD147 exhibits an apparent molecular weight of 45 - 65 kDa (**, **Figure 8.1 B**), ER-resident, immature CD147 migrates at approximately 32 kDa (core glycosylated) (***, **Figure 8.1 B**) or 27 kDa (unglycosylated) (****, **Figure 8.1 B**) [412], [194]. Aminooxy-biotinylation of live U2OS cells for 60 minutes at 4 °C allowed specific affinity capture of cell surface CD147 using streptavidin-conjugated agarose beads (**Figure 8.1 B**, lane 4). In contrast, the intracelluar, ER-resident form did not bind and remained in the supernatant (**Figure 8.1 B**, lane 2). To further confirm that conjugation occurred via the glycan moieties of CD147, on-bead digestion of the aminooxy-biotinylated glycoproteome with Peptide:*N*-glycosidase F (PNGase F) was performed. As expected, PNGase F-catalysed glycan removal led to a marked shift to a lower apparent molecular weight, indicative of partially and fully deglycosylated CD147 (**Figure 8.1 B**, lanes 3 and 5). The presence of partially deglycosylated CD147 likely reflects limited accessibility of the glycosidase to bead-bound polypeptides or titration by other glycoproteins, which could be readily detected by streptavidin-horseradish peroxidase (Strep-HRP) (**Figure 8.1 B**, lanes 1, 4, and 5).

To further confirm the specificity of cell-surface biotinylation in U2OS cells, PMP was performed. The cell surface glycoproteome of U2OS Flp-In cells was aminooxy-biotinylated and affinity-purified on streptavidin-conjugated agarose beads. Tryptic peptides were obtained following on-bead digest. To rule out non-specific binding of proteins to the bead matrix, a separate population of cells was processed identically, but with AOB omitted from the labelling reaction. Using this approach, 587 protein identifications were obtained from AOB-labelled cells, 4.1% (24 proteins) of which were shared with the unlabelled control (**Figure 18.9**). GO analysis (PANTHER classification system [413], www.pantherdb.org) revealed that a majority of unique proteins were either receptors (129) or transporters (55), (**Figure 8.1 C**). Four proteins were classified as transcription factors ('nucleic acid binding'), and can therefore be considered nuclear contaminants. In summary, these results indicate that PMP in U2OS-FlpIn cells is an effective method for profiling cell surface sialoglycoproteins.


A
Streptavidin
Sialic acid
Glycan tree
Aminooxy-biotin
NaIO4, aniline
extracellular
intracellular
B
PNGase F:
AOB:
input (10%)
SN
SN
AP
AP
input (10%)
SN
AP
CD147
CD147
(long exposure)
Strep-HRP
KDEL
kDa
lane #: 1 2 3 4 5 6 7 8


C
number of proteins
receptor
transporter
signaling molecule
cell adhesion molecule
defense/immunity protein
hydrolase
extracellular matrix protein
protease
phosphatase
enzyme modulator
transfer/carrier protein
transferase
lyase
ligase
kinase
cytoskeletal protein
oxidoreductase
membrane traffic protein
cell junction protein
nucleic acid binding
TM receptor regulatory/adaptor protein
calcium-binding protein
chaperone

8.2 SILAC-based PMP (SILAC-PMP) in mEMC-depleted cells

To investigate cell surface proteome changes of mEMC-deficient cells, PMP on SILAC (stable isotope labelling with amino acids in cell culture)-labelled ΔEMC5 and ΔEMC6 U2OS Flp-In cells (SILAC-PMP) was performed. After shortlisting proteins with altered abundance, a set of criteria were established to decrease the likelihood of obtaining false-positives. Firstly, to ensure abundance changes were due to loss of the mEMC and not just individual subunits, genomically edited cell lines lacking either EMC5 or EMC6 were compared. Since the mEMC cannot mature without either, proteins identified from both knockout lines likely reflect the loss of mEMC activity. Secondly, two different single guide RNAs (sgRNAs) per knockout were used to facilitate identification of potential off-target effects. Next, proteins of interest had to be altered in all four independent knockout clones to be considered as a valid hit. Finally, changes in protein abundance below a threshold of 30% were regarded to be technical or biological variation. Proteins that failed to meet any of these criteria were considered unlikely to be modulated by the mEMC.

8.2.1 Constitutive mEMC-deficiency correlates with co-depletion of a set of cell surface proteins

Following the capture and tryptic digest of all biotinylated proteins, peptides were detected by tandem mass spectrometry (**Figure 8.2 A**). The relative abundance of isotopically labelled peptides (M/L and H/L ratios) was determined by processing the dataset using the

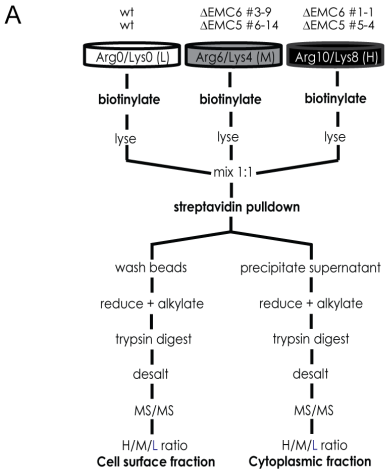
Figure 8.1 ***(previous page)*****: PMP of U2OS Flp-In cells. A.** The principle of PMP. Sialic acid is a common terminal carbohydrate found in the glycan moieties of PM proteins, and can be selectively oxidized by sodium metaperiodate to yield a free aldehyde group. In the presence of the catalyst aniline, aminooxy-biotin (AOB) reacts with the free aldehyde group by oxime ligation, resulting in its covalent incorporation into the glycan structure. Using streptavidin-conjugated agarose beads, aminooxy-biotinylated glycoproteins were enriched by affinity purification and used for downstream applications including MS/MS. **B.** AOB covalently modifies cell surface-localized CD147. Cells were incubated at 4 °C with 100 μM AOB for 60 minutes in the presence of 1 mM sodium metaperiodate and 10 mM aniline. The reaction was quenched by addition of 1 mM glycerol for 30 minutes. Cells were lysed in Triton X-100 lysis buffer and aminooxy-biotinylated proteins were enriched by affinity purification (AP) with streptavidin-conjugated agarose beads. 50% of the beads of were treated with PNGase F for 45 minutes at 37 °C. Proteins that did not bind to streptavidin were retained in the supernatant (SN). ** designates the fully glycosylated form of CD147, whereas *** and **** mark core glycosylated and unglycosylated CD147. **C.** GO analysis of aminooxy-biotinylated proteins. Cells were labelled with AOB for 90 minutes under the same conditions as in (B). Biotinylated proteins were captured by incubation with streptavidin-agarose and peptides released from the beads by tryptic digest. Peptides were identified by MS/MS. All protein IDs were subjected to gene ontology analysis using the PANTHER classification system [413].

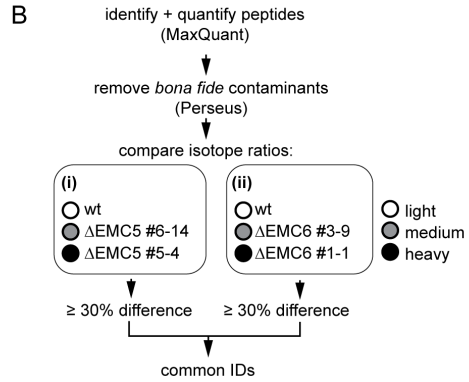
MaxQuant software package [414], [415]. After exclusion of common contaminants (as predefined by MaxQuant) and reverse peptides, 418 and 373 proteins were identified for ΔEMC5 and ΔEMC6 cells, respectively. The majority of these proteins were classified as receptors and transporters according to GO analysis (PANTHER classification system [413], **Supplemental Figure 18.10**). Other identified protein classes included cell adhesion, and signalling molecules, as well as extracellular matrix proteins. Importantly, the abundance of nuclear proteins such as transcription factors was negligible, implying high purity of the cell surface fraction (**Supplemental Figure 18.10**).

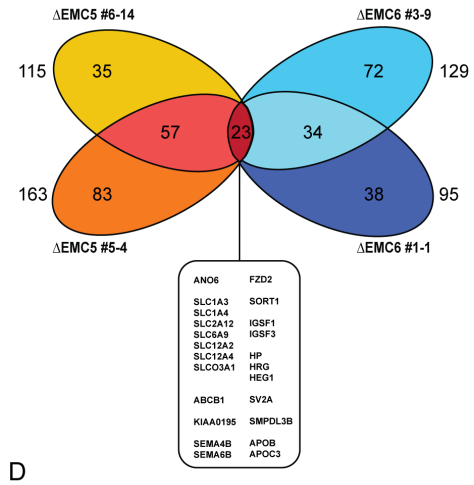
Given the robust cell surface protein enrichment, the relative abundances of all identified proteins of each knockout cell line were compared with those of wild-type cells (**Figure 8.2 B**). To be considered as decreased, a conservative threshold of at least 30% reduction had to be reached (see above). **Figure 8.2 C** shows a comparison of all proteins surpassing that threshold ($\geq$ 30% decrease) identified from ΔEMC5 (x2) and ΔEMC6 (x2) clonal U2OS Flp-In cell lines. All four knockout cell lines shared 23 proteins with reduced abundance (**Figure 8.2 C** and **Figure 8.2 D**). Therefore, this subset represents proteins whose abundance depends upon the mEMC and not just EMC5/6. Of note, 57 proteins were decreased only in the two ΔEMC5 cell lines, while 34 were specific to ΔEMC6 cells (**Figure 8.2 C** and **Supplemental Figure 18.12**). These differences might indicate a selective influence of either EMC5 or EMC6 on certain cell surface proteins. Proteins reduced only in individual EMC5/6 knockout clones were considered to be clone-specific, potentially representing off-target consequences of the sgRNAs used.

As expected, all polypeptides shortlisted as being potentially modulated by the mEMC (**Figure 8.2 C** and **Figure 8.2 D**) had annotated *N*- or *O*-linked glycosylation sites (UniProt, NetNGlyc 1.0 Server, http://www.cbs.dtu.dk/services/NetNGlyc/), consistent with them being trafficked along the secretory pathway. Furthermore, they exhibited a wide range of topologies, with polytopic TM proteins being most common (ABCB1, ANO6, FZD2, IGSF1, KIAA0195, SLC12A2, SLC12A4, SLC1A3, SLC1A4, SLC2A12, SLC6A9, SLCO3A1, and SV2A). Proteins with a single TMD included HEG1, IGSF3, SEMA4B, SEMA6B, SMPDL3B, and SORT1. In contrast, APOB, APOC3, HP, and HRG do not contain any annotated TMDs and might therefore be associated with the PM or integral membrane proteins. The identified transporters are involved in the movement of amino acids (SLC1A3, SLC1A4, and SLC6A9), chloride (ANO6, SLC1A4, SLC12A4, and SLC12A2), anions (SLCO3A1) and cations (ANO6, SLC1A4, SLC2A12, SLC12A4, SLC6A9, and SLC12A2). In this context, the mEMC has recently been reported to interact with the mitochondrial solute carrier (SLC) SLC25A46 [372]

and has previously been shown to affect CFTR-ΔF biogenesis [369]. It can be hypothesized that the mEMC might play a role in chaperoning or trafficking for a class/classes of cell surface proteins in the ER. Notwithstanding, the large number of transporters in the dataset might reflect their high relative overall abundance within the PM proteome rather than a direct, SLC-specific activity of the mEMC [416]. Moreover, it is plausible that loss of the mEMC indirectly alters the subcellular localization or expression of PM proteins by affecting other biological processes. Therefore, careful validation will be needed to confirm the requirement of the mEMC for expression of this distinct set of cell surface proteins. One possible way forward might be to corroborate this observation by antibody staining and flow cytometry analysis of (a subset of) the proteins shortlisted, followed by functional studies (e.g. trafficking to the PM and phenotypic readouts depending on the client protein) in multiple cell lines.







D

			ΔEMC5						ΔEMC6					
Gene	Accession #	Protein	(M/L)*	Fold change	Peptides	(H/L)*	Fold change	Peptides	(M/L)*	Fold change	Peptides	(H/L)*	Fold change	Peptides
ABCB1	P08183	Multidrug resistance protein 1	0.451	2.217	14	0.496	2.016	14	0.611	1.637	10	0.417	2.398	10
ANO6	Q4KMQ2	Anoctamin-6	0.239	4.184	1	0.160	6.250	1	0.188	5.319	3	0.314	3.185	3
APOB	P04114	Apolipoprotein B-100	0.037	27.027	1	0.208	4.808	1	0.027	37.037	2	0.083	12.048	2
APOC3	P02656	Apolipoprotein C-III	0.139	7.194	2	0.038	26.316	2	0.031	32.258	4	0.089	11.236	4
FZD2	Q14332	Frizzled-2	0.497	2.012	5	0.451	2.217	5	0.439	2.278	3	0.620	1.613	3
HEG1	Q9ULI3	Protein HEG homolog 1	0.609	1.642	7	0.375	2.667	7	0.479	2.088	7	0.542	1.845	7
HP	P00738	Haptoglobin	0.036	27.778	5	0.056	17.857	5	0.037	27.027	5	0.070	14.286	5
HRG	P04196	His-rich glycoprotein	0.014	71.429	3	0.047	21.277	3	0.007	142.857	1	0.141	7.092	1
IGSF1	Q8N6C5	Immunoglobulin superfamily member 1	0.575	1.739	1	0.346	2.890	1	0.419	2.387	1	0.435	2.299	1
IGSF3	O75054	Immunoglobulin superfamily member 3	0.419	2.387	1	0.216	4.630	1	0.197	5.076	1	0.258	3.876	1
KIAA0195	Q12767	Uncharacterized protein KIAA0195	0.519	1.927	4	0.208	4.808	4	0.291	3.436	3	0.476	2.101	3
SEMA4B	Q9NPR2	Semaphorin-4B	0.366	2.732	27	0.514	1.946	27	0.437	2.288	17	0.480	2.083	17
SEMA6B	Q9H3T3	Semaphorin-6B	0.643	1.555	3	0.434	2.304	3	0.356	2.809	1	0.644	1.553	1
SLC12A2	P55011	Solute carrier family 12 member 2	0.416	2.404	NaN	0.536	1.866	NaN	0.562	1.779	11	0.679	1.473	11
SLC12A4	Q9UP95	Solute carrier family 12 member 4	0.615	1.626	13	0.453	2.208	13	0.350	2.857	26	0.589	1.698	26
SLC1A3	P43003	Excitatory amino acid transporter 1	0.236	4.237	13	0.259	3.861	13	0.188	5.319	8	0.472	2.119	8
SLC1A4	P43007	Neutral amino acid transporter A4	0.279	3.584	9	0.467	2.141	9	0.425	2.353	8	0.380	2.632	8
SLC2A12	Q8TD20	Solute carrier family 2, facilitated glucose transporter member 12	0.695	1.439	5	0.093	10.753	5	0.090	11.111	3	0.167	5.988	3
SLC6A9	P48067	Sodium- and chloride-dependent glycine transporter 1	0.418	2.392	1	0.400	2.500	1	0.350	2.857	3	0.515	1.942	3
SLCO3A1	Q9UIG8	Solute carrier organic anion transporter family member 3A1	0.633	1.580	5	0.367	2.725	5	0.311	3.215	3	0.401	2.494	3
SMPDL3B	Q92485	Acid sphingomyelinase-like phosphodiesterase 3b	0.457	2.188	1	0.395	2.532	1	0.423	2.364	2	0.511	1.957	2
SORT1	Q99523	Sortilin	0.333	3.003	2	0.096	10.417	2	0.209	4.785	3	0.156	6.410	3
SV2A	Q7L0J3	Synaptic vesicle glycoprotein 2A	0.625	1.600	5	0.472	2.119	5	0.484	2.066	1	0.443	2.257	1

*normalised

Figure legend on next page

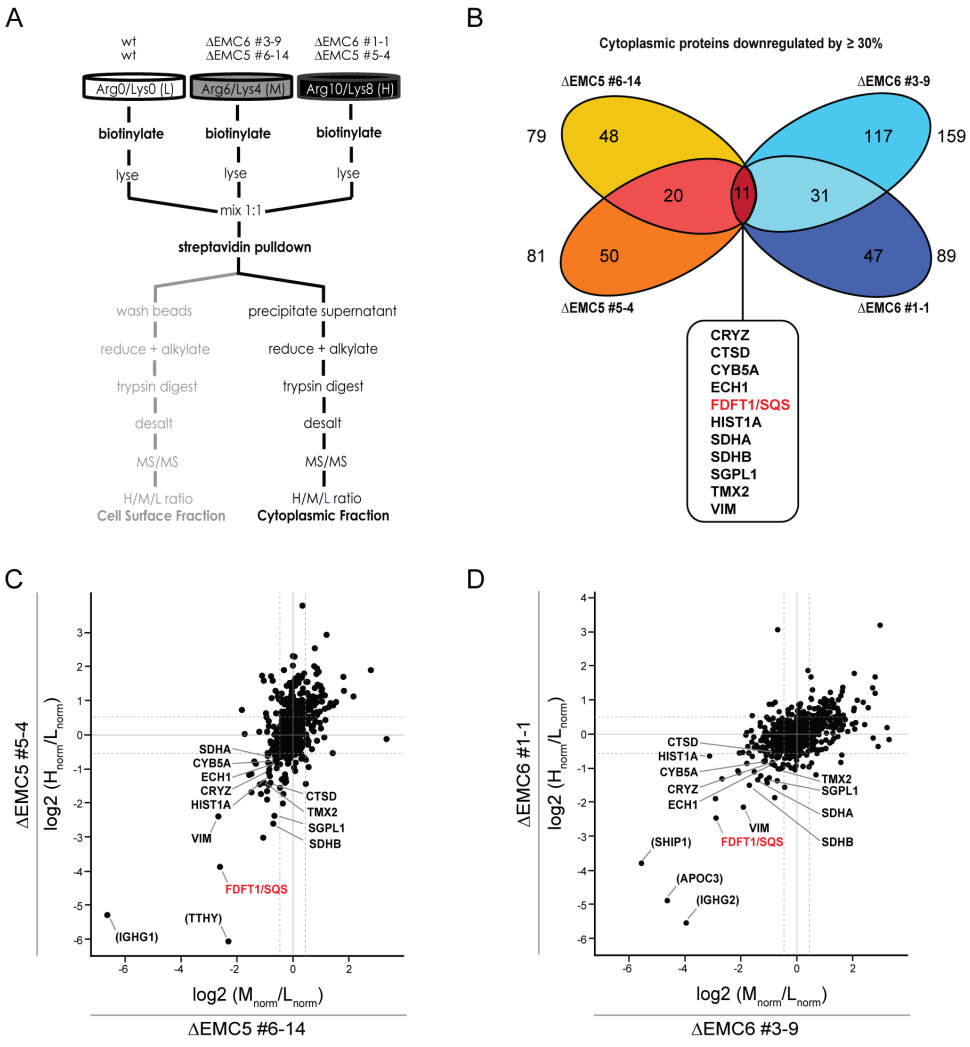
8.2.2 The mEMC is necessary for the expression of a set of intracellular proteins

In the previous section, an approach to quantify proteomic changes in mEMC-deficient cells was delineated. This method was based on the fractionation and MS-aided identification of the cell surface and intracellular proteome. Here, intracellular proteomic changes in ΔEMC5, and ΔEMC6 U2OS Flp-In cells were analysed (**Figure 8.3 A**). In the ΔEMC5 *versus* wild-type sample, 737 proteins were detected (excluding common contaminants and reverse peptide identifications), whereas the ΔEMC6 *versus* wild-type sample yielded 853 different protein identifications. Within these datasets, alterations of the intracellular proteome were quantified using the same technique as described in **Section 8.2.1**. The overall abundance of the majority of proteins remained unchanged by mEMC-depletion, as shown in **Figure 8.3 C** and **Figure 8.3 D**. However, cross-correlation of all isotopic ratios revealed a subset of 11 intracellular proteins that were concomitantly reduced in cells devoid of either EMC5 or EMC6 (**Figure 8.3 B** and **Figure 8.3 E**). Among the most consistently and strongly co-depleted factors were vimentin (VIM) and FDFT1/SQS (**Figure 8.3 E**). Four out of 11 shortlisted proteins were reported to be at least partially localized to the ER (CYB5A, FDFT1/SQS, SGPL1, and TMX2) [418], [419], [420], [421], [422]. Of these, only three (CYB5A, FDFT1/SQS, and TMX2) are anchored to the ER through a TMD. Succinate dehydrogenase complex flavoprotein subunit A, succinate dehydrogenase complex iron sulphur subunit B (SDHA/B), and

Figure 8.2 ***(previous page)*****: mEMC depletion affects the expression of cell surface proteins. A.** PMP workflow. Two clonal U2OS Flp-In cell lines deficient of EMC5 (ΔEMC5 #5-4 and #6-14), and two deficient of ΔEMC6 (#1-1 and #3-9) were labelled with medium R6/K4 (M) or heavy R10/K8 (H) amino acids. The wild-type (wt) cell line remained unlabelled (L). Each knockout line was generated with a distinct CRISPR/Cas9 sequence targeting different regions of the same gene. Sialylated cell surface glycoproteins were then oxidatively *in vivo* biotinylated for 90 minutes using 100 μM aminooxy-biotin. Cell extracts were prepared in Triton-X100 lysis buffer and mixed at equimolar ratios. Subsequently, the biotin-labelled cell surface proteome was separated from intracellular proteins (cytoplasmic fraction) by affinity purification with streptavidin-conjugated agarose beads. Purified glycoproteins were stringently washed and peptide fragments were obtained by on-bead digest with trypsin. Polypeptides of the cytoplasmic fraction were precipitated before trypsin digest. Peptides contained in both fractions were identified and quantified by MS/MS. **B.** Workflow to identify proteins that were affected by loss of both, EMC5, and EMC6. Peptides detected by MS/MS (see (A)), were identified and their isotopic ratios quantified using the MaxQuant software package [414]. Common contaminants were computationally removed from the dataset. The data was then further processed by Perseus [417]. Proteins whose abundance was changed by at least 30% were shortlisted and all lists were compared to find proteins that were mutually depleted (i and ii). **C.** Venn diagram of proteins downregulated in ΔEMC5 and ΔEMC6 cells. The peptide abundance for each protein was decreased by $\geq$ 30% compared to wt. Total numbers of proteins with decreased abundance in each knockout cell line are shown. A set of 23 proteins was commonly affected by loss of EMC5, or EMC6. **D.** Table listing the 23 proteins that had decreased M/L and H/L ratios in all ΔEMC5 and ΔEMC6 cell lines shown. Peptide counts refer to unique and razor peptides. Gaussian curve fitting of M/L, and H/L ratios (normalization) was achieved by MaxQuant. wt, wild-type (U2OS Flp-In)

Δ(3,5)-Δ(2,4)-dienoyl-CoA isomerase (ECH1) are localized to mitochondria (and also to peroxisomes in the case of ECH1) [423], [424]. The remaining proteins are predicted to reside in the nucleus (histone H1.1), cytoplasm (VIM and quinone oxidoreductase (CRYZ)) [425] or lysosomes (cathepsin D (CTSD)) [426].

In summary, changes to the intracellular proteomes of mEMC-deficient cells were quantified to identify proteins whose expression depended upon the mEMC. Eleven proteins were consistently reduced in mEMC-deficient cells. Despite varied topological features and biological function, 36% of these factors were predicted to localize to the ER (i.e. FDFT1/SQS). Since SQS is an important, evolutionarily conserved enzyme and was among the most reduced ER-resident factors in mEMC-deficient cells, the relationship between the mEMC and SQS was chosen for further investigation (**Section 9.1**).



E

			ΔEMC5					
Gene	Accession #	Protein	(M/L)*	Fold change	Peptides	(H/L)*	Fold change	Peptides
CRYZ	Q08257	Quinone oxidoreductase	0.554	1.805	7	0.462	2.165	7
CTSD	P07339	Cathepsin D	0.581	1.721	2	0.379	2.639	2
CYB5A	P00167	Cytochrome b5	0.661	1.513	3	0.595	1.681	3
ECH1	Q13011	Delta(3,5)-Delta(2,4)-dienoyl-CoA isomerase, mitochondrial	0.676	1.479	8	0.570	1.754	8
FDFT1	P37268	Squalene synthase	0.164	6.098	2	0.069	14.493	2
HIST1A	Q02539	Histone H1.1	0.570	1.754	3	0.434	2.304	3
SDHA	P31040	Succinate dehydrogenase [ubiquinone] flavoprotein subunit	0.665	1.504	3	0.605	1.653	3
SDHB	P21912	Succinate dehydrogenase [ubiquinone] iron-sulfur subunit	0.622	1.608	3	0.165	6.061	3
SGPL1	O95470	Sphingosine-1-phosphate lyase 1	0.642	1.558	3	0.194	5.155	3
TMX2	Q9Y320	Thioredoxin-related transmembrane protein 2	0.489	2.045	1	0.378	2.646	1
VIM	P08670	Vimentin	0.156	6.410	NaN	0.192	5.208	NaN

			ΔEMC6					
Gene	Accession #	Protein	(M/L)*	Fold change	Peptides	(H/L)*	Fold change	Peptides
CRYZ	Q08257	Quinone oxidoreductase	0.656	1.524	5	0.633	1.580	1
CTSD	P07339	Cathepsin D	0.565	1.770	1	0.696	1.437	1
CYB5A	P00167	Cytochrome b5	0.462	2.165	4	0.587	1.704	1
ECH1	Q13011	Delta(3,5)-Delta(2,4)-dienoyl-CoA isomerase, mitochondrial	0.548	1.825	7	0.545	1.835	1
FDFT1	P37268	Squalene synthase	0.132	7.576	1	0.182	5.495	2
HIST1A	Q02539	Histone H1.1	0.112	8.929	2	0.640	1.563	3
SDHA	P31040	Succinate dehydrogenase [ubiquinone] flavoprotein subunit	0.380	2.632	8	0.398	2.513	4
SDHB	P21912	Succinate dehydrogenase [ubiquinone] iron-sulfur subunit	0.309	3.236	3	0.354	2.825	5
SGPL1	O95470	Sphingosine-1-phosphate lyase 1	0.482	2.075	1	0.395	2.532	7
TMX2	Q9Y320	Thioredoxin-related transmembrane protein 2	0.689	1.451	1	0.496	2.016	8
VIM	P08670	Vimentin	0.265	3.774	NaN	0.227	4.405	NaN

* normalised

Figure legend on next page

Figure 8.3 ***(previous page)*****: Depletion of the mEMC affects the abundance of intracellular proteins. A.** Workflow of intracellular protein isolation. Isotopically labelled cells were treated as described in **Figure 8.2 A**. After affinity purification of biotinylated sialoglycoproteins, the remaining proteins were extracted, and subjected to tryptic digestion. Peptide masses were determined by tandem mass spectrometry. **B.** Venn diagram of proteins whose abundance was decreased by $\geq 30\%$ in ΔEMC5 and ΔEMC6 cells. Protein identifications shared by all four knockout cell lines were shortlisted for validation and are indicated (boxed, gene names shown). SQS (FDFT1) is shown in red as it was the most notably and consistently reduced ER-resident protein. **C** and **D.** Scatter plots of all identified proteins in ΔEMC5 (C) and ΔEMC6 (D) cells. Knockout cells were isotopically labelled with either heavy (H) or medium (M) amino acids and compared to unlabelled (L) wild-type (wt) cells. H/L, and M/L ratios were converted to a log2 scale and plotted against one another for each knockout cell line. Dashed lines demarcate the log2 = 0.5 threshold (corresponding to a change of at least 30%). Each protein is represented by a single dot. SQS (FDFT1) is highlighted in red. All proteins that were decreased by $\geq 30\%$ are annotated (gene names shown). A selection of shortlisted proteins that were downregulated only in ΔEMC5, or ΔEMC6 cells are shown in brackets. **E.** Table of shortlisted proteins from (B). H/L, and M/L ratios are the normalized ratios (Gaussian curve fitting).

Chapter 9

The mEMC affects cholesterol biosynthesis of U2OS cells

Steroids are found in all kingdoms of life where they serve a plethora of important functions [258]. Sterols are a subclass of steroids characterized by a hydroxyl group at position C-3. Cholesterol is commonly found in animals where it is synthesized in a reaction sequence that requires at least 20 different enzymes [258]. The *de novo* biosynthesis of this compound is highly compartmentalized, encompassing the ER, cytoplasm and peroxisomal reaction compartments (**Section 3.1.3**). Whereas the isoprenoid intermediates of the mevalonate pathway can be used for post-translational protein modification (e.g. geranylgeranylation and farnesylation), or for the synthesis of non-steroids (e.g. dolichol-diphosphate), the formation of squalene by SQS fully commits these isoprenoid precursors (farnesyl-diphosphate) to sterol biosynthesis (**Figure 9.1 B**). SQS has therefore been proposed to act as a 'gatekeeper', controlling the metabolite flux through the cholesterol and isoprenoid pathways [269], [427].

9.1 The mEMC is essential for the biogenesis of SQS in U2OS cells

SQS is an essential enzyme of the sterol biosynthesis pathways in the plant, animal, and fungi kingdoms of life [428], [429]. Over the last two decades, significant progress has been made in solving the structure of this TA protein [430] and determining its transcriptional regulation [431], [432]. Deletion of SQS in mice results in neural tube closure defects and embryonic lethality, stressing its important physiological functions [433]. However, little is known about the biogenesis and post-translational regulation of SQS. This section describes a

hitherto unrecognized role of the mEMC in the biogenesis of mammalian SQS.

9.1.1 Steady-state levels of SQS are significantly reduced upon loss of the mEMC

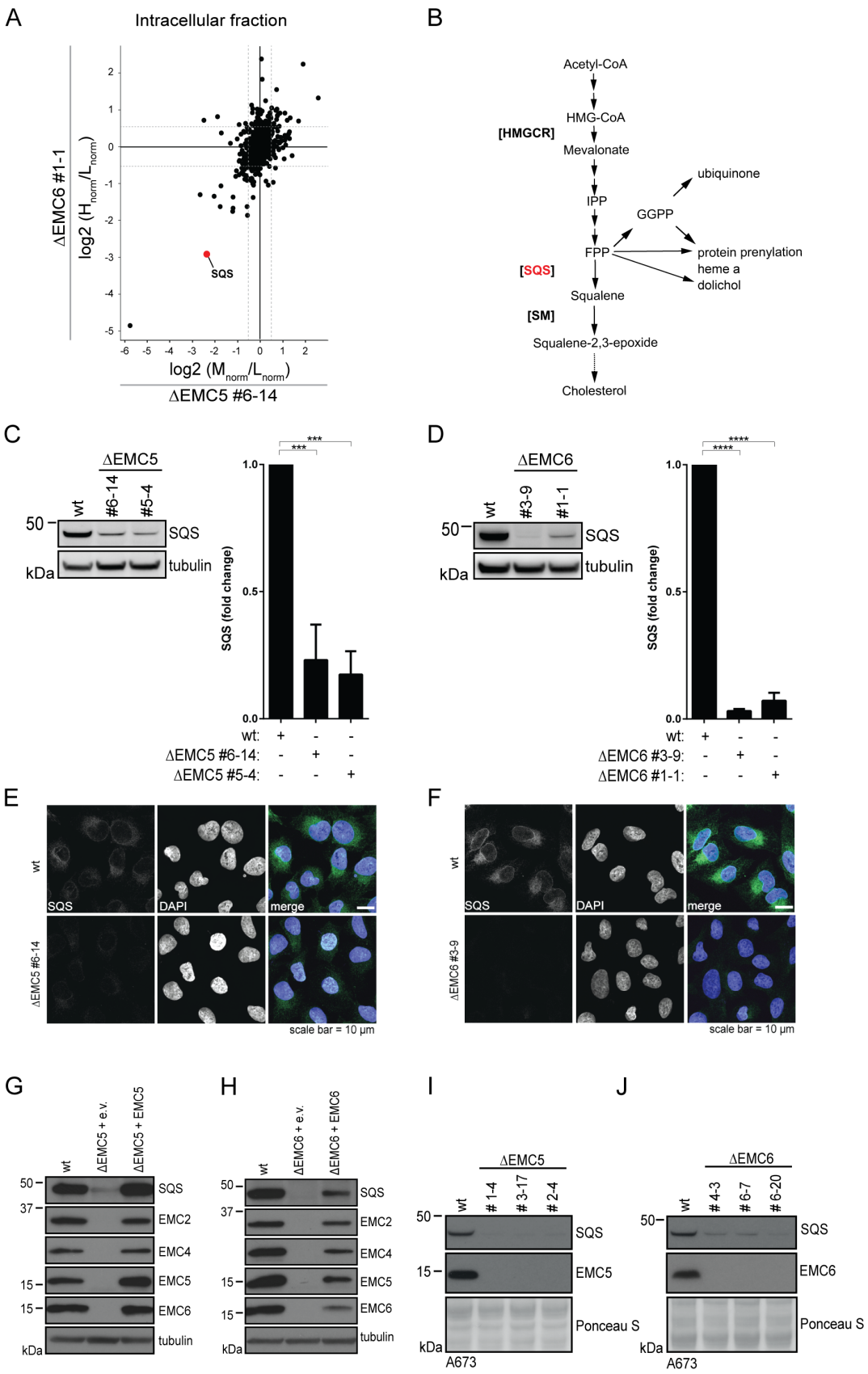
From the previously described SILAC-PMP analysis (**Section 8.2.2**), it was found that the abundance of a group of intracellular proteins was significantly reduced in mEMC-deficient cell lines (ΔEMC5 and ΔEMC6). It was further observed that the most significantly and consistently downregulated protein hit was FDFT1, which is also known as SQS (**Figure 8.3**). **Figure 9.1 A** shows the relative abundance of SQS in ΔEMC5 cells (x-axis) compared to that in ΔEMC6 cells (y-axis) as determined by SILAC analysis. Two EMC5 knockout clones showed a decrease of SQS by 83.6 and 93.1%. In two independent clonal EMC6 knockout cell lines, SQS was reduced by 86.8 and 81.8%. Importantly, the relative abundances of most proteins identified were unaffected by the loss of EMC5 or EMC6 (**Figure 9.1 A**).

To validate the coincidental reduction of SQS with knockout of either EMC5 or EMC6, immunoblotting of whole-cell lysates from ΔEMC5 and ΔEMC6 U2OS Flp-In cells was performed (**Figure 9.1 C/D**). Using an antibody specific for endogenous SQS, its decrease was quantified in all ΔEMC5 and ΔEMC6 cell lines tested (77% (ΔEMC5 #6-14), 83% (ΔEMC5 #5-4), 96.9% (ΔEMC6 #3-9) and 92.9% (ΔEMC5 #1-1) (bar graphs in **Figure 9.1 C** and **D**)). Comparable results were obtained using a different SQS-antibody (data not shown). Confocal microscopy of SQS revealed it to be localized in an ER pattern in wild type cells, and markedly reduced in mEMC-deficient cells (**Figure 9.1 E/F**). The specificity of the SQS antibody for immunoblotting and confocal microscopy was validated in ΔSQS U2OS cells generated by using CRISPR/Cas-9 (**Supplemental Figure 18.13 A**). Localization of SQS to the ER in U2OS cells is in agreement with previous reports that used rat hepatocytes [419].

Next, it was investigated whether the decreased SQS levels occurred concomitantly with mEMC loss and were not due to clonal variation. To test this, full-length EMC5 or EMC6 was re-introduced to knockout cell lines (ΔEMC5 or ΔEMC6) to restore mEMC function. The empty vector backbone (e.v.) was introduced as a negative control. All constructs were expressed under the control of a Dox-inducible CMV-promoter, which permitted the titration and monitoring of expression levels and mEMC restoration over time (see also **Figure 6.1 E**). Indeed, mEMC reconstitution by inducing EMC5/6 expression over 24 hours restored SQS protein levels to near normal (**Figure 9.1 G/H**). The re-appearance of EMC2, EMC4, and EMC5/6 implies that the reintroduction of either EMC5 or EMC6 into the respective knockout lines was sufficient to restore the entire mEMC (compare lanes 2 and 3 in **Figure 9.1 G/H**).

Reassured that the lack of SQS in ΔEMC5 and ΔEMC6 cells resulted from a loss of mEMC functionality, the next step was to address the question of whether the functional link between the mEMC and SQS was a more general phenomenon that extended beyond U2OS cells. Therefore, CRISPR/Cas9-mediated deletion of EMC5 or EMC6 was performed in a range of cell lines, from which single-cell knockout clones were obtained from A673 cells (Ewing's sarcoma). **Figure 9.1 I/J** illustrates that SQS levels were reduced in multiple A673 ΔEMC5 and ΔEMC6 single-cell clones. These observations were supported further by the detection of a moderate reduction in SQS levels from ΔEMC6 HEK293 Flp-In cells (**Supplemental Figure 18.13 B**).

In this section, it has been demonstrated that the mEMC plays a role in regulating the levels of the ER-localized, integral membrane protein SQS. Loss of EMC5 or EMC6 disrupts the mEMC, allowing either to be used as a means to reduce mEMC levels and functionality. Reduction of SQS could be observed in different cell lines and clonal variants, rendering pleiotropic effects of the sgRNAs an unlikely cause. Furthermore, it has been demonstrated that restoration of mEMC expression can reverse the loss of SQS. Finally, these data strongly suggest that the mEMC oversees an aspect of SQS biogenesis. As SQS is essential for *de novo* biosynthesis of cholesterol and other sterols, it is postulated that the mEMC is an important (indirect) regulator of cholesterol homeostasis within cells.



See next page for Figure legend.

9.1.2 EMC5 and EMC6 are necessary but not sufficient for SQS biogenesis

Sufficient levels of EMC5 and EMC6 are necessary for the mature mEMC to form, most likely by promoting the co-translational assembly of the remaining subunits (**Section 6.1.1**). Accordingly, deletion of either component significantly decreased the putative mEMC client protein SQS. In the next stage of this study, it was investigated whether the correct biosynthesis and/or targeting of SQS requires the mature mEMC, or just EMC5 (or EMC6). To test this, each component was expressed in the knockout lines of its counterpart (i.e. ΔEMC5 + EMC6 and ΔEMC6 + EMC5) (**Figure 9.2 A**). Expression of EMC6 for 24 hours in ΔEMC5 cells did not restore SQS expression. Additionally, EMC5 and EMC6 must both be present at the same time in order to stabilize and assemble with other mEMC subunits (**Figure 6.1 F**). This observation is consistent with the view that EMC6 is necessary but not sufficient for SQS stabilization. Since EMC5 was markedly destabilized in ΔEMC6 cells and targeted to the proteasome (**Figure 6.2 B**), it was not possible to establish a cell line in which the

Figure 9.1 ***(previous page)*****: SQS is decreased in mEMC-depleted cells. A.** Representative scatter plot of proteins identified in the intracellular fraction. ΔEMC5 #6-14 and ΔEMC6 #1-1U2OS Flp-In cells were cultured in the presence of medium R6K4 (M) or heavy R10/K8 (H) amino acids, respectively, and the abundance of intracellular proteins was compared to that in unlabelled R0K0 (L) wild-type (wt) cells. The fold change of individual proteins in ΔEMC6 cells compared to wt cells is shown as log2 on the x-axis, whereas that of ΔEMC5 cells is plotted along the y-axis. SQS (red) was consistently downregulated both in ΔEMC5 and ΔEMC6 cells. **B.** Schematic representation of the role of SQS (red) in the cholesterol biosynthesis pathway. SQS catalyses the head-to-head condensation of two FPP molecules to form pre-squalene, which is further converted to squalene by the same enzyme. Dotted arrows represent multiple reaction intermediates. **C** and **D.** Immunoblotting reveals decreased SQS in whole-cell lysate from ΔEMC5 and ΔEMC6 cells. Left: Two EMC5 U2OS Flp-In knockout cell lines (#6-14 and #5-4) were seeded to 10 cm plates and collected after 24 hours. Whole-cell lysate was used for immunoblotting and an SQS-specific antibody in combination with an AlexaFluor-488 secondary antibody was used for detection. Right: Densitometric analysis of the relative abundance of SQS (n = 3). **D.** Left: Cell lysates were obtained and endogenous SQS from two independent knockout cell lines (#3-9 and #1-1) was visualized as described in (C). Right: Quantification of SQS by densitometric analysis as detailed in (C). n = 3. ***, $p \leq 0.001$; ****, $p \leq 0.0001$. **E** and **F.** Decreased immunofluorescence signal of endogenous SQS in ΔEMC5 and ΔEMC6 cells. Cells were seeded to coverslips and subsequently fixed and stained for indirect immunofluorescence confocal microscopy. Scale bars = 10 μm. **F.** Cells were processed as in (E). **G** and **H.** Co-depletion of SQS is reversible and specific to the loss of the mEMC. ΔEMC5 U2OS Flp-In cells were reconstituted either with pcDNA^{TM}/5/FRT/TO empty vector (e.v.) or with full-length EMC5. EMC5 expression was induced by addition of 1 ng/ml doxycycline for 24 hours. SQS expression was analysed by immunoblotting of whole-cell lysate. EMC2/4/6 levels are shown as a surrogate readout for mEMC integrity. **H.** ΔEMC6 U2OS Flp-In cells were complemented with empty vector (e.v.) or full-length EMC6. Expression of EMC6 was induced by 1 ng/ml doxycycline for 24 hours. Whole-cell lysate was separated on a gel and subjected to immunoblotting. EMC2/4/5 serve as indicators for mEMC complex formation. **I** and **J.** The mEMC regulates SQS biogenesis in A673 cells. **I.** Single-cell clones were generated from A673 cells by CRISPR/Cas9 mediated knockout of EMC5. Whole-cell lysates of three independent clones (#1-4, #3-17, and #2-4), each generated using a different Cas9 target sequence, are shown. **J.** EMC6 knockout clones were established from the parental A673 line (wt). Shown are three cell lines (#4-3, #6-7, #6-20). #6-7 and #6-20 share the same Cas9 target sequence.

expression of EMC5 is commensurate with its levels in wild-type cells. The minimal amount of EMC5 detected in ΔEMC6 + EMC5 cells was not sufficient to restore SQS (**Figure 9.2 A**). Consequently, a condition in which EMC5 was isolated from the main complex, while still stable, was required.

As with the loss of EMC5 or EMC6, depletion of EMC2 disrupted mEMC assembly. Unlike the absence of EMC6 in ΔEMC5 cells however, the steady-state amount of EMC6 was markedly reduced in ΔEMC2 cells, but still detectable by immunoblotting (**Figure 6.1 B**). In these cell lines, EMC5 abundance was also only moderately affected by the suppression of EMC2. Importantly, the EMC2 depletion phenocopied the effect of EMC5/6 loss on SQS levels (**Figure 9.2 B**). To further exclude the possibility that the co-depletion of SQS in EMC2-depleted cells was due to the reduced presence of EMC5/6, attempts were made to increase the levels of EMC5/6 by transient expression in ΔEMC2 cells to observe whether this would rescue SQS production (**Figure 9.2 C**). However, exogenous expression of either subunit failed to stabilize SQS levels, further supporting the model where SQS regulation is dependent on the mature mEMC.

Finally, systematic RNAi-mediated depletion of EMC1 - 10 revealed an interdependence between SQS levels and the mEMC subunits that are essential for maintaining an intact mEMC (**Figure 9.2 D**). Albeit to a somewhat milder extent, transient depletion of EMC2, EMC3, EMC5, and EMC6 for 72 hours consistently lowered the steady-state levels of SQS. Interestingly, depletion of EMC4, which does not significantly affect the expression of the remaining mEMC components (**Figure 6.1 A**), still showed a moderate effect on SQS. This might be explained by subtle alterations in the composition of the mature mEMC, as was evidenced by the minor shift of most mEMC components to a lower molecular weight fraction in sucrose gradient sedimentation assays (**Figure 6.3**). Knockdown of EMC7 - 10 had no (or a very mild) impact on SQS levels, consistent with their 'secondary' role in mEMC biogenesis (**Figure 9.2 D**). Despite the absence of direct evidence, it has been suggested that SQS might interact with other proteins of the sterol biosynthesis pathway and form hetero-oligomeric complexes [434]. Therefore, whether or not the reduction of SQS in response to mEMC subunit depletion was the consequence of SQS failing to assemble into homo- or hetero-oligomeric complexes was investigated. Lysates from cells subjected to RNAi-mediated depletion of EMC1/3/4/7 - 10 were fractionated by sucrose gradient sedimentation and SQS distribution was evaluated by immunoblotting. Even though the overall protein levels of SQS were decreased upon RNAi of EMC1, EMC3, and EMC4, no marked shift in its migration pattern was observed, suggesting that SQS was rapidly degraded and did not accumulate in aberrant low molecular weight com-

plexes (**Supplemental Figure 18.14**). Taken together, I suggest that the interdependence between SQS and individual mEMC subunits is an expression of the extent to which the latter support mEMC biogenesis.

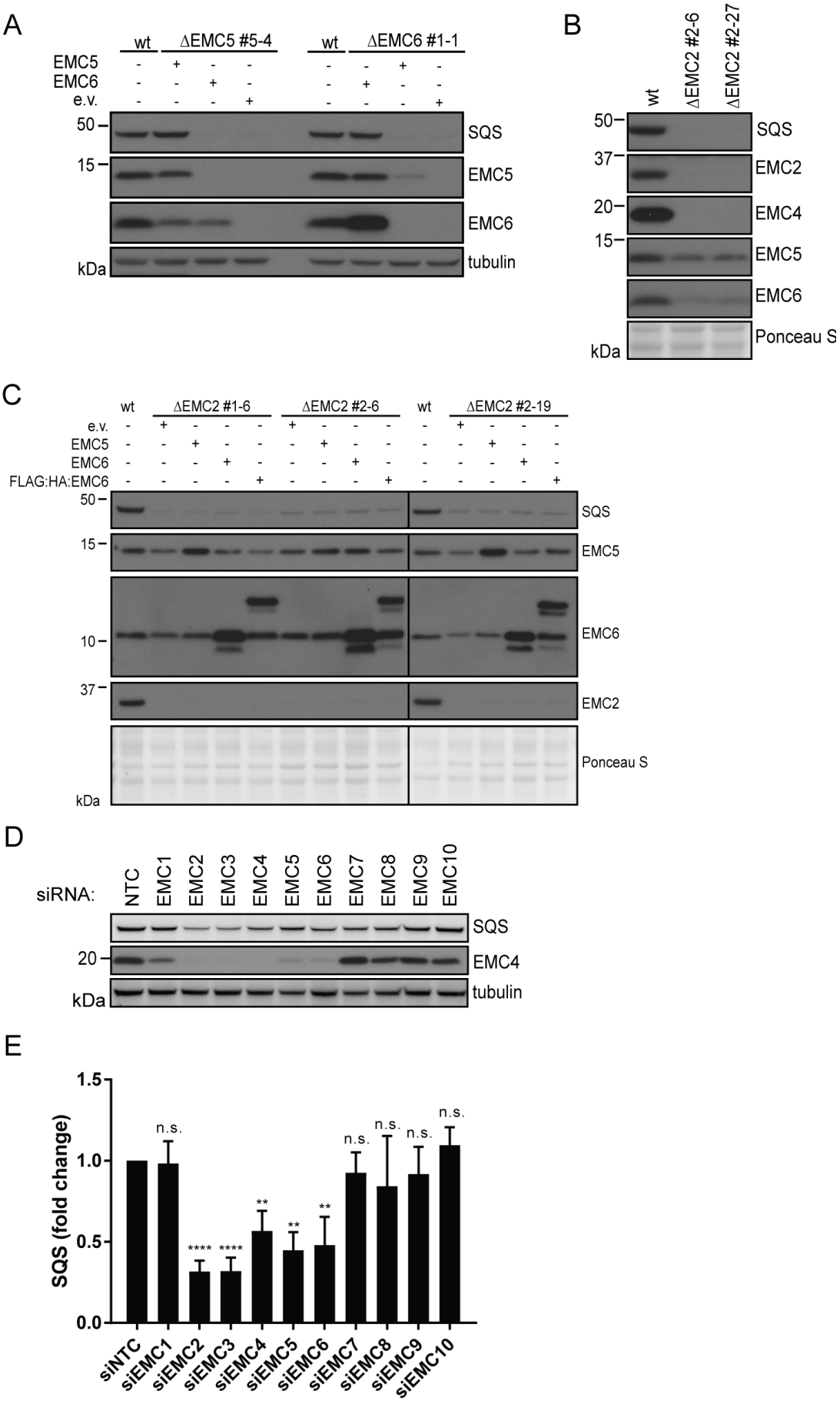


Figure 9.2: *See next page for Figure legend.*

9.2 Depletion of the mEMC perturbs the cholesterol biosynthesis pathway

In mammalian cells, SQS is indispensable for the production of squalene, which serves as an essential precursor for endogenous cholesterol (**Figure 9.1 B**) [435], [436]. Enzymatic inhibition or depletion of SQS has been shown to block *de novo* cholesterol biosynthesis [437], [436] and to sensitize cells to lipid depletion [438]. Therefore, the reduced abundance of this enzyme in mEMC-deficient cells suggests a potential metabolic imbalance in the mevalonate and cholesterol biosynthesis pathways.

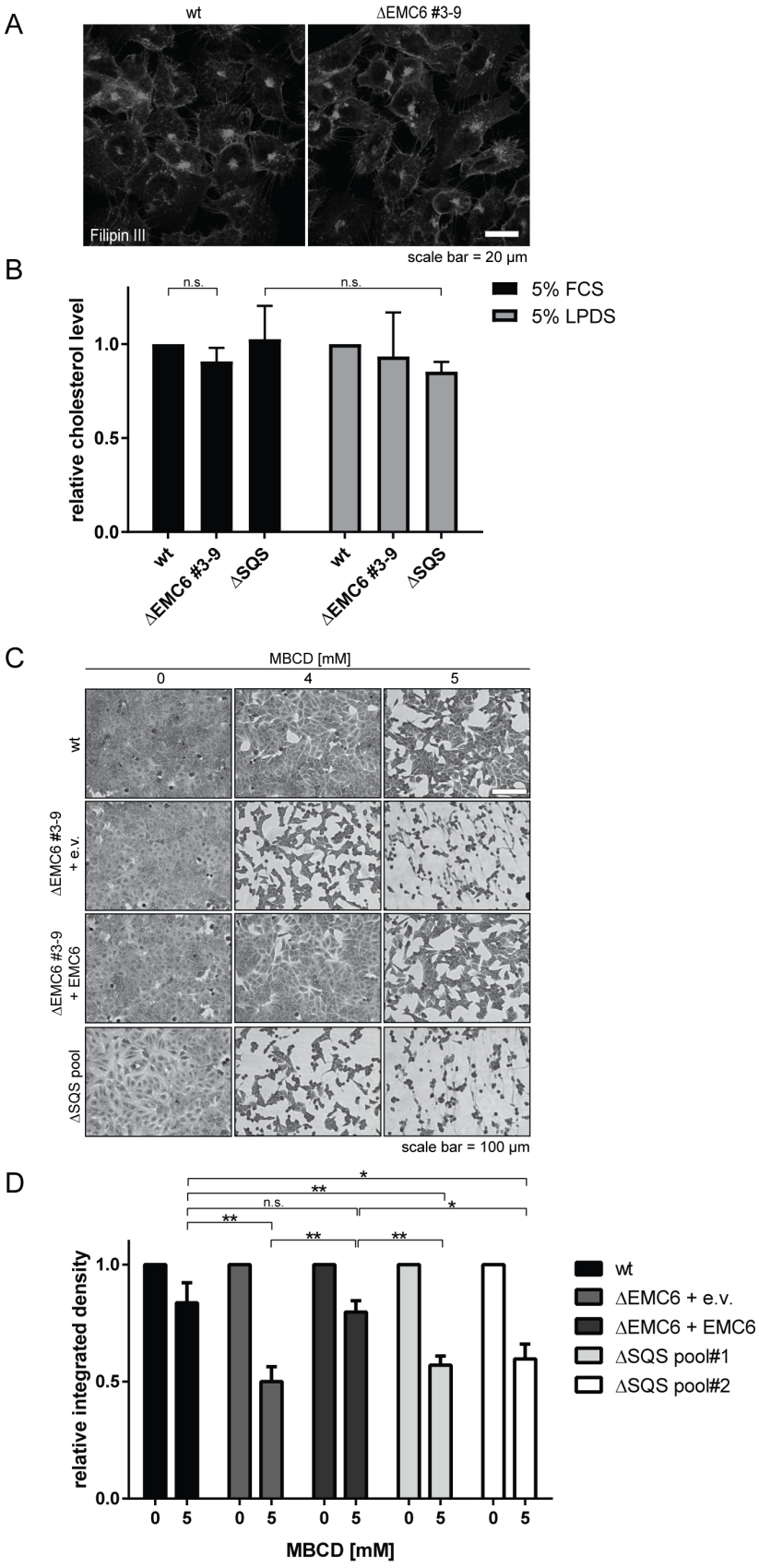
9.2.1 EMC6 knockout cells are sensitized to cholesterol depletion by MBCD

The overall cholesterol content and its subcellular localization was examined in ΔEMC5 and ΔEMC6 cells using Filipin III staining. Filipin III is a polyene macrolide with a high and specific affinity for cholesterol. Due to its autofluorescent properties, it has found widespread application in visualizing cellular cholesterol [439]. No striking abnormalities in either the overall amount or the subcellular localization of cholesterol in mEMC-deficient cells were observed (**Figure 9.3 A**). In this respect, the Filipin III staining pattern was characteristic of a physiological cholesterol distribution with high concentrations in perinuclear structures, which are likely to represent the endocytic recycling compartment [440] or the *trans*-Golgi network [441], [440]. No apparent difference in the intensity of Filipin III staining was observed in ΔEMC6 cells, indicating that cholesterol levels were not reduced. This finding was confirmed

Figure 9.2 *(previous page)*: EMC5 and EMC6 are necessary but not sufficient for SQS biogenesis. A. Restoration of EMC6 in EMC5 knockout cells and vice versa does not rescue SQS expression. ΔEMC5 and ΔEMC6 U2OS Flp-In cells, stably reconstituted with either empty vector (e.v.) or EMC5/6, were seeded onto 6 cm plates (1×10^6 cells per plate) and induced with 100 ng/ml doxycycline for 24 hours. Whole-cell lysate was subjected to immunoblotting. **B.** EMC2 knockout in U2OS Flp-In cells phenocopies the effect of EMC5/6 ablation on SQS. 3×10^6 cells were seeded onto a 10 cm plate and collected after 24 hours. Two different single-cell clones were used. EMC4 was used to indicate loss of mEMC integrity. The immunoblot was performed using whole-cell lysate. **C.** Overexpression of EMC5 or EMC6 does not restore SQS in the absence of EMC2. Three ΔEMC2 single-cell clones were transiently transfected with empty vector (e.v., pcDNA^{TM}/5/FRT/TO), EMC5, EMC6, or FLAG:HA:EMC6. 24 hours after transfection, cells were split to 6 cm plates and induced with 100 ng/ml doxycycline for an additional 24 hours. Whole-cell lysate was collected and used for immunoblotting. **D.** RNAi of EMC1-10 differentially affects SQS biogenesis. U2OS Flp-In cells were transiently transfected with 100 nM siRNA pools targeting each individual subunit. 24 hours after transfection, cells were split and collected after an additional 48 hours. Whole-cell lysate was blotted for SQS and tubulin using specific primary antibodies in conjunction with AlexaFluor 488–conjugated secondary antibodies. **E.** Densitometric quantification of three independent experiments performed as in (D). Student's t-test was used for statistical analysis. Standard deviations are shown. **, $p \leq 0.01$; ****, $p \leq 0.0001$; n.s., not significant.

by the quantification of overall cellular cholesterol levels *via* gas chromatography tandem mass spectrometry (GC-MS/MS). ΔEMC6 cells were grown either under replete conditions (5% foetal calf serum (FCS)/ Dulbecco's Modified Eagle Medium (DMEM)) or in the presence of 5% lipoprotein-deficient serum (LPDS) for cholesterol starvation. Wild-type and ΔSQS cells were treated identically to ΔEMC6 cells and served as controls. Bulk cellular lipids were extracted and overall cholesterol levels were determined by GC-MS/MS. In line with the Filipin III staining above, no pronounced changes to cholesterol levels in EMC6 knockout cells were found (**Figure 9.3 B**). Of note, the lack of SQS did not affect cellular cholesterol content under replete conditions, but led to mild depletion of cholesterol stores in the presence of LPDS (**Figure 9.3 B**). Therefore, it is possible that the residual amounts of SQS in ΔEMC6 cells are sufficient to maintain normal rates of *de novo* cholesterol biosynthesis. Alternatively, cells might import lipoprotein-bound cholesterol from tissue culture media. Indeed, high amounts of cholesterol are present in FCS, a vital constituent of the cell culture media [442]. Lipoprotein receptor-mediated endocytosis of cholesterol from the media would therefore be a way to compensate for shortcomings in intracellular cholesterol biosynthesis and potentially mask any phenotype pertinent to disturbances in cholesterol metabolism.

Accordingly, cells were pharmacologically depleted of cholesterol to increase their dependence on *de novo* cholesterol biosynthesis. Methyl-β-cyclodextrin (MBCD) is a cyclic oligosaccharide shown to potently sequester cholesterol from the PM, resulting in the depletion of cellular cholesterol stores [443], [444]. Prolonged exposure to MBCD can lead to cell death [445], [446]. Careful titration showed that U2OS Flp-In cells were able to tolerate between 4 and 5 mM MBCD for 16 hours with negligible or moderate cell loss, as determined by crystal violet-staining (**Figure 9.3 C**, first row). As an approximation for the number of cells remaining after drug treatment, imaging-based quantification of the crystal violet-stained cells was performed by measuring their dye intensity at 640 nm. Subsequent computational integration of all pixel intensities per well (integrated density) served as a readout for cell viability (**Figure 9.3 D**). In contrast to the wild-type, exposure of ΔEMC6 cells to 4 - 5 mM MBCD led to significant morphological changes and increased cell loss (16.3% (wild-type) *vs.* 50.0% (ΔEMC6 + e.v.)) (**Figure 9.3 C**, row 1 and 2, and **Figure 9.3 D**). This effect was prevented by reconstituting EMC6-deficient cells with the missing subunit (20.3% in ΔEMC6 + EMC6) (**Figure 9.3 C**, row 3 and **Figure 9.3 D**).



See next page for Figure legend.

Despite its high affinity for PM cholesterol, MBCD can also interact with phospholipids such as sphingomyelin [447] [448], or glycosylphosphatidylinositol (GPI)-anchored proteins, albeit to a lesser extent [449], [450], [451]. This increases the probability of inducing unwanted pleiotropic effects unrelated to cholesterol store depletion. To ensure that the pronounced sensitization of mEMC-deficient cells to MBCD was indeed due to its cholesterol-depleting activity, and, more precisely, to the lack of SQS, two polyclonal populations of ΔSQS cells (each generated with sgRNAs targeting different genomic regions) were included in the assay. As shown in **Figure 9.3 C** (row 4) and **Figure 9.3 D**, ΔSQS cells were significantly sensitized to MBCD (43.0% (ΔSQS pool#1) and 40.3% (ΔSQS pool#2)), effectively phenocopying its effect on ΔEMC6 cells. Further support for the dependence of cell viability on SQS under cholesterol-depleting conditions was derived from the pharmacological inhibition of its enzymatic activity by the SQS-specific inhibitor zaragozic acid A (ZA), [452]. When wild-type cells were treated with a combination of MBCD and 100 μM ZA, sensitivity to previously well-tolerated amounts of MBCD was markedly increased to a similar extent as to that observed in a clonal ΔSQS knockout cell line (**Figure 9.4 A**). Of note, exposure to ZA alone did not affect cell viability. Quantification of cells exposed to 5 mM MBCD (**Figure 9.4 B**) revealed that wild-type cells were only mildly affected (91.9% of cells viable), but specific inhibition of SQS by administration of ZA in the presence of 5 mM MBCD resulted in significantly reduced cell viability (49.3% of cells viable). Likewise, genetic deletion of SQS reduced viability to 57.8% when exposed to 5 mM MBCD (**Figure 9.4 B**). These findings support the notion that sensitization of ΔEMC6 cells to MBCD is closely linked to reduced cellular SQS levels.

Figure 9.3 ***(previous page)*****: EMC6 knockout cells are sensitized to cholesterol depletion by MBCD. A.** Filipin III staining of ΔEMC6 cells is comparable to that of the parental line. Cells were grown on glass coverslips for 24 hours under replete conditions (DMEM + 10% FCS) before fixation with 4% paraformaldehyde and staining with Filipin III. Micrographs were acquired using confocal microscopy (63× magnification). **B.** Cellular cholesterol levels of mEMC-deficient cells and wild-type (wt) cells are comparable. Equal cell numbers were seeded and grown either in the presence of 5% FCS or 5% LPDS for 24 hours. Lipids were extracted in methyl t-butyl ether and quantified by GC-MS/MS. Three independent experiments are shown. Error bars are S.D.. **C.** Prolonged cholesterol depletion sensitizes ΔEMC6 cells. 1×10^4 cells per well were seeded to a 96-well plate and were grown in the presence of 1 ng/ml doxycycline for 24 hours, before addition of MBCD to the preconditioned media for 16 hours at the concentrations indicated. Subsequently, the cells were fixed and stained with crystal violet and were imaged by brightfield microscopy (20× magnification). A representative image of at least three independent experiments (n = 3) is shown. Each of the biological replicates was performed in technical quadruplicates. Images were acquired at a magnification of 10×. e.v., empty vector; MBCD, methyl-β-cyclodextrin; wt, wild type; ZA, zaragozic acid A. **D.** Quantification of experiments shown in (C). 96-well plates containing cells stained with crystal violet were scanned at an excitation wavelength of 640 nm. Acquired images were then computationally processed using the ImageJ software. The pixel density was integrated for each well and correlates directly with cell number. Three independent experiments in technical quadruplicate (four wells per condition per experiment) were quantified. Mean values and error bars (S.D.) are indicated. Statistical significance was evaluated by Students t-test. *, $p \leq 0.05$; **, $p \leq 0.01$; n.s., not significant.

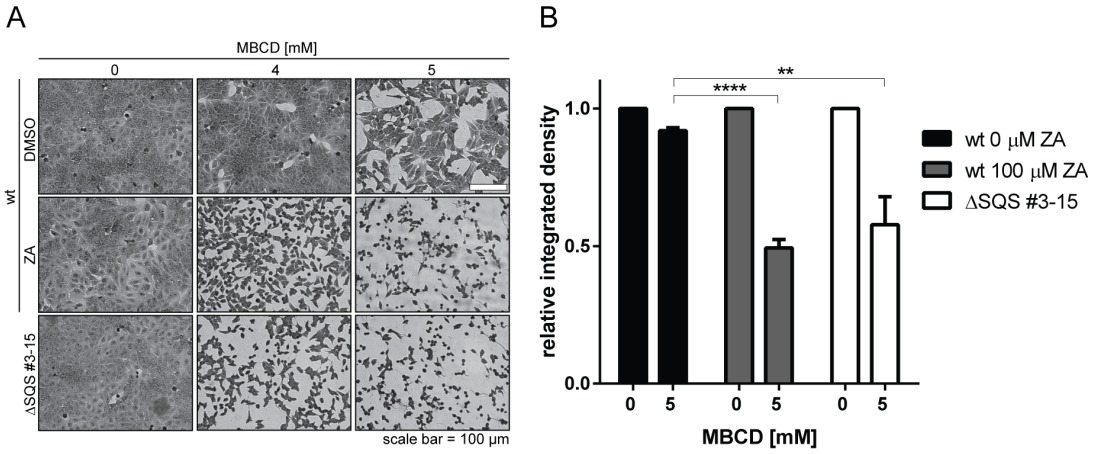


Figure 9.4: SQS inhibition sensitized U2OS Flp-In cells to MBCD. A. Treatment of U2OS Flp-In cells with ZA or deletion of SQS leads to significant morphological changes and cell loss in the presence of MBCD. 10×10^3 cells per well of a 96-well plate were seeded 24 hours before addition of 4 or 5 mM MBCD alone or in combination with 100 μM ZA for 16 hours. ΔSQS cells were not treated with ZA. Cells were fixed with acetone:methanol (1:1) and stained with crystal violet. Micrographs were acquired at 20× magnification. **B.** Loss of SQS or its enzymatic activity significantly sensitizes cells to 5 mM MBCD. Quantification of three independent experiments (n = 3) conducted as in (A). Plates containing stained cells were scanned at an excitation wavelength of 640 nm. The amount of crystal violet correlates with cell number and was derived from the integrated pixel intensities per well. Cells were treated in five replicate wells per condition per experiment. Mean values are shown. Error bars represent S.D.. ****, $p \leq 0.0001$; **, $p \leq 0.01$; MBCD, methyl-β-cyclodextrin; ZA, zaragozic acid A.

Here, the sensitization of mEMC-deficient cells to cholesterol depletion has been demonstrated. This sensitization is likely to be a consequence of the co-incidental decrease of SQS in ΔEMC6 cells. Firstly, SQS protein levels were severely reduced in the absence of EMC6 (and by extension the mEMC), but could be restored by reconstitution with EMC6. Secondly, ΔSQS cells were not able to tolerate prolonged cholesterol depletion. Thirdly, MBCD treatment compromised wild-type cell viability only when SQS activity was blocked by ZA. These findings indicate the loss of SQS to be non-lethal as compensatory mechanisms, such as cholesterol uptake from the surroundings, are in place. Therefore, any impairment of SQS predominantly affected cell viability only when extracellular cholesterol could not be efficiently harnessed. In summary, disruption of mEMC function impairs sterol biosynthesis and may impact cell viability under conditions where intracellular cholesterol stores are exhausted, or exogenous cholesterol sources are limiting.

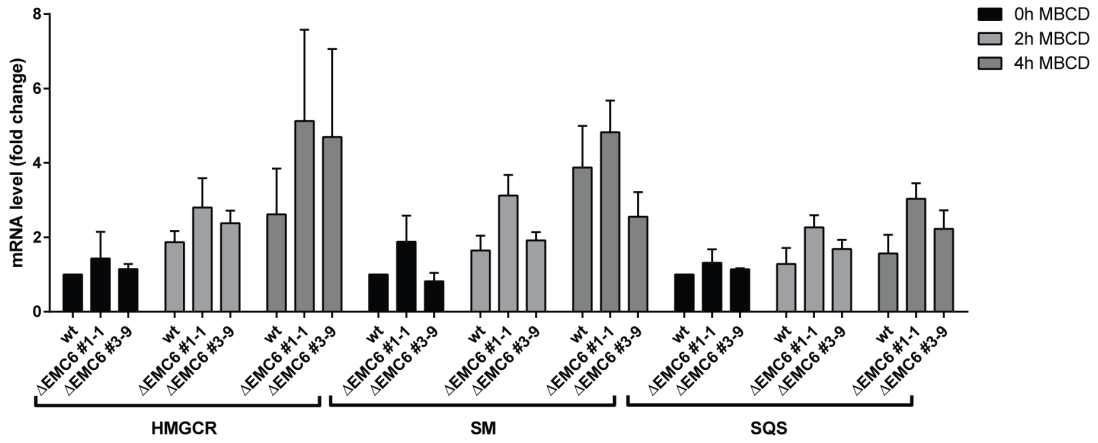
9.2.2 The transcriptional regulation of select SREBP2 target genes remains intact in EMC6 knockout cells

Cholesterogenic enzymes are subject to stringent transcriptional and post-transcriptional regulation [428], [263]. The SQS gene contains three sterol regulatory-like elements (HSS-SRE-1, Inv-SRE-3, and SRE-1(8/10)) in its promoter region [432], which have been shown to be modulated by SREBP2 and SREBP1a [453], [428]. HMGCR and SM, the two rate-limiting enzymes of the isoprenoid/sterol biosynthesis pathways, are also transcriptionally regulated by SREBPs [289]. Having observed an impairment of ΔEMC6 cells to adapt to low cholesterol conditions (**Section 9.2.1**), it was investigated whether a more general disturbance of the SREBP2-dependent transcriptional pathway might be a contributing factor under these circumstances. Aiming to assay the activity of SREBP2 signalling in mEMC-deficient cells, two clonal ΔEMC6 cell lines were treated with 1 mM MBCD for 2 - 4 hours to deplete internal cholesterol stores. SREBP2-dependent transcription of a select set of previously described SREBP2 target genes including HMGCR, SM, and SQS, was monitored by qPCR. Consistent with their role in cholesterol biosynthesis, all three target genes exhibited increased mRNA levels upon exposure to MBCD when compared to wild-type cells (**Figure 9.5 A**). This increase might indicate a stronger transcriptional response in ΔEMC6 cells, reflecting heightened sensitivity to cholesterol starvation. However, it is worth noting that high variation between experiments was sometimes observed (e.g. HMGCR, **Figure 9.5 A**). Therefore, it was concluded that the transcriptional regulation of SREBP2 target genes remains intact in mEMC-deficient cells.

With the SREBP2 pathway intact, it was not clear to what extent the transcriptional upregulation of SQS under low cholesterol conditions could compensate for its stunted biogenesis in mEMC-depleted cells. In accordance with increased SQS gene transcription, **Figure 9.5 C** demonstrates that MBCD treatment can elevate SQS protein levels in ΔEMC6 cells. ΔEMC6 cells with a stably integrated empty vector control (e.v.) were exposed to 4 mM MBCD over a period of 0 - 16 hours, and SQS protein levels were monitored at the indicated times. SQS was detectable after 4 hours of treatment with levels increasing over the 16-hour duration. It remains to be directly shown whether this phenomenon is a manifestation of increased protein stability or a consequence of the rise in transcriptional activity of the SQS gene. Speaking in favour of the latter hypothesis, MBCD treatment did not noticeably affect the UPS, as no alterations of bulk protein ubiquitination were observed (**Figure 9.5 C**). However, specific stabilisation of the SQS protein cannot be ruled out and requires further investigation. It is

also not clear whether *de novo* synthesised SQS is correctly targeted to the ER and enzymatically active. These results imply that the mEMC might be a facilitating factor of SQS biogenesis that is of particular importance for the maintenance of appropriate steady-state levels of this enzyme.

A



B

Target Gene	Cell line	mRNA levels [fold change*] 0 h MBCD	2 h MBCD	4 h MBCD
HMGCR	wt	1	1.87	2.61
	ΔEMC6 #1-1	1.43	2.80	5.12
	ΔEMC6 #3-9	1.15	2.38	4.70
SM	wt	1	1.64	3.88
	ΔEMC6 #1-1	1.88	3.12	4.82
	ΔEMC6 #3-9	0.82	1.91	2.55
SQS	wt	1	1.28	1.56
	ΔEMC6 #1-1	1.32	2.27	3.04
	ΔEMC6 #3-9	1.14	1.69	2.23

* mean of n=3, normalised to wt 0h MBCD

C

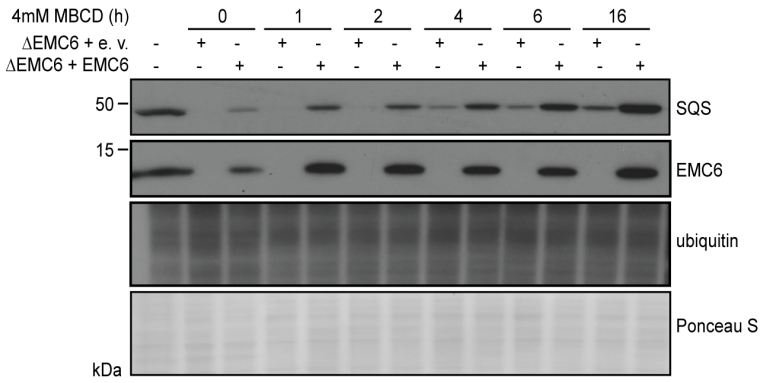


Figure 9.5: The transcriptional regulation of select SREBP2 target genes remains intact in EMC6 knockout cells. A. Transcription of SREBP2 target genes is induced by cholesterol depletion. 4×10^5 cells were seeded to 3.5 cm plates and were treated on the next day with 1 mM MBCD for the indicated period of time. The relative amounts of mRNA transcripts were determined by reverse transcription and qPCR. The fold change of each transcript compared to the 0 hours MBCD condition was calculated using the ΔΔCt method. All transcript levels were normalized to those of actin, which served as an internal standard. **B.** Fold change of mRNA levels as shown in (A). Mean values of three independent biological replicates are shown. **C.** SQS protein levels are upregulated in ΔEMC6 cells when exposed to MBCD. EMC6 expression in reconstituted ΔEMC6 U2OS Flp-In cells (ΔEMC6 + EMC6) was induced by addition of 1 ng/ml doxycycline for 24 hours. Cells were then treated with 4 mM MBCD for 0 - 16 hours. Whole cell lysates were separated on a gel and immunoblotting was performed for SQS and EMC6. e.v., empty vector; HMGCR, HMG-CoA reductase; MBCD, methyl-β-cyclodextrin; SM, squalene monooxygenase.

9.2.3 Prenylation of Rap1a is increased in EMC6 knockout cells

In previous sections a strong correlation has been established between mEMC integrity and SQS biogenesis. Moreover, ΔEMC6 and ΔSQS cells were more sensitive to cholesterol depletion than their parental cell line (**Section 9.1.1** and **Section 9.2.1**). Both observations suggest perturbed metabolite flux through the mevalonate and sterol biosynthesis pathways.

Decreased SQS activity results in the accumulation of its substrate, FPP, and other isoprenoids (e.g. GGPP) [454], [270]. It was hypothesized that an impairment of the committing step in sterol biosynthesis, the formation of squalene, by mEMC deficiency would lead to an increased isoprenoid pool of FPP and GGPP upstream of SQS. Hence, more shunting of FPP into protein prenylation pathways might occur, thereby increasing the ratio of prenylated:unprenylated protein species (**Figure 9.6 A**). Rap1a, a Ras-related family protein, is geranylgeranylated at its C-terminal CAAX motif [455]. The geranylgeranylation status of Rap1a has previously been used to assess the flux of FPP through the steroidogenic pathway [286]. Specifically, Leichner *et al.* (2011) demonstrated that pharmacological inhibition of SQS increases Rap1a prenylation, resulting in lower levels of unprenylated Rap1a, which can be detected using an antibody specific for the unprenylated form of this protein [286], [456]. Therefore, the levels of unprenylated Rap1a were monitored as a surrogate readout for FPP shunting into the prenylation pathway in mEMC-deficient cells. **Figure 9.6 B** shows that the amount of unprenylated Rap1a was decreased in ΔEMC6 cells. When EMC6 was stably added back to the knockout cells (ΔEMC6 + EMC6), prenylation of Rap1a was reverted to levels comparable to those in wild-type cells. Importantly, reconstituting the same EMC6 knockout cell line with an empty vector (ΔEMC6 + e.v.) failed to elevate unprenylated Rap1a. To exclude the possibility that global levels of Rap1a were affected by loss of EMC6, ΔEMC6 cells were treated with the geranylgeranyl transferase 1 (GGT1) inhibitor GGTI-298 for 4 hours to block thioether formation between GGPP and the acceptor cysteine in CAAX motifs. Under these conditions, equal amounts of (unprenylated) global Rap1a were detectable in all cell lines, indicating that there was no notable change in Rap1a synthesis. Similarly, inhibition of the enzymatic activity of SQS by supplementing wild-type cells with ZA (10 μM, 4 hours), also resulted in reduced levels of unprenylated Rap1a (**Figure 9.6 C**). These data support a mechanism in which diminished SQS activity is a causative factor for enhanced Rap1a prenylation.

To conclude, mEMC-deficiency and the consequential reduction of SQS levels and activity, may have a number of knock-on consequences, including the enhancement of geranylgeranyla-

tion of proteins containing a C-terminal CAAX motif. As SQS inhibition elevates isoprenoid levels (e.g. FPP and GGPP) [438], [454], and because the latter can in turn stimulate protein prenylation [457], [286], it is tempting to suggest that mEMC plays an indirect role in FPP shunting into prenylation pathways. This could indicate imbalances in protein prenylation whose consequences have hitherto not been defined in the wake of mEMC loss.

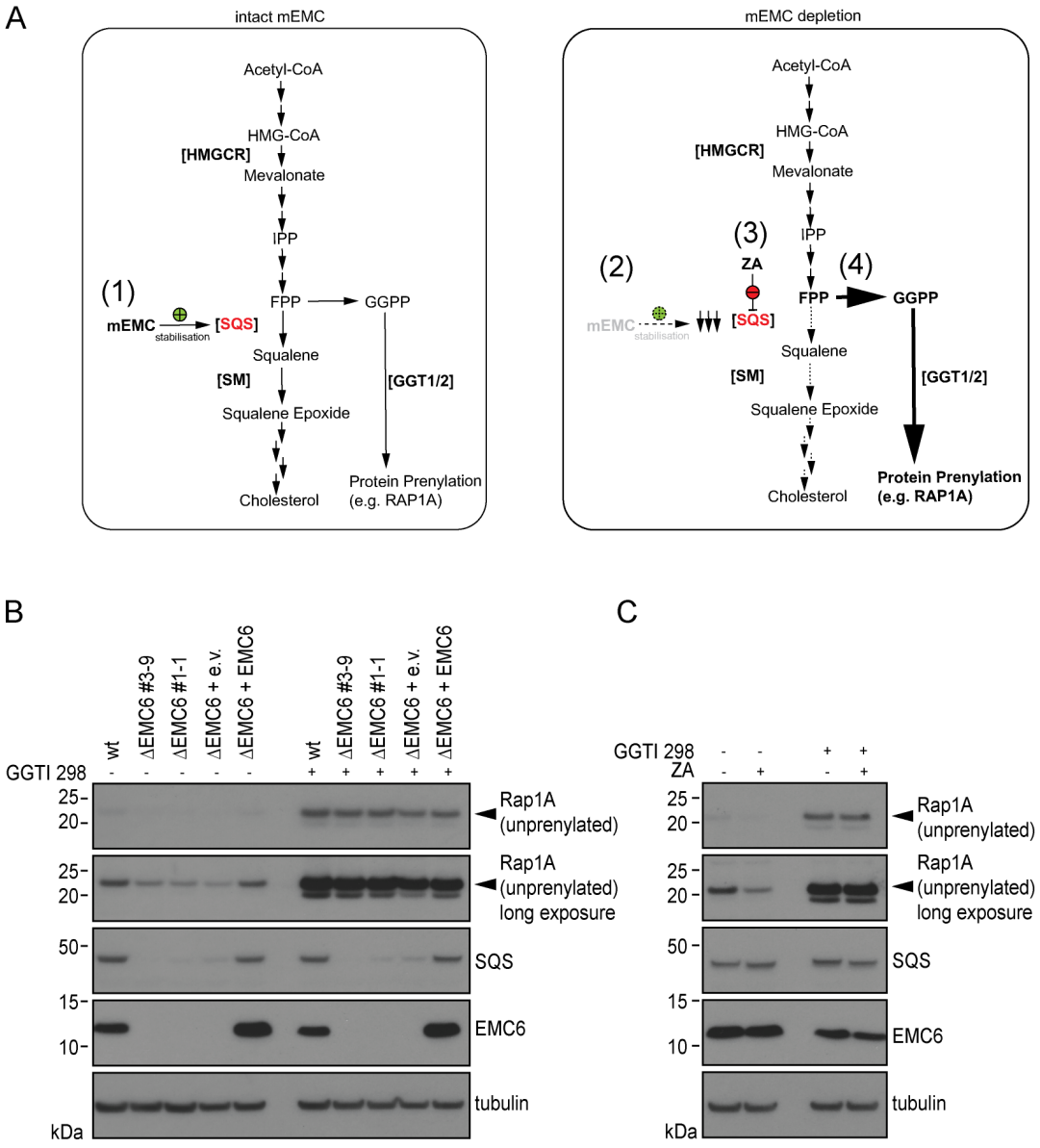


Figure 9.6: Prenylation of Rap1a is increased in EMC6 knockout cells. A. Schematic representation of knock-on effects caused by SQS perturbation. In wild type cells, farnesyl-diphosphate (FPP), the end product of the mevalonate pathway, can either be converted to squalene and therefore committed to sterol biosynthesis, or be shunted into protein prenylation pathways (geranylgeranylation or farnesylation). The mEMC contributes to the sterol biosynthesis branch by facilitating SQS biogenesis (1). If SQS protein levels are decreased in the absence of the mEMC (2) or its activity is impaired by zaragozic acid A (ZA) (3), FPP cannot be efficiently converted to squalene and is increasingly diverted into geranylgeranyl-diphosphate (GGPP) synthesis, a precursor for protein geranylgeranylation. Rap1a is known to be prenylated by geranylgeranyl transferases (GGT1/2). **B.** Rap1a prenylation is increased in ΔEMC6 cells. U2OS Flp-In cells were grown in 1 ng/ml doxycycline for 24 hours. The cells were then incubated with 25 μM GGTI 298 for 4.5 hours. Whole-cell lysates were separated on a gel and further processed by immunoblotting. An antibody specifically recognizing the unprenylated form of Rap1a was used. **C.** SQS inhibition enhances Rap1a prenylation. U2OS Flp-In cells were treated as in (B) and incubated with ZA or DMSO (vehicle control) for 4 hours. Where indicated, 25 μM GGTI 298 or DMSO were added for 30 minutes before addition of 10 μM ZA, and both compounds were present over the course of the 4 hour treatment. e.v., empty vector; GGT1/2, geranylgeranyl transferase 1/2; HMGCR, hydroxymethylglutaryl-CoA reductase; IPP, isopentenyl diphosphate; FPP, farnesyl diphosphate; GGP, geranylgeranyl diphosphate; SM, squalene monooxygenase; ZA, zaragozic acid A.

9.2.4 Lack of the mEMC correlates with increased levels of squalene monooxygenase (SM)

With evidence of increased FPP shunting into protein prenylation pathways in ΔEMC6 cells (**Section 9.2.3**), I investigated whether enzymes whose abundance is regulated by cholesterol or its intermediates might be affected by reduced SQS levels. SM converts squalene to squalene-2,3-epoxide and is therefore located directly downstream of SQS in the reaction sequence of cholesterol biosynthesis. Similar to other enzymes of the pathway, SM is subjected to stringent transcriptional and post-translational regulation [458]. In yeast, inhibition of the SQS orthologue ERG9 by ZA leads to increased steady-state levels and post-translational stabilization of ERG1, the yeast orthologue of SM [196]. Therefore, the effect of reduced SQS levels on SM in mEMC-deficient cells was examined. Immunoblotting of SM in ΔEMC5 and ΔEMC6 U2OS Flp-In cells revealed higher basal levels of SM when compared to wild-type cells (**Figure 9.7 A/B**). Elevated SM was reduced back to basal levels when the mEMC (and thereby SQS) was restored (**Figure 9.7 C**). When ΔEMC5 cells were stably reconstituted with EMC5 (+Dox, 24 hours) SM levels decreased (**Figure 9.7 C**). This reduction correlated inversely with the overall amount of EMC5 and SQS. It should be noted that the minute amounts of EMC5 at 0 hours, resulting from leaky expression in ΔEMC5 + EMC5 cells (**Figure 9.7 C**, see long exposure of EMC5), were already sufficient to partially stabilise SQS and lower SM levels. This finding has also been recapitulated with another reconstituted ΔEMC5 clone (not shown).

In summary, here it has been demonstrated that SQS and SM levels are inversely correlated in mEMC-deficient cells. This finding implies an autoregulatory feedback mechanism to compensate for the partial loss of SQS by upregulating downstream enzymes and thereby increasing metabolic flux through the sterol biosynthesis pathway.

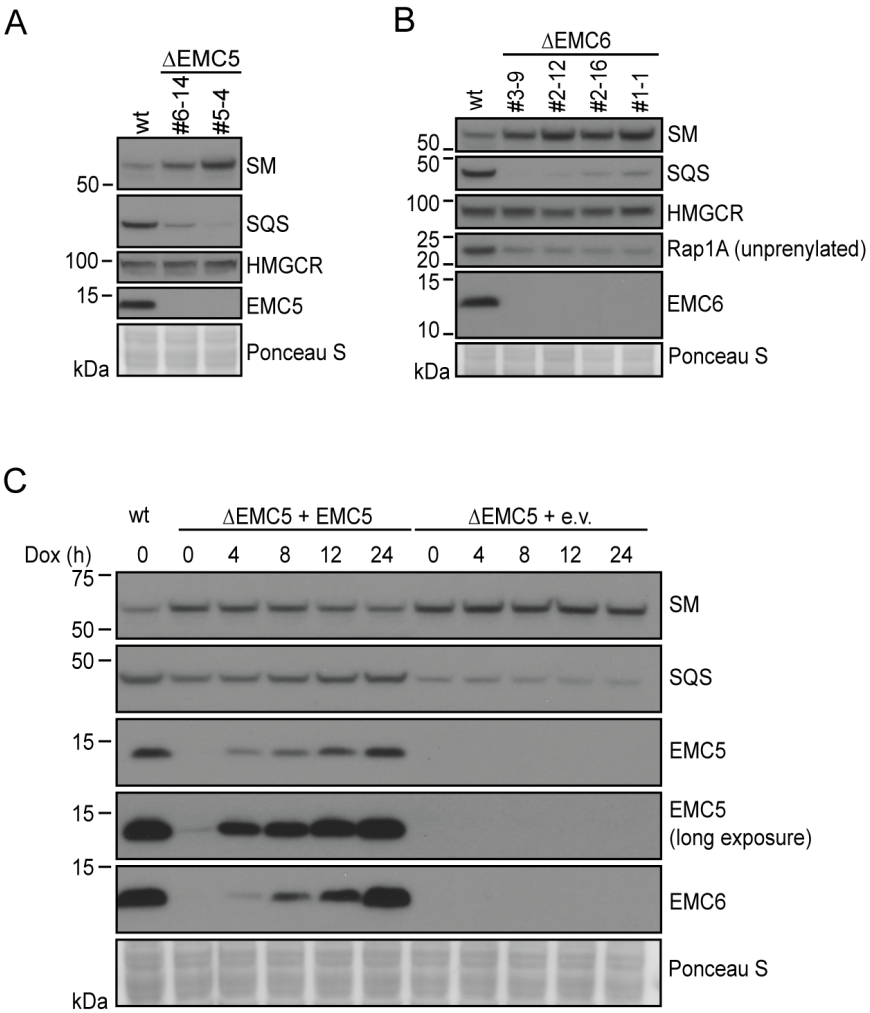


Figure 9.7: SM is increased in mEMC-deficient cells. A. Knockout of EMC5 in U2OS Flp-In cells increases SM. Whole-cell lysate of cells growing in replete conditions (DMEM + 10% FCS) were subjected to immunoblotting. Two independent ΔEMC5 clones are shown. **B.** ΔEMC6 U2OS Flp-In cells exhibit elevates SM protein levels. Cells were grown as described in (A) and whole-cell lysates separated on a gel. **C.** EMC5 expression in ΔEMC5 U2OS Flp-In cells reverses SM accumulation. ΔEMC5 cells stably expressing doxycycline-inducible EMC5 (ΔEMC5 + EMC5) or an empty-vector control (ΔEMC5 + e.v.), were induced with 100 ng/ml Dox for the indicated time. Whole-cell extract was separated by SDS-PAGE. Dox, doxycycline; HMGCR, hydroxymethylglutaryl-CoA reductase; SM, squalene monooxygenase.

Chapter 10

Newly synthesized SQS is destabilized in mEMC-deficient cells

The underlying mechanisms of post-translational regulation of cholesterogenic enzymes are still not fully delineated. In this regard, the elucidation of their degradation pathways has heavily focussed on the two rate-limiting enzymes of sterol biogenesis, HMGCR, and SM [261]. Both are polytopic, ER-resident membrane proteins, whose turnover is regulated in a sterol-dependent manner by E3 ligases within the same compartment [261]. In contrast, post-translational regulation of SQS has been understudied up to now, despite detailed knowledge of its localization [419], catalytic mechanism [266], transcriptional regulation [453], and molecular structure [428]. Unlike HMGCR and SM, SQS is a TA protein [459], and is likely to be targeted to and inserted in the ER membrane post-translationally. Although speculative, its unique topology and role as a potential regulator of FPP flux into protein prenylation pathways, might be reflected in distinctive post-transcriptional control of its protein levels.

10.1 Post-transcriptional downregulation of SQS upon mEMC deficiency

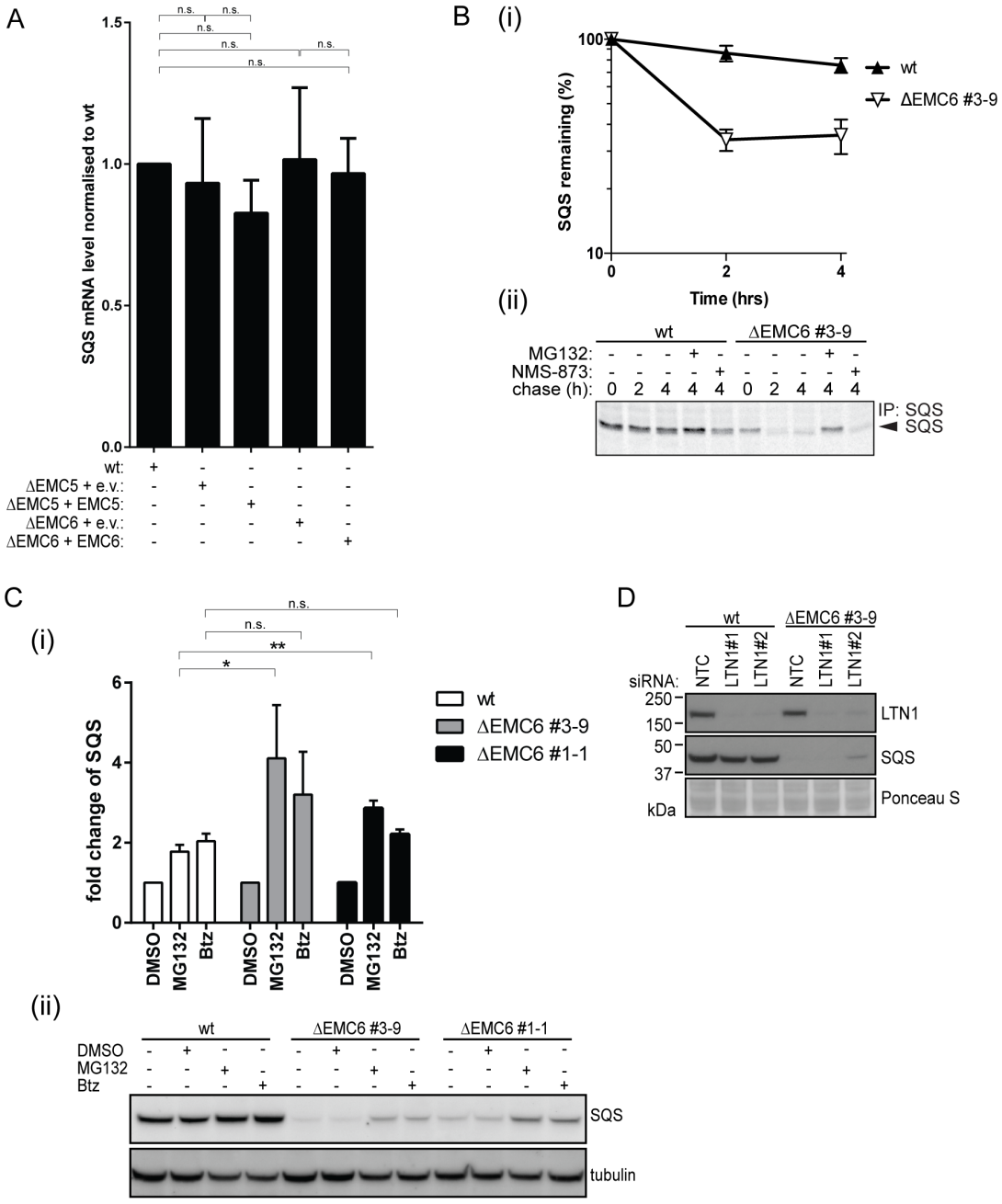
Chapter 9 demonstrated that the steady-state levels of SQS were significantly reduced in mEMC-deficient cells, and that co-depletion of this enzyme affected the steroid *de novo* biosynthesis pathway. Moreover, it was shown that the reduction of SQS was reversible and closely tracked EMC5 and EMC6 protein levels (**Section 9.1.2**, and **Section 9.2.4**). Here, the

molecular mechanism underlying the functional relationship between the mEMC and SQS is investigated.

10.1.1 *De novo*-synthesized SQS is destabilized in EMC6 knockout cells

Since the SREBP pathway strictly regulates SQS transcription [428], I first tested whether reduced protein levels were due to translational attenuation in the absence of the mEMC. SQS transcript levels were measured by qPCR in ΔEMC5, ΔEMC6, and mEMC-reconstituted cells. SQS mRNA levels were near those of wild type in ΔEMC5 (-6.7%) and ΔEMC6 (+1.6%) cells reconstituted with an empty vector (**Figure 10.1 A**). mEMC-reconstituted ΔEMC5 cells (+EMC5) exhibited SQS levels that were moderately decreased (-17.3% *versus* wild-type), whereas reconstituted ΔEMC6 cells (+EMC6) had near wild-type levels (-3%) (**Figure 10.1 A**). These data indicate that the loss of the mEMC does not adversely impact SQS mRNA levels, and point to a model where SQS reduction is due to post-translational events. To test this hypothesis, the stability of SQS in ΔEMC6 and wild-type cells was compared by radiolabel pulse-chase experiments. Wild-type and ΔEMC6 cells were labelled by ^{35}S-Met/Cys and chased for 4 hours. Immunoprecipitated SQS was separated by SDS-PAGE and the appropriate bands subsequently quantified to determine half-lives. SQS exhibited an increased rate of degradation in ΔEMC6 cells compared to wild type (**Figure 10.1 B (i)**). SQS degradation could be stabilized by MG-132 (10 μg/ml), but not with the VCP/p97 inhibitor NMS-873 (**Figure 10.1 B (ii)**). Accelerated SQS degradation was also observed in ΔEMC5 cells (not shown). These results could partially be recapitulated by measuring the increase of total cellular amounts of SQS in two ΔEMC6 cell lines treated with with MG-132 (#3-9, 4.1-fold; #1-1, 2.9-fold) compared to wild type (1.8 fold) (**Figure 10.1 C (i)**). In contrast, for reasons unknown, SQS was not rescued by the proteasome inhibitor bortezomib (Btz) in this assay, (**Figure 10.1 C (i)**). It is worth mentioning that steady-state SQS levels were very low in ΔEMC6 cell lines, and that MG-132 treatment only resulted in a partial rescue (**Figure 10.1 C (ii)**). Similarly, for the pulse-chase experiments described above, SQS levels in ΔEMC6 cells at t = 0 were lower than those of wild-type cells. To test whether there was a decrease in the rate of SQS translation, incorporation of ^{35}S-Met/Cys into SQS in ΔEMC6 cells was assessed by labelling for different durations (10, 20, and 30 minutes). A preliminary experiment revealed that incorporation rates in ΔEMC6 cells were comparable to those in wild type cells (**Supplemental Figure 18.16**). Another plausible explanation for reduced SQS levels in ΔEMC6 cells at t = 0 could be rapid co-translational degradation of nascent

SQS from the ribosome. In yeast, the RING finger domain-type E3 ligase Listerin (LTN1) is implicated in the ubiquitination and subsequent degradation of stalled translation products [460]. To test whether nascent SQS might be subject to this type of degradation, the human LTN1 homologue was knocked down in ΔEMC6 cells. However, despite efficient knockdown of LTN1, wild-type equivalent levels of SQS could not be restored in ΔEMC6 cells, rendering co-translational LTN1-mediated degradation unlikely (**Figure 10.1 D**). In summary, here it has been demonstrated that *de novo* synthesized SQS was unstable without the mEMC and was degraded in a proteasome-dependent manner.



See next page for Figure legend.

10.2 SQS is an ER-localized membrane protein

SQS is predicted to have TA protein topology, spanning the ER membrane via a single C-terminal TMD [54]. The N-terminal catalytic domain has been crystallized previously [430], and expression of a truncated variant of SQS lacking the TMD clearly shows it to be essential for membrane integration [461]. Moreover, SQS was exclusively found to be localized to the ER [462], [419], [429]. To validate SQS localization in U2OS Flp-In cells, an N-terminally epitope-tagged variant of SQS, FLAG:HA:SQS, was transiently co-expressed with an ER-targeted form of mCherry (ER-mCherry). SQS was visualized in fixed cells using an anti-HA antibody. Confocal microscopy confirmed extensive overlap of SQS and mCherry, reminiscent of an ER pattern (**Figure 10.2 A**). To demonstrate that SQS is a *bona fide* integral membrane protein, subcellular fractionation into cytosolic and membrane fractions was performed. As shown in **Figure 10.2 B**, the majority of SQS was found in the membrane-bound fraction (M). However, small amounts of SQS could also be detected in the cytosolic fraction (C), possibly representing SQS that was in the process of being post-translationally targeted to the ER membrane, or which had been extracted from the membrane for degradation. Sucrose gradient sedimentation was performed to interrogate whether SQS oligomerizes or forms higher molecular weight complexes. SQS exhibited a sedimentation pattern reminiscent of a protein of approximately 150 - 200 kDa (**Figure 10.2 C**). Since the native molecular weight of SQS is 48

Figure 10.1 ***(previous page)*****: *De novo*-synthesized SQS was destabilized in EMC6 knockout cells.A.** Transcript levels of SQS in mEMC-deficient cells were not significantly altered. qPCR analysis of SQS mRNA levels. ΔEMC5, and ΔEMC6 U2OS Flp-In cells were reconstituted with either an empty vector control (e.v.), EMC5, or EMC6. Expression of EMC5/6 was induced with 1 ng/ml doxycycline for 24 hours. SQS mRNA levels were quantified by qPCR and normalized to the wild-type (wt) control. Three independent experiments (n = 3) are shown. Statistics are based on Student's t-test. n.s., not significant. **B.** SQS shows faster degradation kinetics in ΔEMC6 U2OS Flp-In cells. Cells were starved for 10 minutes before ^{32}S-labelling for an additional 10 minutes. Cycloheximide was added for the indicated periods of time. Endogenous SQS was then co-immunoprecipitated (IP) using a specific anti-SQS antibody, and visualized by phosphoimaging. (i): Line graph showing remaining SQS over 0 - 4 hours of cycloheximide treatment in three independent experiments (n = 3). The amount of SQS was normalized to that in the absence of cycloheximide (0 h time point). Error bars are S.D.. A representative pulse-chase experiment performed as in (i) is shown in (ii). Where indicated, cells were additionally treated with 10 μg/ml MG-132, or the VCP inhibitor NMS-873 (10 μM). Pulse-chase experiments were performed with the help of John C. Christianson. **C.** Proteasome inhibition partially restores SQS in ΔEMC6 U2OS Flp-In cells. Four million cells per 10 cm tissue culture plate were seeded. After 24 hours, the cells were treated with DMSO (vehicle control), 10 μg/ml MG132, or 25 nM bortezomib (Btz), for 6 hours. The absolute levels of SQS were determined by densitometry using an AlexaFluor-488 conjugated secondary antibody (i). Each sample was internally normalized to tubulin, to account for loading differences, and then converted to fold-increase when compared with SQS levels in DMSO-treated cells. Mean values of three independent experiments (n = 3) and error bars (S.D.) are shown. Statistical significance was evaluated by Students t-test. A representative immunoblot is shown in (ii). *, $p \leq 0.05$; **, $p \leq 0.01$; n.s., not significant; Btz, bortezomib. **D.** Knockdown of LTN1 does not rescue SQS in ΔEMC6 cells. LTN was depleted for 72 hours using two different LTN1-specific siRNAs (LTN1#1/2).

kDa, it is possible that SQS could be part of larger complexes. The sedimentation behaviour of SM was similar to that of SQS (**Figure 10.2 D**). A confounding factor in this type of protein complex analysis could be the use of the mild detergent LMNG, which forms relatively large micelles, potentially affecting the sedimentation pattern of TM proteins including SQS and SM (please refer to **Section 11.2.2** for further discussion). Separation of cellular protein extracts by gel filtration would be required to more accurately determine the size and stoichiometry of such putative SQS complexes. In conclusion, the subcellular localization of SQS in U2OS Flp-In cells is consistent with that of an ER-localized integral membrane protein.

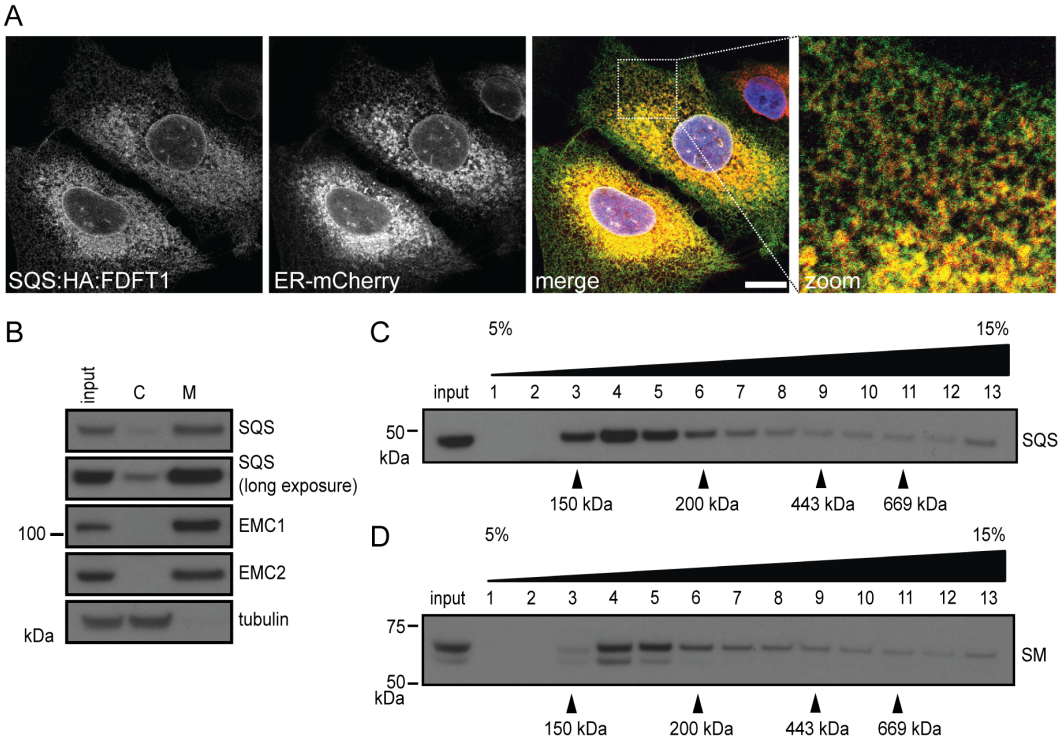


Figure 10.2: SQS is an ER-localized TM protein. A. SQS co-localizes with ER-mCherry. 3.5×10^5 U2OS Flp-In cells were co-transfected with 0.5 μg FLAG:HA:SQS and 1 μg ER-mCherry. After 24 hours, cells were seeded onto coverslips in the presence of 100 ng/ml Dox and cultured for an additional 24 hours. Cells were fixed with 4% paraformaldehyde. FLAG:HA:SQS was stained with an anti-HA antibody and visualized by confocal microscopy. Nuclei were stained by DAPI (blue). Scale bar = 10 μM. **B.** SQS is membrane-bound. Subcellular fractionation into cytoplasmic (C) and membrane (M) fractions was performed with U2OS Flp-In cells. Cells were lysed by hypotonic shock and cytoplasmic and subcellular fractions were purified by ultracentrifugation. Equivalent amounts of M and C fractions were subjected to SDS-PAGE analysis. EMC1, and EMC2, serve as positive controls for the membrane fraction (EMC2 is a cytosolic protein bound to a TM protein complex, the mEMC). Tubulin was used as a cytoplasmic marker. **C.** SQS sediments between 150 and 200 kDa under mild detergent conditions. U2OS Flp-In whole-cell lysate was isolated by lysis with 1% LMNG and was subsequently separated on a 5 - 15% sucrose gradient. 13 fractions were collected. **D.** SM shows a similar sedimentation pattern to SQS. Samples were prepared as described in (C).

10.3 SQS biogenesis is sensitive to disruption of components of the GET/TRC40 pathway

The prominent topological feature shared by all TA proteins is their single C-terminal TMD [73], [463]. Since the TMD of TA proteins is synthesized last, co-translational integration into the membrane bilayer via the SRP is not possible. Therefore, a variety of TA proteins (but not all) utilize the GET/TRC40 pathway for correct membrane insertion [55] (**Section 1.3.2**).

SQS is anchored to the ER membrane by integration of its C-terminal TMD (aa 384 - 404) and is predicted to expose 13 amino acids (aa 405 - 417) to the ER lumen [459], [434], (**Figure 10.3 A**). Given its activity, the large catalytic domain is expected to be oriented towards the cytoplasm. Currently, our knowledge of the factors mediating SQS biogenesis (including insertion into the ER) is limited. Mistargeted TM proteins, or proteins containing long hydrophobic stretches, are prone to aggregation and/or degradation [53]. Therefore, it was investigated whether the co-depletion of SQS (and its destabilization) in mEMC-deficient cells might be an expression of its mistargeting. Steady-state SQS levels were measured in cells where the GET pathway was targeted by siRNA-mediated depletion of Bag6, and TRC40 (**Figure 10.3 B**). Reducing TRC40 levels, but not Bag6, coincided with a decrease of SQS by 45.9 % (**Figure 10.3 C**). Assuming that SQS is a TRC40 client, it is possible that, with insufficient TRC40 levels, SQS cannot be targeted to the ER membrane and thus becomes a substrate for UPS-dependent degradation (for a discussion of SQS as a putative TRC40 client, please refer to **Section 11.2.3**). Consistent with this, TRC40 depletion can prevent targeting and instead shunt proteins containing long hydrophobic domains into Bag6-dependent degradation pathways [53], [108]. Failure of Bag6 depletion to reduce SQS could indicate that the residual Bag6 levels are sufficient to mediate efficient SQS biogenesis, consistent with reports that Bag6 also performs GET/TRC40-independent functions [464].

Given TRC40s apparent influence on SQS expression, it was next tested whether the GET/TRC40 pathway was altered by mEMC depletion. GET pathway impairment would result in mislocalization of TA proteins and potentially decrease their steady-state levels [53]). Levels of Bag6, TRC40, and of the TA proteins Ube2j1 [58], [54], and Sec61β [75], [54] were quantified in ΔEMC5 and ΔEMC6 cells (**Figure 10.3 D/E**). Bag6 levels were not significantly affected in three of four cell lines tested, with the exception of ΔEMC5 #6-14, where a significant decrease (-14.1%) was observed. TRC40 was consistently reduced in all cells lacking the mEMC (ΔEMC5: -27.2% and -34.3%, ΔEMC6: -22.9% and -11.1%). Neither Sec61β nor Ube2j1 showed consistent trends.

In this section, evidence is presented for a role of TRC40, a targeting factor within the GET/TRC40 pathway, in SQS biogenesis. Steady-state TRC40 levels were reduced in cells missing either EMC5 or EMC6, and hence the mEMC. It is not yet clear whether TRC40 plays a role in SQS biogenesis, stability, or localization, or whether its influence is direct (e.g. by mislocalization and degradation), or indirect. In addition to the role of TRC40, the involvement of the remaining GET/TRC40 pathway components, such as CAML and WRB, in SQS biogenesis remains to be clarified. Finally, the variability of the effects of EMC5 or EMC6 loss on Sec61β and Ube2j1 prevents a broader conclusion being made regarding the involvement of the mEMC in general TA protein biogenesis.

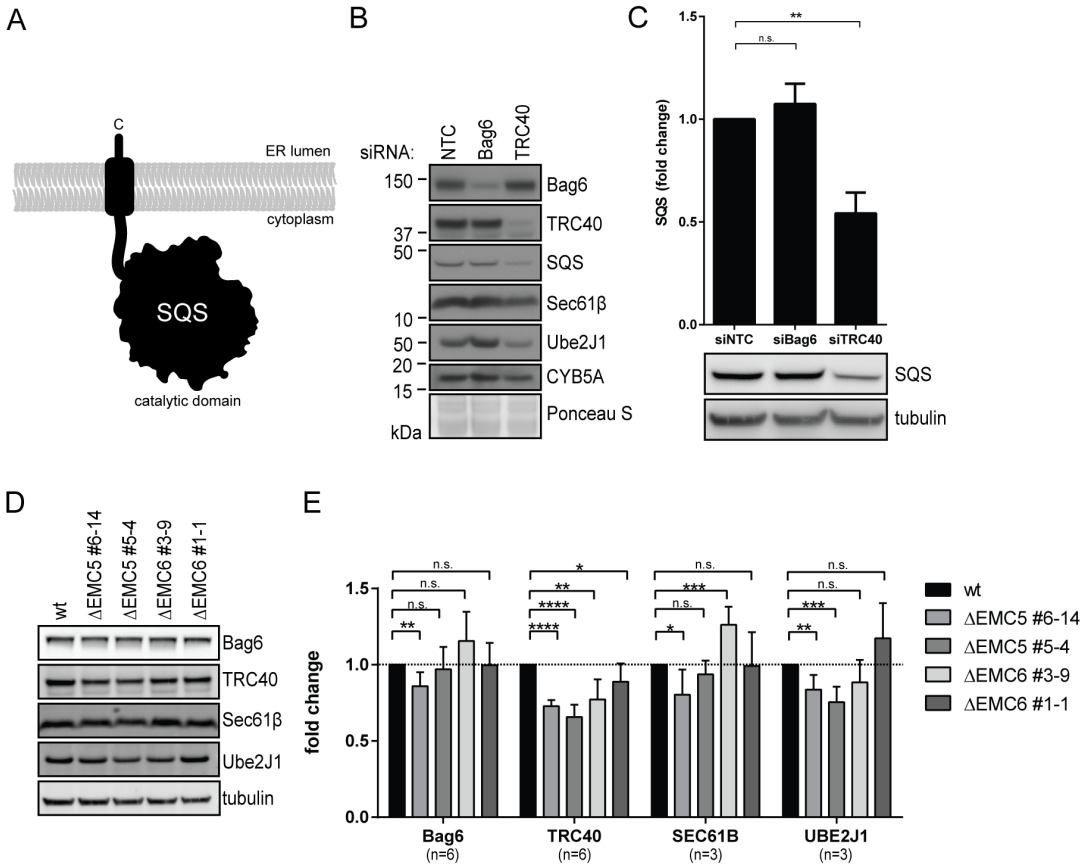


Figure 10.3: SQS biogenesis was affected by depleting components of the GET pathway. **A.** Schematic representation of SQS topology. SQS possesses a single, C-terminal TMD (aa 388 - 404), with 13 residues predicted to be exposed to the ER lumen. The catalytic centre is contained within the large cytoplasmic domain (aa 1 - 383), which is entirely composed of α helices. **B.** Co-depletion of SQS by knockdown of GET-pathway components. Bag6 and TRC40 were depleted from U2OS Flp-In cells by siRNA-mediated knockdown for 72 hours. Non-targeting siRNA (siNTC) served as a negative control. Whole-cell extracts were subjected to immunoblotting. Sec61β, Ube2J1, and CYB5A were used to interrogate the effect of GET pathway disruption on other TA proteins. **C.** Quantification of SQS co-depletion. Cells were treated as in (B). Immunoblotting was performed and SQS was quantified after detection with AlexaFluor 488-conjugated secondary antibodies. The bar graph represents three independent experiments (n = 3) performed as described in. Absolute amounts of SQS were normalized to tubulin (internal standard) and represented as fold change compared to siNTC transfected cells. Mean values and error bars (S.D.) are indicated. Statistical significance was evaluated by Student's t-test. **, $p \leq 0.01$; n.s., not significant. **D.** The steady-state levels of TRC40 are decreased in ΔEMC5 and ΔEMC6 cells. Whole-cell lysates from ΔEMC5 and ΔEMC6 U2OS Flp-In cells was separated by SDS-PAGE and immunoblotting was performed for TRC40, Bag6, Sec61β, and Ube2J1 using specific antibodies. **E.** Densitometric quantification of GET pathway components and of tail-anchored proteins in mEMC-deficient cells. Experiments were performed as delineated in (D). For quantification, AlexaFluor 488-conjugated secondary antibodies were used. Bar graphs show mean values of 3 - 6 independent experiments (n = 3 $\leq$ 6) normalized to wild-type. Error bars represent S.D. Student's t-test was used for statistical analysis. *, $p \leq 0.05$; **, $p \leq 0.01$; ***, $p \leq 0.001$; ****, $p \leq 0.0001$; n.s., not significant. NTC, non-targeting control; TMD, transmembrane domain.

10.4 The mEMC and SQS do not form a stable complex

In **Sections 9.1** and **10.1.1**, evidence has been provided of an involvement of the mEMC in SQS biogenesis. Since both the mEMC and SQS are ER-resident, it was investigated whether both factors were interacting to form a stable complex. Epitope-tagged SQS was expressed in U2OS Flp-In cells and affinity purified under low stringency lysis conditions (1% LMNG) to enrich for transient or weaker interactions. Under these conditions, the mEMC did not co-purify with epitope-tagged SQS (**Figure 10.4 A**). Likewise, physical interaction between SQS and the mEMC seems unlikely under the conditions tested, as the majority of SQS sedimented in fractions 3 - 5 on sucrose gradients (5 - 15%), whereas the mEMC was found in fractions 7 - 9 (**Figure 10.2 C** and **Figure 5.2**). This suggests that the mEMC and SQS do not constitute a stable complex under steady-state conditions. Nevertheless, it cannot be rule out that the lysis conditions might not preserve interactions of a transient mEMC-SQS complex (see also **Section 11.2**).

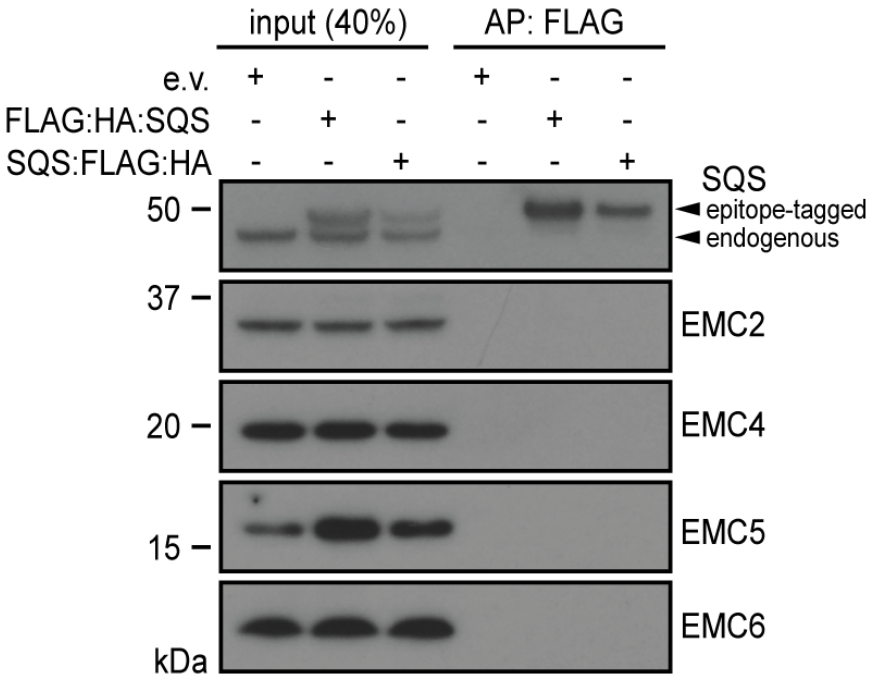


Figure 10.4: SQS and the mEMC did not form a stable complex. N-terminally or C-terminally epitope-tagged variants of SQS (FLAG:HA:SQS and SQS:FLAG:HA) were stably introduced into U2OS Flp-In cells and expression was induced with 100 ng/ml Dox for 24 hours. SQS was affinity-purified (AP) by the FLAG-tag from whole-cell extracts under mild lysis conditions (1% LMNG) to preserve weak interactions.

10.5 mEMC-deficient cells do not accumulate SQS cleavage intermediates

The ER-resident TA protein haem oxygenase-1 (HO-1) is proteolytically processed by SPP [58]. An intramembrane cleavage event might facilitate the release of the cytoplasmic domain, and could represent a general principle for TA protein degradation. To interrogate whether SQS cleavage occurred in mEMC-deficient cells, resulting in epitope loss, N- and C-terminally tagged SQS variants were expressed in wild-type and ΔEMC6 cells. To stabilize potential degradation intermediates, cells were concomitantly treated with MG-132 (5 μg/ml, 4 hours). SQS was detected from whole-cell lysate by anti-HA or anti-SQS recognizing an N-terminal epitope within its first 255 amino acids. This approach enabled detection of both putative N- and C-terminal cleavage fragments. As shown in **Figure 10.5**, both tagged variants of SQS expressed at lower levels in ΔEMC6 cells when compared wild-type cells, potentially reflecting a requirement for the mEMC in SQS biosynthesis. Additionally, proteasome inhibition led to an accumulation of lower molecular weight forms in wild-type and EMC6-deficient cells (denoted as 'a' and 'b' in **Figure 10.5**). The low molecular weight form 'b' was not recognized by the anti-HA antibody, but was immunoreactive with the SQS-specific antibody. This indicates loss of the C-terminal FLAG:HA epitope, possibly by proteolytic cleavage. However, a putative C-terminal cleavage fragment could not be detected. As the occurrence of these lower molecular weight variants of SQS was mEMC-independent, they are likely to reflect aspects of SQS biology that do not necessitate the presence of this complex.

Despite failing to detect additional cleavage fragments in mEMC-deficient cells, degradation intermediates might be difficult to detect due their size, and potential PTMs such as ubiquitination. Further study is required to fully rule out this hypothesis. If mEMC loss renders SQS a substrate for intramembrane proteases, pharmacological inhibition of SPP and other proteases might be a worthwhile attempt to restore SQS levels in these cells.

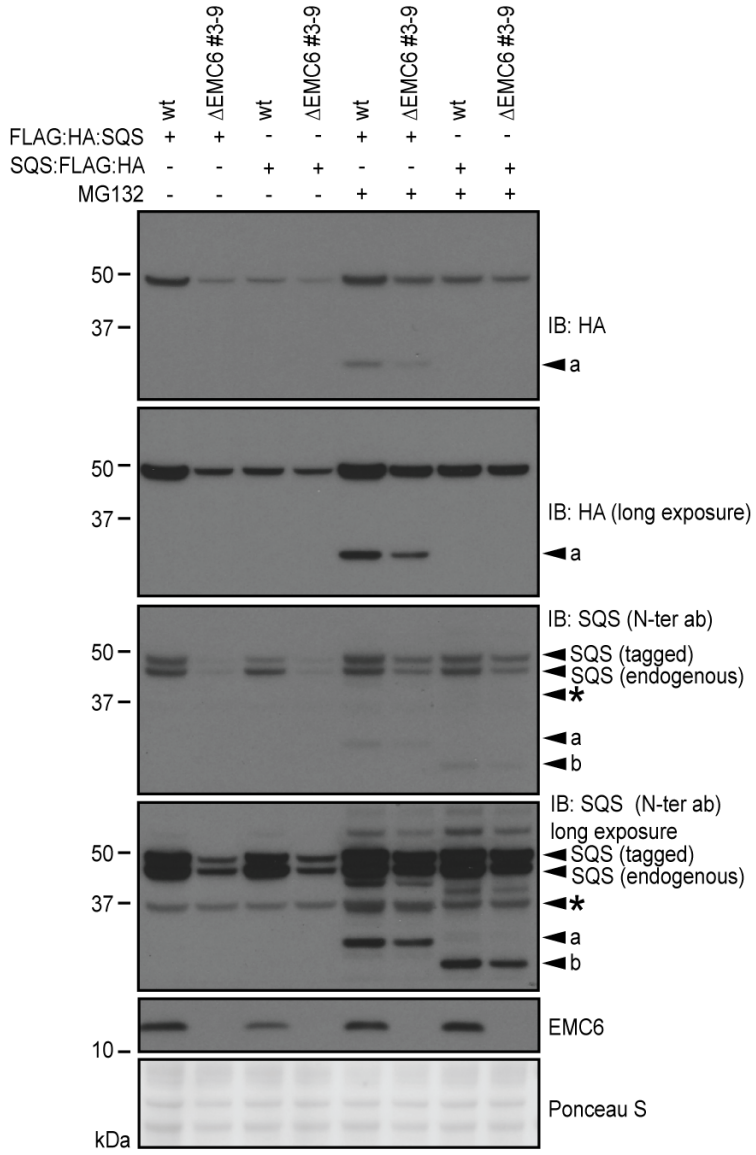


Figure 10.5: mEMC-deficient cells did not accumulate SQS cleavage intermediates. ΔEMC6 U2OS Flp-In cells were reconstituted with FLAG:HA:SQS or SQS:FLAG:HA, and expression of the transgene was induced with 100 ng/ml Dox for 24 hours before addition of 5 μg/ml MG-132 for 4 hours. Whole-cell extracts were isolated and separated on a 4 - 12% gradient gel. Additional bands could be detected in MG-132 treated cells (a, b). Unspecific bands are marked by an asterisk (*).

Chapter 11

Conclusions and working model

The data presented in this study support the following conclusions:

(1) The biogenesis and assembly of individual EMC proteins are interdependent. CRISPR/Cas9-mediated deletion or RNAi-mediated downregulation of five EMC proteins (EMC1 - 3/5/6) caused marked co-dependent reduction of the remaining mEMC subunits. In contrast, depletion of EMC4 or EMC7 - 10 had a relatively mild impact on the steady-state levels of other EMC proteins.

Based on these findings, I suggest a hierarchy of 'primary' and 'secondary' subunits that enable mEMC biogenesis (**Figure 11.1 A, B**). Co-dependent degradation of EMC5 in ΔEMC6 cells occurred in a UPS-dependent manner. Moreover, residual EMC2 in ΔEMC5 and ΔEMC6 cells was also destabilized. Deletion of either EMC5 or EMC6 led to the most pronounced mEMC biogenesis defect, giving rise to cells that were virtually deficient of the mature complex. EMC2 depletion had similar repercussions for mEMC assembly, but in these cells EMC5 and EMC6 formed a sub-complex, which is likely to be a dead-end assembly intermediate. These observations indicate a crucial role for EMC5 and EMC6 in mEMC biogenesis (**Figure 11.1 B**). Notably, exogenous expression of EMC6 in ΔEMC5 cells did not restore the mEMC, indicating a defined assembly process and essential subunits for the mEMC. Intriguingly, knockdown of EMC8 caused increased steady-state levels of its close homologue, EMC9, potentially replacing the lost subunit. These results demonstrate that the formation of the mEMC involves a remarkable degree of coordination between individual subunits and, potentially, other accessory factors.

(2) The mEMC supports SQS biogenesis in U2OS cells. mEMC-deficient cells showed reduced steady-state levels of SQS. Consistent with the mEMC functioning as a maturation/stabilization factor, *de novo*-synthesized SQS was unstable in ΔEMC6 cells. However,

physical association between the mEMC and SQS could not be observed. Therefore, it is conceivable that the mEMC facilitates SQS biogenesis, and/or stability indirectly *via* an intermediate factor, by an as yet unidentified activity, or directly *via* transient interactions, the detection of which would require complex stabilisation i.e. by a protein cross-linking approach (**Figure 11.1 C (i)**). As a TA protein, SQS is likely to be post-translationally targeted and inserted into the ER membrane. The mEMC might promote efficient targeting and/or insertion of SQS into the lipid bilayer. Reduced mEMC activity could lead to mislocalization of newly synthesized SQS, and consequently to its degradation by the UPS (**Figure 11.1 C (ii)**). SQS catalyses the committing step in the cholesterol biosynthesis pathway. Phenotypes associated with impaired SQS activity correlated with mEMC disruption. Specifically, sensitization and impaired viability by depleting cholesterol in cells lacking SQS activity was phenocopied by mEMC depletion *via* loss of EMC6. Like suppressing SQS activity, deletion of EMC6 led to elevated Rap1a prenylation, likely due to the increased availability of FPP for GGPP biosynthesis. Despite compromising SQS capabilities, the total cholesterol content in mEMC-deficient (and ΔSQS) cells was comparable to that in wild-type cells, implying complex compensatory mechanisms controlling cellular cholesterol import.

(3) Based on quantitative mass-spectrometry, loss of either EMC5 or EMC6, affected the abundance of a subpopulation of intracellular and cell surface proteins (**Figure 11.1 D**).

In summary, these data support a model wherein the mEMC is involved the biogenesis of a variety of proteins in the ER.

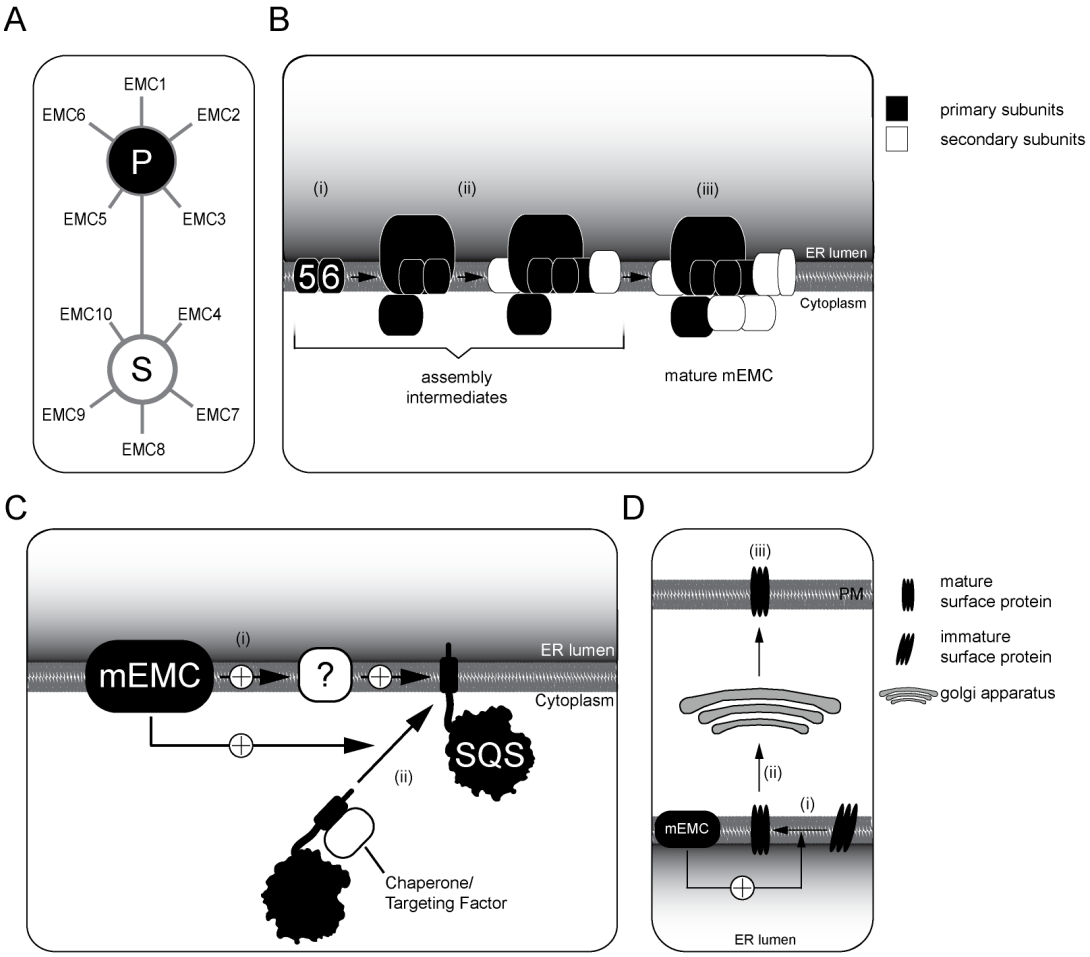


Figure 11.1: Working model. A. Subunit hierarchy in mEMC biogenesis. Depletion of a subset of EMC proteins (EMC1 - 3/5/6) severely impaired the formation of the mature complex, and are referred to as 'primary subunits' (P). In contrast, knockdown of the 'secondary subunits' (S) EMC4/7 - 10 had a more moderate effect on the steady-state levels of the mEMC. **B.** This distinction of primary and secondary subunits likely reflects their role in stabilizing complex assembly intermediates. EMC5 and EMC6 (indicated) might be of particular importance at early steps of mEMC assembly. According to this hypothesis, EMC5/6 act as a 'nucleation core' for the remaining subunits (i). Primary subunits (black) might be recruited first, whereas secondary subunits (white) join later, forming distinct, unstable assembly intermediates (ii), giving rise to the mature, stable mEMC (iii). **C.** The mEMC promotes biogenesis of SQS by an intermediary factor, or by an as yet unrecognized activity (i), stabilizing SQS and preventing its degradation by the UPS. Alternatively, the mEMC might facilitate the correct post-translational targeting/membrane insertion of chaperoned SQS (ii). According to this hypothesis, mEMC loss would lead to SQS mislocalization and degradation. **D.** The mEMC modulates the expression of a subset of PM glycoproteins, potentially by promoting their maturation in the ER (i). Once these mEMC clients acquire their correct conformation/oligomerization state, they are trafficked along the secretory pathway (ii) to the PM (iii).

Part III

Discussion and Perspective

This study has tried to address fundamental and outstanding questions surrounding the mEMC, such as the interrelationships and assembly parameters of its subunits and the molecular function of the mature complex. A clear and striking interdependence of mEMC subunit biogenesis has been demonstrated. This study has confirmed that the endogenous mEMC is comprised of 10 distinct subunits. Importantly, the data suggest that their assembly into the mature mEMC is strictly regulated and occurs via distinct oligomeric complex intermediates. Specific subunits (i.e. EMC2, EMC5, and EMC6) were essential for mEMC formation; cells lacking any one of these formed unstable complex intermediates that severely attenuated mEMC abundance. Altered mEMC abundance impacted the steady-state levels of SQS, an ER-resident, TA protein involved in cholesterol biosynthesis. Accordingly, mEMC deficiency (and loss of SQS) resulted in significantly reduced cell viability under conditions of acute cholesterol starvation. The following sections will critically assess these observations.

11.1 Architecture, biogenesis, and stability of the mEMC

In this study, I have demonstrated that a subset of EMC proteins (EMC1 - 3/5/6) are necessary to maintain the steady-state levels and assembly of other mEMC subunits. Accordingly, a hierarchy of subunits required for mEMC assembly has been determined. When diminished or lost, primary subunits (EMC1 - 3/5/6), caused severe defects in mEMC biogenesis that preclude its assembly. In contrast, depletion of secondary subunits (EMC4/7 - 10) only moderately affected mEMC assembly. This differential impact of mEMC subunit depletion on the integrity of the mature mEMC is consistent with a vectorial assembly process. Therefore, I propose that the consequential destabilization of mEMC subunits that ensues with loss of primary subunits, reflects a severe and irreparable assembly defect (**Figure 6.1 A**). Primary subunits might be crucial for early mEMC assembly steps or required to stabilize later assembly intermediates. Without them, incomplete complexes and unassembled subunits may accumulate and would require rapid disposal to avoid formation of dysfunctional and potentially detrimental mEMC forms. However, the complex pattern of co-dependent degradation of individual subunits has prevented the establishment of a detailed assembly sequence and linkage map for the 10 EMC proteins. Collectively, though, data presented here support several conclusions.

Firstly, I propose that the primary subunits (EMC1 - 3/5/6), are indispensable for the formation of early mEMC assembly intermediates. This is supported by the dramatic depletion of the mEMC upon the loss of any one of these subunits. Transient, intermediate mEMC complexes that may form in their absence remain elusive and are likely to be cleared

by cellular degradation mechanisms. This is strikingly reflected by the UPS-dependent degradation of EMC5 when expressed in ΔEMC6 cells (**Figure 6.2 B**). Similarly, residual EMC2 was destabilized and degraded by the UPS in both ΔEMC5 and Δ EMC6 cells (**Figure 6.2 C**), indicating cooperative stability [465]. However, restoring individual subunit expression in cells lacking EMC5/6 just by inhibiting degradation proved difficult. In an alternative interpretation, some (or all) primary subunits would be required to maintain the mature complex rather than for assembly, perhaps by interacting with hitherto unidentified stabilizing factors (e.g. chaperones) or by regulating post-translational modifications. Finally, interactions with primary subunits could be masking destabilizing degrons, preventing access of degradation factors, or enhancing the thermodynamic stability of the complex [466]. It should be noted that mutual stabilization of individual subunits of hetero- and homo-oligomeric protein complexes is a common phenomenon [466], [467], [465], [173].

Secondly, it appears that some assembly intermediates are more stable than others. CRISPR/Cas9-mediated depletion of EMC2 led to a dramatic disruption of the mature mEMC, but did not entirely deplete the cells of EMC5, EMC6, or EMC10. EMC5 and EMC6 formed a complex under these conditions that did not include EMC10, suggesting a stable EMC5-EMC6 assembly intermediate. In contrast to EMC5 instability in ΔEMC6 cells, exogenous EMC6 could be stably expressed in ΔEMC5 cells (**Figure 6.1 F**). Furthermore, depleting a secondary subunit, EMC4, affected the ability of EMC6 to bind EMC10 and *vice versa* (**Figure 6.4 D**). This was accompanied by a changed EMC10 sedimentation pattern in siEMC4 cells, suggesting that EMC10 was no longer able to assemble (**Figure 6.3 A** and **Figure 6.4 E**). Yet, despite failing to interact with EMC6, EMC4 could still join the complex when EMC10 was knocked down (**Figure 6.3 A** and **Figure 6.4 E**). This suggests that EMC4 and EMC10 are mutually dependent for incorporation into the complex.

Thirdly, mEMC loss from cells was reversible, with complex assembly and reconstitution requiring both EMC5 and EMC6 (**Figure 6.1 F, G**). Among the primary subunits, loss of EMC5/6 was most disruptive to the mEMC (**Figure 6.1 A**). EMC5 and EMC6 are the smallest subunits of the complex (14.7 and 12 kDa, respectively), and a considerable proportion of their structure appears to be buried within the membrane. In protein complexes of the respiratory chain, small subunits serve an important function in the assembly and overall stability of the holo-complex [468], [469]. Hence, it is conceivable that EMC5 and EMC6 represent structural subunits that form the core of the mEMC, around which the other subunits assemble. It would be interesting to investigate which structural features of EMC6 are responsible for the stabilization of the complex. The C-terminal region of EMC6 is conserved with the

last seven amino acids showing the highest degree of sequence conservation (**Supplemental Figure 18.19**). This supports the notion that the C-terminus of EMC6 serves an important structural function and could be an essential contact site for other subunits.

Finally, our observations imply strict post-transcriptional regulation of the mEMC and any assembly intermediates. EMC6 depletion did not attenuate mRNA levels of any of the remaining subunits, while corresponding protein levels were considerably reduced (**Figure 6.2 A**). To fully understand the molecular architecture of the mEMC, purification and *in vitro* reconstitution will be required. Large-scale purification of the complex is favoured due to its extraordinary resistance to high detergent concentrations (1% Triton X-100), but could be compromised by the fact that 7 out of 10 subunits contain TMDs. Additionally, it is not known whether efficient mEMC assembly requires co-factors or chaperones. It is worth noting that, depending on the model organism and experimental readout, depletion of individual EMC subunits did not necessarily produce as severe outcomes as would be predicted by our subunit hierarchy. In this respect, knockdown of EMC1 - 3/4 and EMC6 in *C. elegans* dramatically affected L-AChR biogenesis but depletion of EMC5 had no effect [336]. Similarly, in a yeast model for CFTR-ΔF508 biogenesis, only EMC7 was observed to affect the translation rate of CFTR-ΔF508 [369]. This heterogeneity is at odds with our observation that EMC6 loss is catastrophic for the remaining subunits and precludes assembly. One explanation for this apparent conundrum might be differences in the EMC assembly programme for different model organisms. This view is supported by phylogenetic analyses that show the loss of the EMC5 or EMC6 gene from a number of lineages while retaining other EMC subunits [329]. However, it should be noted that some organismal genomes have not been fully annotated and EMC expression remains to be demonstrated at the protein level. It is also possible that in these organisms one or more mEMC subunits have been functionally replaced by other proteins. Alternatively, the efficacy of transient depletion/knockdown reagents is likely to play a major role in the phenotypic outcome of manipulating EMC protein levels. In this regard, I have observed recovery of SQS expression, with just minute amounts of EMC5 (**Figure 9.7 C**).

The physiological contribution of the EMC on an organismal level is reflected by the loss of viability when subunits are removed. Knockout of EMC3 (dPob) in *D. melanogaster* and *D. rerio* causes lethality during early development [357], [358]. Loss of EMC4 and EMC6 was accompanied by embryonic lethality in *C. elegans* [336], while depletion of EMC1, or EMC2, caused developmental arrest [336]. Of note, homozygous knockout of individual subunits (EMC3, EMC4, EMC6, but not EMC10) is embryonic lethal (International Mouse Phenotyping Consortium: http://www.mousephenotype.org/). These observations stress the importance of

maintaining integrity within the mature EMC.

11.1.1 Examples for co-dependent expression of protein complex subunits

It is not currently clear which processes underlie co-dependent loss of mEMC subunits in cells lacking EMC5 or EMC6. EMC5 and EMC6 may be essential to form the core of the mEMC on which other subunits rely for assembly cues to give rise to the mature mEMC. Alternatively, EMC5/6 might be required to stabilize the mature mEMC and maintain it, and may be entirely dispensable for early stage assembly. Finally, EMC5/6 could play roles in both processes. Co-dependent subunit expression/degradation is common in higher-order complexes, and several relevant examples are discussed below.

11.1.1.1 The MICOS complex

The ancient mitochondrial contact site and cristae organizing system (MICOS) complex is localized at cristae junctions of the inner mitochondrial membrane and is crucial for cristae formation and maintenance [470], [471], [472]. The mammalian 700 kDa MICOS complex contains nine MIC subunits (MIC14/19/25/60, MIC13 (QIL1), MIC10/26/27, and DNAJC11), and is part of the larger (2200 kDa) mitochondrial intermembrane space bridging (MIB) complex [469], [473]. MIC19, MIC25, and MIC60 form a lower molecular weight (450 kDa) subcomplex that serves as a nucleation centre in the assembly of the mature complex [469], [473]. MIC13/QIL1 is the most recently identified subunit of the mammalian MICOS complex [469], [472], [473], [474]. RNAi-mediated QIL1 depletion drives MICOS complex fragmentation, accompanied by the dramatic post-transcriptional co-depletion of several MICOS subunits (MIC10, MIC26, and MIC27) and sub-complex formation [469], [475]. Therefore, it seems that QIL1 connects these three subunits with the core of the MICOS complex (MIC19/25/60). The effect of QIL1 depletion is reversible and steady-state levels of the 'core' components MIC60 and MIC19 are interdependent [372]. Similar to the effects of deleting 'primary' mEMC subunits, knockdown of the core complex component MIC60 causes severe reduction of the MICOS complex [476]. According to the role of the MICOS complex in mitochondrial membrane organization, MIC60 depletion results in the loss of normal cristae morphology [476]. These observations suggest that controlling complex formation and maintenance by one or more individual subunits is a fundamental property of hetero-oligomeric protein assemblies.

11.1.1.2 Cytochrome c oxidase

In the condition Leigh Syndrome, the amount of cytochrome c oxidase (COX) is suppressed due to severe assembly defects of the COX complex [477]. Similar to the putative assembly defect of the mEMC, the mRNA levels of COX subunits are unaffected or increased, while the protein levels of individual subunits are significantly reduced [478]. Functional loss of the COX assembly factor SURF1 (Surfeit 1) has been shown to disrupt COX biogenesis post-translationally [478], [479].

11.1.1.3 The apicomplexa *P. falciparum* CC multi-domain adhesion proteins

Plasmodium falciparum LCCL (Limulus coagulation factor C, cochlear protein Coch-5b2, and late gestation lung protein Lgl1) domain-containing proteins (pfCCp's) are members of a highly conserved protein family within the *apicomplexa* clade. In *P. falciparum*, *pf*CCP1p - 5p and *pf*FNPA form a hetero-oligomeric protein complex (the *pf*CCp complex), which is expressed exclusively during the sexual gametocyte stage of the malaria parasite. The complex is localized to the PM of gametocytes. The function of the *pf*CCp complex is not known, but the presence of multiple lectin-like adhesion domains implies a role in macrogamete cell adhesion during sexual reproduction of the parasite [480]. Intriguingly, reminiscent of the mEMC, the subunits of the *pf*CCp complex show a high degree of co-dependent expression when one or more complex members are lost [481], [482]. The subunits of the *pf*CCp complex also exhibited a certain degree of hierarchy in terms of the extent of co-dependent depletion. Knockout of *pf*CC1p - 3p, leads to loss of the remaining complex subunits, whereas deletion of *pf*CC4p or *pf*FNPA causes only mild depletion of other *pf*CCp's [482]. Notably, as is the case with EMC proteins, co-depletion of *pf*CCp complex subunits is not a result of decreased transcript levels, suggesting post-translational or co-translational regulation [481]. Co-dependent expression has also been confirmed for *P. berghei* LCCL-lectin adhesive-like proteins (*pb*LAPs), the *P. berghei* homologues of *pf*CCp's [483]. Loss of *pb*LAP1p (*pf*CCP1p homologue) concomitantly suppresses GFP fluorescence of a *pb*LAP1p (*pf*CCP3p homologue) - GFP fusion protein (*pb*LAP:GFP), even though expression of *pb*LAP:GFP is unaffected by *pb*LAP3p knockout [484]. Therefore, the authors suggest that the loss of the *pb*LAP:GFP could be explained by a conformational change of GFP, indicative of misfolding of the *pb*LAP3p fusion protein in *pb*LAP1p knockout gametocytes [484]. As the gametocytes progressed to the ookinete developmental stage, the fusion protein was lost when *pb*LAP1 was absent, suggesting removal by

protein quality control systems [484]. In conclusion, the *pf*CCp complex and its homologues (*pb*LAPs) imply some degree of co-stabilization of its subunits, potentially by template-assisted folding.

These three examples demonstrate that co-dependency among protein complex subunits is not unique to the mEMC. They further suggest that multiple molecular mechanisms might contribute to the interdependence of complex components. On the one hand, imposed loss of individual subunits can interfere with the ordered assembly process of protein complexes. Notwithstanding, in some cases, complex subunits which are co-translationally assembled, might be conformationally interdependent and require other subunits to reach their native fold. Both scenarios could be manifest in the same complex and would lead to co-dependent degradation.

11.2 mEMC involvement in SQS biogenesis

SQS is an essential ER-localized enzyme within the cholesterol biosynthesis pathway. Homozygous disruption of the SQS gene in mice causes early embryonic lethality and neural tube closure defects [433], while exogenous expression of SQS in mice enhances cholesterol biosynthesis and leads to hypercholesterolemia [485]. In this study a strong correlation is reported between SQS protein levels and the integrity of the mEMC in multiple human model cell lines, and it has been demonstrated that EMC5 or EMC6 deletion leads to reduced mEMC levels and adversely impacts steady-state levels SQS in the ER (**Figure 9.1**). It is further shown that SQS nascent chains are unstable without the mEMC (**Figure 10.1 B**), but could be fully rescued by restoring mEMC levels in U2OS cells (**Figure 9.1 G** and **H**).The data presented here support a requirement for at least a minimal mEMC composition, since transient (or constitutive) impairment of other primary subunits (EMC2 and EMC3) reduced SQS levels while attenuation of secondary subunits (EMC7 - 10) did not (**Figure 9.2**). No single EMC subunit alone appeared to govern SQS biogenesis, as depletion of several primary subunits caused severe mEMC biogenesis defects. EMC2-depleted cells retained reduced levels of EMC5 and EMC6, but were not able to rescue SQS (**Figure 9.2 B**). Moreover, expressing EMC5 or EMC6 exogenously in these cells also failed to restore SQS levels (**Figure 9.2 C**). Transient depletion of EMC3 reduced steady-state SQS levels and all remaining EMCs except EMC2 (**Figure 9.2 D** and **Figure 6.1 A**). Knockdown of EMC3 caused a marked shift in EMC2 sedimentation, indicating that monomeric EMC2 or EMC2 trapped in dead-end assembly intermediates was itself unable to support SQS expression (**Figure 6.3 A**). Currently, the

possibility that EMC3 alone might be limiting for SQS protein levels cannot be excluded, since the basal amount of EMC3 was strongly decreased by deletion/depletion of EMC2, EMC5, or EMC6.

Regardless of mEMC-dependence of SQS biosynthesis, several arguments speak against a specialized role for the mEMC supervising only SQS biogenesis or the regulation of steroidogenic pathways. Firstly, despite the extensive evolutionary conservation of both the mEMC [329] and SQS [459], most invertebrates are auxotrophic for cholesterol and its derivatives while still expressing EMC proteins [486]. Accordingly, the SQS gene is absent in *C. elegans* and *D. melanogaster* [486], [487]. Secondly, a study in *D. melanogaster* reported that the loss of EMC3 (dPob) had no effect on a limited set of type I/ II integral membrane proteins [357]. Thirdly, the mEMC did not stably bind to to SQS under mild detergent conditions. Hence, several models could explain the dependency of SQS biogenesis on the mEMC:

A - The mEMC is necessary for efficient (post-translational) membrane insertion of SQS. Predicted SQS TMDs from different organisms contain several hydrophilic amino acids (i.e. Ser, Tyr, Thr, Gln, Asn, and His) (**Supplemental Figure 18.17**), increasing their overall hydrophilicity, which might render them poor substrates for the GET/TRC40 pathway (**Table 1.1**). The mEMC might assist in the membrane integration of relatively hydrophilic TMDs bearing resemblance to that of SQS. In this paradigm, the mEMC could be acting directly as an insertase or indirectly by promoting the biogenesis/activity of a dedicated insertase (complex).

B - The overall structure and localization of the mEMC suggests a role in orchestrating post-insertion processes, such as the assembly of TM protein complexes containing SQS. Whereas such complexes have been described in yeast [488], orthologous complexes in mammalian cells remain a matter of speculation [434].

The following sections aim to dissect these competing models in the light of current evidence.

11.2.1 Model A - The mEMC as a putative membrane insertion factor for SQS

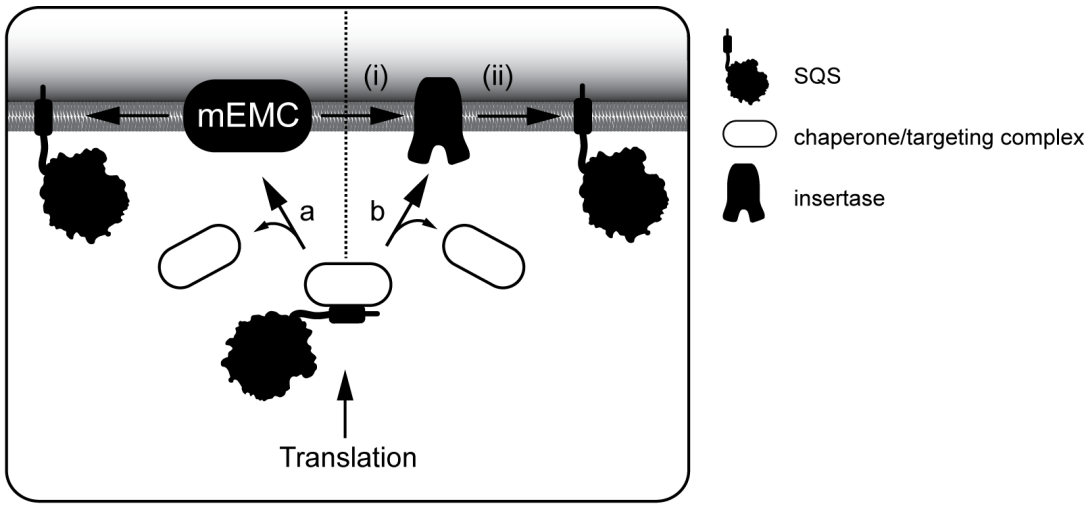


Figure 11.2: Insertase model. Two hypothetical models of SQS insertion. SQS is translated in the cytosol where its hydrophobic TMD is prevented from aggregating by the chaperone activity of a targeting complex. SQS is then transferred to the mEMC, which could act as an insertase and directly facilitates SQS membrane integration (a). In model (b), the mEMC acts as a maturation factor for an insertase (i), which accepts SQS from a chaperone/targeting complex for subsequent membrane insertion (ii).

SQS exhibits typical TA protein topology [54]. Accordingly, ER-localization of SQS is dependent on its predicted C-terminal TMD [461], [462], [419], [429]. If TA proteins fail to insert post-translationally into their target membranes, they become mislocalized and are removed by the UPS [53]. This study reports the post-translational destabilization and proteasome-dependent degradation of SQS in EMC6 knockout cells (**Section 10.1.1**). Consequently, the mEMC might be required for the post-translational insertion of SQS into the ER lipid bilayer. Loss of mEMC function (i.e. in ΔEMC6 cells) could cause cytoplasmic sequestration or mislocalization of SQS. Interestingly, sequence analysis of human SQS reveals a divergent TMD (aa 384-404). The presence of polar residues (i.e. Gln, Tyr, Thr and Ser) accounts for low hydrophobicity and an overall amphipathic character of this domain (**Table 1.1** and **Figure 18.17 A**). These properties disfavour SQS as a *bona fide* client of the GET/TRC40 pathway, which shows a predilection for TMDs with comparatively higher hydrophobicity (**Table 1.1**). Consistent with these observations, it was found that CYB5A, whose TMD is similarly hydrophilic, was moderately decreased in the initial SILAC screen (**Table 1.1** and **Figure 8.3**). This observation requires further investigation, but might indicate that the mEMC is involved in the biogenesis of multiple proteins with degenerate TMDs that are not obligate clients of the GET/TRC40 pathway. Alternative targeting pathways with some specificity for

TA proteins containing relatively hydrophilic TMDs have been suggested by reconstitution assays [61], [103], [102], but remain to be definitively characterized *in vivo* [60]. A dedicated insertase for non-GET/TRC40 client TA proteins still remains elusive.

Although it is a matter of conjecture, the idea of the mEMC being a candidate for such an insertase is explored below. In mammalian cells, the polytopic membrane proteins CAML and WRB form a hetero-oligomeric insertase [97]. WRB is the mammalian orthologue of Get1 in yeast [489], whereas CAML is functionally but not structurally analogous to Get2 [96]. Despite the lack of definitive mechanistic evidence, detailed analyses of domains involved in mediating TA protein insertion into the lipid bilayer allocated an important role to the TMDs of CAML/WRB and Get1/2 [97], [98], [490]. Incoming clients are transferred to the insertase from TRC40, which is recruited by docking to the cytoplasmic coiled-coil domain of WRB and the N-terminal cytoplasmic domain of CAML [489], [96]. It follows that an insertase can serve interdependent functions mediated by different domains: 1) recruitment of the cytosolic cargo-chaperone complex, and 2) subsequent membrane integration of the TA protein. 3) The bacterial insertase YidC can cooperate with the Sec translocase in inserting polytopic TM proteins [491], [492]. In the case of the mEMC, (some of) these functions might be allocated to different subunits. In such a model, EMC2 would be ideally situated on the cytosolic face of the ER to interact with chaperones that could maintain a TA protein (e.g. SQS) in an insertion-competent state. Interaction could be mediated by the three TPR motifs present in EMC2. TPRs are found in a wide range of proteins with diverse functions, and have been shown to mediate protein-protein interactions [346], [347], [141]. Additionally, EMC3 contains three predicted TM segments (**Supplemental Figure 18.18 A**), which have been classified as part of the DUF106 protein family (Pfam database, http://pfam.xfam.org/, [349]). DUF106 proteins, such as Mj0480, are found in archaea, where they likely function as insertases and bear structural similarity to the bacterial insertase YidC [350], [493]. Interestingly, YidC comprises six TMDs [494], [493], whereas Mj0480 has only three [350]. The insertase TMDs form a hydrophilic groove that can accept client polypeptides [493]. It is conceivable that multiple subunits of the mEMC might function to contribute additional TMDs to EMC3. Based on a model where the mEMC exhibits insertase activity (the 'mEMC insertase model', **Figure 11.2**), the following predictions are testable:

(1) If mEMC deficiency leads to SQS degradation as a consequence of failed insertion into the ER membrane, exogenously expressed SQS would likewise be mislocalized. Using recombinant SQS variants containing a C-terminal *N*-glycosylation consensus site, targeting and insertion can be tested using the glycosylation efficiency as a surrogate readout.

(2) The model posits that the degenerate TMD of SQS determines the stability of the holo-enzyme in mEMC-deficient cells. Therefore, expression of the TMD in isolation, or fused to a reporter, should be equally destabilizing.

(3) If the TPRs of EMC2 are involved in contacting cytosolic chaperones bound to a TA client protein pre-insertion, mutation of essential TPR residues should prevent targeting. Since EMC2 was identified as a 'primary subunit', TPRs could also be important for mEMC assembly. Therefore, potential mEMC biogenesis defects due to interference with TPR function must be taken into account.

(4) EMC3 sequence similarity to DUF106 proteins could indicate EMC3 as (part of) a putative insertase. The distribution of hydrophilic amino acid side chains in insertase TMDs (e.g. YidC and Mj0480) is essential for insertase activity [495], [350]. Targeted mutagenesis of charged (Arg) or hydrophilic (Asn/Ser) amino acids in the TMDs of EMC3 (especially the unusually hydrophilic third TMD (aa 167 - 187) (**Supplemental Figure 18.18 B**)) may interfere with mEMC activity.

(5) Analogous to the interaction of TA proteins with the TMDs of CAML/WRB during membrane insertion, client proteins of the mEMC should transiently interact with TMDs of one or more mEMC subunits. A transient mEMC-client interaction could explain why the mEMC was not found in complex with SQS (**Section 10.4**). Similar to dissecting the contribution of Get1/2 TMDs to translocation, cross-linking studies may be used to test this hypothesis [98], [350].

A variant of the mEMC insertase model is the mEMC serving as a maturation complex for an elusive intermediary factor that communicates mEMC loss to processes that determine SQS stability. This model is compatible with the aforementioned hypothesis as the intermediate factor might mediate TMD insertion into the lipid bilayer. Given an accumulating body of literature suggesting a role of the EMC in the biogenesis of polytopic membrane proteins [336], [369], [357], such a factor could share a similar topology (multiple TMDs) and is likely to be confined to the ER membrane. According to this paradigm, loss of an mEMC-mediated co-chaperoning function perturbs the biogenesis of a polytopic TM protein, which in turn controls the stability of SQS. By introducing one or several intermediate factors, SQS biogenesis would be controlled by multiple variables, with the mEMC being one of these. Therefore, different cell lines might depend on the mEMC for SQS biogenesis/maintenance to varying, cell type-specific degrees. To unravel which other factors might be involved in SQS biogenesis, the system described in this study is amenable to genetic or drug screens that would aim to identify proteins or pathways which could potentially rescue SQS expression in EMC6 knockout cells.

11.2.2 Model B - The mEMC operating at a post-insertion step

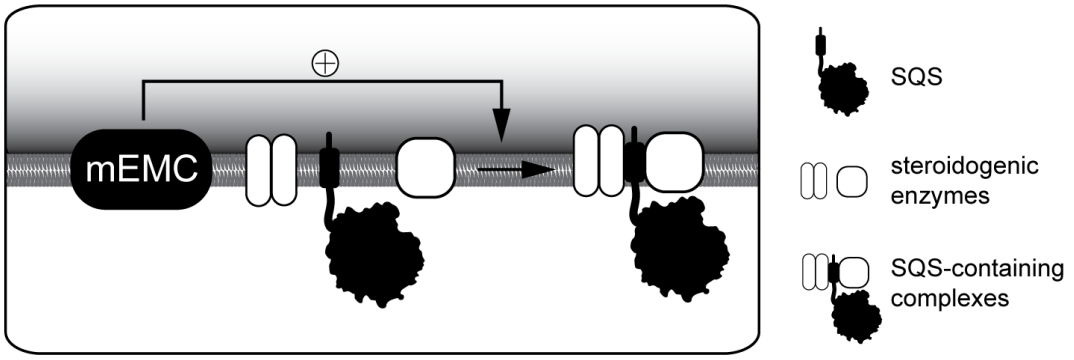


Figure 11.3: The mEMC acting at a post-insertion step. The mEMC could stabilize SQS post-insertion. In this model, SQS is stabilized in the ER membrane by formation of larger multi-protein complexes. According to this hypothesis, the mEMC stabilizes these complexes, potentially by facilitating their assembly/maturation.

Consistent with a notion of the mEMC being a putative maturation factor for proteins with multiple TMDs, the mEMC could either directly or indirectly influence the ability of SQS to form higher order complexes with other steroidogenic enzymes. This assumption is consistent with the presence of multiple charged residues in the TMD of SQS, which could be involved in interacting with TMDs of other membrane proteins via hydrogen bond formation or electrostatic interactions. Some metabolic enzymes have been found to form larger complexes [496], [497]. Multi-enzyme complexes facilitate cooperation between enzymes that work in the same pathway and enable metabolite channelling [498], [497], [499]. Several groups have embraced the concept of the 'ergosome', an ER-resident protein complex of multiple enzymes involved in the ergosterol biosynthesis pathway of *S. cerevisiae* [488]. Ergosterol is the yeast analogue of cholesterol. Using a split-ubiquitin system, Mo and Bard (2005) postulated the existence of a 'core complex', encompassing the enzymes ERG11/25/27/28 [488]. This core complex, the authors suggest, would then interact with other enzymes of the same pathway to facilitate metabolite channelling. Previous work from the same group has identified a 66 - 200 kDa C-4 demethylation complex consisting of ERG25/26/27, and the polytopic ER-resident membrane protein ERG28, which serves as a scaffold [500], [501], [502], [503].

Remarkably, many enzymes of the ergosterol biosynthesis pathway are evolutionarily conserved, and the majority of mammalian ERG orthologues operating in cholesterol biosynthesis functionally substituted their fungal counterparts in a complementation assay [504]. Nonetheless, human SQS (hSQS) was found to be one of two enzymes of the cholesterol pathway that was unable to rescue the lethal growth defect resulting from ERG9 loss (ERG9 is the yeast homologue of hSQS) [504]. Similarly, SQS from *A. thaliana* could not complement ΔERG9 yeast

strains [505]. In a recent publication, it was suggested that a kingdom-specific 26-amino acid hinge region of SQS, connecting the TMD and the catalytic domain, mediates protein-protein interactions with other enzymes of the cholesterol biosynthesis pathway [434]. However, little is known about the protein interaction networks of steroidogenic enzymes in mammalian cells. On a sucrose gradient, endogenous SQS sedimented with the characteristics of a protein of approximately 150 - 200 kDa, indicating that mammalian SQS might indeed participate in larger complexes (**Figure 10.2**). The composition of these putative SQS complexes is not known, but the scarcity of observed interactions of SQS in large-scale protein-protein interaction studies suggests that such complexes might be transient or characterized by weak interactions. Alternatively, complexes involving SQS might be dynamic and could preferentially be formed under certain conditions, such as nutrient starvation [496], [497].

Nonetheless, it cannot be claimed with certainty that SQS transiently or stably associates with other steroidogenic enzymes or the ER-resident folding machinery. A confounding factor in estimating the size of such putative complexes by sucrose gradient sedimentation under mild detergent conditions might be the formation of large SQS-containing lipid-detergent micelles. When subjected to velocity sedimentation, these structures can lead to an overestimation of the approximate molecular weight of SQS. To test this hypothesis, SQS was separated on a sucrse gradient in the presence of 1% Triton X-100 leading to a pronounced shift to lower molecular weight fractions (**Supplemental Figure 18.15**). However, as Triton X-100 potently disrupts weak protein-protein interactions formed by TMDs, the possibility that this shift was solely due to the formation of smaller micelles compared to LMNG cannot be excluded.

Equally, it cannot be ruled out that the mEMC negatively regulates a putative suppressor of SQS. This scenario predicts that the mEMC prevents ERAD or the activity of a destabilizing factor of SQS. In support of this model, the mEMC is connected to the ERAD network [189], and has repeatedly been implicated in ERAD-related processes [366], [364], [336]. An SQS-destabilizing factor would therefore allow to rapidly change the balance of cholesterol and isoprenoid intermediates upstream of SM. However, the isoprenoid/cholesterol pathway is already under strict regulation by HMGCR and SM.

11.2.3 The GET/TRC40 pathway in SQS biogenesis

By depleting components of the GET/TRC40 pathway, this study found that the steady-state levels of SQS were partly dependent on TRC40, an ATPase that delivers TA proteins to the hetero-oligomeric CAML/WRB receptor complex in the ER membrane. It is therefore tempting to presume that *de novo*-synthesized SQS could not be targeted correctly to the

ER membrane of TRC40-depleted cells and was degraded by the ubiquitin-proteasome system (UPS). However, these data should be interpreted with care. In a bioinformatics approach, Kalbfleisch and colleagues (2007) have identified over 400 human proteins with TA topology, a subset of which are regulated by the GET/TRC40 pathway [54]. Impairment of TRC40 is therefore likely to have pleiotropic effects on cells. For instance, TRC40 knockout mice show perturbed ER-Golgi retrograde transport and ER stress induction in pancreatic β-cells [506]. Consequently, it cannot be ruled out that the reduction of SQS in TRC40-depleted cells may be caused by knock-on effects unrelated to SQS targeting and membrane insertion.

Interestingly, depletion of Bag6, a component of the pre-targeting complex upstream of TRC40, did not significantly affect SQS protein levels. In addition to its function as a holdase in the GET/TRC40 pathway, Bag6 is involved in a variety of cellular processes including targeting substrates to the UPS [234], [507]. Hence, it is possible that a subpopulation of Bag6 is engaged in the GET/TRC40 pathway at any one time, and that low amounts of Bag6 are sufficient to maintain SQS biogenesis. Consequently, the residual Bag6 activity in Bag6-depleted cells might have been sufficient to engage the GET/TRC40 pathway. It is also possible that Bag6 is compensated for by other holdases. Accordingly, knockdown of Bag6 did not affect the biogenesis of TA proteins [234], similar to observations presented here. Alternatively, Bag6, and by extension the GET/TRC40 pathway, may not be involved at all in SQS biogenesis. The degenerate TMD of SQS, which is predicted to be an unfavourable substrate of TRC40 (**Table 1.1**), could be seen to support this view. Moreover, loss of the mEMC did not consistently affect the steady-state levels of two endogenous TA proteins (Ube2j1 and Sec61β), where the latter is a validated TRC40 client. Taken together, it seems unlikely that decreased SQS levels in mEMC-depleted cells are the result of decreased GET/TRC40 pathway activity.

11.3 Metabolic flux through the mevalonate/cholesterol biosynthesis pathways in mEMC-deficient cells

The observations presented here indicate that mEMC depletion alters the metabolic flux of mevalonate/cholesterol biosynthesis pathway intermediates. In particular, it was found that the loss of EMC6 (and of SQS) increased the total cellular fraction of geranylgeranylated Rap1a (**Figure 9.6 B**), [508]. This observation is consistent with previous reports. Inhibition of SQS with ZA, increased detection of the GGPP precursor FPP in HepG2 cells, lymphoblasts, and fibroblasts [270]. ZA also increased Rap1a prenylation in UT-2 cells, but could be reversed by inhibiting either geranylgeranyl-diphosphate synthase or GGTI [286]. Prenylation (i.e. far-

nesylation/geranylgeranylation) of otherwise cytoplasmic protein species promotes subcellular compartmentalization to membrane domains, and has been shown to promote protein-protein interaction [509], [510], [511]. Thus, it is possible that mEMC levels could indirectly modulate protein prenylation and signal transduction pathways. It is worth noting that the unprenylated population of Rap1a is small compared to the total cellular pool, and the decrease in the small fraction observed in mEMC-deficient cells is therefore unlikely to have broad functional consequences. Nonetheless, it cannot be ruled out that the prenylation of other proteins may be increased at a greater extent than for Rap1a and may have a more profound cellular impact. In this study, the FPP pool in mEMC-deficient cells was not assessed. Since FPP is a precursor of GGPP, it is likely that FPP and other isoprenoid derivatives (e.g. dolichol and haem A) could be elevated as well [512], but these were not monitored in this study.

Residual SQS in mEMC-deficient cells might still contribute significantly to the metabolite flux along the steroid biosynthesis pathway as the enzyme is likely to be present in excess under basal conditions [283]. Nonetheless, Brown and Goldstein have noted that suppression of SQS activity might not significantly slow the net flux through the pathway, but still be sufficient to lead to notable FPP accumulation [283].

Here, it has been shown that SM was markedly increased in mEMC-deficient cells (**Figure 9.7**), and it is tempting to speculate that SM upregulation is a consequence of reduced SQS levels. As SM mRNA levels were not significantly increased in ΔEMC6 cells (**Figure 9.5 A**), it is reasonable to suspect that SM is stabilized, but this remains to be demonstrated. Importantly, ZA treatment stabilized the yeast orthologue of SM, ERG1p, elevating protein levels and increasing its half-life [196].

Not unexpectedly, HMGCR mRNA and protein levels remained unaffected in mEMC-deficient cells (**Figure 9.5 A** and **Figure 9.7 A/B**). Peffley *et al.* (1995) have shown previously that inhibition of SQS by ZA has no effect on HMGCR synthesis in lovastatin-treated Syrian hamster cells [513].

Deletion of EMC6 or SQS did not adversely affect overall cholesterol levels under nutrient-rich steady-state conditions (**Figure 9.3 A/B**). Therefore, SQS-deficient U2OS cells were likely able to satisfy the cellular demand for cholesterol by LDLR-mediated lipoprotein endocytosis from the FCS-containing tissue culture medium. Intriguingly, work on DCG fibroblasts shows a moderate decrease (15 - 30%) of cellular cholesterol levels when these cells were exposed to 100 μM ZA for 10 days [514]. This discrepancy implies that the *net* contribution of cholesterol *de novo* biosynthesis and import pathways is cell-type specific and that, in U2OS cells, cholesterol import at basal conditions might be critical to maintain sterol homeostasis.

11.4 Sensitization of mEMC-deficient cells to cholesterol depletion

EMC6 knockout cells were markedly and specifically sensitized to the cholesterol-chelating agent MBCD (**Figure 9.3 C/D** and **Figure 9.4**). MBCD is advantageous for cholesterol depletion since it acts rapidly [515], [516], and does not integrate into, or bind to, the PM [449], thereby lowering the risk of pleiotropic effects. MBCD also interferes with the formation of clathrin-coated endocytic vesicles, potentially preventing LDLR-mediated endocytic uptake of extracellular lipoprotein-bound cholesterol [517]. However, it should be noted that MBCD shows some capacity to extract dipalmitoylphosphatidylcholine, sphingolipids [447], [448], and GPI-anchored proteins from the PM of human cells, especially upon prolonged exposure [450]. Therefore, MBCD treatment is generally used for acute and transient depletion of cholesterol over shorter time periods. Nevertheless, the drug has also been employed in assessing the effects of prolonged cholesterol starvation (e.g. 16 - 24 hours) on cell survival or gene transcription [518], [519]. Since the treatment regimen employed in this study commonly included extended MBCD exposure (16 hours), potential detrimental off-target effects cannot be completely ruled out. However, there is strong evidence that the increased sensitivity to MBCD is a consequence of reduced SQS activity. Firstly, MBCD-induced cell death of ΔEMC6 cells correlated with substantially reduced steady-state levels of SQS (**Figure 9.3 C/D** and **Figure 9.1**). Exogenous expression of EMC6, and therefore reconstitution of the mEMC, led to restoration of SQS with a concomitant increase in MBCD resistance (**Figure 9.3 C/D**). Secondly, wild-type cells treated with ZA became significantly sensitized to MBCD-induced cell death (**Figure 9.4**). Thirdly, although ΔSQS cells were viable, they were unable to tolerate minimally cytotoxic concentrations of MBCD (**Figure 9.3 C/D** and **Figure 9.1**). Nevertheless, to unequivocally exclude off-target effects, repletion experiments using MBCD complexed with cholesterol should be performed [515]. A milder form of cellular cholesterol depletion is commonly achieved by growing cells in medium supplemented with lipoprotein-free serum (LPDS) and/or exposure to HDL. In contrast to MBCD, these treatments show slower cholesterol depletion kinetics, thereby allowing cells to adapt to the slowly increasing sterol demand [516].

Intriguingly, upon MBCD-treated mEMC-deficient cells were able to upregulate SREBP2 target genes, including HMGCR, SM, and SQS. Increased SQS gene transcription was likely responsible for elevated (but not fully restored) SQS protein levels when ΔEMC6 cells were exposed to MBCD (**Figure 9.5**), stressing that the mEMC facilitated, but was not absolutely

essential for, SQS biogenesis. Whether or not newly synthesized SQS can insert into the ER membrane and is fully functional in mEMC-deficient cells remains to be shown.

11.4.1 The mEMC and SQS in the context of mevalonate/cholesterol biosynthesis and virus propagation

The identification of factors involved in the biogenesis of SQS and, more broadly, in the maintenance of cellular cholesterol homeostasis, could have several important implications for therapeutic intervention in a number of pathologies. Cellular cholesterol plays an essential role in the life cycle of viruses within the *Flaviviridae* family, such as HCV [520], WNV [521], or DNV [522]. Interestingly, the mEMC has repeatedly been associated with modulating the propagation of *Flaviviridae*, notably WNV [366], and has recently been described to be a host factor in Zika Virus and DNV infections [383] (**Section 4.8**). The ability of certain viruses in the *Flaviviridae* family to manipulate the cholesterol homeostasis pathways of their host cell is a crucial factor determining viral infection and replication. In the following section, work emphasizing the role of SQS and cellular cholesterol levels in virus propagation will be summmarized.

Cholesterol-rich PM microdomains ('lipid rafts') are sites of virus-host cell interaction [523]. Their cholesterol content is dependent on SQS activity [436]. Concordantly, Park *et al.* (2014) identified SQS as a positive regulator of HCV propagation[520]. HCV replication was impaired upon SQS knockdown and SQS was post-translationally stabilized in HCV-infected cells [520]. This implies that SQS enables HCV replication by promoting cholesterol synthesis. It would be interesting to determine whether the mEMC is also important for the susceptibility to HCV infection and propagation in these cells.

Similarly, the WNV harnesses cellular cholesterol for host cell entry and viral propagation. Acute depletion of PM cholesterol inhibits viral entry into host cells, most likely by perturbing receptor assemblies within cholesterol-rich microdomains [524]. Intracellular cholesterol appears to be essential for WNV replication. In this regard, Mackenzie *et al.* (2007) observed a striking redistribution of internal cholesterol stores to perinuclear sites of WNV replication [521]. Furthermore, WNV infection potentiated the mevalonate pathway by upregulating HMGCR. Accordingly, HMGCR inhibition by lovastatin had detrimental effects on WNV replication [521]. Addition of exogenous cholesterol inhibited virus replication, presumably by downregulating HMGCR activity. Inhibition of geranylgeranylation pathways showed a similar outcome [521]. Consequently, efficient WNV replication is dependent on both host cell *de novo* cholesterol biosynthesis and protein prenylation pathways. EMC2 and EMC3 were found

to promote WNV-mediated neuronal cell death [366]. Of note, whereas knockout of EMC2/3 caused resistance to WNV-induced cell death, deletion of HMGCR and therefore impairment of the mevalonate/cholesterol pathway was not protective [366]. Given the mEMC link to ERAD [189], [364], and since other ERAD genes also modulate WNV cytotoxicity [366], it may be that an ERAD-related function of the mEMC plays a role in virus infection and propagation. This argues against a connection between the mEMC and the cholesterol biosynthesis pathway *via* SQS as a role of this complex as a host factor.

DNV pathogenicity is also heavily modulated by cellular cholesterol stores [522], [525]. In this regard, inhibition of SQS prevented infection of lymphoblast cells with dengue type 2 New Guinea C (DEN-2 NGC) in a dose-dependent manner [522]. Importantly, reduced levels of the mEMC (EMC1 - EMC5), prevented DNV from efficiently entering HeLa cells [383]. To date, it is not clear whether SQS modulation by the mEMC might contribute to DNV entry. However, it should be mentioned that, even though Savidis *et al.* (2016) did identify genes involved in lipid metabolism as host factors, SQS was not one of them [383]. Hence, mEMC depletion might impair DNV infection and propagation in an SQS-independent manner. In summary, Flaviviruses manipulate the lipid metabolomic pathways of their host cells, which in the case of HCV is directly mediated by SQS. Although the mEMC has been shown to be a potent host factor for a number of Flaviviruses, it is unlikely that SQS regulation by the mEMC plays a major causative role.

11.5 SQS and cell viability

SQS plays an essential role in embryonic development. Consequently, homozygous SQS knockout mice exhibit severe defects in neural tube closure and die early in embryonic development [433]. Cholesterol is an important structural component of lipid rafts, which are thought to serve signalling functions in the PM [243]. Furthermore, the activity of the mevalonate/steroid biosynthesis pathway is indispensable for cell division [526]. The rapid proliferation rate of cancer cells necessitates enhanced membrane biogenesis and therefore a high demand of lipids including cholesterol [527]. Accordingly, depletion of SQS has been demonstrated to negatively affect the viability of prostate cancer cell lines, where reduced SQS activity is sufficient to alter cellular cholesterol content and induce apoptosis [436]. In contrast, cerebellar granule cells are unaffected by a loss of SQS [528]. Differential dependence of various cells and tissues on SQS could imply cell type-specific differences in their ability to satisfy the cellular demand for cholesterol by increased cholesterol uptake from the cellular microenvironment. The high

demand of cancer cells for a continuous supply of cholesterol renders the mevalonate/steroid pathway an attractive drug target for therapeutic intervention [529], [267]. Hence, it would be worthwhile to investigate the mEMC as a potential modulator of cholesterol biosynthesis in cancer cells, and interrogate whether loss of EMC6 induces cytotoxicity under steady-state conditions in cancer cells that are dependent on endogenous cholesterol production.

11.6 Changes to the cell-surface glycoproteome in mEMC-deficient cells

Aiming to interrogate potential protein maturation defects in the secretory pathway in mEMC-deficient cells, cell surface proteomic changes in EMC5, and EMC6 knockout cell lines were quantified in this study. The levels of 23 proteins were reduced, the majority of which were transporters (**Figure 8.2**). These observations are consistent with reports implicating the EMC as an ER-resident maturation factor for polytopic TM proteins [369], [336], [357]. Even though the molecular function of the mEMC still remains elusive, a role in chaperoning TMDs and in facilitating the assembly of larger protein complexes destined for the PM (e.g. receptors, and transporters) has been suggested in *C. elegans* [336], and *D. melanogaster* [357].

The analysis of the cell surface proteome of mEMC-deficient human cell lines provides new insights into an apparently mEMC-dependent sub-population of the membrane proteome. However, the topological and functional heterogeneity of this population raises a number of questions.

What are the defining molecular features of proteins being translocated along the secretory pathway that dictate mEMC-dependence? Many of the potential mEMC client proteins identified appear to lack compelling unifying features (except for proteins of the same family). In this respect, they differ in functionality, size, oligomerization state and number of TMDs. A possible explanation for this discrepancy might be that mEMC-deficiency affects a variety of cellular processes. More specifically, the mEMC might aid maturation of certain proteins directly (e.g. by chaperoning), whereas others are affected indirectly by (unspecific) knock-on effects. Alternatively, the mEMC could cooperate with maturation factors of broad specificity, such as the OST complex. In support of this idea, Savidis *et al.* (2016) described an interaction of several EMC proteins with components of the OST complex [383]. This leads into the question of whether the mEMC has a wide range of disparate substrates (an example of such behaviour would be the chaperone BiP) or has more limited, specific activity? Even though the data presented here indicate a broader spectrum of clients, our approach does not address

whether the observed changes are directly dependent on the mEMC alone. Furthermore, is the decreased surface expression of putative mEMC clients a consequence of enhanced ER retention and degradation of immature, or dead-end assembly intermediates? Loss of cell-surface expression of a particular protein can have a range of causes, including trafficking defects, degradation, internalization, or transcriptional attenuation. It should also be noted that long-term adaptation to mEMC-deficiency by engagement of compensatory mechanisms cannot be excluded. Therefore, the effect of mEMC loss on non-obligatory client proteins could be underestimated and further confound the analysis.

A large number of sialylated cell surface proteins were downregulated in ΔEMC5, but not ΔEMC6 cells, and *vice versa* (**Supplemental Figure 18.12**). The reproducibility and physiological significance of this observation remain to be determined. In some cases, different members of the same protein family were found to be depleted only in EMC5 or EMC6 knockout cells. For example, markedly decreased cell surface expression of the metazoan-specific solute carriers Choline transporter-like protein 1 (CTL1) and CTL2 was detected in Δ EMC6 and ΔEMC5 cells, respectively. CTL1 and CTL2 were shown to be localized to the PM (CTL1/2) as well as to mitochondria (CTL2), where they mediate choline import [530], [531]. Decreased CTL1/2 expression could therefore affect PC biosynthesis. Interestingly, a recent report in genetically engineered yeast lacking five EMC subunits implicated the EMC in PC metabolism by preventing ER-mitochondrial tethering [331]. Despite the conceptual difference between ER-mitochondrial uncoupling and depletion of choline transporters, both observations indicate that loss of the EMC might impair PC metabolism. Further research is required to validate our initial findings and determine whether diminished levels of cell surface proteins are a consequence of enhanced ER retention due to impaired co- and post-translational maturation.

11.7 Conclusion

In this study, a first description of the fundamental principles guiding the biogenesis of the mammalian homologue of the ER membrane protein complex (mEMC) is provided. The consequences of mEMC depletion in a tissue culture model have been explored, leading to the discovery of a novel correlation between this complex and SQS, an enzyme catalysing the committing step in cholesterol *de novo* biosynthesis. No doubt, further study of the mechanistic details of this correlation will shed light on the molecular function of the mEMC as a putative maturation factor for transmembrane proteins.

Part IV

Materials and Methods

Chapter 12

Materials

Primer	Description	Sequence (5'-3')
N11	HMGCR forward primer	GGACCCCTTTGCTTAGATGAAA
N12	HMGCR reverse primer	CCACCAAGACCTATTGCTCTG
N15	SM forward primer	CTATGGCAGAGCCCAATGCAAAGT
N16	SM reverse primer	ACAACAGTCAGTGGAGCATGGAGT
N17	SQS forward primer	GGCAAGCGGAAGGTGATG
N18	SQS reverse primer	CTGGTCTGATTGAGATACTTGTAGCAA
N64	Actin forward primer	GAGGCACTCTTCCAGCCTT
N65	Actin reverse primer	AAGGTAGTTTCGTGGATGCC
N66	EMC1 forward primer	GGAATGTCTTGCGACAGCTA
N67	EMC1 reverse primer	AGATCCTTTCGAAGCCGATA
N68	EMC2 forward primer	TCCAACTAACACTGCTGCAA
N69	EMC2 reverse primer	AAGTTCATGCCAGGCTTCTT
N70	EMC3 forward primer	GCCAAGATAATGCCGCTGAC
N71	EMC3 reverse primer	TCGAAGTGGAGGTCTTTGGC
N72	EMC4 forward primer	TTCAGCCACTTTCAAGATGTTAG
N73	EMC4 reverse primer	GTCCTCCACCACTGAACTCC
N74	EMC5 forward primer	CTGCGCAGCATCGTTCTTAT
N75	EMC5 reverse primer	GCCGGAAAAGTACTCGACCA
N76	EMC6 forward primer	GCCGCCGTCCTGGATTATT
N77	EMC6 reverse primer	GGAGGCGAGCAGGTAGAAGA
N78	EMC7 forward primer	CTGACATGAGACGGGAAATG
N79	EMC7 reverse primer	GCTGCTAGATTTGCCAGATG
N80	EMC8 forward primer	CTGCGCTCATCATGGTAGAC
N81	EMC8 reverse primer	CCATCTGTTCTCATGGTGCT
N82	EMC9 forward primer	TCAACCAGGTGGATGTGTGG
N83	EMC9 reverse primer	GACCTTGGTTCTCCAGGACG
N84	EMC10 forward primer	TGAGATCGATGACAGTGCCAA
N85	EMC10 reverse primer	GCAGGGACAAAGGAGGAGAC

Table 12.1: qPCR primers used in this study

Compound/Enzyme	**Solvent**	**Manufacturer**
Aniline hydrochloride	H_2O	Sigma-Aldrich
Aminooxybiotin (AOB)	DMSO	Biotium
Bafilomycin A1 (BafA1)	DMSO	Viva Bioscience
Bortezomib (Btz)	DMSO	Cell Signaling
Cycloheximide (CHX)	DMSO	Abcam
4',6-Diamidino-2-Phenylindole (DAPI)	H_2O	Sigma-Aldrich
Dimethylsulfoxide (DMSO)	n.a.	Sigma-Aldrich
Dithiothreitol (DTT)	H_2O	Sigma-Aldrich
Doxycycline (Dox)	DMSO	Sigma-Aldrich
Filipin III	DMSO	Santa Cruz Biotechnology
Gel filtration markers kit MWGF1000	50 mM Tris-HCl, pH 7.5, 100 mM KCl	Sigma-Aldrich
Glycerol	H_2O	Sigma-Aldrich
GGTI 298 trifluoroacetate salt hydrate	DMSO	Sigma-Aldrich
Harringtonin (HT)	DMSO	Abcam
Iodoactammide (IAA)	H_2O	Roche
Foetal bovine lipoprotein depleted serum (LPDS)	n.a.	BIOTREND
Methyl-β-cyclodextrin (MBCD)	H_2O	Sigma-Aldrich
MitoTracker®Red CMα Ros	DMSO	Life Technologies
MG-132	DMSO	CalBiochem
NEM	ethanol	Acrose Organics
NMS-873	DMSO	Sigma-Aldrich
Paraformaldehyde solution	PBS	Alfa-Aesar
Phenylmethane sulfonyl fluoride (PMSF) 100%	ethanol	Sigma-Aldrich
PNGase F	n.a.	NEB
Polybrene	H_2O	Sigma-Aldrich
SILAC Lys-8-Arg-10 kit (282986444)	n.a.	Silantes GmbH
Sodium-meta-periodate	H_2O	Sigma-Aldrich
Tunicamycin (TM)	DMSO	Abcam
Trypsin (mass spectrometry grade)	100 mM ammonium bicarbonate	Sigma-Aldrich
Zaragozic acid A (ZA)	DMSO	Santa Cruz Biotechnology

Table 12.2: Compounds used in this study.

Target/Antibody	Species	Dilution in 2% (w/v) BSA/PBST	Product number/Clone	Manufacturer
AlexaFluor®488 Anti-mouse IgG (H+L)	Donkey	1:4000 (IB), 1:400 (IF)	A21202	Invitrogen
AlexaFluor®488 Anti-rabbit IgG (H+L)	Goat	1:4000 (IB), 1:400 (IF)	A11008	Invitrogen
Anti-mouse IgG-HRP	Goat	1:10000	sc-2005	Santa Cruz Biotechnology
Anti-rabbit IgG-HRP	Goat	1:10000	sc-2030	Santa Cruz Biotechnology
Bag6 (1-250)	Rabbit	1:10.000	-	Kind gift from R. Hegde lab
BiP	Rabbit	1:5000	3183	Cell Signalling Technoligies
CYB5A	Rabbit	1:1000	sc-33174/H-114	Santa Cruz Biotechnology
CD147	Mouse	1:1000	sc-25273	Santa Cruz Biotechnology
CHOP	Mouse	1:1000	L63F7	Cell Signaling Technologies
EMC1	Rabbit	1:1000	-	Kind gift from E. Espreafico lab
EMC2	Rabbit	1:2000	25443-1-AP	Proteintech
EMC3	Rabbit	1:500	ab175537	Abcam
EMC4	Rabbit	1:1000	ab123719	Abcam
EMC5	Rabbit	1:1000	ab174366	Abcam
EMC6	Rabbit	1:1000	ab84902	Abcam
EMC7	Rabbit	1:500	AP11145c	Abgent
EMC8	Rabbit	1:500	ab180065	Abcam
EMC9	Rabbit	1:500	AP5632b	Abgent
EMC10	Rabbit	1:1000	ab180148	Abcam
HA	Mouse	1:1000	Clone 12CA5	Purified from hybridoma
HERP	Rabbit	1:1000	ab150424	Abcam
HMGCR	Rabbit	1:1000	ab174830	Abcam
KDEL	Mouse	1:200 (IF)	ADI-SPA-827 (10C3)	Enzo
Lamin B	Goat	1:3000	sc-6216	Santa Cruz Biotechnology
LTN1	Rabbit	1:1000	ab104375	Abcam
Rap1a	Rabbit	1:1000	sc-1482/C-17	Santa Cruz Biotechnology
S-tag	Mouse	1:1000	MA1-981	Thermo Fisher
Sel1L	Goat	1:1000	sc-48081	Santa Cruz Biotechnology
SM	Rabbit	1:1000	12544-1-AP	Proteintech
SQS (C-terminus)	Rabbit	1:2000	ab109723	Abcam
SQS (N-terminus)	Rabbit	1:2000	ab195046	Abcam
Step-HRP	-	1:1000	474-3000	KPL
TRC40	Rabbit	1:1000	-	Kind gift from R. Hegde lab
Tubulin	Mouse	1:1000	T5168/b-5-1-2	Sigma-Aldrich
Ube2J1	Rabbit	1:5000	NBP1-59757	Novus Biologicals
Ubiquitin	Rabbit	1:1000	3933S	Cell Signaling Technologies

Table 12.3: Antibodies used in this study. IB, immunoblotting; IF immunofluorescence microscopy.

Plasmid	Description	Vector backbone	Source (ID)
pcDNA™/3:EGFP	Empty expression vector	pcDNA™/3:EGFP	Thermo Fisher
pcDNA™/5/FRT/TO	Empty expression vector	pcDNA™/5/FRT/TO	Thermo Fisher
pFL001	pcDNA™/5/FRT/TO encoding N-terminal FLAG:HA	pcDNA™/5/FRT/TO	F. Lari
pFL002	pcDNA™/5/FRT/TO encoding C-terminal FLAG:HA	pcDNA™/5/FRT/TO	F. Lari
pNV001	SQS wt expression vector	pcDNA™5/FRT/TO	This study (528.1)
pNV002	FLAG:HA:SQS expression vector	pFL001 (pcDNA™/5/FRT/TO:FLAG:HA, N-terminal FLAG:HA)	This study (528.2)
pNV003	SQS:FLAG:HA expression vector	pFL002 (pcDNA™/5/FRT/TO:FLAG:HA, C-terminal FLAG:HA)	This study (528.3)
pNV010	FLAG:HA:EMC6 expression vector	pFL001 (pcDNA™/5/FRT/TO:FLAG:HA, N-terminal FLAG:HA)	This study
pNV011	EMC6 wt expression vector	pcDNA™/5/FRT/TO	This study
pNV012	EMC5 wt expression vector	pcDNA™/5/FRT/TO	This study
pNV013	EMC5 expression vector	pcDNA™/5/FRT/TO	This study
AT40	SQS wt cDNA library vector		
EMC7:S	EMC7:S expression vector	pcDNA™/3	Kopito lab
EMC9:S	EMC9:S expression vector	pcDNA™/3	Kopito lab
ER-mCherry	Expression vector for SS-myc-mCherry-KDEL	pcDNA™/3	Hartl lab
S:EMC6:S	S:EMC6 expression vector	pcDNA™/3	Kopito lab

Table 12.4: Plasmids used in this study

Primer	Used to Generate	Description	Sequence (5'-3')
N5	SQS:FLAG:HA	fw primer for cloning SQS into FL002	GTTGCTAGCGCCACCATGGAGTTCGTGAAATGC
N6	SQS:FLAG:HA	rev primer for cloning SQS into FL002	CTTGGTACCGTGTTCTCCAGTCTGAAC
N21	FLAG:HA:SQS	fw primer for cloning SQS into FL001	GTTACCGGTGAGTTCGTGAAATGCCTTGG
N22	FLAG:HA:SQS	rev primer for cloning SQS into FL001	CTTGCTAGCTCAGTGTTCTCCAGTCTG
N86	EMC6	fw primer for cloning EMC6 into pcDNA^{TM}/5/FRT/TO	GCGGGATCCGCCACCATGGCCGCGGTGGTGGCCAA
N87	EMC6	rev primer for cloning EMC6 into pcDNA^{TM}/5/FRT/TO	CCGGCTCGAGTCAGTAGACGTGCACCATG
N88	FLAG:HA:EMC6	fw primer for cloning EMC6 into FL001	GTTACCGGTGCCGCGGTGGTGGCCAAG
N89	FLAG:HA:EMC6	rev primer for cloning EMC6 into FL001	CTTGCTAGCTCAGTAGACGTGCACCATGCCGTAG
N90	EMC5	fw primer for cloning EMC5 into pcDNA^{TM}/5/FRT/TO	GCGGGATCCGCCACCATGGCGCCGTCGCTGTGGAAG
N91	EMC5	rev primer for cloning EMC5 into pcDNA^{TM}/5/FRT/TO	CCGGCTCGAGTTAACGACGCAGTGATTCGAG

Table 12.5: Primers used for cloning. fw, forward; rev, reverse.

Plasmid (Vector Number)	Target Gene	Target Site	Vector Backbone	Antibiotic Resistance	Source
NV_EMC2_1 (853)	EMC2	AGACTATGGTCGGGATGACTTGG	pX459v2	Puromycin	This study (A. Bassett)
NV_EMC2_2 (854)	EMC2	CACAGAGTCAAGCGATTAACAGG	pX459v2	Puromycin	This study (A. Bassett)
JC_hMMGT_1 (410)	EMC5	GCATCATGGCGCCGTCGCTGTGG	pX459v2	Puromycin	This study (A. Bassett)
JC_hMMGT_2 (411)	EMC5	CGCAGCGGAAAAGGCGGCGTGGG	pX459v2	Puromycin	This study (A. Bassett)
JC_hMMGT_3 (412)	EMC5	CACTGCCAATAGATGTAAGTTGG	pX459v2	Puromycin	This study (A. Bassett)
JC_hEMC6_1 (401B)	EMC6	GCCGCCTCGCTGATGAACGGCGG	pX459v2	Puromycin	This study (A. Bassett)
JC_hEMC6_2 (402)	EMC6	CCGAGGTCCGGCAATAATCCAGG	pX459v2	Puromycin	This study (A. Bassett)
JC_hEMC6_3 (403)	EMC6	GAACGGCGGCCCTTCCCGCTTGG	pX459v2	Puromycin	This study (A. Bassett)
NV_FDFT1_1 (855)	SQS	GCCGACATTTGCCGGAGAATGGG	pX459v2	Puromycin	This study (A. Bassett)
NV_FDFT1_2 (856)	SQS	ACGGCCAAGTCAATATTCTCCGG	pX459v2	Puromycin	This study (A. Bassett)

Table 12.6: CRISPR/Cas9 plasmids used in this study

siRNA/shRNA Plasmid	Target Gene	siRNA Sequence (5'-3')/ Full Hairpin shRNA Sequence (5'-3')	Vector Backbone	Catalogue Number	Source	Reference
Set of 4: ON-TARGETplus EMC1 siRNA	EMC1	AGUCAUGGCCUGUCGGAAU	n.a.	LQ-014146-01-0002 2 nmol	GE Healthcare/Dharmacon	n.a.
	EMC1	AGAUACACGCAGAGCGAUU	n.a.	LQ-014146-01-0002 2 nmol	GE Healthcare/Dharmacon	n.a.
	EMC1	GUGGAUAUCGGCUUCGAAA	n.a.	LQ-014146-01-0002 2 nmol	GE Healthcare/Dharmacon	n.a.
	EMC1	UGAAAGAGGUACACUCGAA	n.a.	LQ-014146-01-0002 2 nmol	GE Healthcare/Dharmacon	n.a.
Set of 4: ON-TARGETplus EMC2 siRNA	EMC2	UUGGGCAGCUAGUCAAAUA	n.a.	LQ-010631-00-0002 2 nmol	GE Healthcare/Dharmacon	n.a.
	EMC2	GCGAUUAACAGGCAUGAGA	n.a.	LQ-010631-00-0002 2 nmol	GE Healthcare/Dharmacon	n.a.
	EMC2	GAGCUUUGUUUGGACUUUA	n.a.	LQ-010631-00-0002 2 nmol	GE Healthcare/Dharmacon	n.a.
	EMC2	UUCGGGAGCUGAAUGAGUA	n.a.	LQ-010631-00-0002 2 nmol	GE Healthcare/Dharmacon	n.a.
Set of 4: ON-TARGETplus EMC3 siRNA	EMC3	CCGCUGACCAAUCACGAAU	n.a.	LQ-010715-02-0002 2 nmol	GE Healthcare/Dharmacon	n.a.
	EMC3	ACUAGAUGAUGUCGAAGAA	n.a.	LQ-010715-02-0002 2 nmol	GE Healthcare/Dharmacon	n.a.
	EMC3	ACAGCAAGGAAUCGAGCUA	n.a.	LQ-010715-02-0002 2 nmol	GE Healthcare/Dharmacon	n.a.
	EMC3	CAGUCUUUCUUGACACGAA	n.a.	LQ-010715-02-0002 2 nmol	GE Healthcare/Dharmacon	n.a.
Set of 4: ON-TARGETplus EMC4 siRNA	EMC4	CUACUAUGAUGGUGUGUAU	n.a.	LQ-021126-00-0002 2 nmol	GE Healthcare/Dharmacon	n.a.
	EMC4	GCAAGUGCCUGAUACCAGC	n.a.	LQ-021126-00-0002 2 nmol	GE Healthcare/Dharmacon	n.a.
	EMC4	UGGUCUAUCUCAUUGGGAA	n.a.	LQ-021126-00-0002 2 nmol	GE Healthcare/Dharmacon	n.a.
	EMC4	UUAGAAAGUUCAAGCCAGA	n.a.	LQ-021126-00-0002 2 nmol	GE Healthcare/Dharmacon	n.a.
Set of 4: ON-TARGETplus EMC5 siRNA	EMC5	GCCAAUAGAUAUAGUUCUU	n.a.	LQ-018365-00-0002 2 nmol	GE Healthcare/Dharmacon	n.a.
	EMC5	UCGAAUCACUGCGUCGUUA	n.a.	LQ-018365-00-0002 2 nmol	GE Healthcare/Dharmacon	n.a.
	EMC5	GCGCAGCAUCGUUCUUAUA	n.a.	LQ-018365-00-0002 2 nmol	GE Healthcare/Dharmacon	n.a.
	EMC5	CAAGAUGCAUUGUCCUCUA	n.a.	LQ-018365-00-0002 2 nmol	GE Healthcare/Dharmacon	n.a.
Set of 4: ON-TARGETplus EMC6 siRNA	EMC6	CAGAUUAAAUGAAGCGUGA	n.a.	LQ-014711-02-0002 2 nmol	GE Healthcare/Dharmacon	n.a.
	EMC6	ACGGAGAGCCUGUAAUAUU	n.a.	LQ-014711-02-0002 2 nmol	GE Healthcare/Dharmacon	n.a.
	EMC6	GAAGGAGGUGGAACAAAUA	n.a.	LQ-014711-02-0002 2 nmol	GE Healthcare/Dharmacon	n.a.
	EMC6	ACGGCAUGGUGCACGUCUA	n.a.	LQ-014711-02-0002 2 nmol	GE Healthcare/Dharmacon	n.a.
Set of 4: ON-TARGETplus EMC7 siRNA	EMC7	CCUGACAUGAGACGGGAAA	n.a.	LQ-021215-01-0002 2 nmol	GE Healthcare/Dharmacon	n.a.
	EMC7	CGGCAUAGGAGAUCGCUUC	n.a.	LQ-021215-01-0002 2 nmol	GE Healthcare/Dharmacon	n.a.
	EMC7	GAGAAGAGCACGUCGGUUU	n.a.	LQ-021215-01-0002 2 nmol	GE Healthcare/Dharmacon	n.a.
	EMC7	GAGCAAGAUAUGUGAAUUA	n.a.	LQ-021215-01-0002 2 nmol	GE Healthcare/Dharmacon	n.a.
Set of 4: ON-TARGETplus EMC8 siRNA	EMC8	UUAUCAAGCUAAUGAGCGA	n.a.	LQ-032511-02-0002 2 nmol	GE Healthcare/Dharmacon	n.a.
	EMC8	GAGAACAGAUGGCGGUGCA	n.a.	LQ-032511-02-0002 2 nmol	GE Healthcare/Dharmacon	n.a.
	EMC8	UGUGGAAAGCUGACCGUUU	n.a.	LQ-032511-02-0002 2 nmol	GE Healthcare/Dharmacon	n.a.
	EMC8	GCUCGUGGAUUUCGAUAAC	n.a.	LQ-032511-02-0002 2 nmol	GE Healthcare/Dharmacon	n.a.
Set of 4: ON-TARGETplus EMC9 siRNA	EMC9	CCAAUGCAGCUGUGAACGA	n.a.	LQ-017638-02-0002 2 nmol	GE Healthcare/Dharmacon	n.a.
	EMC9	CUUGAAAAUUGCUGGGCGA	n.a.	LQ-017638-02-0002 2 nmol	GE Healthcare/Dharmacon	n.a.
	EMC9	CGCUGGGUCCCUAAGGAUA	n.a.	LQ-017638-02-0002 2 nmol	GE Healthcare/Dharmacon	n.a.
	EMC9	GUCUGGUGGUGGCUGGUUA	n.a.	LQ-017638-02-0002 2 nmol	GE Healthcare/Dharmacon	n.a.
Set of 4: ON-TARGETplus EMC10 siRNA	EMC10	GUACAAGCUUGAUUGAAAU	n.a.	LQ-018434-02-0002 2 nmol	GE Healthcare/Dharmac	n.a.
	EMC10	UCACUUUGACACUGGACUA	n.a.	LQ-018434-02-0002 2 nmol	GE Healthcare/Dharmac	n.a.
	EMC10	AGUCCUUCUUCGCCAAAUA	n.a.	LQ-018434-02-0002 2 nmol	GE Healthcare/Dharmac	n.a.
	EMC10	CUGCUCACUUGAUACGUUA	n.a.	LQ-018434-02-0002 2 nmol	GE Healthcare/Dharmac	n.a.
ON-TARGETplus BAG6 siRNA	Bag6	GCGCAUGUGCUGCAUUGCACAGAUA (3' UU overhang)	n.a.	Custom	GE Healthcare/Dharmacon	[532]
ON-TARGETplus TRC40 siRNA	TRC40	CAGACAACUUUCAUCUGCGUAUGCA (3' UU overhang)	n.a.	Custom	GE Healthcare/Dharmacon	[532]
siGENOME LTN1 siRNA#1	LTN1	GAGAGUACCUUCCUACAUU	n.a.	D-006968-02-0002	GE Healthcare/Dharmacon	n.a.
siGENOME LTN1 siRNA#2	LTN1	GCACUUACCUCACCCAUCA	n.a.	D-006968-03-0002	GE Healthcare/Dharmacon	n.a.
siGENOME NTC#1 siRNA	Scramble/Unspecific	UAGCGACUAAAACACAUCAA	n.a.	D-001210-01-05	GE Healthcare/Dharmac	n.a.
ON-TARGETplus Non-targeting Pool siRNA	Scramble/Unspecific	UGGUUUACAUGUCGACUAA	n.a.	D-001810-10-20 20 nmol	GE Healthcare/Dharmac	n.a.
	Scramble/unspecific	UGGUUUACAUGUUGUGUGA	n.a.	D-001810-10-20 20 nmol	GE Healthcare/Dharmac	n.a.
	Scramble/unspecific	UGGUUUACAUGUUUUCUGA	n.a.	D-001810-10-20 20 nmol	GE Healthcare/Dharmac	n.a.
	Scramble/unspecific	UGGUUUACAUGUUUUCCUA	n.a.	D-001810-10-20 20 nmol	GE Healthcare/Dharmac	n.a.
376_0493 (V2LHS_259758)	EMC2	TGCTGTTGACAGTGAGCGAGCCTGTAACTTATTTACTAAATAGTGAAGCCACAGATGTATTTAGTAAATAAGTTACAGGCCTGCCTACTGCCTCGGA	pGIPZ	RHS6066-200197615	Sigma-Aldrich	n.a.
376_0512 (V2LHS_79107)	EMC2	TGCTGTTGACAGTGAGCGCACTTATTGGCCTGTAACTTATTAGTGAAGCCACAGATGTAATAAGTTACAGGCCAATAAGTTTGCCTACTGCCTCGGA	pGIPZ	RHS6066-200215010	Sigma-Aldrich	n.a.
376_0230 (V3LHS_396311)	EMC6	TGCTGTTGACAGTGAGCGACGGGAAGGAGGTGGAACAAATTAGTGAAGCCACAGATGTAATTTGTTCCACCTCCTTCCCGCTGCCTACTGCCTCGGA	pGIPZ	RHS6066-200272512	Sigma-Aldrich	n.a.
376_0389 (V3LHS_396312)	EMC6	TGCTGTTGACAGTGAGCGAAAGGAGGTGGAACAAATATTTTAGTGAAGCCACAGATGTAAAATATTTGTTCCACCTCCTTCTGCCTACTGCCTCGGA	pGIPZ	RHS6066-200304418	Sigma-Aldrich	n.a.
V3LHS_405505	EMC5 (3' UTR)	TGCTGTTGACAGTGAGCGCCAGACCTACTTTAGTAAAAAATAGTGAAGCCACAGATGTATTTTTTACTAAAGTAGGTCTGATGCCTACTGCCTCGGA	pGIPZ	RHS6066-200245877	Sigma-Aldrich	n.a.
V3LHS_405504	EMC5 (3' UTR)	TGCTGTTGACAGTGAGCGCTTGGATTGTACAGGTATAAAATAGTGAAGCCACAGATGTATTTTATACCTGTACAATCCAAATGCCTACTGCCTCGGA	pGIPZ	RHS6066-200249451	Sigma-Aldrich	n.a.
NM_031298.2-536s21c1	EMC6 (3'UTR)	CCGGGCCAGCAATTAACACCATGTACTCGAGTACATGGTGTTAATTGCTGGCTTTTTG	pLKO.1-puro	TRCN0000257006	Sigma-Aldrich	n.a.
shNTC	Non-specific	CCGGCAACAAGATGAAGAGCACCAACTCGAGTTGGTGCTCTTCATCTTGTTGTTTTT	pLKO.1-puro	SHC002	Sigma-Aldrich	n.a.
shNTC			pGIPZ			n.a.

Table 12.7: siRNAs and shRNA plasmids used in this study. n.a., not applicable.

Beads	**Manufacturer**
Sepharose®CL-2B beads	Pharmacia Fine Chemicals
Anti-FLAG®M2 affinity gel	Sigma-Aldrich
Monoclonal anti-HA agarose antibody	Sigma-Aldrich
Protein G resin	Roche
S-protein agarose	GenScript
Streptavidin agarose resin	GenScript

Table 12.8: Beads used for affinity purification

Antibiotic	**Concentration [μg/ml]**	**Manufacturer**
Ampicillin	100	Thermo Fisher Scientific
Carbenicillin	100	Thermo Fisher Scientific
Hygromycin B	variable (see **Table 12.10**)	InvivoGen
Normocin	50	InvivoGen
Puromycin	variable (see **Table 12.10**)	InvivoGen

Table 12.9: Antibiotics

Cell line	**Antibiotic**	**Selection [μg/ml]**	**Maintenance [μg/ml]**
A673	Puromycin	1	1
U2OS Flp-In	Hygromycin B	250	100
	Puromycin	1.6	1
HEK293 Flp-In	Hygromycin B	100	100
	Puromycin	2	1
C2C12	Puromycin	1.4	1
CN21	Puromycin	1	1
TE671	Puromycin	1	1

Table 12.10: Antibiotics used for the selection and maintenance of stable cell lines.

Buffer/Solution	Component	Concentration
Blocking solution	1x PBST	
	Fat-free milk powder	5% (w/v)
IP buffer	NP-40	1% (v/v)
	EDTA	2 mM
	NaCl	150 mM
	Tris HCl pH 7.4	50 mM
	1x Complete Protease Inhibitor Cocktail (supplied freshly)	
	PMSF (supplied freshly)	1 mM
Hypotonic buffer (HB)	KOAc	10 mM
	HEPES pH 7.5	10 mM
	$MgOAc_2$	2.5 mM
	PMSF (supplied freshly)	1 mM
	1x Complete Protease Inhibitor Cocktail (supplied freshly)	
High Salt (HS) buffer	Tris-HCl pH 8.0	10 mM
	NaCl	0.5 M
	PMSF (supplied freshly)	1 mM
	1x Complete Protease Inhibitor Cocktail (supplied freshly)	
Na_2CO_3 buffer	Na_2CO_3 pH 11.5	100 mM
	1x Complete Protease Inhibitor Cocktail (supplied freshly)	
	PMSF (supplied freshly)	1 mM
LMNG lysis buffer	Tris-HCl pH 7.5	50 mM
	NaCl	150 mM
	LMNG	1% (v/v)
	EDTA	5 mM
	NEM	2 mM
	PMSF	1 mM
	Roche Protease Inhibitor Cocktail	1x
Paraformaldehyde solution	Paraformaldehyde	16% (w/v)
PBS (phosphate-buffered saline)	Na_2HPO_4/KH_2HPO_4	12 mM
	KCl	2.7 mM
	NaCl	137 mM
PBST (PBS/Tween™ 20)	1x PBS	1x
	Tween™ 20	0.1% (v/v)
Ponceau S staining solution	Ponceau S	0.5% (w/v)
	Acetic acid	1%(v/v)

Table 12.11: Buffers and solutions

Buffer/Solution	Component	Concentration
RIPA	SDS	0.1% (w/v)
	Sodium deoxycholate	1% (w/v)
	NP-40	1% (v/v)
	EDTA	2 mM
	NaCl	150 mM
	Tris HCl pH 7.4	50 mM
	1x Complete Protease Inhibitor Cocktail (supplied freshly)	
	PMSF (supplied freshly)	1 mM
SDS buffer	SDS	1% (w/v)
	PBS	
	1x Complete Protease Inhibitor Cocktail (supplied freshly)	
	PMSF (supplied freshly)	1 mM
SDS electrophoresis buffer, 10x stock solution	Tris pH 8.3	250 mM
	SDS	1% (w/v)
	Glycine	1.9 M
SDS resolving gel	Tris-HCl pH 8.8	350 mM
	SDS	0.1% (w/v)
	Acrylamide/bisacrylamide (37.5:1)	8.5 - 12% (v/v)
	APS	0.04% (v/v)
	TEMED	0.075 (v/v)
SDS sample buffer, 5x stock solution	Tis-HCl pH 6.8	312.5 mM
	Glycerol	50% (v/v)
	SDS	10% (w/v)
	DTT	60 mM
	Bromophenol blue	0.05% (w/v)
SDS stacking gel	Tris-HCl pH 6.8	125 mM
	SDS	0.1% (w/v)
	Acrylamide/bisacrylamide (37.5:1)	5% (v/v)
	APS	0.04% (v/v)
	TEMED	0.075 (v/v)

Table 12.12: Buffers and solutions (continued)

Buffer/Solution	Component	Concentration
Sucrose buffer (5%)	Tris pH 7.4	50 mM
	NaCl	150 mM
	EDTA	5 mM
	sucrose	5% (w/v)
	LMNG (or Triton X-100)	1% (w/v)/(1% (w/v) for Triton X-100)
	PMSF	1 mM
Sucrose buffer (15%)	Tris pH 7.4	50 mM
	NaCl	150 mM
	EDTA	5 mM
	sucrose	15% (w/v)
	LMNG (or Triton X-100)	1% (w/v)/(1% (w/v) for Triton X-100)
	PMSF	1 mM
Transfer buffer	Tris pH 8.3	25 mM
	glycine	190 mM
	MeOH	20% (v/v)
Triton X-100 lysis buffer	Tris-HCl pH 7.5	50 mM
	NaCl	150 mM
	Triton X-100	1% (v/v)
	EDTA	5 mM
	NEM	2 mM
	PMSF	1 mM
	Roche Protease Inhibitor Cocktail	1x
UC buffer	Tris-HCl pH 8.5	100 mM
	urea	6M
Urea buffer	urea	8M
	thiourea	1M
	CHAPS	0.5% (w/v)
	DTT	50 mM
	spermine tetrahydrochloride	24 mM

Table 12.13: Buffers and solutions (continued)

Description	Manufacturer
3.5 cm tissue culture plate	Corning
6 cm tissue culture plate	Corning
10 cm tissue culture plate	Corning
15 cm tissue culture plate	Corning
6-well tissue culture plate	Corning
12-well tissue culture plate	Corning
24-well tissue culture plate	Corning
96-well tissue culture plate	Corning
0.05% Trypsin/EDTA	Life Technologies
Dulbecco's Modified Eagle Medium (DMEM)	Life Technologies
L-Glutamine 200 mM (100×)	Life Technologies
1.5 ml reaction tube	Sarstedt
1.5 ml Axygen®reaction tube	Corning
2 ml reaction tube	Eppendorf
15 ml reaction tube	Corning
50 ml reaction tube	Corning
Acrylamide:Bisacrylamide 29:1 (40%)	Thermo Fisher Scientific
Bovine Serum Albumin	Sigma-Aldrich
Hybond^{TM}P 0.45 PVDF	Amersham
Clarity^{TM}Western ECL Substrate	Bio-Rad
MES running buffer (20×)	Invitrogen
Pierce®ECL Western Blot Substrate	Thermo Fisher Scientific
Super Signal^{TM}West Femto	Thermo Fisher Scientific
Tetramethylethylenediamine (TEMED)	Thermo Fisher Scientific
S-protein HRP conjugate	Novagen
ddH_2O deionized, filtered by MilliQ water purifier	n.a.

Table 12.14: Miscellaneous materials

Chapter 13

Methods in Molecular Biology

13.1 Polymerase chain reaction (PCR)

DNA (approximately 100 ng) was amplified using Phusion® Hot Start II DNA polymerase (NEB) and 0.5 μM of each primer in the presence of 1M betaine. The PCR reaction was performed on a C1000^{TM}Thermal Cycler (Bio-Rad).

13.2 Purification of PCR products

PCR products were purified using the QIAquick PCR Purification Kit (Qiagen) according to the manufacturer's instructions. DNA was eluted in 30 μl EB buffer. Digested plasmids and digested PCR products were separated on an agarose gel, bands excised, and DNA was extracated using the QIAquick Gel Extraction Kit (Qiagen). DNA elution was performed in 30 μl EB buffer.

13.3 Restriction endonuclease digestion

For PCR products, 15 μl of the reaction mixture was supplemented with 1 x BSA (NEB) and, restriction enzyme buffer (NEB) and 1 μl of the corresponding restriction enzyme(s) (NEB). This digest mixture was adjusted to 20 μl with H_2O. For plasmids, 1 μg DNA was used for digest in the presence of excess restriction endonuclease. The digestion reaction was allowed to proceed for 60 minutes at 37 °C. Digest efficiency was validated by agarose gel electrophoresis.

13.4 DNA ligation

The restriction endonucleas-treated vector backbone was incubated with Alkaline Phosphatase (Invitrogen) for 30 minutes at 37 °C. The ligation reaction was performed using the T4 DNA ligase H.C. (Invitrogen) at a vector backbone:insert ratio of 1:3.

13.5 Bacterial transformation

Competent DH5α bacterial cells were prepared using the $CaCl_2$ method and kept at −80 °C. For transformation, aliquots were defrosted on ice for 10 minutes. DNA was added to 100 μl bacterial suspension, and the mixture was incubated on ice for an additional 15 minutes. Heat-induced transformation was performed by raising the temperature to 42 °C for 45 seconds. The bacteria were transferred back on ice for 2 minutes and 100 μl super optimal broth containing glucose (S.O.C.) medium was added. 100 μl of bacterial suspension was plated on agarose plates containing appropriate antibiotics (**Table 12.9**). The plates were incubated for 18 hours at 37 °C.

13.6 DNA preparation

Small-scale DNA preparation was performed using the PureYield^{TM}system (Promega) according to the manufacturer's instructions. The final elution volume was 30 μl. For large-scale DNA preparations, the Plasmid Midiprep Kit^{TM}(Qiagen) was used according to the manufacturer's instructions. Purified DNA was eluted in 100 μl TE buffer. DNA concentrations were determined using a NanoDrop^{TM}2000 spectrometer (Fisher Scientific).

13.7 RNA isolation, reverse transcription, and qPCR

RNA isolation from cells was performed according to the manufacturer's instructions using the RNeasy Mini Kit (Qiagen). 500 ng RNA were used for gDNA removal and the reverse transcription reaction with the QuantiTect Reverse Transcription Kit (Qiagen) according to the manufacturer's instructions. For the qPCR reaction, the cDNA was diluted 1:10 (for the quantification of EMCs) or 1:50 (for the quantification of SREBP2 target genes), and 5 μl diluted cDNA sample were then mixed with 0.45 μl forward and 0.45 μl reverse amplification primers, 1.6 μl H_2O, and 7.5 μl GoTaq®qPCR Master Mix (Promega). The amplification reaction was performed on a Rotor Gene 6000 real time PCR cycler (Corbett Life Science). The following settings were used: holding step for 2 minutes at 95 °C melting step from 72 -

95 °C (1 °C per step); with 90 seconds of pre-melt conditioning at the first step and waiting for 5 seconds for reach step; 60 °C annealing temperature, 40 cycles. Transcription of actin was used for normalization. Calculation of relative mRNA levels was performed according to the ddCT method.

Chapter 14

Methods in Cell Biology

14.1 Cell culture

The human osteosarcoma line U2OS Flp-In was a kind gift from the Gyrd-Hansen laboratory. HEK293 Flp-In cells were a donation by the Kopito lab. Ewing sarcoma A673 cells were a kind gift from Prof. Udo Oppermann. TE671 cells and CN21 cells were kindly provided by Prof. Dr. David Beeson. All cell lines were maintained in Gibco® GlutaMAX® Dulbecco's Modified Eagle Medium (DMEM; Life Technologies) containing 10% v/v foetal calf serum (FCS) and 2 mM L-glutamine (Life Technologies). Stable expression cell lines generated by Flp recombinase-mediated integration of the GOI were continuously cultured in the presence of hygromycin B (Hygromycin B Gold, InvivoGen). Stable cell lines derived by lentiviral transduction were maintained in puromycin-containing media. All cell lines were cultured in a humidified incubator at 5% CO_2 and 37 °C.

14.2 Cryopreservation of cells

Cells were trypsinized, resuspended in GlutaMAX® DMEM (Thermo Fisher Scientific)/10%FCS (v/v) /2 mM L-glutamine (Gln) (Thermo Fisher Scientific) and centrifuged for 5 minutes at 1000 × g. After resuspension in FCS containing 10% dimethylsulfoxide (DMSO) (Sigma-Aldrich) as cryopreservant, cells were transferred into cryovials, placed into a freezing container (Mr Frosty, Nalgene) and frozen at −80 °C overnight. For long-term storage, the frozen cells were kept in vapour phase nitrogen.

14.3 Transfection of plasmids

Transfection with Lipofectamine^{TM}2000: On the day before transfection, U2OS FlpIn cells were seeded to 6-well plates (3.5×10^5 cells per well) or 6 cm plates (1×10^6 cells per plate). For transfection, the ratio of DNA:Lipofectamine^{TM}2000 was 1:2.5 to 1:5. For one well of a 6-well plate, Lipofectamine^{TM}2000 (Invitrogen) was mixed with 250 μl OptiMEM (Thermo Fisher Scientific) and incubated at room temperature for 5 min. The appropriate amount of DNA was diluted in 250 μl OptiMEM and added to the OptiMEM/Lipofectamine^{TM}2000 mixture to obtain the transfection mixture. The transfection mixture was incubated for 20 min at room temperature and then added drop wise to the cells in 2 ml preconditioned cell culture medium. The cells were transferred back to a humidified incubator and left for After 3.5 hours at 37 °C. Subsequently, the mixture was aspirated, and replaced with DMEM + 10% FCS (v/v) /2 mM L-Gln. The following day, cells were trypsinized and transferred to a larger plate. Cells were processed at the indicated time points after addition of the transfection mixture to the cells.
Transfection with Fugene^{TM}HD: The same cell number as for transfection with Lipofectamine^{TM}2000 (Invitrogen) was seeded. Cells were transfected with a 1:4 ratio of DNA: Fugene^{TM}HD (Promega). An appropriate amount of Fugene^{TM}HD was added to 250 - 500 μl OptiMEM (Thermo Fisher Scientific) and incubated at room temperature for 10 minutes. The DNA was directly added to the thus diluted Fugene^{TM}HD and the mixture was incubated for an additional 20 minutes at room temperature before dropwise addition to the cells in 2 ml preconditioned DMEM + 10% (v/v) FCS/2 mM L-Gln per well of a 6-well plate. Cells were left overnight in a humidified incubator at 37 °C, and the next day transferred to a larger plate. Transfected cells were further processed at the indicate time points after supplementation with the transfection mixture.

14.4 siRNA-mediated knockdown

Cells were transfected with either non-targeting siRNA or siRNA targeting the gene of interest. For a detailed list of the siRNAs used, please refer to **Table 12.7**. The following amounts were used to transfect cells in a single well of a 6-well, or 3.5 cm plate. On the evening before transfection, 3×10^5 - 3.5×10^5 cells (U2OS Flp-In) were seeded in 1.6 ml DMEM/10% (v/v) FCS/2 mM L-Gln. For transfection, 4 μl Dharmafect 1 (Dharmacon) were mixed with 196 μl HBSS (Thermo Fisher Scientific) and incubated at room temperature for 10 minutes (A). In a separate tube, 10 μl of 20 μM SMARTpool (GE Healthcare) or individual siRNAs (GE Healthcare, Sigma-Aldrich) were added to 190 μl HBSS (Thermo Fisher Scientific) (B). A and

B were mixed and left at room temperature for 20 minutes. The transfection mixture (A+B) was then added dropwise to the cells. 24 hours after transfection, the cells were split to 10 cm plates (one plate per well) and incubated for an additional 48 hours.

14.5 Genome editing

14.5.1 gRNAs

A list of gRNAs can be found in **Table 12.6**. Before transfection, the efficiency of each individual gRNA was evaluated by high resolution melting analysis (HRMA).

14.5.2 Transfection and selection

Cells were seeded to 6 cm tissue culture plates 24 hours before transfection at a density of 6×10^5 cells per plate. Each plate was transfected with 3 μg DNA using either Lipofectamine^{TM}2000 or Fugene^{TM}HD. The following day, the cells were trypsinized and the content of one 6 cm plate transferred to a 10 cm tissue culture plate. 48 hours after transfection, the medium was supplemented with 1 μg/ml puromycin (InvivoGen) for 72 hours. Surviving cells were then expanded and served as a polyclonal 'knockout pool' or were used for the derivation of single-cell clones by limiting dilution.

14.5.3 Establishment of single cell clones

Polyclonal 'knockout pools' were trypsinized and adjusted to a concentration of 100 cells/ml. 100 μl of cell suspension was seeded to each well of a 96-well plate. Two 96-well plates per construct were seeded. Cells were then left at 37 °C, 5% CO_2 until individual colonies were discernible. Wells containing single colonies were treated with trypsin and the cells were then sequentially expanded for validation by immunoblotting.

14.6 Gene knockdown using lentiviruses

14.6.1 Production of lentivirus

For the production of lentivirus, 2×10^6 HEK293T cells were seeded to a 10 cm tissue culture plate the evening before transfection. The cells were then transfected with 10 μg shRNA vector and the lentiviral packaging vectors pMD2 (1 μg) and pCMV-R (10 μg), according to the calcium phosphate transfection method [533]. The medium was changed to DMEM + 10% FCS 4 - 5 hours after transfection. Culture media containing lentivirus particles was

collected 72 hours after transfection, and was filtered through a 0.45 μm membrane. For future use, lentivirus-containing medium was aliquoted, flash-frozen in liquid nitrogen, and stored at $-80\,^{\circ}$C.

14.6.2 Transduction and selection

Lentivirus-containing media was diluted in DMEM + 10% FCS and added to the target cells in the presence of 6*mu*g/ml polybrene for 16 hours. To remove residual virus, cells were then washed three times with PBS. Transduction efficiency was monitored by determining the amount of GFP positive cells (in the case of GIPZ lentiviral constructs) *via* FACS analysis (FACS Canto, BD Biosciences). To maximize the probability of a single integration event per cell, a transduction rate of 3 - 5 % was aimed for. The cells were split to a new tissue culture plate and stable populations were selected by adding 1.6 μg/ml puromycin (InvivoGen) 48 hours after infection at a confluency of approximately 20%. Selection was considered successful at the outgrowth of stable colonies and the complete loss of untransduced cells in the presence of 1.6 μg/ml puromycin. Cells were subsequently maintained in 1 μg/ml puromycin.

14.7 Generation of stable cell lines using the Flp-In system

Cells were seeded to a 6 cm tissue culture plate and transfected with 3 μg of the gene of interest in pcDNA$^{\text{TM}}$/5/FRT/TO and 1 μ g of Flp recombinase (pOG44) using Lipofectamine$^{\text{TM}}$2000 (**Section 14.3**). The following day, cells were trypsinized and seeded to 10 cm tissue culture plates in order to achieve 20 - 40% confluency the following day. 48 hours after transfection, 250 μg/ml (U2OS Flp-In) or 100 μg/ml (HEK293 Flp-In) hygromycin B (InvivoGen) was added to the cells. The same amount was supplemented to a plate of the parental untransfected cell line at the same confluency (negative control). Selection was finished when all cells of the negative control had died (typically 7 - 10 days of exposure). For sub-culturing, cells were selected cells were routinely supplemented with 100 μg/ml hygromycin B.

14.8 Cholesterol depletion

PM-bound cholesterol was depleted by treating cells with 3 - 6 mM methyl-β-cyclodextrin (MBCD) over different periods of time (commonly 16 hours). On the day before MBCD treatment, 1×10^4 cells were seeded to each well of a 96-well plate. After 24 hours, some of the

medium was removed from each well, mixed with MBCD, and added back. This premixing step ensured equal volumes of MBCD in each well. Each treatment regimen was repeated in four wells per cell line (technical quadruplicates) per experiment. Cells were transferred back into the incubator and were processed 16 hours later (**Section 14.9**).

14.9 Crystal violet-staining

Cells were seeded to a 96-well plate and treated for different periods of time. To fixate the cells, the medium was completely removed and 100 μl per well of cold methanol/acetone (1:1) were added per well for 10 minutes. The fixative was aspirated and 100 μl staining solution (0.1% (w/v) crystal violet, 10% EtOH) was added for 10 minutes. After removal of the staining solution, cells were washed with ultrapure water and air-dried. Microscopy was performed on the stained cells.

14.10 Imaging-based quantification of crystal violet-staining

Crystal violet-stained cells were scanned with a Typhoon^{TM}FLA9500 laser scanner (GE Healthcare) at 50 mum resolution and at an excitation wavelength of 640 nm. The relative integrated pixel intensity was determined using the ImageJ software package.

14.11 Lipid extraction from cells and cholesterol quantification

Quantification of cellular cholesterol levels was performed by GC-MS/MS. 1.5×10^6 cells were seeded to a 10 cm tissue culture plate. After 24 hours, the medium was aspirated and cells were washed three times with PBS before addition of DMEM/L-Gln containing either 5% FCS or 5% LPDS. Cells were then allowed to grow for another 24 hours before washing three times with ice-cold PBS and collection using a cell scraper. Cells were resuspended in 1 ml ice-cold PBS and 10% of the cell suspension (100 μl) was used for protein quantification by Bradford assay (**Section 15.2**). Protein concentrations were assumed to be proportional to cell number and were used for normalization. The remaining cell suspension (900 μl) was centrifuged and resuspended in 400 μl MeOH:H_2O, and a spatula tip of glass beads was added. Myristic acid was added to each sample to control for any losses during lipid extraction. Cells were subjected to four cycles of homogenization by shaking at 6500 Hz for 40 seconds. In between each cycle, the cells were placed on dry ice to avoid overheating. 1 ml methyl t-butyl ether

was added and an additional homogenization cycle (6500 Hz, 40 seconds) was performed. The homogenates were centrifuged at 13000 × g for 20 minutes at 4 °C. 800 μl of the organic phase were collected, transferred to glass vials, and evaporated by vacuum centrifugation. The dry metabolite film was resuspended in 50 μl of 20 μg/μl methoxyamine hydrochloride (MOX) in pyridine and incubated at 30 °C for 90 minutes under constant agitation (vortexing). Next, 30 μl pyridine and 70 μl *N*-Methyl-*N*-trimethylsilyltrifluoroacetamide (MSTFA) were added and incubated at 60 °C for 60 minutes. Samples were cooled down and directly injected into the mass spectrometer. For quantification, the area under the curve for each cholesterol peak was measured and normalized to both, the internal control (myristic acid) and the protein concentration (as determined by Bradford assay).

14.12 Scratch assay

To perform the scratch assay, 5×10^5 cells per well were seeded to a 12-well tissue culture plate. After 18 hours, three vertical 'scratches' were inflicted by locally removing a confluent monolayer of cells using a P10 micro pipette tip. The scratches were equidistant from each other by approximately 2 - 3 mm. Detached cells were removed by washing the monolayer with PBS, and DMEM/10% FCS/2 mM L-Gln was subsequently added back to the attached cells. The plate was then immediately transferred into a humidified microscopy chamber and monitored for 18-24 hours at 37 °C, 5% CO_2. At least three different fields of view per well were selected. Selection criteria included comparable scratch width, comparable cell density and a homogeneous cell border. Images were recorded at 15 minute intervals. All images were batch-compiled into a movie and the scratch surface area was determined using the ImageJ software package (NIH). For each time point, three different fields of view per experiment per cell line were scored and averaged. The scratch area at t = 0 min was set as 100% for each individual cell line. Areas determined in subsequent time points were then normalized to the averaged scratch area at t = 0 minutes for each individual cell line. Data were plotted with Prism 6 (GraphPad Software).

Chapter 15

Methods in protein biochemistry

15.1 Preparation of whole-cell protein lysates

Cells grown in tissue culture dishes were placed on ice, growth medium was aspirated, and cells were rinsed with ice-cold PBS. Cells were then collected by scraping in cold PBS using a cell strainer (Greiner). Next, cells were transferred to 1.5 ml Eppendorf tubes or 15 ml conical tubes and centrifuged at 1000×g at 4 °C for 5 minutes. PBS was removed and cells were resusupended in the appropriate lysis buffer (**Table 12.11**) and incubated on ice for 45 min. Cell lysates were centrifuged at 21.000×g at 4 °C for 20 minutes to precipitate cellular debris, the overall volume was adjusted with cold lysis buffer, and 5× Laemmli buffer containing DTT was added. The final concentration of DTT in the samples was 17.5 mM. Lysates were heated to 56 °C for 10 min and stored at -80 °C for further processing (**Section 15.3**).

15.2 Determination of protein concentration

Protein concentration in whole-cell lysates was determined using the Bradford method. Cell lysates were diluted 1:5 in 1% Triton X-100 lysis buffer. 1 μl of this dilution was then transferred to a 96-well cell culture plate and supplemented with 200 μl of detection reagent (Quick Start® Bradford Protein Assay, Bio-Rad; the detection reagent was prepared according to the manufacturer's instructions). Purified BSA was used to create a standard curve in the range of 0 - 1.5 μg/ml. Absorption was measured at 570 nm on a microplate reader.

15.3 SDS-PAGE

Proteins were separated by SDS-polyacrylamide gel electrophoresis (SDS-PAGE). Protein samples were prepared as described in **Section 15.1** and applied to SDS-polyacrylamide gels (7.5/10/12/15% (v/v)). The Mini Protean® III system (Bio-Rad) was used to perform discontinuous electrophoresis. Polyacrylamide gels were cast using a Mini Protean® III casting stand (Bio-Rad). Alternatively, pre-cast NuPAGE™ Novex™ 4 - 12% Bis-Tris Protein Gels (Thermo Fisher Scientific) were used in combination with 1× NuPAGE® MES running buffer (Thermo Fisher Scientific). The latter gels were run at 150V for 105 minutes under constant cooling.

15.4 Immunoblotting and detection

A tank blotting system was used to transfer electrophoretically separated proteins (Section 15.3) from the polyacrylamide gel to a polyvinylidene fluoride (PVDF) membrane (Hybond™ P; GE Healthcare). PVDF membranes were solubilized in 100% MeOH for 1 minute. Whatman filter papers and sponges were equilibrated in transfer buffer. In a basin with sufficient transfer buffer, the protein gel was assembled into a 'sandwich' of a plastic fastener, two sponges, two Whatman filter papers, and one PVDF membrane. Protein transfer occurred for 90 minutes at 110 V and 4 °C. Thereafter, the 'sandwich' was disassembled and the membrane transferred to blocking buffer (5% milk powder (w/v) in PBST) to saturate free protein binding sites. After 60 minutes of incubation on a shaker at room temperature, the membranes were transferred to 50 ml conical tubes containing primary antibodies in 5 ml blocking buffer. The tubes were left for 60 minutes at room temperature or overnight at 4 °C under constant agitation. The following day, the membranes were washed for at least 15 - 30 min in PBST, immersed in horseraddish peroxidase (HRP)-conjugated secondary antibody in blocking buffer (1:10.000 (v/v)), and incubated on a shaker for 60 minutes. Membranes were then extensively washed in PBST buffer and detection was performed by incubation with luminol-based enhanced chemiluminescence (ECL) HRP substrates (Thermo Fisher Scientific) according to the manufacturers instructions. In some cases, HRP was irreversibly inhibited by adding 10% sodium azide to the membrane for 12 hours at 4 °C and under constant agitation. The membrane was subsequently extensively washed with PBST and re-probed with primary and secondary antibodies as described above. Images were acquired by exposure of X-ray films (Fuji). Alternatively, image acquisition was performed using the ChemiDoc™ MP Imaging System (Bio-Rad).

15.5 Densitometry

Proteins were quantified by densitometry of immunoblots obtained by incubation with a target-specific primary antibody, followed by signal amplification using secondary AlexaFluor 488-conjugated antibodies. Image acquisition was performed using the ChemiDoc system (Bio-Rad). Care was taken not to saturate the signal, and only signal intensities below the saturation threshold, as indicated by the Image Lab 5.1 software package (Bio-Rad), were used for subsequent quantification. Bands were then quantified by the ImageJ software package. Areas containing individual protein bands were defined and the area under the curve for the integrated pixel intensities of each band was measured for both the protein of interest and an internal control (usually tubulin). Each intensity was normalized to that of tubulin belonging to the same sample. Depending on the experiment, signal intensities were then further normalized to positive or negative control samples.

15.6 SILAC-PMP

15.6.1 SILAC labelling and cell surface biotinylation

The PMP procedure was adapted from Weekes *et al.* (2012) [133]. Several modifications were introduced to the protocol. Cells were maintained for at least six passages in media supplemented with either light (K0/R0), medium (K4/R6), or heavy (K8/R10) amino acids. Incorporation efficiency under these culturing conditions was determined to be greater than 98%. 3.5 days prior to the experiment, 6 million cells per 15 cm tissue culture plate were seeded. On the day of the experiment, cells were washed twice with ice-cold PBS, pH 6.7. To each plate, 8 ml of the biotinylation/oxidation mixture (1 mM sodium meta-periodate, 10 mM aniline, and 100 mM aminooxy-biotin, PBS pH 6.7) were added and incubated for 90 minutes at 4 °C and under constant agitation in the dark. The reaction was quenched by addition of glycerol to a final concentration of 1 mM for 30 minutes. The reaction mixture was removed and cells were first washed with PBS pH 7.4/5% FCS and then with PBS pH7.4/1mM $CaCl_2$/0.5mM $MgCl_2$.

15.6.2 Sample preparation for MS/MS

Cells were collected in ice-cold PBS using a cell strainer, centrifuged at 1500 × g for 5 minutes, and the resulting cell pellet was resuspended on ice in 300 μl of Triton lysis buffer per 15 cm plate for 45 minutes. Cell debris was removed by centrifugation for 25 minutes at 17.000 ×

g. The protein concentration of the supernatant was determined by Bradford assay in three independent triplicates. Equal amounts of cell lysate from K0/R0, K4/R6, or K8R10 cells were mixed, 77.8 μl of 50% streptavidin/agarose slurry was added per mg of whole-cell lysate, and incubated for 90 minutes on a spinning wheel at 4 °C. Subsequently, the beads were washed using Micro Bio-Spin Chromatography Columns (Bio-Rad, Cat. No. #732-6204). All washing and modification steps were performed with 600 μl buffer and centrifugation steps were performed at 1000 × g for 1 minute at 4 °C. Beads were washed twice with Triton X-100 lysis buffer, followed by two washes with PBS/0.5% (w/v) SDS. Disulphide bonds were then reduced by incubation with PBS/0.5% (w/v) SDS/100 mM DTT at 300 rpm (Eppendorf Thermomixer) at room temperature for 20 minutes. Subsequently, beads were washed twice with UC buffer and treated with UC buffer/50 mM iodacetamide at 300 rpm at room temperature for 20 minutes. Additional washing was performed with UC buffer (2×), 5 M NaCl (2×), 100 mM Na_2CO_3 (2×), PBS (2×) and H_2O (2×). The amount of enriched proteins was estimated by visualization of 1/10 of the sample via SDS-PAGE and subsequent silver staining. Proteins were digested overnight at 350 rpm (Eppendorf Thermomixer) at 37 °C in 200 μl ammonium bicarbonate buffer containing 300 ng trypsin. Trypsin was then inactivated by adding trifluoroacetic acid (TFA) to a final concentration of 1%. The sample was transferred to a SpinX spin column (Sigma) and tryptic peptides were isolated by centrifugation at 1000 × g for 1 minute. Peptides were desalted using a C18 Sep-Pak cartridges (Waters) according to the manufacturer's instructions. The cartridge was pre-conditioned with 5 ml Solution B (0.1% TFA in 65% CH_3CN), and equilibrated with 10 ml of Solution A (0.1% TFA in 98% H2O). Tryptic peptides were added to bind to the cartridge and washed with 10 ml solution A. The peptides were eluted in 2 × 600 μl Solution B. The samples were dried in a vacuum concentrator and resuspended in 20 μl 2% CH_3CN/0.1% TFA.

15.6.2.1 Sample preparation of cytoplasmic fractions

The cytoplasmic fraction was obtained from the supernatant after affinity purification of biotinylated proteins. 10 μl supernantant was trypsinized for LC-MS/MS analysis. The samples were reduced with a 5 mM DTT (final concentration) for 30 minutes, followed by incubation with a final concentration of 20 mM iodoacetamide (IAA) for 30 minutes. Proteins were enriched by chloroform/methanol precipitation and resuspended in 6 M urea, 0.1 M Tris pH 7.8. The solution was diluted 1:6 with H_2O and trypsin was supplemented at a trypsin:protein ratio of 1:50. Trypsinization was allowed to proceed overnight at 37 °C and 300 rpm (Eppendorf Thermomixer). Trypsin was inactivated by adding TFA to a final concentration of

1%. Samples were applied to a SpinX spin column and tryptic peptides were enriched by centrifugation at 1000 × g for one minute. Desalting was performed in C18 Sep-Pak cartridges (Waters). The cartridges were conditioned with 5 ml Solution B (0.1% TFA in 65% CH_3CN), and equilibrated with 10 ml of Solution A (0.1% TFA in 98% H_2O). Tryptic peptides were added to the cartridge, washed with 10 ml Solution A, and eluted in 2 × 600 μl Solution B. All samples were dried by a vacuum concentrator and resuspended in 20 μl 2% CH_3CN/0.1% TFA.

15.6.3 Peptide analysis by UHPLC-coupled mass spectrometry

Peptide analysis was performed by ultra-high performance liquid chromatography (Dionex Ultimate 3000 UHPLC, Thermo Fisher Scientific) coupled with tandem mass spectrometry (Q Exactive, Thermo Fisher Scientific) on a PepMap RSLC column (C18, 2 μm, 100 A, 75 μm × 50 cm). Samples were loaded in 0.1% TFA/99% H_2O and analysed on a 2 hour linear gradient at a flow rate of 250 nl/minute. The gradient for peptide elution started at 3 minutes with 2 % buffer B (0.1% TFA/5% DMSO in CH_3CN), increasing to 5% buffer B by 6 minutes, followed by an increase to 35% after 123 minutes. The column was washed twice with 99% buffer B for 10 minutes. The total analysis length was 170 min to allow column re-equilibration. Data acquisition was performed at a resolution of 70,000 full-width half maximum at mass/charge of 400 with lockmass enabled (445.120025 m/z), Top 15 precursor ion selection, Dynamic Exclusion of 27 seconds, and fragmentation was performed in Higher-energy C-trap dissociation (HCD) mode with a Normalized Collision Energy of 28.

15.6.4 Data processing

Raw MS files were processed by using MaxQuant v. 1.5.1.2 [414]. The FASTA file used for protein identification was downloaded from Uniprot in April 2015 using the database of reviewed human proteins. A maximum of two missed tryptic cleavages sites was allowed and the peptide ion tolerance was adjusted to 0.5 Da. Variable modifications included in protein quantification were N-terminal acetylation, methionine oxidation, and deamidation (NQ). Carbamidomethyl cysteine was defined as a fixed modification. The false discovery rate for peptides and proteins was defined as 0.01 against a reversed decoy database. For protein quantification, unique and razor peptides were used with a minimum ratio count of 1. Re-quantify was enabled. Data generated by MaxQuant was further analysed using Perseus v. 1.5.0.31 [417]. Reverse peptides, proteins only identified by site, and potential contaminants were removed from the dataset. Normalized H/L or normalized M/L ratios were transformed into log2 values. Intensities were

transformed into log10 values. Significance B values were calculated by Perseus. Proteins with a decrease in abundance of at least 30 percent were classified as downregulated; those with an increase of at least 30 percent were scored as upregulated. Proteins commonly down- or upregulated in multiple cell lines were identified by using Perseus and Microsoft Excel 2010. Venn diagrams were drawn with Adobe Illustrator CS6.

15.7 ^{35}S-methionine/cysteine pulse-chase

U2OS Flp-In cells (wt/ΔEMC6) were subjected to radiolabel pulse-chase assays according to Christianson *et al.* (2008) [139]. 4×10^6 cells were seeded to a 10 cm tissue culture plate. Cells were then starved in methionine/cysteine-free DMEM (Lonza) + 10% FCS for 10 minutes, and metabolically labelled by adding ^{35}S-methionine/cysteine (EXPRE^{35}S^{35}S Protein Labelling Mix (PerkinElmer)) for 10 minutes. The medium was removed, cells were washed three times with PBS, and incubated in DMEM containing methionine/cysteine (50 mM each) + 10% FCS for the indicated time periods. Cell lysis was performed in 1% Triton-X100 lysis buffer and SQS was immunoprecipitated from the detergent-soluble fraction using protein G resin (Roche) + anti-SQS antibody (ab195046). Immuno-captured material was resuspended in Laemmli buffer + 20 mM DTT, separated on a gel, and radiolabelled proteins were visualized and quantified using a phosphoimager and the QuantityOne software package (Bio-Rad).

15.8 Velocity gradient sedimentation

Whole-cell lysates were prepared in LMNG lysis buffer. The protein concentration was determined by Bradford assay and 0.5 - 1 mg whole-cell lysate was applied to a 5 - 15% continuous sucrose gradient. Velocity gradient sedimentation was performed in a physiological salt solution (150 mM NaCl, 50 mM Tris pH7.4, 5 mM EDTA, and 1 mM PMSF) in the presence of 1% LMNG (Affymetrix). Sucrose gradients were generated by carefully layering 5% sucrose solution onto a 15% sucrose solution and using GradientMaster 108® (Biocomp) to form a continuous sucrose gradient (parameters: 5 - 15% sucrose, short, S1/1; t = 2:50 min; angle = 81.5; speed = 15 rpm). Sucrose gradients were then spun in an SW41 rotor at 36.000 rpm (OptimaTM L-100 XP) for 16 hours at 4 °C. Subsequently, 13 fractions were collected by hand (940 μl per fraction) and proteins were precipitated by adding trichloroacetic acid (TCA) to a final concentration of 8.4%. After incubation for 1 hour on ice, protein pellets were obtained by centrifugation at 21.000 × g for 5 min, washed twice with ice-cold acetone and resuspended in 200 μl 2 × Laemmli buffer containing 35 mM DTT. If necessary, the pH was adjusted with

1M Tris (pH 9). Before SDS-PAGE analysis, the samples were heated to 56 °C for 10 minutes.

15.8.1 Molecular weight markers

Native gel filtration standards (Gel Filtration Markers Kit, MWGF1000, Sigma) were mixed and subsequently separated on a 5 - 15% sucrose gradient in a physiological salt solution (150 mM NaCl, 50 mM Tris pH7.4, 5 mM EDTA, and 1 mM PMSF) with 1% LMNG (Affymetrix) present. The gel filtration markers used were alcohol dehydrogenase (150 kDa), β-amylase (200 kDa), apoferritin (443 kDa), and thyroglobulin (663 kDa). Thirteen fractions were collected by hand and further processed as outlined above (**Section 15.8**). Each isolated and processed fraction was subjected to SDS-PAGE analysis. The molecular size of each complex was correlated with the fraction number in which its monomeric subunits could be detected by silver staining (Silver Stain for Mass Spectrometry, Pierce).

15.9 Membrane fractionation

Membrane fractionation was performed to specifically enrich membrane-bound proteins. 1×10^7 cells were seeded to 15 cm tissue culture plates 24 hours before harvesting. Cells were collected by scraping in cold PBS and pelleted by centrifugation at 4 °C. The cell pellet was resuspended in 1 ml ice-cold HB per plate and incubated on ice for 5 minutes. Cells were then homogenized *via* mechanical disruption by 40 strokes on ice with a size B glass pestle. Cell debris was removed by centrifugation at 10.000 × g, 4 °C for 10 minutes. To isolate the membrane fraction, the supernatant (input) was centrifuged at 100,000 × g for 60 min. The resulting supernatant was collected (cytoplasmic fraction) and the membrane pellet (membrane fraction) was gently washed in 2 × 1 ml ice-cold HB, before adding 1 ml 1% cold Triton-X 100, vortexing and incubation on ice for an additional 30 minutes. This resulted in the solubilization of membrane-bound proteins. Proteins from input, cytoplasmic, and membrane fractions were concentrated by TCA precipitation (**Section 15.10**). Proteins of all three fractions (input/cytoplasmic/membrane) were resuspended in 100 μl 2 × Laemmli buffer and heated at 56 °C for 10 minutes. Equal volumes were loaded on an SDS-PAGE gel.

15.10 Protein precipitation with TCA

Protein samples were supplemented with trichloroacetic acid (TCA) at a final concentration of 0.61 M and incubated on ice for 60 minutes. The samples were then centrifuged at 14.000 × g for 5 minutes at 4 °C. The supernatant was discarded and the protein pellet washed twice

with ice-cold acetone. Residual acetone was evaporated at room temperature and proteins were resuspended in 2 × Laemmli buffer + 35 mM DTT.

15.11 Affinity purification and co-immunoprecipitation

15.11.1 Affinity purification of epitope-tagged proteins

Whole-cell lysates were isolated according to **Section 15.1** by resuspending the cells in the appropriate lysis buffer (Triton X-100 lysis buffer or LMNG lysis buffer). Lysates were pre-cleared by adding 100 μl of 50% sepharose bead slurry and overhead rotation for 1 hour at 4 °C. Beads were pelleted by centrifugation for 1 minute at 3000 × g, 4 °C. After determination of the protein concentration in the supernatant by Bradford assay (**Section 15.2**), an appropriate amount of protein lysate (300 - 1000 μg) was adjusted to 500 μl using the same lysis buffer. 20 - 40 μl of 50% antibody-conjugated bead slurry was added to each tube and rotated for 2 hours at 4 °C. For S-tag pulldowns, 40 μl 50% S-protein agarose (GenScript) was added to the lysate and incubated at 4 °C on an overhead rotor for 1 hour. The resin was collected by centrifugation for 1 minute at 3000 × g, 4 °C and washed once in high-salt buffer (lysis buffer containing 0.5M NaCl) followed by two washes with detergent-free buffer. The beads were then resuspended in 2 × Laemmli buffer containing 35 mM DTT and heated at 56 °C for 10 minutes.

15.11.2 Affinity purification of epitope-tagged proteins from sucrose gradient fractions

1 mg of Whole-cell protein lysate was subjected to velocity gradient sedimentation as described in **Section 15.8**. 50% of each fraction (470 μl) were supplemented with 12 μl HA beads and 38 μl sepharose 4B beads. Binding to the HA beads was allowed to occur for 2 hours at 4 °C on an overhead rotor. The supernatant was saved as a post-AP sample. Beads were washed twice with lysis buffer without detergent and resuspended in 100 μl 1x Laemmli buffer + 17.5 mM DTT. Samples were heated for 10 minutes at 56 °C, and 10 μl of each sample were loaded onto a Novex^{TM} 4 - 12% Bis-Tris gel (Thermo Fisher Scientific) for further analysis.

15.12 Solubilization of RIPA-insoluble protein fractions

For isolation of whole-cell lysate, 15×10^6 U2OS Flp-In cells were seeded to a 15 cm tissue culture plate 24 hours before lysis by resuspension in 200 μl RIPA buffer for 45 minutes on ice.

After centrifugation at 17.000 g for 25 minutes, the RIPA insoluble fraction was washed with 1 ml RIPA buffer, spun at 17.000 g for 25 minutes, and resuspended in 200 μl urea lysis buffer for 45 min on ice. The urea soluble fraction was then isolated by centrifugation at 17.000 g for 25 minutes. Protein concentration of the RIPA-soluble fraction was adjusted with RIPA buffer and an equal amount of urea buffer was added to the urea-soluble fraction. After addition of equal amounts of Laemmli buffer, the samples were heated at 56 degrees for 10 minutes.

Chapter 16

Purification and quantification of lipids

16.1 Lipid extraction, derivatization, and quantification

Equal numbers of cells were seeded to 10 cm tissue culture plates. 24 hours after seeding, the cells were washed three times with PBS and either DMEM + 2 mM L-Gln + 5% FCS or DMEM + 2 mM L-Gln + 5% LPDS was added and left for another 24 hours. Cells were washed three times with cold PBS and collected by scraping and centrifugation at 1000 × g, 5 minutes, 4 °C. Cell pellets (approximately 5×10^6 cells) were resuspended in 400 μl 50% Methanol/H_2O. 1 μg myristic acid was added as an internal standard. A spatula tip of glass beads was added to each sample. For cell disruption, the samples were homogenized using a Precellys^{TM}24 tissue homogenizer (Bertin Instruments) for 4 cycles of 40 seconds at 6500 Hz, with cooling for 1 min on dry ice after each cycle. 1 ml methyl-*tert*-butyl ether was added and an additional homogenization cycle (40 seconds, 6500 Hz) was performed. The samples were subsequently centrifuged at 13.000 × g for 20 minutes at 4 °C. Equal volumes of the organic phase were collected, transferred to a glass vial and dried in a vacuum centrifuge. Dried metabolites were resuspended in 50 μl of 20 μg/μl methoxyamine hydrochloride in pyridine, and incubated at 30 °C for 90 minutes under constant agitation (1200 rpm), followed by addition of 30 μl pyridine and 70 μl *N*-Methyl-*N*-trimethylsilyltrifluoroacetamide/1% chlorotrimethylsilane, and incubation for 60 minutes at 60 °C on a shaker at 1200 rpm. Samples were cooled down and directly injected into the GCxGC-MS system, consisting of a chromatograph, a quadrupole mass spectrometer (Shimadzu GCMS QP2010 Ultra), and a Shimadzu AOC-20i/s auto sampler. Metabolite separation was performed in two dimensions: a SHM5MS capillary

column (30 m × 0.25 mm internal diameter × 0.25 μm film thickness, Shimadzu), followed by a BPX-50 capillary column (5 m × 0.15 mm internal diameter × 0.15 μm film thickness, SGE). The carrier was helium gas at a constant inlet head pressure of 73 psi and the modulation period was 6 seconds. Sample injection was performed at 280 °C. The oven temperature was increased from 60 °C to 320 °C at 10 °C per minute and was held constant at 320 °C over a period of 8 minutes. The mass spectrometer interface temperature was 330 °C. The ion source was at 230 °C. MS scan speeds were 5000 - 20000 amu (m/z = 45 - 600). The recording of electron ionization spectra was carried out at 70 eV. Data analysis was performed using the following software packages: GCMSsolution (v2.72/4.20 Shimadzu), Chromsquare (v2.1.6, Shimadzu), and GC Image (v2.3).

16.1.1 Quantification of cholesterol

The absolute amount of cholesterol for each sample was normalized to its internal standard (myristic acid) to account for any losses during the extraction and derivatization procedure, and to the relative protein concentration of each sample, as determined by Bradford Assay (Bio-Rad). The relative protein concentration of wild-type cells was set to 100%.

Chapter 17

Microscopy

17.1 Confocal microscopy

Cells were seeded on 12-mm glass coverslips (Nunc). The following day, the adherent cells on the coverslips were washed twice with PBS and fixated with 4% paraformaldehyde (PFA) for 20 min. PFA was removed by washing twice with PBS and cells were permeabilized by incubation with 0.1% Triton™ X-100 in PBS for 5 min, washed twice with PBS, and then blocked with 0.2% fish skin gelatine (FSG) in PBS for 1 h. The blocking solution was aspirated and 100 μl primary antibody in PBS + 0.2% FSG were applied to the coverslips and left for 1 hour at room temperature. After removal of the primary antibody solution, the coverslips were washed twice with PBS and 100 μl Alexa Fluor® 488- or Alexa Fluor® 647-conjugated secondary antibodies in PBS + 3% BSA were added and incubated for 1 hour in the dark. Secondary antibodies were removed, and the coverslips were washed twice with PBS and once with H_2O. DNA was stained using 5 μg/ml DAPI before mounting in Fluoromount G® (Southern Biotech). Prior to microscopy, the coverslip was sealed with transparent nail polish. Visualization of immunofluorescence signals was performed and images were acquired using an LSM 710 (Zeiss) confocal microscope. Images were processed using ImageJ and Adobe Illustrator software.

Chapter 18

Bioinformatics

18.1 Gene Ontology (GO) analysis

GO analysis was performed by uploading all protein IDs excluding potential contaminants, or proteins identified by reverse peptides or only by site, to the Panther classification system [413] (http://pantherdb.org/).

18.2 Domain and motif annotation

Primary polypeptide sequences for human EMC1 - 10 and human SQS were extracted from Uniprot (http://www.uniprot.org/). Common motifs were annotated using the Pfam database (http://pfam.xfam.org/, [349]). For the identification of putative TMDs, the TOPCONS database [340] was used (http://topcons.net/). *N*-linked glycosylation sites were mapped by the NetNGlyc 1.0 Server (http://www.cbs.dtu.dk/services/NetNGlyc/).

18.3 Helical wheel prediction

Helical wheels were of annotated TMDs (Uniprot and TOPCONS [340]) were generated using wheel.pl, v. 1.4 (http://rzlab.ucr.edu/scripts/wheel/wheel.cgi).

18.4 Multiple sequence alignment

Primary protein sequences for human EMC1 - 10 were obtained from UniProt and aligned using the Clustal Omega web tool (https://www.ebi.ac.uk/Tools/msa/clustalo/, [352]).

18.5 Expression profiling

RNAseq data for the human EMC1 - 10 were extracted from the GTEx database as listed in the supplementary FPKM data table in [387].

Part V

Supplemental Data

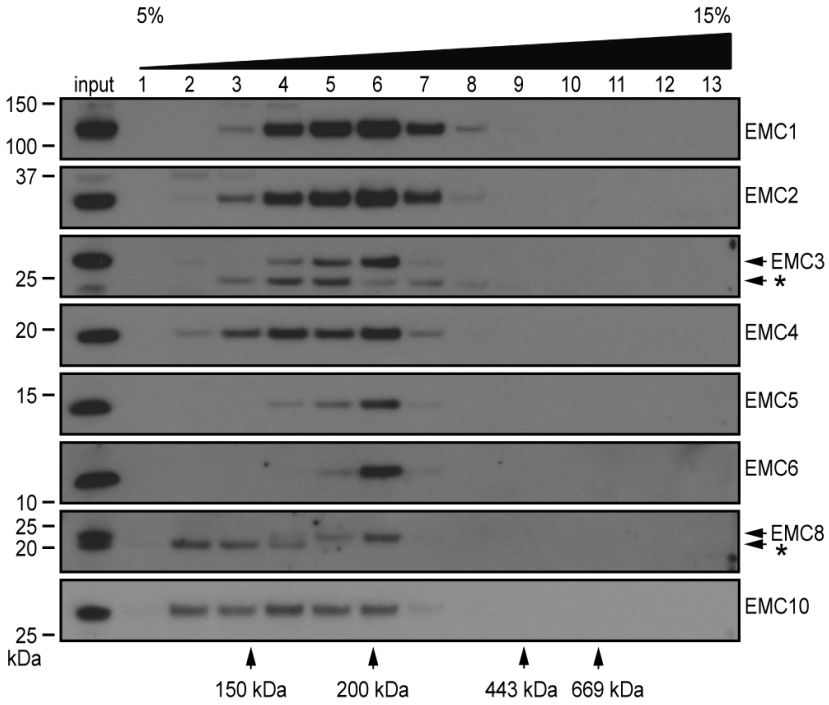


Figure 18.1: Velocity gradient sedimentation in 1% Triton X-100. Whole-cell lysate was subjected to sucrose gradient sedimentation in the presence of 1% Triton X-100. Endogenous EMC proteins were detected using specific antibodies.

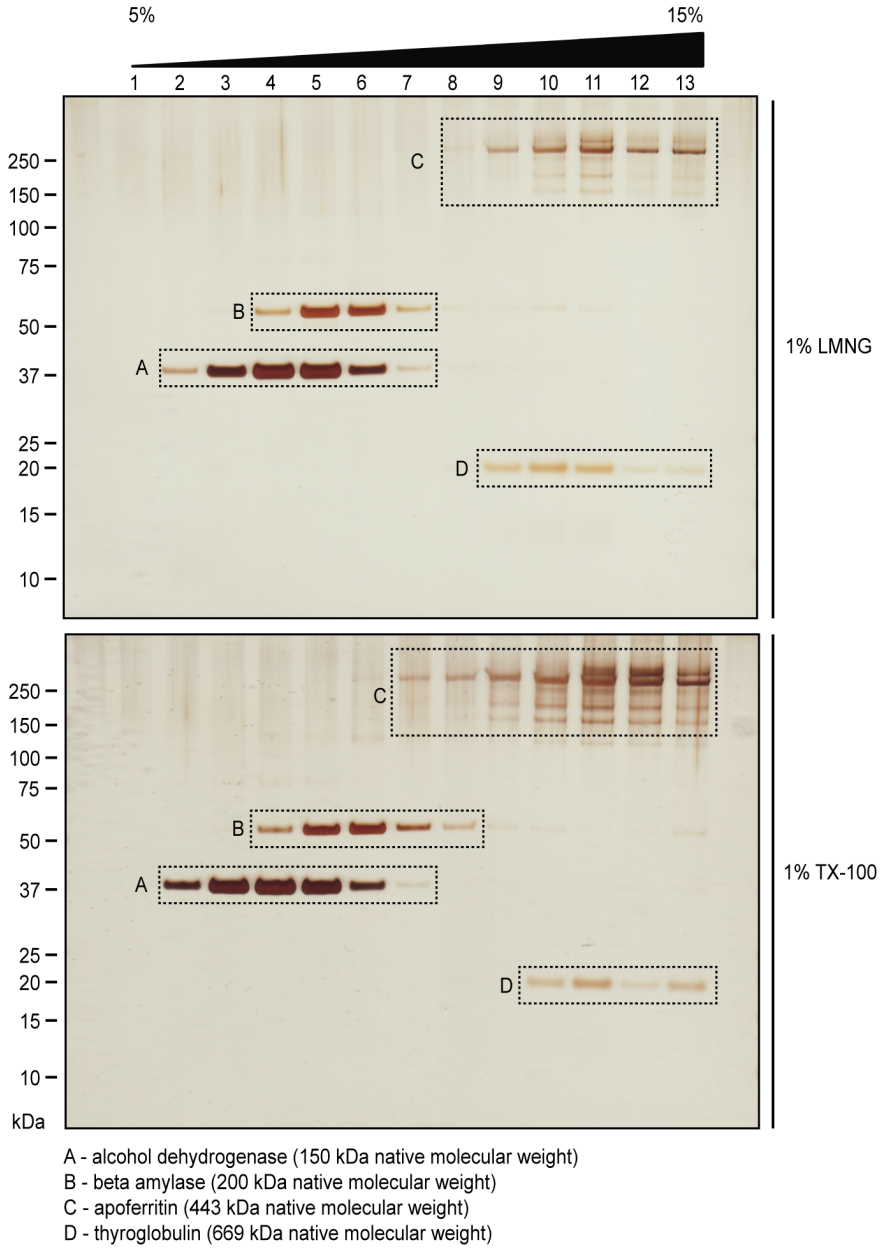


Figure 18.2: Velocity gradient sedimentation of gel filtration markers. Gel filtration markers (A - D, boxed) were resuspended in 1% LMNG lysis buffer or 1% Triton X-100 (TX-100) lysis buffer and subjected to sucrose gradient sedimentation. After fraction collection, proteins were precipitated, denatured, separated on a gel, and visualized by silver staining. Fractions 1 - 13 are indicated.

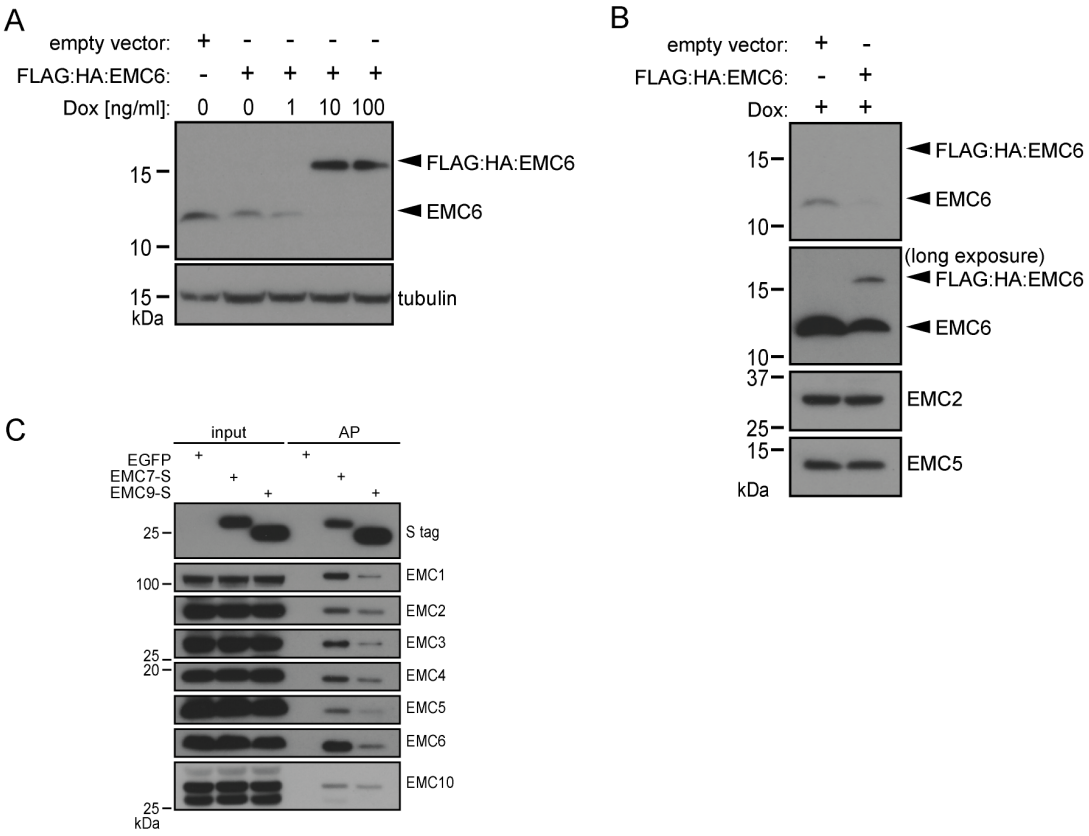


Figure 18.3: Exogenous expression of EMC subunits. A. Displacement of endogenous EMC6 by FLAG:HA:EMC6. U2OS Flp-In cells carrying a stably integrated FLAG:HA:EMC6 transgene were induced with Dox for 24 hours. Whole-cell lysate was separated on a gel and EMC6 was visualized by immunoblotting with a specific anti-EMC6 antibody. **B.** Expression levels of epitope-tagged EMC6 in stable U2OS Flp-In cells. Expression of FLAG:HA:EMC6 was induced with 1 ng/ml doxycycline for 18 hours. SDS-PAGE and immunoblotting was performed on whole-cell lysate. EMC6 was detected using a specific anti-EMC6 antibody. **C.** EMC7 and EMC9 are part of the mEMC in U2OS cells. U2OS cells were transiently transfected with epitope-tagged EMC7, EMC9, or EGFP (negative control) for 48 hours. Affinity purification (AP) of the mEMC was performed using S-protein conjugated agarose beads. AP, affinity purification.

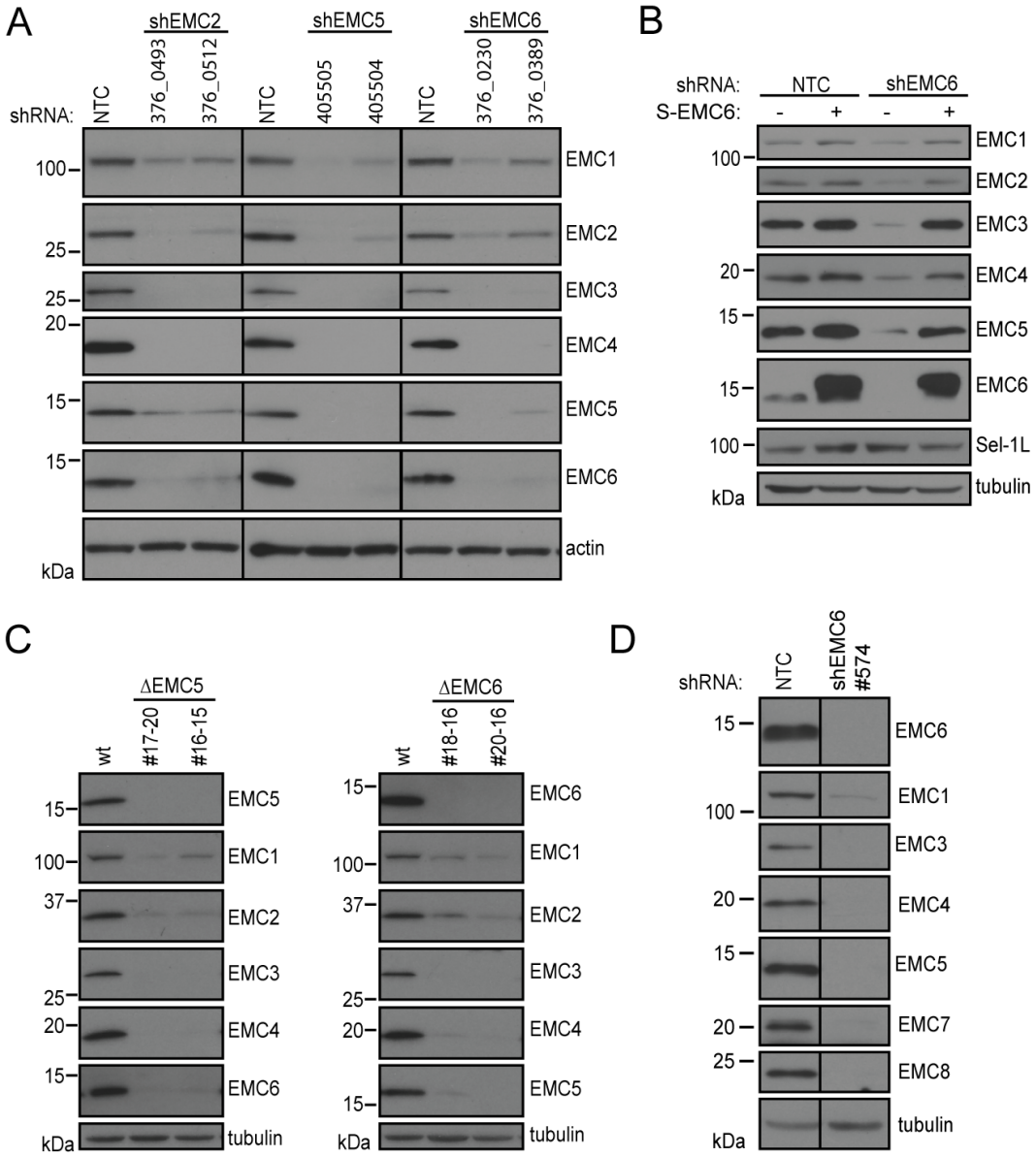


Figure 18.4: Co-dependent EMC depletion in multiple mammalian cell lines. A. Stable depletion of EMC2, EMC5, or EMC6, caused co-depletion of other EMC proteins. U2OS Flp-In cells were stably transduced with lentiviruses containing EMC5-, or EMC6-specific shRNA. Transduction with an non-targeting shRNA (NTC) served as a negative control. Whole-cell lysates were subjected to SDS-PAGE and immunoblotting. **B.** Reconstitution of EMC6 expression rescues the mEMC in shEMC6 cells. U2OS Flp-In cells were stably depleted of EMC6 using an shRNA specifically binding the 3' UTR of EMC6 mRNA. S-EMC6 was then transiently expressed for 48 hours. Whole-cell extract is shown. Sel1-L served as a negative control. **C.** EMC5/6 knockout in TE671 cells caused mEMC deficiency. EMC5, or EMC6 were deleted in TE671 cells using CRISPR/Cas9-mediated genomic editing. Whole-cell lysates from two ΔEMC5 single-cell clones (#17-20 and #16-15), and two ΔEMC6 clones (#18-16 and #20-16) are shown. **D.** Co-depletion of the mEMC in EMC6-depleted C2C12 cells. C2C12 cells were stably depleted of EMC6, and whole-cell extract was subjected to SDS-PAGE and immunoblotting. NTC, non-targeting control.

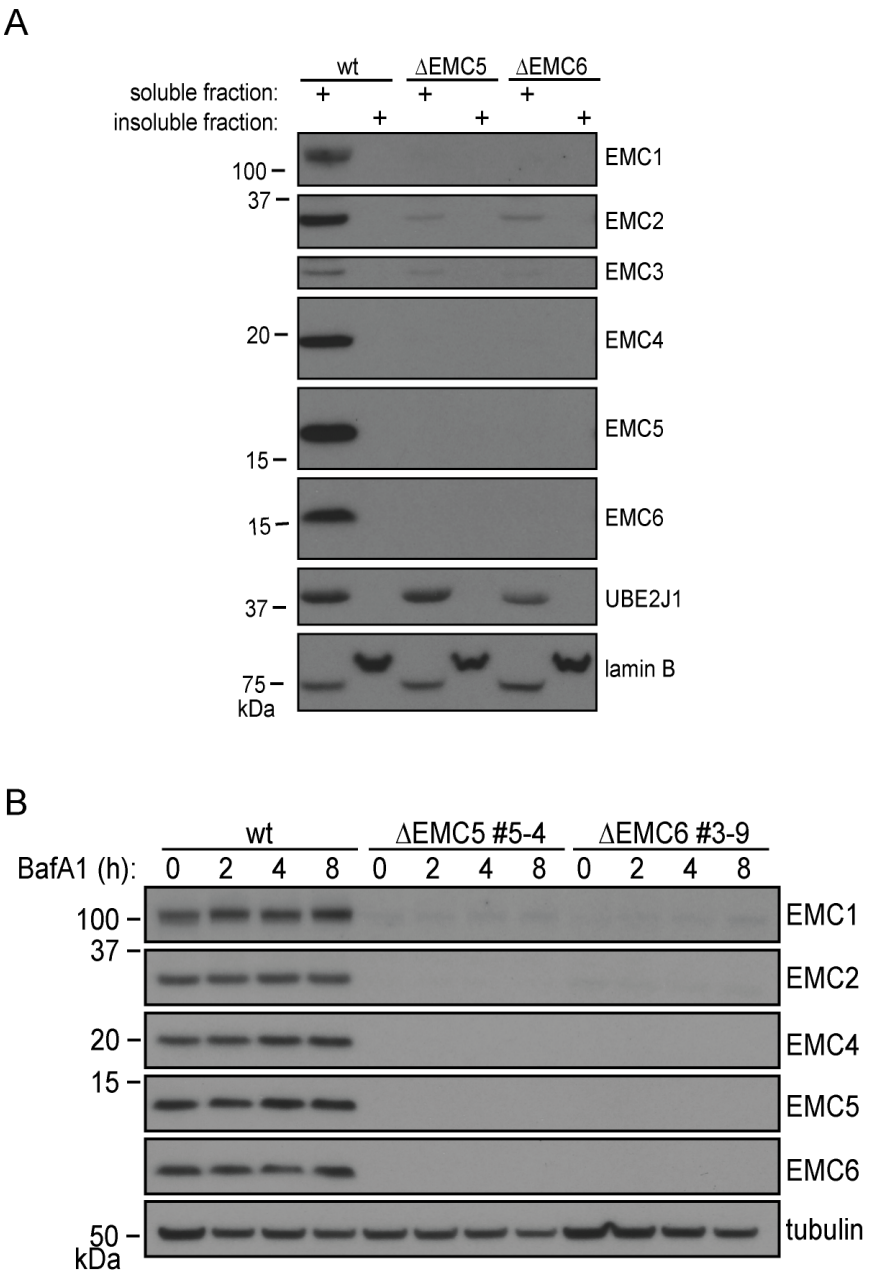


Figure 18.5: A. ΔEMC5/6 cells were lysed in RIPA buffer (soluble fraction) and RIPA-insoluble material was resuspended in an equal volume of urea buffer (insoluble fraction). Lamin B served as positive control for the RIPA-insoluble fraction, whereas Ube2J1 is RIPA-soluble. **B.** mEMC subunit levels were not restored by autophagy inhibition. ΔEMC5 and ΔEMC6 cells were treated with 100 nM Bafilomycin A1 for the indicated times. Whole-cell lysates were subjected to SDS-PAGE and immunoblotting.

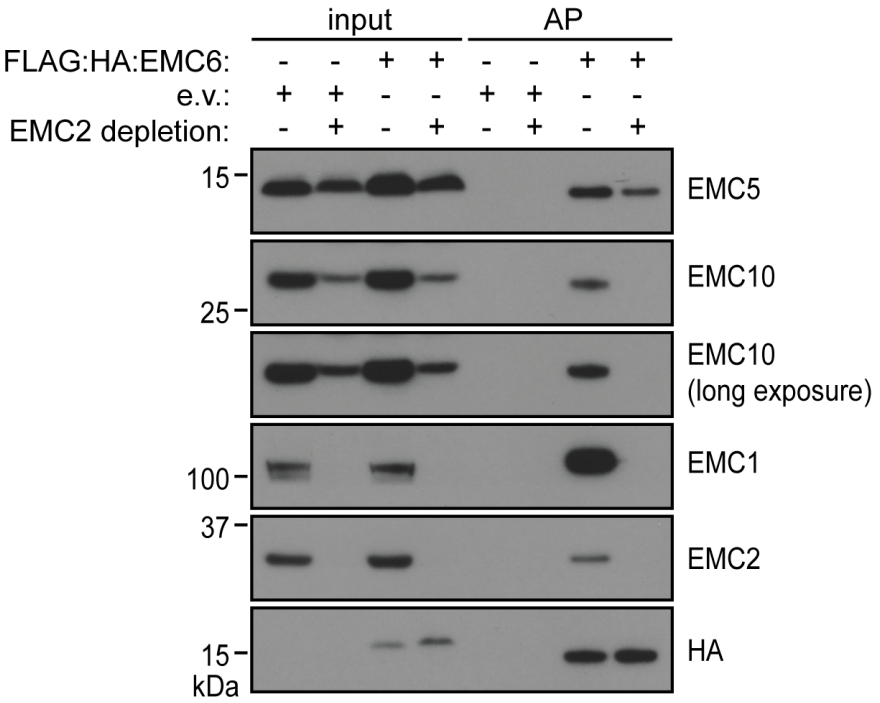


Figure 18.6: Isolation of an mEMC assembly intermediate. A. EMC5 and EMC6 formed a complex in EMC2 depleted cells, but did not bind EMC10. EMC2-depleted cells (ΔEMC2 #2-6) were stably transfected with FLAG:HA:EMC6, or an empty vector control (e.v.; pcDNA^{TM}/5/FRT/TO). FLAG:HA:EMC6 expression was induced with 10 ng/ml Dox for 24 hours and associated proteins were affinity-captured by a monoclonal anti-HA agarose-conjugated antibody.

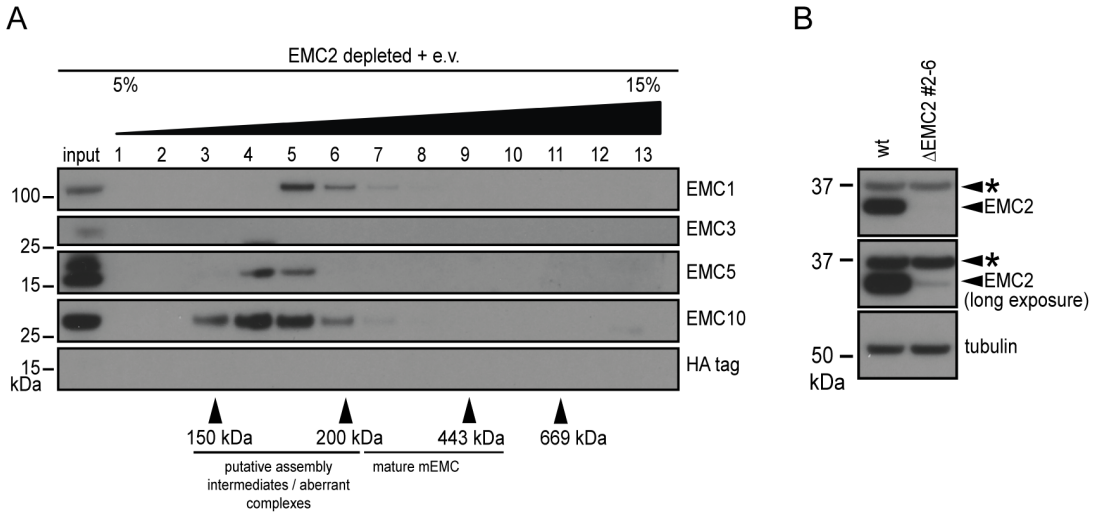


Figure 18.7: Sucrose gradient sedimentation of mEMC subunits from EMC2-depleted cells. A. Whole-cell lysate from EMC2-depleted cells (ΔEMC2 #2-6) with a stably integrated empty vector control (e.v.; pcDNA^{TM}/5/FRT/TO) was subjected to velocity gradient sedimentation. Endogenous EMC1/3/5/10 are shown. **B.** ΔEMC2 cells retain low levels of EMC2.

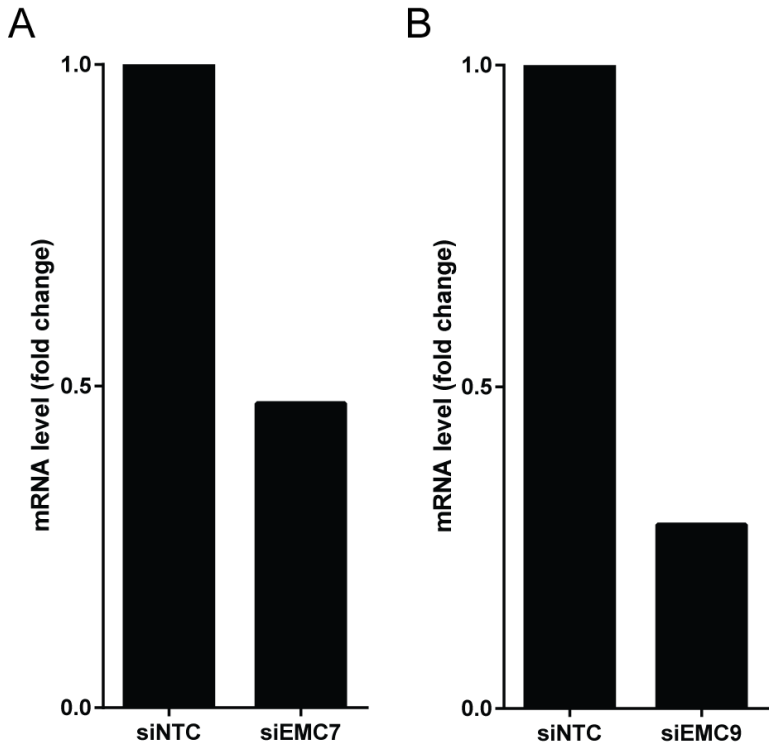


Figure 18.8: EMC7/9 knockdown efficiency as determined by qPCR. mRNA was isolated, reverse transcribed, and quantified by qPCR from cells transiently depleted of EMC7 (siEMC7), or EMC9 (siEMC9) for 72 hours. The mRNA levels of EMC7 and EMC9 in the knockdown cells were normalized to those from cells transfected with a non-targeted siRNA control (siNTC).

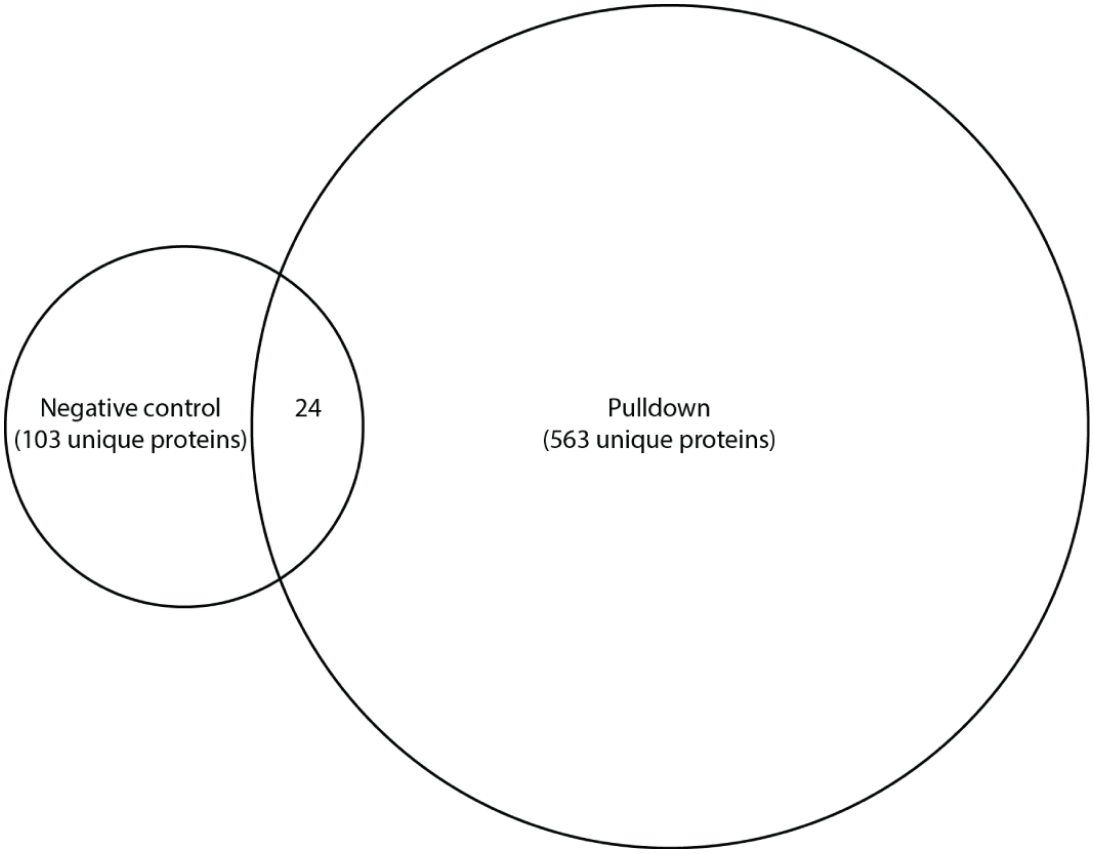
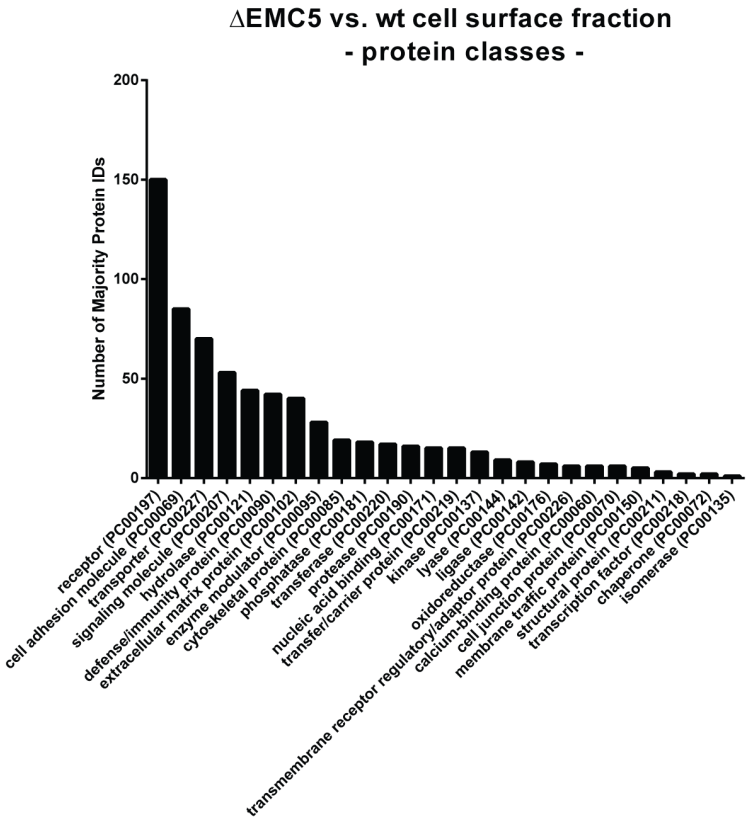
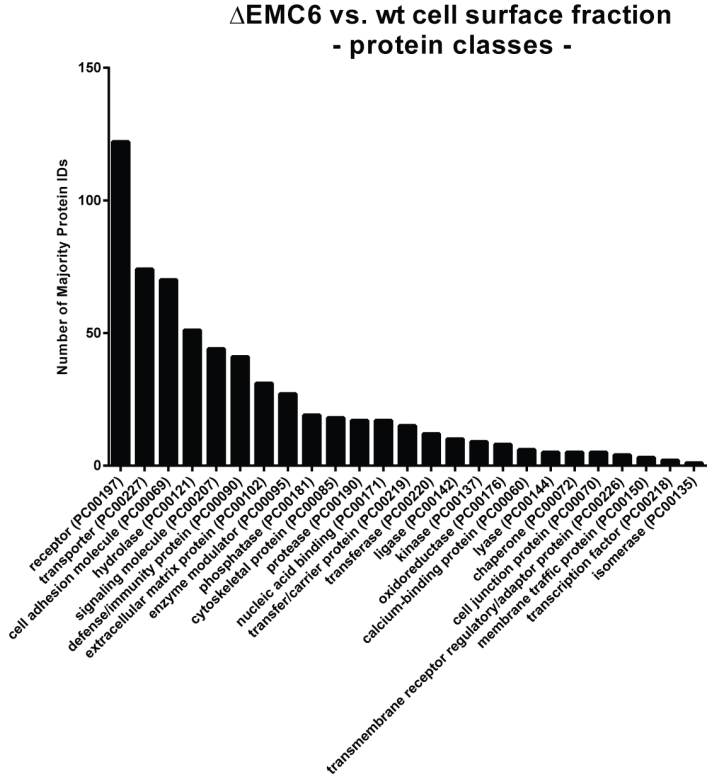


Figure 18.9: Specificity of PM protein enrichment. A. Biotinylated cell surface sialoglycoproteins were enriched U2OS Flp-In cells by affinity capture using streptavidin agarose beads ('Pulldown'). Alternatively, aminooxy-biotin was omitted from the reaction mixture before affinity purification with streptavidin agarose resin ('Negative control'). The total number of proteins unique to each sample and found in both samples are shown.

A


ΔEMC5 vs. wt cell surface fraction
- protein classes -
Number of Majority Protein IDs
200
150
100
50
0
receptor (PC00197)
cell adhesion molecule (PC00069)
transporter (PC00227)
signaling molecule (PC00207)
hydrolase (PC00121)
defense/immunity protein (PC00090)
extracellular matrix protein (PC00102)
enzyme modulator (PC00095)
cytoskeletal protein (PC00085)
phosphatase (PC00181)
transferase (PC00220)
protease (PC00190)
nucleic acid binding (PC00171)
transfer/carrier protein (PC00219)
kinase (PC00137)
ligase (PC00144)
lyase (PC00142)
oxidoreductase (PC00176)
transmembrane receptor regulatory/adaptor protein (PC00226)
calcium-binding protein (PC00060)
cell junction protein (PC00070)
membrane traffic protein (PC00150)
structural protein (PC00211)
transcription factor (PC00218)
chaperone (PC00072)
isomerase (PC00135)

B


ΔEMC6 vs. wt cell surface fraction
- protein classes -
Number of Majority Protein IDs
150
100
50
0
receptor (PC00197)
transporter (PC00227)
cell adhesion molecule (PC00069)
hydrolase (PC00121)
signaling molecule (PC00207)
defense/immunity protein (PC00090)
extracellular matrix protein (PC00102)
enzyme modulator (PC00095)
phosphatase (PC00181)
cytoskeletal protein (PC00085)
protease (PC00190)
nucleic acid binding (PC00171)
transfer/carrier protein (PC00219)
transferase (PC00220)
ligase (PC00142)
kinase (PC00137)
oxidoreductase (PC00176)
calcium-binding protein (PC00060)
lyase (PC00144)
chaperone (PC00072)
cell junction protein (PC00070)
transmembrane receptor regulatory/adaptor protein (PC00226)
membrane traffic protein (PC00150)
transcription factor (PC00218)
isomerase (PC00135)

A

Gene	Protein	# TMDs	Structural Features	# of Glycosylation sites (N-linked/O-linked)
ABCB1	Multidrug resistance protein 1	12	2 nucleotide-binding motifs, AAA+ ATPase domain	3/0
ANO6	Anoctamin-6	8	-	6/0
APOB	Apolipoprotein B-100	0	signal peptide, Vitellogenin domain	19/0
APOC3	Apolipoprotein C-III	0	signal peptide, lipid-binding domain	0/1
FZD2	Frizzled-2	7	Lys-Thr-X-X-X-Trp motif, PDZ binding	2/0
HEG1	Protein HEG homolog 1	1	signal peptide, 2 EGF-like domains, Ser-rich motif	8/1
HP	Haptoglobin	0	signal peptide, Sushi 1, Sushi 2, pepdidase S1	4/0
HRG	His-rich glycoprotein	0	signal peptide, His/Pro-rich (HRR) region	4/0
IGSF1	Immunoglobulin superfamily member 1	2	12 Ig-like C2-type domains	14/0
IGSF3	Immunoglobulin superfamily member 3	1	8 Ig-like C2-type domains, EWI motif	5/0
KIAA0195	Uncharacterized protein KIAA0195	10	-	4/0
SEMA4B	Semaphorin-4B	1	signal peptide, 1 Ig-like C2-type domain (by similarity)	6/0
SEMA6B	Semaphorin-6B	1	signal peptide, WD40/YVTN repeat-like domain	7/0
SLC12A2	Solute carrier family 12 member 2	12	-	2 (NetNGlyc 1.0 Server)
SLC12A4	Solute carrier family 12 member 4	12	poly-Cys motif	5/0
SLC1A3	Excitatory amino acid transporter 1	6	-	3 (NetNGlyc 1.0 Server)
SLC1A4	Neutral amino acid transporter A4	9	-	2/0
SLC2A12	Solute carrier family 2, facilitated glucose transporter member 12	12	-	4/0
SLC6A9	Sodium- and chloride-dependent glycine transporter 1	12	-	2/0
SLCO3A1	Solute carrier organic anion transporter family member 3A1	12	Kazal-like domain	7/0
SMPDL3B	Acid sphingomyelinase-like phosphodiesterase 3b	1 (TOPCONS)	signal peptide	3/0
SORT1	Sortilin	1 (TOPCONS)	signal peptide, BNR repeats, endocytosis signal	7/0
SV2A	Synaptic vesicle glycoprotein 2A	12	-	3/0

B

	Ratio M/L norm		Ratio H/L norm	
Gene	ΔEMC5 vs. wt	ΔEMC6 vs. wt	ΔEMC5 vs. wt	ΔEMC6 vs. wt
ABCB1	0.451	0.611	0.496	0.417
ANO6	0.239	0.188	0.160	0.314
APOB	0.037	0.027	0.208	0.083
APOC3	0.139	0.031	0.038	0.089
FZD2	0.497	0.439	0.451	0.620
HEG1	0.609	0.479	0.375	0.542
HP	0.036	0.037	0.056	0.070
HRG	0.014	0.007	0.047	0.141
IGSF1	0.575	0.419	0.346	0.435
IGSF3	0.419	0.197	0.216	0.258
KIAA0195	0.519	0.291	0.208	0.476
SEMA4B	0.366	0.437	0.514	0.480
SEMA6B	0.643	0.356	0.434	0.644
SLC12A2	0.416	0.562	0.536	0.679
SLC12A4	0.615	0.350	0.453	0.589
SLC1A3	0.236	0.188	0.259	0.472
SLC1A4	0.279	0.425	0.467	0.380
SLC2A12	0.695	0.090	0.093	0.167
SLC6A9	0.418	0.350	0.400	0.515
SLCO3A1	0.633	0.311	0.367	0.401
SMPDL3B	0.457	0.423	0.395	0.511
SORT1	0.333	0.209	0.096	0.156
SV2A	0.625	0.484	0.472	0.443

C

	Ratio M/L norm		Ratio H/L norm	
Gene	ΔEMC5 vs. wt	ΔEMC6 vs. wt	ΔEMC5 vs. wt	ΔEMC6 vs. wt
CRYZ	0.554	0.656	0.462	0.633
CTSD	0.581	0.565	0.379	0.696
CYB5A	0.661	0.462	0.595	0.587
ECH1	0.676	0.548	0.570	0.545
FDFT1	0.164	0.132	0.069	0.182
HIST1A	0.570	0.112	0.434	0.640
SDHA	0.665	0.380	0.605	0.398
SDHB	0.622	0.309	0.165	0.354
SGPL1	0.642	0.482	0.194	0.395
TMX2	0.489	0.689	0.378	0.496
VIM	0.156	0.265	0.192	0.227

Figure 18.11: Proteins downregulated in both ΔEMC5 and ΔEMC6 cells. A. Structural features of cell surface proteins that were depleted in ΔEMC5 and ΔEMC6 cells. **B.** M/L and H/L ratios of co-depleted cell-surface proteins. **C.** M/L and H/L ratios of intracellular proteins whose abundance was reduced in ΔEMC5 and ΔEMC6 cells.

Figure 18.10 ***(previous page)*****: GO annotation of cell surface fraction A.** GO annotation of proteins identified in the ΔEMC5 *versus* wild-type (wt) SILAC-PMP cell surface sample. Common contaminants and reverse peptides were excluded from the analysis. GO classification was performed using the PANTHER classification system [413]. **B.** GO annotation of proteins identified in the ΔEMC6 *versus* wt SILAC-PMP cell surface sample. Data was obtained as described in (A).

A

Gene Name	Accession #	Protein Name	(M/L)*	peptides	(H/L)*	peptides
ADCY3	O60266	Adenylate cyclase type 3	0.0199917	3	0.200880579	3
ADCY6	O43306	Adenylate cyclase type 6	0.148628	NaN	0.528589986	NaN
ADCY9	O60503	Adenylate cyclase type 9	0.149574	3	0.185650358	3
ADK	P55263	Adenosine kinase	0.110745	1	0.178039591	1
AT133	Q9H7F0	Probable cation-transporting ATPase 13A3	0.04226	3	0.248679588	3
AT1B1	P05026	Sodium/potassium-transporting ATPase subunit beta-1	0.282779	19	0.652449886	19
B3A2	P04920	Anion exchange protein 2	0.0942237	9	0.571169956	9
BBS12	Q6ZW61	Bardet-Biedl syndrome 12 protein	2.25488E-35	1	0.034602018	1
BMR1A	P36894	Bone morphogenetic protein receptor type-1A	0.396476	5	0.306139265	5
CADM3	Q8N126	Cell adhesion molecule 3	0.596772	6	0.158219574	6
CAHD1	Q5VU97	VWFA and cache domain-containing protein 1	0.189017	4	0.267079287	4
CC50A	Q9NV96	Cell cycle control protein 50A	0.562908	NaN	0.465750751	NaN
CD34	P28906	Hematopoietic progenitor cell antigen CD34	0.403231	2	0.266050127	2
CELR2	Q9HCU4	Cadherin EGF LAG seven-pass G-type receptor 2	0.465227	3	0.498190702	3
CTL2	Q8IWA5	Choline transporter-like protein 2	0.0154457	2	0.299789134	2
CTR1	P30825	High affinity cationic amino acid transporter 1	0.34188	9	0.603749921	9
DOS	Q8N350	Protein Dos	0.00446646	2	0.274789732	2
ELFN1	P0C7U0	Protein ELFN1	0.492556	15	0.672710182	15
EPCAM	P16422	Epithelial cell adhesion molecule	0.413972	7	0.597810027	7
EPHA5	P54756	Ephrin type-A receptor 5	0.322135	NaN	0.28843937	NaN
FZD6	O60353	Frizzled-6	0.0890097	5	0.496580667	5
GNAT1	P11488	Guanine nucleotide-binding protein G(t) subunit alpha-1	0.337276	NaN	0.682290011	NaN
GP176	Q14439	Probable G-protein coupled receptor 176	0.000835104	1	0.497548821	1
GSLG1	Q92896	Golgi apparatus protein 1	0.00671716	2	0.516420079	2
HRH1	P35367	Histamine H1 receptor	0.317311	1	0.645529978	1
IMB1	Q14974	Importin subunit beta-1	0.0283629	1	0.647460013	1
ITB4	P16144	Integrin beta-4	0.591528	28	0.53482989	28
LAMC1	P11047	Laminin subunit gamma-1	0.476333	2	0.280760134	2
LCAP	Q9UIQ6	Leucyl-cystinyl aminopeptidase	0.572255	2	0.292609801	2
LPP3	O14495	Lipid phosphate phosphohydrolase 3	0.000635146	2	0.386869795	2
LRC8C	Q8TDW0	Volume-regulated anion channel subunit LRRC8C	0.214018	10	0.589339962	10
LRC8D	Q7L1W4	Volume-regulated anion channel subunit LRRC8D	0.376806	2	0.685699797	2
LRC8E	Q6NSJ5	Volume-regulated anion channel subunit LRRC8E	0.0979168	4	0.616320208	4
LUC7L	Q9NQ29	Putative RNA-binding protein Luc7-like 1	0.299937	2	0.557660117	2
MPRI	P11717	Cation-independent mannose-6-phosphate receptor	0.543111	12	0.137159837	12
MRP3	O15438	Canalicular multispecific organic anion transporter 2	0.120523	4	0.403748834	4
NOTC3	Q9UM47	Neurogenic locus notch homolog protein 3	0.451584	2	0.432979312	2
NPTN	Q9Y639	Neuroplastin	0.213018	11	0.695710018	11
PCFT	Q96NT5	Proton-coupled folate transporter	0.312111	1	0.458511556	1
PIEZ1	Q92508	Piezo-type mechanosensitive ion channel component 1	0.343212	15	0.610100154	15
PR38A	Q8NAV1	Pre-mRNA-splicing factor 38A	0.0360294	1	0.358540998	1
PRRT3	Q5FWE3	Proline-rich transmembrane protein 3	0.310457	3	0.464229465	3
R4RL2	Q86UN3	Reticulon-4 receptor-like 2	0.312748	3	0.59638009	3
S23A2	Q9UGH3	Solute carrier family 23 member 2	0.536722	2	0.699900139	2
S26A2	P50443	Sulfate transporter	0.520202	7	0.528900044	7
S29A2	Q14542	Equilibrative nucleoside transporter 2	0.148536	3	0.383091255	3
S4A7	Q9Y6M7	Sodium bicarbonate cotransporter 3	0.103269	NaN	0.363719959	NaN
S6A11	P48066	Sodium- and chloride-dependent GABA transporter 3	0.105208	1	0.687510189	1
SC5A6	Q9Y289	Sodium-dependent multivitamin transporter	0.572946	8	0.619959983	8
SC6A6	P31641	Sodium- and chloride-dependent taurine transporter	0.0589533	4	0.534140062	4
SMAGP	Q0VAQ4	Small cell adhesion glycoprotein	0.130911	3	0.699159732	3
SRSF1	Q07955	Serine/arginine-rich splicing factor 1	0.0233587	1	0.466979136	1
SRSF3	P84103	Serine/arginine-rich splicing factor 3	0.333027	5	0.551919973	5
STRA6	Q9BX79	Stimulated by retinoic acid gene 6 protein homolog	0.0542995	2	0.675440223	2
TGFR1	P36897	TGF-beta receptor type-1	0.259646	1	0.636129766	1

B

Gene Name	Accession #	Protein Name	(M/L)*	peptides	(H/L)*	peptides
ANO1	Q5XXA6	Anoctamin-1	0.157790254	1	0.0052	1
AOC2, AOC3	O75106, Q16853	Retina-specific copper amine oxidase	0.147410378	1	0.112	1
ARAP1	Q96P48	Arf-GAP with Rho-GAP domain, ANK repeat and PH domain-containing protein 1	0.266870178	1	0.4974	1
C1TC	P11586	C-1-tetrahydrofolate synthase, cytoplasmic	0.039131114	1	0.0549	1
CLUS	P10909	Clusterin	0.283289689	3	0.5933	3
CTL1	Q8WWI5	Choline transporter-like protein 1	0.151610334	1	0.3919	1
ECE1	P42892	Endothelin-converting enzyme 1	0.619020031	7	0.6892	7
EPHA5	P54756	Ephrin type-A receptor 5	0.502109874	1	0.5479	1
F1712	A8MVW0	Protein FAM171A2	0.18579969	1	0.3996	1
GLU2B	P14314	Glucosidase 2 subunit beta	0.604029954	5	0.2688	5
GPR45	Q9Y5Y3	Probable G-protein coupled receptor 45	0.339560371	1	0.4434	1
GPR56	Q9Y653	G-protein coupled receptor 56	0.195429478	2	0.3044	2
HXK1	P19367	Hexokinase-1	0.496140282	1	0.6617	1
IGF1R	P08069	Insulin-like growth factor 1 receptor	0.641450125	17	0.63	17
ITA7	Q13683	Integrin alpha-7	0.417248856	1	0.6052	1
ITB3	P05106	Integrin beta-3	0.288009838	12	0.3787	12
JAM3	Q9BX67	Junctional adhesion molecule C	0.632040101	7	0.6702	7
LRC15	Q8TF66	Leucine-rich repeat-containing protein 15	0.541790124	4	0.5427	4
LRC4B	Q9NT99	Leucine-rich repeat-containing protein 4B	0.451779277	8	0.6073	8
LRP1	Q07954	Prolow-density lipoprotein receptor-related protein 1	0.187390536	24	0.4507	24
MPRD	P20645	Cation-dependent mannose-6-phosphate receptor	0.515649976	2	0.5231	2
NAC2	Q9UPR5	Sodium/calcium exchanger 2	0.192530645	1	0.4338	1
PCDB5	Q9Y5E4	Protocadherin beta-5	0.266600243	1	0.6074	1
PTPRJ	Q12913	Receptor-type tyrosine-protein phosphatase eta	0.318039971	10	0.652	10
RAI3	Q8NFJ5	Retinoic acid-induced protein 3	0.184669818	2	0.1847	2
ROR1	Q01973	Tyrosine-protein kinase transmembrane receptor R	0.141330035	8	0.5334	8
S12A7	Q9Y666	Solute carrier family 12 member 7	0.205749382	29	0.6317	29
S39A6	Q13433	Zinc transporter ZIP6	0.630280092	4	0.6567	4
SSR2	P30874	Somatostatin receptor type 2	0.343721023	2	0.1975	2
SYPL1	Q16563	Synaptophysin-like protein 1	0.204390493	3	0.5089	3
TEN3	Q9P273	Teneurin-3	0.281030769	15	0.5836	15
TMEM2	Q9UHN6	Transmembrane protein 2	0.54720981	18	0.6112	18
TSN9	O75954	Tetraspanin-9	0.612870004	3	0.5889	3
VP6	A4ZCW7	TH3 Intermediate capsid protein VP6	0.201329432	1	0.0818	1

Figure 18.12: Cell surface proteins downregulated only in ΔEMC5 and ΔEMC6 cells. **A.** Cell surface proteins that were downregulated by $\geq 30\%$ in two EMC5 knockout clones. **B.** As in (A), but downregulated proteins exclusive for two ΔEMC6 cell lines ares shown. The data presented here are from the same experiment as shown in **Figure 8.2**.

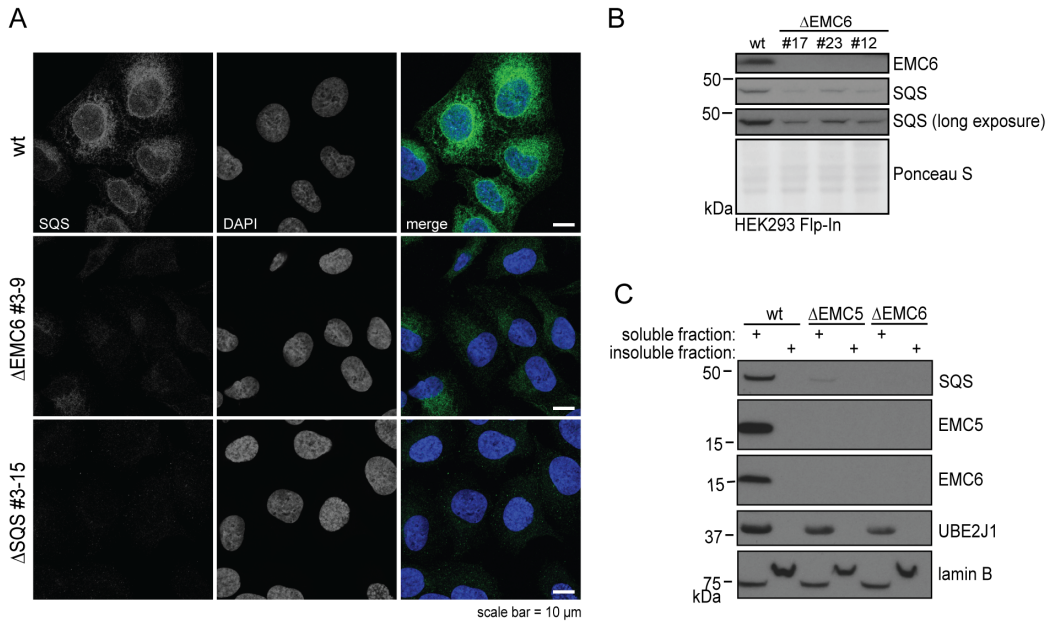


Figure 18.13: SQS is decreased in ΔEMC6 cells. A. Validation of anti-SQS for immunofluorescence microscopy. Cells were prepared and stained with anti-SQS anntibody as described in Figure 9.1 E/F. Reduction of the SQS signal in ΔEMC6 cells and its loss in ΔSQS cells shows that the antibody is specific for SQS. **B.** SQS levels are reduced in HEK293 Flp-In ΔEMC6 cells. Whole-cell lysates were separated on a gel and SQS was detected by immunoblotting with an SQS-specific antibody. Three different single-cell ΔEMC6 clones are shown.

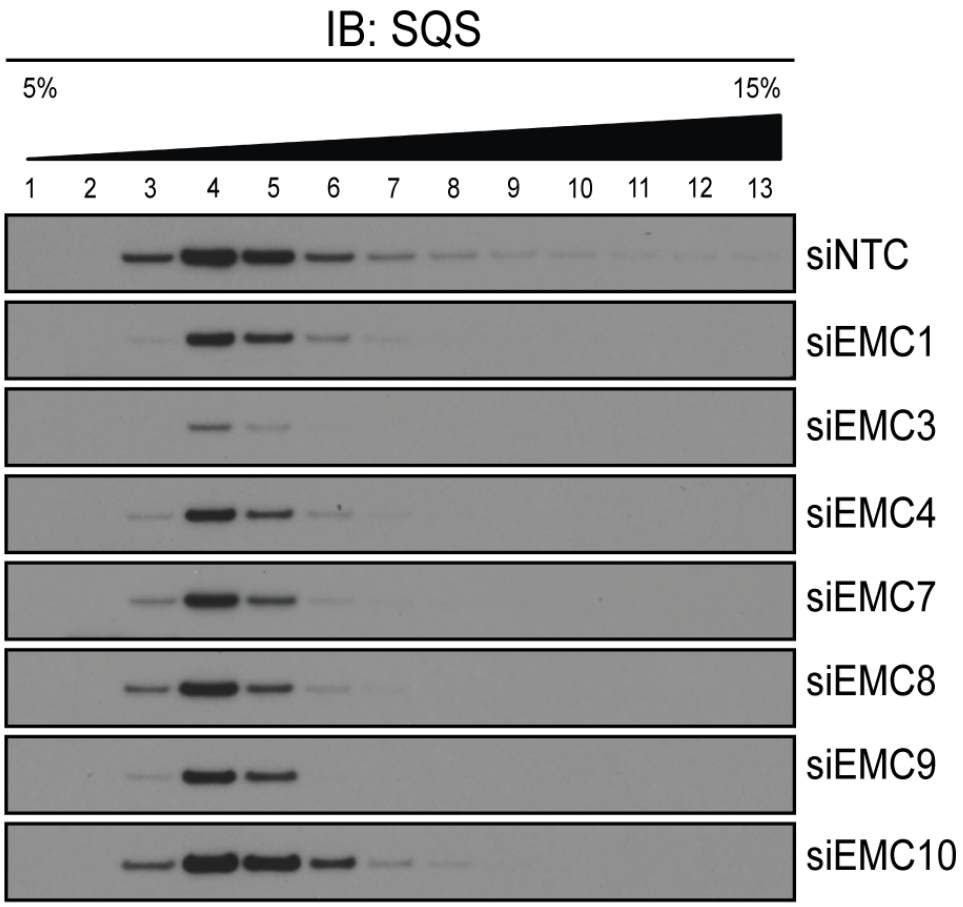


Figure 18.14: The velocity gradient sedimentation pattern of SQS is not affected by EMC RNAi. A. U2OS Flp-In cells were transfected with ON-Target siRNA pools directed against EMC1/3/4/7 - 10 or a non-targeting control (NTC) pool. After 72 hours, whole-cell lysates were isolated in LMNG lysis buffer and sucrose gradient velocity centrifugation was performed. Endogenous SQS was detected by immunoblotting. NTC, non-targeting control.

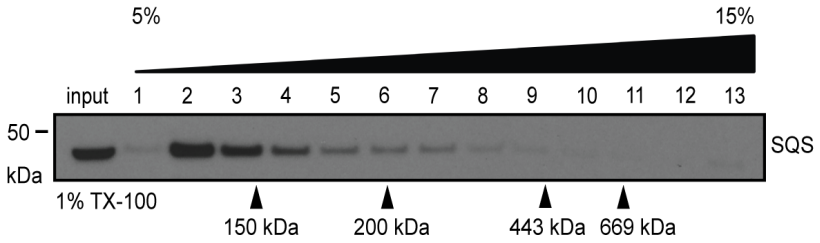


Figure 18.15: Velocity gradient centrifugation in the presence of 1% Triton-X 100. Whole-cell lysate was obtained by resuspending U2OS Flp-In cells in Triton-X 100 lysis buffer and subjecting them to sucrose gradient sedimentation. 13 fractions were collected and separated on a gel.

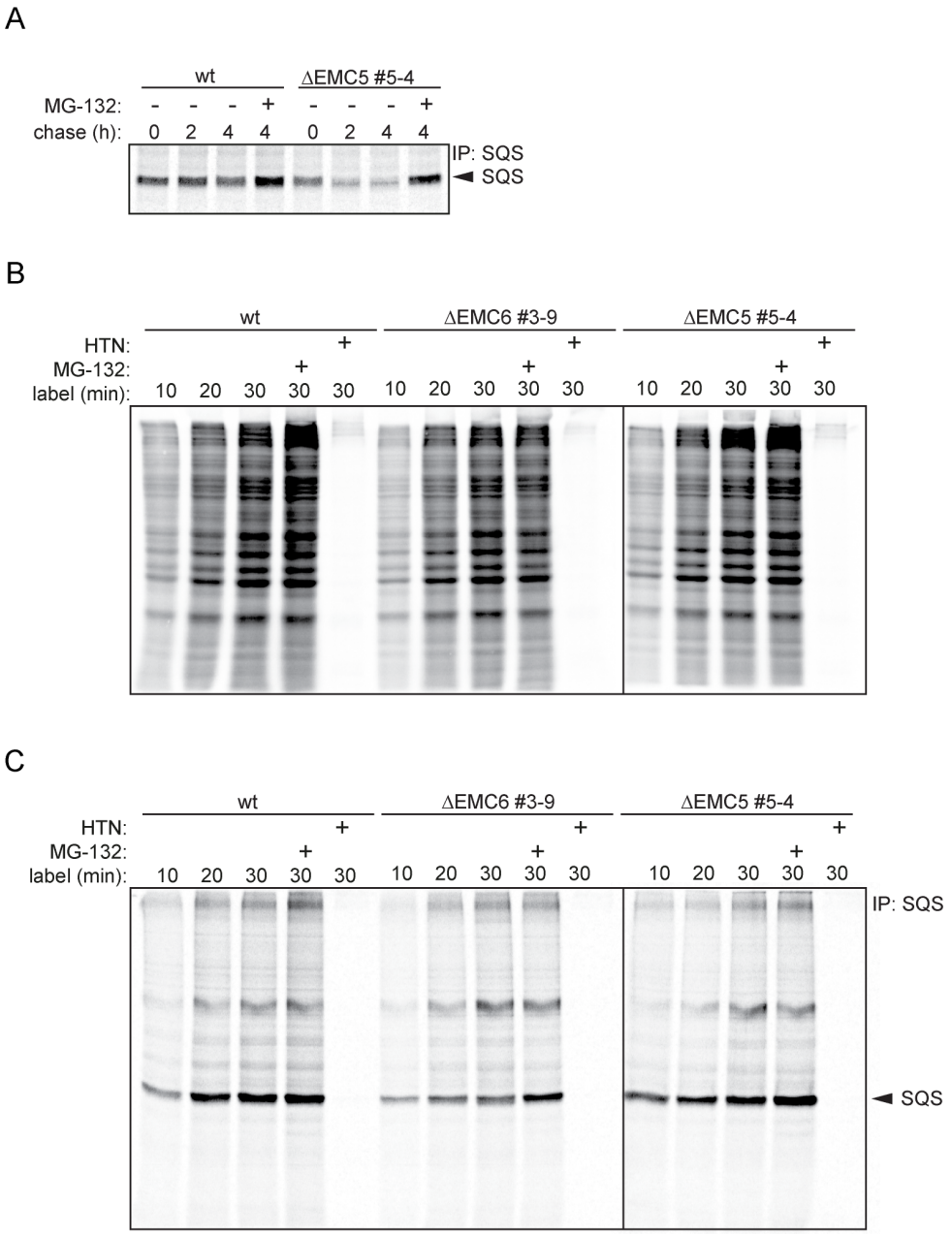
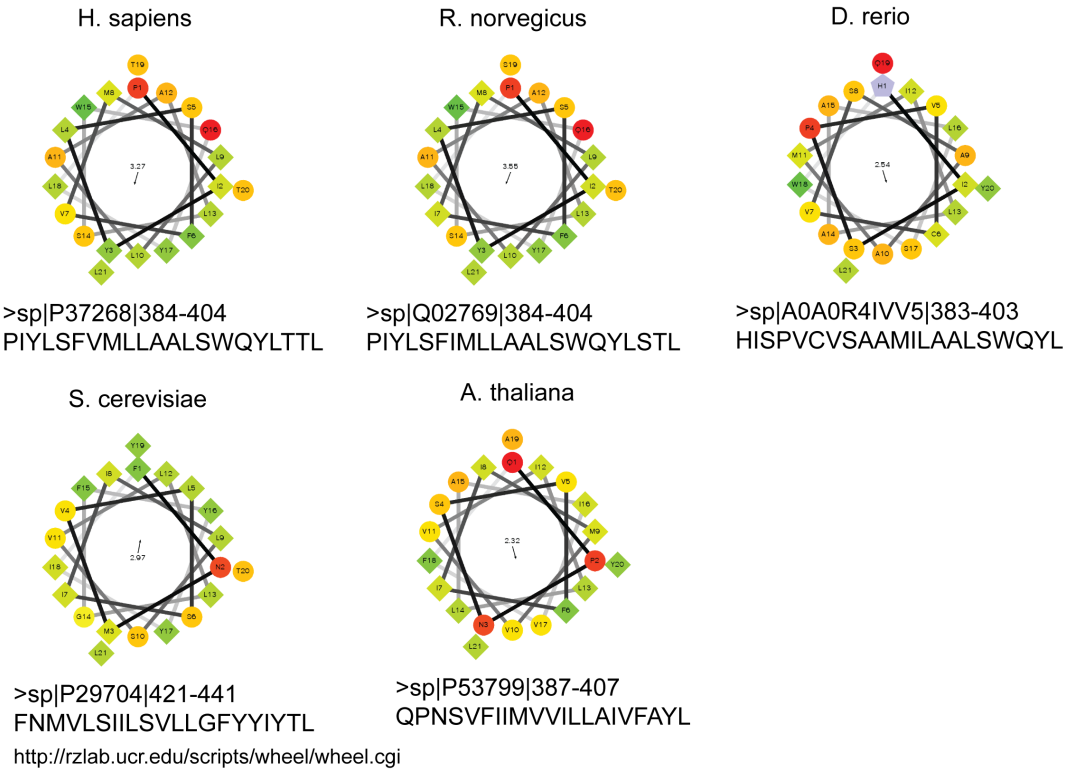


Figure 18.16: SQS is destabilised in ΔEMC5 cells. A. ΔEMC5 cells were radiolabeled, chased for 0 - 4 hours +/- MG-132 and SQS was subsequently captured from whole-cell extract as described in Figure 10.1. **B.** Radiolabel incorporation effiency in ΔEMC5 and ΔEMC6 U2OS Flp-In cells. Cells were labelled with ^{35}S-Met/Cys for the indicated periods in the presence or absence of MG-132 or harringtoninn (HTN) and whole-cell lysate was seperated on a gel. **C.** SQS biosynthesis rates in ΔEMC5 and ΔEMC6 cells are comparable to those in wild-type (wt) cells. Endogenous SQS was immunoproecipitated from whole-cell extracts in (B) using anti-SQS. Data shown in (A) - (C) were acquired with the help of John C. Christianson. HTN, harringtonin; IP, immunoprecipitation.

A



B

```
sp|P29704|FDFT_YEAST          SFWPKEIWSQYAPQLKDFMKPENEQLGLDCINHLVLNALSHVIDVLTYLAGIHEQSTFQF
sp|P53799|FDFT_ARATH          MFWPREIWGKYADKLEDLKYEENTNKSVQCLNEMVTNALMHIEDCLKYMVSLRDPSIFRF
tr|A0A0R4IVV5|A0A0R4IVV5_DANRE AFWPEEAWSQYASGLEDLAQPQHLSSALSCLNLLVTDALRHVPDVMLYLSRLRNQSVFNF
sp|P37268|FDFT_HUMAN          EFWPQEVWSRYVKKLGDFAKPENIDLAVQCLNELITNALHHIPDVITYLSRLRNQSVFNF
sp|Q02769|FDFT_RAT            QFWPQEVWGKYVKKLEDFVKPENVDVAVKCLNELITNALQHIPDVITYLSRLRNQSVFNF
                               ***.* *.:*.  * *:   :. . .:.*:* :: :** *: * : *:  ::: * *.*

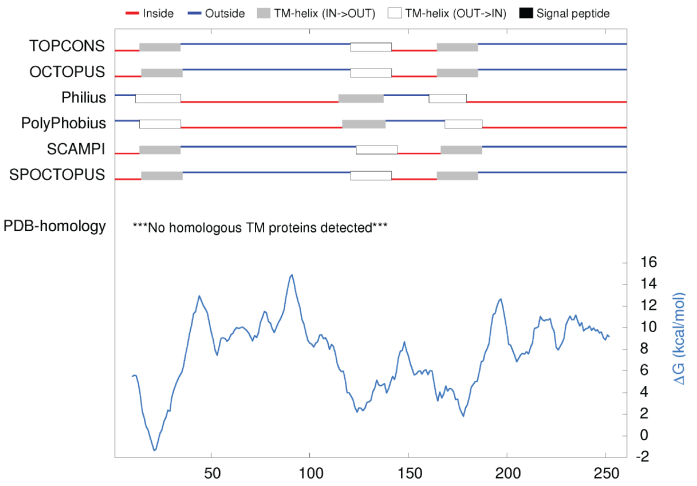
sp|P29704|FDFT_YEAST          CAIPQVMAIATLALVFNNREVLHGNVKIRKGTTCYLILKSRTLRGCVEIFDYYLRDIKSK
sp|P53799|FDFT_ARATH          CAIPQIMAIGTLALCYNNEQVFRGVVKLRRGLTAKVIDRTKTMADVYGAFYDFSCMLKTK
tr|A0A0R4IVV5|A0A0R4IVV5_DANRE CAIPQVMAIATLSACYNNPQVFQGVVKIRKGQAVTLMMQATNMSAVYSIITQYSHEILQK
sp|P37268|FDFT_HUMAN          CAIPQVMAIATLAACYNNQQVFKGAVKIRKGQAVTLMMDATNMPAVKAIIYQYMEEIYHR
sp|Q02769|FDFT_RAT            CAIPQVMAIATLAACYNNHQVFKGVVKIRKGQAVTLMMDATNMPAVKAIIYQYIEEIYHR
                               *****:***.**:  :** ::*::* **:*:* :  ::  : .:      :  :   :  :

sp|P29704|FDFT_YEAST          LAVQDPNFLKLNIQISKIEQFMEEMYQDKLPPNVKPNETPIFLKVKERSRYDDELVPTQQ
sp|P53799|FDFT_ARATH          VDKNDPNASKTLNRLEAVQKLC-------RDAGVLQN----------RKSYVND------
tr|A0A0R4IVV5|A0A0R4IVV5_DANRE VSISDPSREKTLQILSVIREKS-------VHEGCVSS----------RA----------
sp|P37268|FDFT_HUMAN          IPDSDPSSSKTRQIISTIRTQN-------LPNCQLIS----------R-----------
sp|Q02769|FDFT_RAT            VPNSDPSASKAKQLISNIRTQS-------LPNCQLIS----------R-----------
                               :  .**.  *    :. :.                .          *

sp|P29704|FDFT_YEAST          EEEYKFNMVLSIILSVLLGFYYIYTLHRA----------
sp|P53799|FDFT_ARATH          KGQPNSVFIIMVVILLAIVFAYLRAN-------------
tr|A0A0R4IVV5|A0A0R4IVV5_DANRE HHHISPVCVSAAMILAALSWQYLNTTAGPAGGADMQGH-
sp|P37268|FDFT_HUMAN          -SHYSPIYLSFVMLLAALSWQYLTTLSQVTEDYVQTGEH
sp|Q02769|FDFT_RAT            -SHYSPIYLSFIMLLAALSWQYLSTLSQVTEDYVQREH-
                                 . .   :   ::   : : *: :
```

Figure 18.17: SQS contains a predicted hydrophilic TMD. A. Helical wheel projections of the predicted SQS TMDs from different species. The primary sequences and accession numbers (UniProt/Swiss-Prot) are indicated. **B.** Multiple sequence alignment of the SQS C-terminal segment. TMDs are boxed. TMD, transmembrane domain.

A



B

```
sp|Q9P0I2|EMC3_HUMAN       MAGPELLLDSNIRLWVVLPIVIITFFVGMIRHYVSILLQ---SDKKLTQE
sp|Q99KI3|EMC3_MOUSE       MAGPELLLDSNIRLWVVLPIVIITFFVGMIRHYVSILLQ---SDKKLTQE
sp|Q7SXW4|EMC3_DANRE       MAEPELLLDSNIRLWVVLPIVFITFLVGVIRHYVSILLQ---SDKKLTLE
tr|Q9VKR0|Q9VKR0_DROME     --MTELLIDPDIRVWVFLPIVLITFLVGIVRHYVSILIS---TQKKAEIT
sp|P36039|EMC3_YEAST       -----MLLDDQLKYWVLLPISIVMVLTGVLKQYIMTLITGSSANEAQPRV
                                :*:* ::: **.*** :: .:.*::::*:  *:    :::

sp|Q9P0I2|EMC3_HUMAN       QVSDSQVLIRSRVLRENGKYIPKQSFLTRKYYFNNPEDGFFKKTKR----
sp|Q99KI3|EMC3_MOUSE       QVSDSQVLIRSRVLRENGKYIPKQSFLTRKYYFNNPEDGFFKKTKR----
sp|Q7SXW4|EMC3_DANRE       QVSDSQVLIRSRVLRENGKYIPKQSFLMRKFYFNNQEDGFFKKTKR----
tr|Q9VKR0|Q9VKR0_DROME     QIQDSQAMIRARLLRENGKYLSAQSFSMRKNYFNNEETGYFKTQKR----
sp|P36039|EMC3_YEAST       KLTEWQYLQWAQLLIGNGGNLSSDAFAAKKEFLVKDLTEERHLAKAKQQD
                           :: : * :  :::*  **  :. ::*  :* :: :      :  *

sp|Q9P0I2|EMC3_HUMAN       ------KVVPPSPMTDPTMLTDMMKGNVTNVLPMILIGGWINMTFSGFVT
sp|Q99KI3|EMC3_MOUSE       ------KVVPPSPMTDPTMLTDMMKGNVTNVLPMILIGGWINMTFSGFVT
sp|Q7SXW4|EMC3_DANRE       ------KVVPPSPMTDPSMLTDMMKGNVTNVLPMILIGGWINWTFSGFVT
tr|Q9VKR0|Q9VKR0_DROME     ------APVAQN---SSAMLTDMVKGNFINVLPMVVIGGWINWMFSGFVT
sp|P36039|EMC3_YEAST       GSQAGEVPNPFNDPSMSNAMMNMAKGNMASFIPQTIIMWWVNHFFAGFIL
                                    . .    .  : :* ***. ..:*  :*  *:*  *:**:

sp|Q9P0I2|EMC3_HUMAN       TKVPFPLTLRFKPMLQQGIELLTLDASWVSSASWYFLNVFGLRSIYSLIL
sp|Q99KI3|EMC3_MOUSE       TKVPFPLTLRFKPMLQQGIELLTLDASWVSSASWYFLNVFGLRSIYSLIL
sp|Q7SXW4|EMC3_DANRE       TKVPFPLTLRFKPMLQQGIELLSLDASWVSSASWYFLNVFGLRSMYSLIL
tr|Q9VKR0|Q9VKR0_DROME     TKVPFPLTLRFKPMLQRGVELASLDAAWVSSASWYFLNVFGLRSIYTLVL
sp|P36039|EMC3_YEAST       MQLPFPLTAKFKEMLQTGIICQDLDVRWVSSISWYFISVLGLNPVYNLIG
                            ::***** :** *** *:    **. **** ****:.*:**..:*.*:

sp|Q9P0I2|EMC3_HUMAN       GQDNAADQSRMMQEQMTGAAMAMPADTNKAFKTEWEALELTDHQWALDDV
sp|Q99KI3|EMC3_MOUSE       GQDNAADQSRMMQEQMTGAAMAMPADTNKAFKTEWEALELTDHQWALDDV
sp|Q7SXW4|EMC3_DANRE       GQDNGADQSRIMQEQMSGAAMAMPADTNKAFKAEWEALELTDHQWALENV
tr|Q9VKR0|Q9VKR0_DROME     GENNHADQTQAQADAMTGAAMTMPQDPKAAFKAEWEALEITEYHNALKNI
sp|P36039|EMC3_YEAST       LNDQDMG-IQAGIGGPQGPQGPPQSQVDKAMHAMANDLTIIQHETCLDNV
                            :::  .  :       *.  .   : . *:::  : * : ::. .*.::

sp|Q9P0I2|EMC3_HUMAN       EEELMAKDLHFEGMFKKELQTSIF
sp|Q99KI3|EMC3_MOUSE       EEELMARDLHFEGMFKKELQTSIF
sp|Q7SXW4|EMC3_DANRE       EEDLMSKDLDLSGMFSKDLPTGIF
tr|Q9VKR0|Q9VKR0_DROME     DADMLAIASAPAASS---------
sp|P36039|EMC3_YEAST       EQRVLKQYM---------------
                           :  ::
```

Figure 18.18: Predicted topology of EMC3. A. The topology of EMC3 (UniProt/Swiss-Prot entry Q9P0I2) is shown as predicted by TOPCONS [340] (http://topcons.cbr.su.se/). Segments marked in red correspond to cytoplasmic regions, whereas blue signifies exposure to the ER lumen. TMDs are represented as white and grey boxes. **B.** Multiple sequence alignment of EMC3 in different species. The predicted TMDs in human EMC3 are boxed.

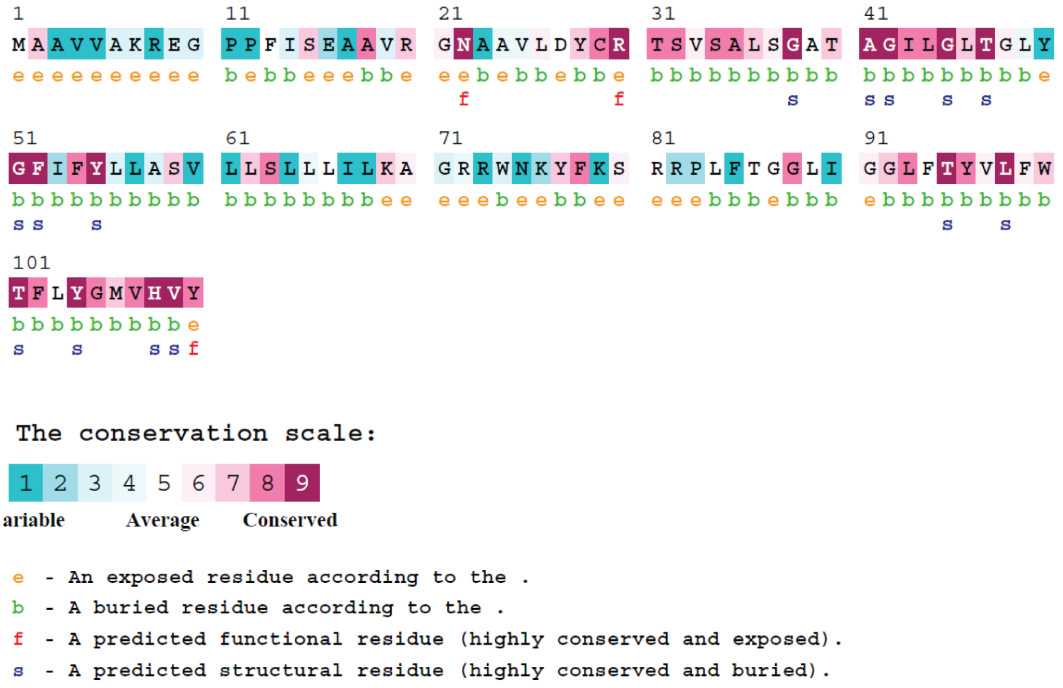


Figure 18.19: Conservation of EMC6 primary structure Sequence conservation of the human EMC6. Computational analysis was performed using the ConSurf Database [534].

Bibliography

[1] M. K. Park, O. H. Petersen, and A. V. Tepikin. The endoplasmic reticulum as one continuous Ca pool: visualization of rapid Ca movements and equilibration. *The EMBO Journal*, 19(21):5729–5739, 2000.

[2] G. E. Palade. The endoplasmic reticulum. *Journal of Biophysical and Biochemical Cytology*, 2(4):85–98, 1956.

[3] Y. Shibata, G. K. Voeltz, and T. A. Rapoport. Rough sheets and smooth tubules. *Cell*, 126(3):435–439, 2006.

[4] L. M. Westrate, J. E. Lee, W. A. Prinz, and G. K. Voeltz. Form follows function: The importance of endoplasmic reticulum shape. *Annual Review of Biochemistry*, 84:791–811, 2015.

[5] D. S. Schwarz and M. D. Blower. The endoplasmic reticulum: structure, function and response to cellular signaling. *Cellular and Molecular Life Sciences*, 73(1):79–94, 2016.

[6] J. Nixon-Abell, C. Obara, A. Weigel, D. Li, W. Legant, C. Xu, H. Pasolli, K. Harvey, H. Hess, E. Betzig, C. Blackstone, and J. Lippincott-Schwartz. Increased spatiotemporal resolution reveals highly dynamic dense tubular matrices in the peripheral ER. *Science*, 354(6311):aaf3928, 2016.

[7] J. Hu, W. A. Prinz, and T. A. Rapoport. Weaving the web of ER tubules. *Cell*, 147(6):1226–1231, 2011.

[8] A. A. Rowland and G. K. Voeltz. Endoplasmic reticulum-mitochondria contacts: function of the junction. *Nature Reviews. Molecular Cell Biology*, 13(10):607–625, oct 2012.

[9] A. R. English and G. K. Voeltz. Endoplasmic reticulum structure and interconnections with other organelles. *Cold Spring Harbor Perspectives in Biology*, 5(4):a013227, apr 2013.

[10] T. Blom, P. Somerharju, and E. Ikonen. Synthesis and biosynthetic trafficking of membrane lipids. *Cold Spring Harbor Perspectives in Biology*, 3(8):a004713, 2011.

[11] S. Lev. Nonvesicular Lipid Transfer from the Endoplasmic Reticulum. *Cold Spring Harbor Perspectives in Biology*, 4:a013300, 2012.

[12] L. Biwer and B. E. Isakson. Endoplasmic reticulum mediated signaling in cellular microdomains. *Acta Physiologica*, page doi:10.1111/apha.12675, 2016.

[13] G. Agrawal and S. Subramani. De novo peroxisome biogenesis: Evolving concepts and conundrums. *Biochimica et Biophysica Acta - Molecular Cell Research*, 1863(5):892–901, 2016.

[14] M. Aebi. N-linked protein glycosylation in the ER. *Biochimica et Biophysica Acta - Molecular Cell Research*, 1833(11):2430–2437, 2013.

[15] I. Braakman and N. J. Bulleid. Protein folding and modification in the mammalian endoplasmic reticulum. *Annual Reviews of Biochemistry*, 80:71–99, jan 2011.

[16] J. C. Christianson and Y. Ye. Cleaning up in the endoplasmic reticulum: Ubiquitin in charge. *Nature Structural & Molecular Biology*, 21(4):325–335, 2014.

[17] O. Foresti, V. Rodriguez-vaello, C. Funaya, and P. Carvalho. Quality control of inner nuclear membrane proteins by the Asi complex. *Science*, 994(2002):2962–2967, 2013.

[18] C. K. Barlowe and E. A. Miller. Secretory protein biogenesis and traffic in the early secretory pathway. *Genetics*, 193(2):383–410, 2013.

[19] E. C. Mandon, S. F. Trueman, and R. Gilmore. Protein translocation across the rough endoplasmic reticulum. *Cold Spring Harbor Perspectives in Biology*, 5(2):a013342, feb 2013.

[20] X. A. Cui, H. Zhang, and A. F. Palazzo. P180 promotes the ribosome-independent localization of a subset of mRNA to the endoplasmic reticulum. *PLoS Biology*, 10(5):e1001336, 2012.

[21] X. A. Cui and A. F. Palazzo. Localization of mRNAs to the endoplasmic reticulum. *Wiley Interdisciplinary Reviews: RNA*, 5(4):481–492, 2014.

[22] J. Dudek, S. Pfeffer, P.-H. Lee, M. Jung, A. Cavalié, V. Helms, F. Förster, and R. Zimmermann. Protein transport into the human endoplasmic reticulum. *Journal of Molecular Biology*, 427:1159–1175, 2015.

[23] G. Blobel and B. Dobberstein. Transfer of Proteins Across Membranes I. Presence of the proteolytically processed and unprocessed nascent immunoglobin light chains on membrane-bound ribosomes of murine meyloma. *The Journal of Cell Biology*, 67(3):835–851, 1975.

[24] G. von Heijne. Patterns of amino acids near signal-sequence cleavage sites. *European Journal of Biochemistry*, 133(1):17–21, 1983.

[25] N. K. Mize, D. W. Andrews, and V. R. Lingappa. A stop transfer sequence recognizes receptors for nascent chain translocation across the endoplasmic reticulum membrane. *Cell*, 47(5):711–719, 1986.

[26] G. von Heijne. Signal sequences. The limits of variation. *Journal of Molecular Biology*, 184(1):99–105, 1985.

[27] P. Walter and G. Blobel. Purification of a membrane-associated protein complex required for protein translocation across the endoplasmic reticulum. *Proceedings of the National Academy of Sciences of the United States of America*, 77(12):7112–7116, 1980.

[28] P. Walter and G. Blobel. Signal recognition particle contains a 7S RNA essential for protein translocation across the endoplasmic reticulum. *Nature*, 299(5885):691 – 698, 1982.

[29] P. Walter and G. Blobel. Translocation of proteins across membranes III. Signal recognition protein (SRP) causes signal sequence- dependent and site specific arrest of chain elongation that is released by microsomal membranes. *Journal of Cell Biology*, 91(4):557–561, 1981.

[30] D. I. Meyer and B. Dobberstein. Identification and characterization of a membrane component essential for the translocation of nascent proteins across the membrane of the endoplasmic reticulum. *The Journal of Cell Biology*, 87:503–508, 1980.

[31] P. Walter, I. Ibrahimi, and G. Blobel. Traslocation of proteins across the endoplasmic reticulum. I. Signal recognition protein (SRP) binds to in vitro assembled polysomes synthesizing secretory proteins. *Journal of Cell Biology*, 91:545–550, 1981.

[32] D. I. Meyer, E. Krause, and B. Dobberstein. Secretory protein translocation across membranes - the role of the "docking protein". *Nature*, 297:647–650, 1982.

[33] R. Gilmore, G. Blobel, and P. Walter. Protein translocation across the endoplasmic reticulum. I. Detection in the microsomal membrane of a receptor for the signal recognition particle. *The Journal of Cell Biology*, 95:463–469, 1982.

[34] R. Gilmore, P. Walter, and G. Blobel. Protein translocation across the endoplasmic reticulum. II. Isolation and characterization of the signal recognition particle receptor. *The Journal of Cell Biology*, 95:470–477, 1982.

[35] Y. Jiang, Z. Cheng, E. C. Mandon, and R. Gilmore. An interaction between the SRP receptor and the translocon is critical during cotranslational protein translocation. *Journal of Cell Biology*, 180(6):1149–1161, 2008.

[36] T. Connolly and R. Gilmore. GTP hydrolysis by complexes of the signal recognition particle and the signal recognition particle receptor. *The Journal of Cell Biology*, 123(4):799–807, 1993.

[37] J. D. Miller, H. Wilhelm, L. Gierasch, R. Gilmore, and P. Walter. GTP binding and hydrolysis by the signal recognition particle during initiation of protein translocation. *Nature*, 366(6453):351–354, 1993.

[38] T. Connolly, P. J. Rapiejko, and R. Gilmore. Requirement of GTP hydrolysis for dissociation of the signal recognition particle from its receptor. *Science*, 252(5010):1171–1173, 1991.

[39] J. D. Miller and P. Walter. A GTPase cycle in initiation of protein translocation across the endoplasmic reticulum membrane. *Ciba Foundation Symposium*, 176:147–163, 1993.

[40] T. A. Fulga, I. Sinning, B. Dobberstein, and M. R. Pool. SR beta coordinates signal sequence release from SRP with ribosome binding to the translocon. *EMBO Journal*, 20(9):2338–2347, 2001.

[41] R. J. Deshaies and R. Schekman. A yeast mutant defective at an early stage in import of secretory protein precursors into the endoplasmic reticulum. *Journal of Cell Biology*, 105(2):633–645, 1987.

[42] J. A. Rothblatt, R. J. Deshaies, S. L. Sanders, G. Daum, and R. Schekman. Multiple genes are required for proper insertion of secretory proteins into the endoplasmic reticulum in yeast. *The Journal of Cell Biology*, 109(6 Pt 1):2641–2652, 1989.

[43] R. J. Deshaies, S. L. Sanders, D. A. Feldheim, and R. Schekman. Assembly of yeast Sec proteins involved in translocation into the endoplasmic reticulum into a membrane-bound multisubunit complex. *Nature*, 349(6312):806–808, 1991.

[44] D. Goerlich and T. A. Rapoport. Protein translocation into proteoliposomes reconstituted from purified components of the endoplasmic reticulum membrane. *Cell*, 75(4):615–630, 1993.

[45] B. van den Berg, W. M. C. Jr, I. Collinson, Y. Modis, E. Hartmann4, S. C. Harrison, and Tom A. Rapoport. X-ray structure of a protein-conducting channel. *Nature*, 427(6969):36–44, 2004.

[46] F. Cymer, G. Von Heijne, and S. H. White. Mechanisms of integral membrane protein insertion and folding. *Journal of Molecular Biology*, 427(5):999–1022, 2015.

[47] K. Denks, A. Vogt, I. Sachelaru, N.-A. Petriman, R. Kudva, and H.-G. Koch. The Sec translocon mediated protein transport in prokaryotes and eukaryotes. *Molecular Membrane Biology*, 31(2-3):58–84, 2014.

[48] D. J. Kelleher and R. Gilmore. An evolving view of the eukaryotic oligosaccharyltransferase. *Glycobiology*, 16(4):47–62, 2006.

[49] B. C. S. Cross and S. High. Dissecting the physiological role of selective transmembrane-segment retention at the ER translocon. *Journal of Cell Science*, 122(11):1768–1777, 2009.

[50] S. Tamborero, M. Vilar, L. Martínez-Gil, A. E. Johnson, and I. Mingarro. Membrane insertion and topology of the translocating chain-associating membrane protein (TRAM). *Journal of Molecular Biology*, 406(4):571–582, 2011.

[51] N. Sommer, T. Junne, K. U. Kalies, M. Spiess, and E. Hartmann. TRAP assists membrane protein topogenesis at the mammalian ER membrane. *Biochimica et Biophysica Acta - Molecular Cell Research*, 1833(12):3104–3111, 2013.

[52] E. Wallin and G. von Heijne. Genome-wide analysis of integral membrane proteins from eubacterial, archaean, and eukaryotic organisms. *Protein Science*, 7:1029–1038, 1998.

[53] T. Hessa, A. Sharma, M. Mariappan, H. D. Eshleman, E. Gutierrez, and R. S. Hegde. Protein targeting and degradation are coupled for elimination of mislocalized proteins. *Nature*, 475(7356):394–397, 2011.

[54] T. Kalbfleisch, A. Cambon, and B. W. Wattenberg. A bioinformatics approach to identifying tail-anchored proteins in the human genome. *Traffic*, 8(12):1687–1694, 2007.

[55] V. Denic. A portrait of the GET pathway as a surprisingly complicated young man. *Trends in Biochemical Sciences*, 37(10):411–417, 2012.

[56] T. Beilharz, B. Egan, P. A. Silver, K. Hofmann, and T. Lithgow. Bipartite signals mediate subcellular targeting of tail-anchored membrane proteins in Saccharomyces cerevisiae. *Journal of Biological Chemistry*, 278(10):8219–8223, 2003.

[57] S. Stefanovic and R. S. Hegde. Identification of a targeting factor for posttranslational membrane protein insertion into the ER. *Cell*, 128(6):1147–1159, 2007.

[58] J. M. Boname, S. Bloor, M. P. Wandel, J. A. Nathan, R. Antrobus, K. S. Dingwell, T. L. Thurston, D. L. Smith, J. C. Smith, F. Randow, and P. J. Lehner. Cleavage by signal peptide peptidase is required for the degradation of selected tail-anchored proteins. *The Journal of Cell Biology*, 205(6):847–862, 2014.

[59] B. Wegiel, Z. Nemeth, M. Correa-Costa, A. C. Bulmer, and L. E. Otterbein. Heme oxygenase-1: A metabolic nike. *Antioxidants & Redox Signaling*, 20(11):1709–1722, 2014.

[60] C. Rabu, V. Schmid, B. Schwappach, and S. High. Biogenesis of tail-anchored proteins: The beginning for the end? *Journal of Cell Science*, 122(Pt 20):3605–3612, 2009.

[61] B. M. Abell, M. R. Pool, O. Schlenker, I. Sinning, and S. High. Signal recognition particle mediates post-translational targeting in eukaryotes. *The EMBO Journal*, 23(14):2755–2764, 2004.

[62] U. Berndt, S. Oellerer, Y. Zhang, A. E. Johnson, and S. Rospert. A signal-anchor sequence stimulates signal recognition particle binding to ribosomes from inside the exit tunnel. *Proceedings of the National Academy of Sciences of the United States of America*, 106(5):1398–1403, 2009.

[63] B. M. Abell, M. Jung, J. D. Oliver, B. C. Knight, J. Tyedmers, R. Zimmermann, and S. High. Tail-anchored and signal-anchored proteins utilize overlapping pathways during membrane insertion. *Journal of Biological Chemistry*, 278(8):5669–5678, 2003.

[64] D. T. W. Ng, J. D. Brown, and P. Walter. Signal sequences specify the targeting route to the endoplasmic reticulum membrane. *Journal of Cell Biology*, 134(2):269–278, 1996.

[65] R. J. Deshaies and R. Schekman. Structural and functional dissection of Sec62p, a membrane-bound component of the yeast endoplasmic reticulum protein import machinery. *Molecular and Cellular Biology*, 10(11):6024–6035, 1990.

[66] S. Panzner, L. Dreier, E. Hartmann, S. Kostka, and T. A. Rapoport. Posttranslational protein transport in yeast reconstituted with a purified complex of Sec proteins and Kar2p. *Cell*, 81(4):561–570, 1995.

[67] H. A. Meyer, H. Grau, R. Kraft, S. Kostka, S. Prehn, K. U. Kalies, and E. Hartmann. Mammalian Sec61 is associated with Sec62 and Sec63. *Journal of Biological Chemistry*, 275(19):14550–14557, 2000.

[68] A. Mades, K. Gotthardt, K. Awe, J. Stieler, T. Doering, S. Fueser, and R. Prange. Role of human Sec63 in modulating the steady-state levels of multi-spanning membrane proteins. *PLoS ONE*, 7(11):e49243. doi:10.1371/journal.pone.0049243, 2012.

[69] S. K. Lyman and R. Schekman. Interaction between BiP and Sec63p is required for the completion of protein translocation into the ER of Saccharomyces cerevisiae. *Journal of Cell Biology*, 131(5):1163–1171, 1995.

[70] K. E. S. Matlack, B. Misselwitz, K. Plath, and T. A. Rapoport. BIP acts as a molecular ratchet during posttranslational transport of prepro-α factor across the ER membrane. *Cell*, 97(5):553–564, 1999.

[71] L. I. Malkin and A. Rich. Partial resistance of nascent polypeptide chains to proteolytic digestion due to ribosomal shielding. *Journal of Molecular Biology*, 26(2):329–346, 1967.

[72] G. Blobel and D. D. Sabatini. Controlled proteolysis of nascent polypeptides in rat liver cell fractions. *The Journal of Cell Biology*, 45(1):130–145, 1970.

[73] U. Kutay, G. Ahnert-Hilger, E. Hartmann, B. Wiedenmann, and T. A. Rapoport. Transport route for synaptobrevin via a novel pathway of insertion into the endoplasmic reticulum membrane. *The EMBO Journal*, 14(2):217–23, 1995.

[74] M. Schuldiner, J. Metz, V. Schmid, V. Denic, M. Rakwalska, H. D. Schmitt, B. Schwappach, and J. S. Weissman. The GET complex mediates insertion of tail-anchored proteins into the ER membrane. *Cell*, 134(4):634–645, 2008.

[75] V. Favaloro, F. Vilardi, R. Schlecht, M. P. Mayer, and B. Dobberstein. Asna1/TRC40-mediated membrane insertion of tail-anchored proteins. *Journal of Cell Science*, 123(9):1522–1530, 2010.

[76] F. Wang, E. C. Brown, G. Mak, J. Zhuang, and V. Denic. A chaperone cascade sorts proteins for posttranslational membrane insertion into the endoplasmic reticulum. *Molecular Cell*, 40(1):159–171, 2010.

[77] M. Mariappan, X. Li, S. Stefanovic, A. Sharma, A. Mateja, R. J. Keenan, and R. S. Hegde. A ribosome-associating factor chaperones tail-anchored membrane proteins. *Nature*, 466(7310):1120–1124, 2010.

[78] Y. Xu, Y. Liu, J. G. Lee, and Y. Ye. A Ubiquitin-like domain recruits an oligomeric chaperone to a retrotranslocation complex in endoplasmic reticulum-associated degradation. *Journal of Biological Chemistry*, 288(25):18068–18076, 2013.

[79] P. Leznicki, Q. P. Roebuck, L. Wunderley, A. Clancy, E. M. Krysztofinska, R. L. Isaacson, J. Warwicker, B. Schwappach, and S. High. The association of BAG6 with SGTA and tail-anchored proteins. *PLoS ONE*, 8(3):e59590, 2013.

[80] J. F. Darby, E. M. Krysztofinska, P. J. Simpson, A. C. Simon, P. Leznicki, N. Sriskandarajah, D. S. Bishop, L. R. Hale, C. Alfano, M. R. Conte, S. Martinez-Lumbreras, A. Thapaliya, S. High, and R. L. Isaacson. Solution structure of the SGTA dimerisation domain and investigation of its interactions with the ubiquitin-like domains of BAG6 and UBL4A. *PLoS ONE*, 9(11):e113281, 2014.

[81] J.-Y. Mock, J. W. Chartron, M. Zaslaver, Y. Xu, Y. Ye, and W. M. Clemons. Bag6 complex contains a minimal tail-anchor-targeting module and a mock BAG domain. *Proceedings of the National Academy of Sciences of the United States of America*, 112(1):106–111, 2015.

[82] N. Kuwabara, R. Minami, N. Yokota, H. Matsumoto, T. Senda, H. Kawahara, and R. Kato. Structure of a BAG6 (Bcl-2-associated athanogene 6)-Ubl4a (ubiquitin-like protein 4a) complex reveals a novel binding interface that functions in tail-anchored protein biogenesis. *Journal of Biological Chemistry*, 290(15):9387–9398, 2015.

[83] M. Kabbage and M. B. Dickman. The BAG proteins: a ubiquitous family of chaperone regulators. *Cellular and Molecular Life Sciences: CMLS*, 65(9):1390–402, may 2008.

[84] S. T. Liou and C. Wang. Small glutamine-rich tetratricopeptide repeat-containing protein is composed of three structural units with distinct functions. *Archives of Biochemistry and Biophysics*, 435(2):253–263, 2005.

[85] Y. Xu, M. Cai, Y. Yang, L. Huang, and Y. Ye. SGTA recognizes a noncanonical ubiquitin-like domain in the Bag6-Ubl4A-Trc35 complex to promote endoplasmic reticulum-associated degradation. *Cell Reports*, 2(6):1633–1644, 2012.

[86] R. Minami, A. Hayakawa, H. Kagawa, Y. Yanagi, H. Yokosawa, and H. Kawahara. BAG-6 is essential for selective elimination of defective proteasomal substrates. *Journal of Cell Biology*, 190(4):637–650, 2010.

[87] P. Leznicki, A. Clancy, B. Schwappach, and S. High. Bat3 promotes the membrane integration of tail-anchored proteins. *Journal of Cell Science*, 123(Pt 13):2170–2178, 2010.

[88] G. Bozkurt, G. Stjepanovic, F. Vilardi, S. Amlacher, K. Wild, G. Bange, V. Favaloro, K. Rippe, E. Hurt, B. Dobberstein, and I. Sinning. Structural insights into tail-anchored protein binding and membrane insertion by Get3. *Proceedings of the National Academy of Sciences of the United States of America*, 106(50):21131–21136, 2009.

[89] S. Shao and R. S. Hegde. Membrane protein insertion at the endoplasmic reticulum. *Annual Review of Cell and Developmental Biology*, 27:25–56, 2011.

[90] Y. W. Chang, Y. C. Chuang, Y. C. Ho, M. Y. Cheng, Y. J. Sun, C. D. Hsiao, and C. Wang. Crystal structure of Get4-Get5 complex and its interactions with Sgt2, Get3, and Ydj1. *Journal of Biological Chemistry*, 285(13):9962–9970, 2010.

[91] J. W. Chartron, C. J. M. Suloway, M. Zaslaver, and W. M. Clemons. Structural characterization of the Get4/Get5 complex and its interaction with Get3. *Proceedings of the National Academy of Sciences of the United States of America*, 107(27):12127–12132, 2010.

[92] H. B. Gristick, M. E. Rome, J. W. Chartron, M. Rao, S. Hess, S.-o. Shan, and W. M. Clemons. Mechanism of assembly of a substrate-transfer complex during tail-anchored protein targeting. *Journal of Biological Chemistry*, 290:30006–30017, 2015.

[93] A. Mateja, A. Szlachcic, M. E. Downing, M. Dobosz, M. Mariappan, R. S. Hegde, and R. J. Keenan. The structural basis of tail-anchored membrane protein recognition by Get3. *Nature*, 461(7262):361–366, 2009.

[94] A. Mateja, M. Paduch, H.-y. Chang, A. Szydlowska, A. A. Kossiakoff, R. S. Hegde, and R. J. Keenan. Structure of the Get3 targeting factor in complex with its membrane protein cargo. *Science*, 347(6226):1152–1155, 2015.

[95] M. C. Jonikas, S. R. Collins, V. Denic, E. Oh, E. M. Quan, V. Schmid, J. Weibezahn, B. Schwappach, P. Walter, J. S. Weissman, and M. Schuldiner. Comprehensive characterization of genes required for protein folding in the endoplasmic reticulum. *Science*, 323(5922):1693–1697, mar 2009.

[96] Y. Yamamoto and T. Sakisaka. Molecular machinery for insertion of tail-anchored membrane proteins into the endoplasmic reticulum membrane in mammalian cells. *Molecular Cell*, 48(3):387–397, 2012.

[97] F. Vilardi, M. Stephan, A. Clancy, A. Janshoff, and B. Schwappach. WRB and CAML are necessary and sufficient to mediate tail-anchored protein targeting to the ER membrane. *PloS ONE*, 9(1):e85033, 2014.

[98] F. Wang, C. Chan, N. R. Weir, and V. Denic. The Get1/2 transmembrane complex is an endoplasmic-reticulum membrane protein insertase. *Nature*, 512(7515):441–444, 2014.

[99] S. Stefer, S. Reitz, F. Wang, K. Wild, Y. Pang, J. Bomke, C. Hein, F. Löhr, and F. Bernhard. Structural basis for tail-anchored membrane protein biogenesis by the Get3-receptor complex. *Science*, 333(6043):758–762, 2011.

[100] F. Wang, A. Whynot, M. Tung, and V. Denic. The mechanism of tail-anchored protein insertion into the ER membrane. *Molecular Cell*, 43(5):738–750, 2011.

[101] Sara Francesca Colombo, S. Cardani, A. Marol, A. Vitiello, P. Soffientini, A. Crespi, R. F. Bram, R. Benfante, and N. Borgese. Tail-anchored protein biogenesis in mammals: Function and reciprocal interactions of the two subunits of the TRC40 receptor. *Journal of Biological Chemistry*, 291(29):15292–15306, 2016.

[102] C. Rabu, P. Wipf, J. L. Brodsky, and S. High. A precursor-specific role for Hsp40/Hsc70 during tail-anchored protein integration at the endoplasmic reticulum. *Journal of Biological Chemistry*, 283(41):27504–27513, 2008.

[103] B. M. Abell, C. Rabu, P. Leznicki, J. C. Young, and S. High. Post-translational integration of tail-anchored proteins is facilitated by defined molecular chaperones. *Journal of Cell Science*, 120(Pt 10):1743–1751, 2007.

[104] J. C. Young, J. M. Barral, and F. U. Hartl. More than folding: Localized functions of cytosolic chaperones. *Trends in Biochemical Sciences*, 28(10):541–547, 2003.

[105] J. Soll and E. Schleiff. Protein import into chloroplasts. *Nature Reviews Molecular Cell Biology*, 5:198–208, 2004.

[106] S. Brambillasca, M. Yabal, P. Soffientini, S. Stefanovic, M. Makarow, R. S. Hegde, and N. Borgese. Transmembrane topogenesis of a tail-anchored protein is modulated by membrane lipid composition. *The EMBO Journal*, 24(14):2533–2542, 2005.

[107] Y.-C. Chen, G. K. E. Umanah, N. Dephoure, S. A. Andrabi, S. P. Gygi, T. M. Dawson, V. L. Dawson, and J. Rutter. Msp1/ATAD1 maintains mitochondrial function by facilitating the degradation of mislocalized tail-anchored proteins. *The EMBO Journal*, 33(14):1548–1564, 2014.

[108] M. C. Rodrigo-Brenni, E. Gutierrez, and R. S. Hegde. Cytosolic quality control of mislocalized proteins requires RNF126 recruitment to Bag6. *Molecular Cell*, 55(2):227–237, 2014.

[109] E. Itakura, E. Zavodszky, S. Shao, M. L. Wohlever, R. J. Keenan, and R. S. Hegde. Ubiquilins chaperone and triage mitochondrial membrane proteins for degradation. *Molecular Cell*, 63(1):21–33, 2016.

[110] R. Suzuki and H. Kawahara. UBQLN4 recognizes mislocalized transmembrane domain proteins and targets these to proteasomal degradation. *EMBO reports*, 1111:1–16, 2016.

[111] D. Y. Lee and E. J. Brown. Ubiquilins in the crosstalk among proteolytic pathways. *Journal of Biological Chemistry*, 393:441–447, 2012.

[112] F. U. Hartl. Molecular chaperones in cellular protein folding, 1996.

[113] Y. E. Kim, M. S. Hipp, A. Bracher, M. Hayer-Hartl, and F. U. Hartl. *Molecular chaperone functions in protein folding and proteostasis*, volume 82. jan 2013.

[114] J. G. Lee and Y. Ye. Bag6/Bat3/Scythe: A novel chaperone activity with diverse regulatory functions in protein biogenesis and degradation. *BioEssays*, 35(4):377–385, 2013.

[115] M. Marzec, D. Eletto, and Y. Argon. GRP94: An HSP90-like protein specialized for protein folding and quality control in the endoplasmic reticulum. *Biochimica et Biophysica Acta - Molecular Cell Research*, 1823(3):774–787, 2012.

[116] H. H. Kampinga and E. A. Craig. The HSP70 chaperone machinery: J proteins as drivers of functional specificity. *Nature Reviews. Molecular Cell Biology*, 11(8):579–92, 2010.

[117] L. Ellgaard, N. McCaul, A. Chatsisvili, and I. Braakman. Co- and post-translational protein folding in the ER. *Traffic*, (17):615–638, 2016.

[118] M. Gething. Role and regulation of the ER chaperone BiP. *Cell and Develpomental Biology*, 10:465–472, 1999.

[119] J. Yang, M. Nune, Y. Zong, L. Zhou, and Q. Liu. Close and allosteric opening of the polypeptide-binding site in a human Hsp70 chaperone BiP. *Structure*, 23(12):2191–2203, 2015.

[120] M. P. Mayer and B. Bukau. Hsp70 chaperones: Cellular functions and molecular mechanism. *Cellular and Molecular Life Sciences*, 62(6):670–684, 2005.

[121] T. A. Rapoport, K. E. S. Matlack, K. Plath, B. Misselwitz, and O. Staeck. Posttranslational protein translocation across the membrane of the endoplasmic reticulum, 1999.

[122] J. Behnke, M. J. Feige, and L. M. Hendershot. BiP and its nucleotide exchange factors Grp170 and Sil1: Mechanisms of action and biological functions. *Journal of Molecular Biology*, 427(7):1589–1608, 2015.

[123] A. Melnyk, H. Rieger, and R. Zimmermann. *The Networking of Chaperones by Co-chaperones*, volume Chapter 9. 2015.

[124] Y. Shen and L. M. Hendershot. ERdj3, a stress-inducible endoplasmic reticulum DnaJ homologue, serves as a cofactor for BiP's interactions with unfolded substrates. *Molecular Biology of the Cell*, 16(8):40–50, 2005.

[125] K. Petrova, S. Oyadomari, L. M. Hendershot, and D. Ron. Regulated association of misfolded endoplasmic reticulum lumenal proteins with P58/DNAJc3. *The EMBO Journal*, 27(21):2862–2872, 2008.

[126] M. Marzec, D. Eletto, and Y. Argon. GRP94: An HSP90-like protein specialized for protein folding and quality control in the endoplasmic reticulum. *Biochimica et Biophysica Acta*, 1823(3):774–787, mar 2012.

[127] O. Ostrovsky, C. Makarewich, E. L. Snapp, and Y. Argon. An essential role for ATP binding and hydrolysis in the chaperone activity of GRP94 in cells. *Proceedings of the National Academy of Sciences of the United States of America*, 106(28):11600–11605, 2009.

[128] K. A. Krukenberg, U. M. K. Boettcher, D. R. Southworth, and D. A. Agard. Grp94, the endoplasmic reticulum Hsp90, has a similar solution conformation to cytosolic Hsp90 in the absence of nucleotide. *Protein Science*, 18(9):1815–1827, 2009.

[129] T. Gidalevitz, F. Stevens, and Y. Argon. Orchestration of secretory protein folding by ER chaperones. *Biochimica et Biophysica Acta - Molecular Cell Research*, 1833(11):2410–2424, 2013.

[130] J. Melnick, J. L. Dul, and Y. Argon. Sequential interaction of the chaperones BiP and GRP94 with immunoglobulin chains in the endoplasmic reticulum. *Nature*, 370(6488):373–375, 1994.

[131] F. Randow and B. Seed. Endoplasmic reticulum chaperone gp96 is required for innate immunity but not cell viability. *Nature Cell Biology*, 3(10):891–896, 2001.

[132] Y. Yang, B. Liu, J. Dai, P. K. Srivastava, D. J. Zammit, L. Lefrancois, and Z. Li. Heat shock protein gp96 is a master chaperone for Toll-like receptors and is important in the innate function of macrophages. *Immunity*, 26(2):215–226, 2007.

[133] M. P. Weekes, R. Antrobus, S. Talbot, S. Hör, N. Simecek, D. L. Smith, S. Bloor, F. Randow, and P. J. Lehner. Proteomic plasma membrane profiling reveals an essential role for gp96 in the cell surface expression of LDLR family members, including the LDL receptor and LRP6. *Journal of proteome research*, 11(3):1475–84, mar 2012.

[134] C. Morales, S. Wu, Y. Yang, B. Hao, and Z. Li. Drosophila glycoprotein 93 Is an ortholog of mammalian heat shock protein gp96 (grp94, HSP90b1, HSPC4) and retains disulfide bond-independent chaperone function for TLRs and integrins. *Journal of Immunology*, 183(8):5121–5128, 2009.

[135] O. Ostrovsky, N. T. Ahmed, and Y. Argon. The chaperone activity of GRP94 toward insulin-like growth factor II is necessary for the stress response to serum deprivation. *Molecular Biology of the Cell*, 20(6):1855–1864, 2009.

[136] L. R. Ferreira, K. Norris, T. Smith, C. Hebert, and J. J. Sauk. Association of Hsp47, Grp78, and Grp94 with procollagen supports the successive or coupled action of molecular chaperones. *Journal of Cellular Biochemistry*, 56(4):518–526, 1994.

[137] B. Liu, Y. Yang, Z. Qiu, M. Staron, F. Hong, Y. Li, S. Wu, Y. Li, B. Hao, R. Bona, D. Han, and Z. Li. Folding of Toll-like receptors by the HSP90 paralogue gp96 requires a substrate-specific cochaperone. *Nature Communications*, 1(79):DOI: 10.1038/ncomms1070, 2010.

[138] T. Anelli and E. Van Anken. Missing links in antibody assembly control. *International Journal of Cell Biology*, Article ID:http://dx.doi.org/10.1155/2013/606703, 2013.

[139] J. C. Christianson, T. A. Shaler, R. E. Tyler, and R. R. Kopito. OS-9 and GRP94 deliver mutant alpha1-antitrypsin to the Hrd1-SEL1L ubiquitin ligase complex for ERAD. *Nature Cell Biology*, 10(3):272–282, 2008.

[140] J. Melnick, J. L. Dul, and Y. Argon. Sequential interaction of the chaperones BiP and GRP94 with immunoglobulin chains in the endoplasmic reticulum. *Nature*, 370(6488):373–375, 1994.

[141] C. Scheufler, A. Brinker, G. Bourenkov, S. Pegoraro, L. Moroder, H. Bartunik, F. U. Hartl, and I. Moarefi. Structure of TPR domain-peptide complexes: Critical elements in the assembly of the Hsp70-Hsp90 multichaperone machine. *Cell*, 101(2):199–210, 2000.

[142] J. C. Young. The role of the cytosolic HSP70 chaperone system in diseases caused by misfolding and aberrant trafficking of ion channels. *Disease Models & Mechanisms*, 7(3):319–329, 2014.

[143] I. M. Pranke and I. Sermet-Gaudelus. Biosynthesis of cystic fibrosis transmembrane conductance regulator. *The International Journal of Biochemistry & Cell Biology*, 52:26–38, 2014.

[144] E. L. Turnbull, M. F. N. Rosser, and D. M. Cyr. The role of the UPS in cystic fibrosis. *BMC Biochemistry*, 8(S11):doi:10.1186/1471–2091–8–S1–S11, 2007.

[145] B. P. O'Sullivan and S. D. Freedman. Cystic fibrosis. *The Lancet*, 373(9678):1891–1904, 2009.

[146] C. L. Ward and R. R. Kopito. Intracellular turnover of cystic fibrosis transmembrane conductance regulator. Inefficient processing and rapid degradation of wild-type and mutant proteins. *Journal of Biological Chemistry*, 269(41):25710–25718, 1994.

[147] S. Pind, J. R. Riordan, and D. B. Williams. Participation of the endoplasmic reticulum chaperone calnexin (p88, IP90) in the biogenesis of the cystic fibrosis transmembrane conductance regulator. *Journal of Biological Chemistry*, 269(17):12784–12788, 1994.

[148] G. C. Meacham, Z. Lu, S. King, E. Sorscher, A. Tousson, and D. M. Cyr. The Hdj-2/Hsc70 chaperone pair facilitates early steps in CFTR biogenesis. *The EMBO Journal*, 18(6):1492–1505, 1999.

[149] D. E. Grove, C. Fan, H. Ren, and D. M. Cyr. The endoplasmic reticulum-associated Hsp40 DNAJB12 and Hsc70 cooperate to facilitate RMA1 E3-dependent degradation of nascent CFTRDeltaF508. *Molecular Biology of the Cell*, 22(3):301–314, 2011.

[150] G. C. Meacham, C. Patterson, W. Zhang, J. M. Younger, and D. M. Cyr. The Hsc70 co-chaperone CHIP targets immature CFTR for proteasomal degradation. *Nature Cell Biology*, 3:100–105, 2001.

[151] U. C. Krieg, A. E. Johnson, and P. Walter. Protein translocation across the endoplasmic reticulum membrane: Identification by photocross-linking of a 39-kD integral membrane glycoprotein as part of a putative translocation tunnel. *Journal of Cell Biology*, 109(5):2033–2043, 1989.

[152] D. Goerlich, E. Hartmann, S. Prehn, and T. A. Rapoport. A protein of the endoplasmic reticulum involved early in polypeptide translocation. *Nature*, 357(6373):47–52, 1992.

[153] S. Voigt, B. Jungnickel, E. Hartmann, and T. A. Rapoport. Signal sequence-dependent function of the TRAM protein during early phases of protein transport across the endoplasmic reticulum membrane. *Journal of Cell Biology*, 134(1):25–35, 1996.

[154] S. U. Heinrich, W. Mothes, J. Brunner, and T. A. Rapoport. The Sec61p complex mediates the integration of a membrane protein by allowing lipid partitioning of the transmembrane domain. *Cell*, 102(2):233–244, 2000.

[155] D. Hung, D. Falcone, J. Lin, D. W. Andrews, and A. E. Johnson. The cotranslational integration of membrane proteins into the phospholipid bilayer is a multistep process. *Cell*, 85(3):369–378, 1996.

[156] V. E. Walker, M. J. H. Wong, R. Atanasiu, C. Hantouche, J. C. Young, and A. Shrier. Hsp40 chaperones promote degradation of the hERG potassium channel. *Journal of Biological Chemistry*, 285(5):3319–3329, 2010.

[157] M. Nguyen, A. Alfonso, C. D. Johnson, and J. B. Rand. Caenorhabditis elegans mutants resistant to inhibitors of acetylcholinesterase. *Genetics*, 140(2):527–535, 1995.

[158] S. Halevi, L. Yassin, M. Eshel, F. Sala, S. Sala, M. Criado, and M. Treinin. Conservation within the RIC-3 gene family: Effectors of mammalian nicotinic acetylcholine receptor expression. *Journal of Biological Chemistry*, 278(36):34411–34417, 2003.

[159] S. J. Lansdell, V. J. Gee, P. C. Harkness, A. I. Doward, E. R. Baker, A. J. Gibb, and N. S. Millar. RIC-3 enhances functional expression of multiple nicotinic acetylcholine receptor subtypes in mammalian cells. *Molecular Pharmacology*, 68(5):1431–1438, 2005.

[160] A. S. Vallés, A. M. Roccamo, and F. J. Barrantes. Ric-3 chaperone-mediated stable cell-surface expression of the neuronal alpha7 nicotinic acetylcholine receptor in mammalian cells. *Acta Pharmacologica Sinica*, 30(6):818–827, 2009.

[161] A. Dau, P. Komal, M. Truong, G. Morris, G. Evans, and R. Nashmi. RIC-3 differentially modulates alpha4beta2 and alpha7 nicotinic receptor assembly, expression, and nicotine-induced receptor upregulation. *BMC Neuroscience*, 14(47):doi: 10.1186/1471–2202–14–47, 2013.

[162] N. S. Millar. RIC-3: a nicotinic acetylcholine receptor chaperone. *British Journal of Pharmacology*, 153:S177–S183, 2008.

[163] H. C. Ben-Ami, L. Yassin, H. Farah, A. Michaeli, M. Eshel, and M. Treinin. RIC-3 affects properties and quantity of nicotinic acetylcholine receptors via a mechanism that does not require the coiled-coil domains. *Journal of Biological Chemistry*, 280(30):28053–28060, 2005.

[164] S. L. Meacock, F. J. L. Lecomte, S. G. Crawshaw, and S. High. Different transmembrane domains associate with distinct endoplasmic reticulum components during membrane integration of a polytopic protein. *Molecular Biology of the Cell*, 13:4114–4129, 2002.

[165] N. Ismail, S. G. Crawshaw, B. C. S. Cross, A. C. Haagsma, and S. High. Specific transmembrane segments are selectively delayed at the ER translocon during opsin biogenesis. *The Biochemical Journal*, 411(3):495–506, 2008.

[166] D. O. Daley. The assembly of membrane proteins into complexes. *Current Opinion in Structural Biology*, 18(4):420–424, 2008.

[167] L. Hendershot, D. Bole, and J. F. Kearney. The role of immunoglobulin heavy chain binding protein. *Immunology Today*, 8(4):111–114, 1987.

[168] Y. K. Lee, J. W. Brewer, R. Hellman, and L. M. Hendershot. BiP and immunoglobulin light chain cooperate to control the folding of heavy chain and ensure the fidelity of immunoglobulin assembly. *Molecular Biology of the Cell*, 10(7):2209–2219, 1999.

[169] M. Vanhove, Y. K. Usherwood, and L. M. Hendershot. Unassembled Ig heavy chains do not cycle from BiP in vivo but require light chains to trigger their release. *Immunity*, 15(1):105–114, 2001.

[170] M. J. Feige, J. Behnke, T. Mittag, and L. M. Hendershot. Dimerization-dependent folding underlies assembly control of the clonotypic $\alpha\beta$ T cell receptor chains. *Journal of Biological Chemistry*, 290(44):26821–26831, 2015.

[171] P. Blount and J. P. Merlie. Native folding of an acetylcholine receptor alpha subunit expressed in the absence of other receptor subunits. *The Journal of biological chemistry*, 263(2):1072–80, jan 1988.

[172] R. D. Klausner. Pre-Golgi degradation of newly synthesized T-cell antigen receptor chains: intrinsic sensitivity and the role of subunit assembly. *Journal of Cell Biology*, 109(1):73–83, 1989.

[173] S. Mueller, A. Wahlander, N. Selevsek, C. Otto, E. Mankah, and R. Gilmore. Protein degradation corrects for imbalanced subunit stoichiometry in OST complex assembly. *Molecular Biology of the Cell*, 26(14):2596–2608, 2015.

[174] M. E. Call, J. Pyrdol, M. Wiedmann, and K. W. Wucherpfennig. The organizing principle in the formation of the T cell receptor-CD3 complex. *Cell*, 111(7):967–979, 2002.

[175] M. J. Feige and L. M. Hendershot. Quality control of integral membrane proteins by assembly-dependent membrane integration. *Molecular Cell*, 51(3):297–309, 2013.

[176] H. Safavi-Hemami, G. Bulaj, B. M. Olivera, N. A. Williamson, and A. W. Purcell. Identification of Conus peptidylprolyl cis-trans isomerases (PPIases) and assessment of their role in the oxidative folding of conotoxins. *Journal of Biological Chemistry*, 285(17):12735–12746, 2010.

[177] M. Schwaller, B. Wilkinson, and H. F. Gilbert. Reduction-reoxidation cycles contribute to catalysis of disulfide isomerization by protein-disulfide isomerase. *Journal of Biological Chemistry*, 278(9):7154–7159, 2003.

[178] J. G. Elliott, J. D. Oliver, and S. High. The thiol-dependent reductase ERp57 interacts specifically with N- glycosylated integral membrane proteins. *Journal of Biological Chemistry*, 272(21):13849–13855, 1997.

[179] J. D. Oliver, F. J. van der Wal, N. J. Bulleid, and S. High. Interaction of the thiol-dependent reductase ERp57 with nascent glycoproteins. *Science*, 275(5296):86–88, 1997.

[180] A. Helenius and M. Aebi. Roles of N-linked glycans in the endoplasmic reticulum. *Annual Review of Biochemistry*, 73:1019–49, 2004.

[181] P. Orlean and A. K. Menon. Thematic review series: lipid posttranslational modifications. GPI anchoring of protein in yeast and mammalian cells, or: how we learned to stop worrying and love glycophospholipids. *Journal Of Lipid Research*, 48:993–1011, 2007.

[182] R. Wilson, J. F. Lees, and N. J. Bulleid. Protein disulfide isomerase acts as a molecular chaperone during the assembly of procollagen. *Journal of Biological Chemistry*, 273(16):9637–9643, 1998.

[183] D. M. Hudson and D. R. Eyre. Collagen prolyl 3-hydroxylation: a major role for a minor post-translational modification? *Connective Tissue Research*, 54(4-5):245–251, 2013.

[184] K. L. Gorres and R. T. Raines. *Prolyl 4-Hydroxylase*, volume 45. 2010.

[185] S. M. Auclair, M. K. Bhanu, and D. A. Kendall. Signal peptidase I: Cleaving the way to mature proteins. *Protein Science*, 21(1):13–25, 2012.

[186] J. A. Olzmann, R. R. Kopito, and J. C. Christianson. The mammalian endoplasmic reticulum-associated degradation system. *Cold Spring Harbor Perspectives in Biology*, 5:a013185, 2013.

[187] M. P. Hamon, A. L. Bulteau, and B. Friguet. Mitochondrial proteases and protein quality control in ageing and longevity. *Ageing Research Reviews*, 23(PA):56–66, 2015.

[188] Z. Tong, M.-S. Kim, A. Pandey, and P. J. Espenshade. Identification of candidate substrates for the Golgi Tul1 E3 ligase using quantitative diGly proteomics in yeast. *Molecular & Cellular Proteomics*, 13(11):2871–82, 2014.

[189] J. C. Christianson, J. A. Olzmann, T. A. Shaler, M. E. Sowa, E. J. Bennett, C. M. Richter, R. E. Tyler, E. J. Greenblatt, J. W. Harper, and R. R. Kopito. Defining human ERAD networks through an integrative mapping strategy. *Nature Cell Biology*, 14(1):93–105, jan 2012.

[190] C. L. Ward, S. Omura, and R. R. Kopito. Degradation of CFTR by the ubiquitin-proteasome pathway. *Cell*, 83(1):121–127, 1995.

[191] T. Claudio, H. L. Paulson, W. N. Green, A. E. Ross, D. S. Hartman, and D. Hayden. Fibroblasts transfected with Torpedo acetylcholine receptor beta-, gamma-, and delta-subunit cDNAs express functional receptors when infected with a retroviral alpha recombinant. *Journal of Cell Biology*, 108:2277–2290, 1989.

[192] P. Blount and J. P. Merlie. Mutational analysis of muscle nicotinic acetylcholine receptor subunit assembly. *Journal of Cell Biology*, 111(6):2613–2622, 1990.

[193] J. C. Christianson and W. N. Green. Regulation of nicotinic receptor expression by the ubiquitin-proteasome system. *The EMBO Journal*, 23(21):4156–4165, 2004.

[194] R. E. Tyler, M. M. P. Pearce, T. A. Shaler, J. A. Olzmann, E. J. Greenblatt, and R. R. Kopito. Unassembled CD147 is an endogenous endoplasmic reticulum-associated degradation substrate. *Molecular Biology of the Cell*, 23(24):4668–4678, dec 2012.

[195] M. Kikkert, R. Doolman, M. Dai, R. Avner, G. Hassink, S. Van Voorden, S. Thanedar, J. Roitelman, V. Chau, and E. Wiertz. Human HRD1 is an E3 ubiquitin ligase involved in degradation of proteins from the endoplasmic reticulum. *Journal of Biological Chemistry*, 279(5):3525–3534, 2004.

[196] O. Foresti, A. Ruggiano, H. K. Hannibal-Bach, C. S. Ejsing, and P. Carvalho. Sterol homeostasis requires regulated degradation of squalene monooxygenase by the ubiquitin ligase Doa10/Teb4. *eLife*, 2:e00953, 2013.

[197] D. N. Herbert, B. Foellmer, and A. Helenius. Glucose trimming and reglucosylatioin determines glycoprotein association with calnexin. *Cell*, 81(3):425–433, 1995.

[198] C. Hammond, I. Braakman, and A. Helenius. Role of N-linked oligosaccharide recognition, glucose trimming, and calnexin in glycoprotein folding and quality control. *Proceedings of the National Academy of Sciences*, 91(3):913–917, 1994.

[199] H. Coe and M. Michalak. ERp57, a multifunctional endoplasmic reticulum resident oxidoreductase. *International Journal of Biochemistry and Cell Biology*, 42(6):796–799, 2010.

[200] T. Solda, N. Garbi, G. J. Haemmerling, and M. Molinari. Consequences of ERp57 deletion on oxidative folding of obligate and facultative clients of the calnexin cycle. *Journal of Biological Chemistry*, 281(10):6219–6226, 2006.

[201] M. Sousa and A. J. Parodi. The molecular basis for the recognition of misfolded glycoproteins by the UDP-Glc:glycoprotein glucosyltransferase. *The EMBO Journal*, 14(17):4196–203, 1995.

[202] O. Linda and A. Herscovics. Cloning and expression of a specific human alpha 1,2-mannosidase that trims trims Man9GlcNAc2 to Man8GlcNAc2 isomer B during N-glycan biosynthesis. *Glycobiology*, 9(10):1073–1078, 1999.

[203] D. S. Gonzalez, K. Karaveg, A. S. Vandersall-Nairn, A. Lal, and K. W. Moremen. Identification, expression, and characterization of a cDNA encoding human endoplasmic reticulum mannosidase I, the enzyme that catalyzes the first mannose. *Journal of Biological Chemistry*, 274(30):21375–21386, 1999.

[204] S. Olivari, T. Cali, K. E. H. Salo, P. Paganetti, L. W. Ruddock, and M. Molinari. EDEM1 regulates ER-associated degradation by accelerating de-mannosylation of folding-defective polypeptides and by inhibiting their covalent aggregation. *Biochemical and Biophysical Research Communications*, 349(4):1278–1284, 2006.

[205] K. Hirao, Y. Natsuka, T. Tamura, I. Wada, D. Morito, S. Natsuka, P. Romero, B. Sleno, L. O. Tremblay, A. Herscovics, K. Nagata, and N. Hosokawa. EDEM3, a soluble EDEM homolog, enhances glycoprotein endoplasmic reticulum-associated degradation and mannose trimming. *Journal of Biological Chemistry*, 281(14):9650–9658, 2006.

[206] N. Hosokawa, Z. You, L. O. Tremblay, K. Nagata, and A. Herscovics. Stimulation of ERAD of misfolded null Hong Kong alpha1-antitrypsin by Golgi alpha1,2-mannosidases. *Biochemical and Biophysical Research Communications*, 362(3):626–632, 2007.

[207] B. K. Sato, D. Schulz, P. H. Do, and R. Y. Hampton. Misfolded membrane proteins are specifically recognized by the transmembrane domain of the Hrd1p ubiquitin ligase. *Molecular Cell*, 34(2):212–222, 2009.

[208] K. Briant, Y.-H. Koay, Y. Otsuka, and E. Swanton. ERAD of proteins containing aberrant transmembrane domains requires ubiquitylation of cytoplasmic lysine residues. *Journal of Cell Science*, 128(22):4112–4125, 2015.

[209] F. Sun, R. Zhang, X. Gong, X. Geng, P. F. Drain, and R. A. Frizzell. Derlin-1 promotes the efficient degradation of the cystic fibrosis transmembrane conductance regulator (CFTR) and CFTR folding mutants. *Journal of Biological Chemistry*, 281(48):36856–36863, 2006.

[210] W. W. A. Schamel, S. Kuppig, B. Becker, K. Gimborn, H.-P. Hauri, and M. Reth. A high-molecular-weight complex of membrane proteins BAP29/BAP31 is involved in the retention of membrane-bound IgD in the endoplasmic reticulum. *Proceedings of the National Academy of Sciences of the United States of America*, 100(17):9861–9866, 2003.

[211] W. G. Annaert, B. Becker, U. Kistner, M. Reth, and R. Jahn. Export of cellubrevin from the endoplasmic reticulum is controlled by BAP31. *Journal of Cell Biology*, 139(6):1397–1410, 1997.

[212] E. Szczesna-Skorupa and B. Kemper. BAP31 is involved in the retention of cytochrome P450 2C2 in the endoplasmic reticulum. *Journal of Biological Chemistry*, 281(7):4142–4148, 2006.

[213] D. N. Hebert, R. Bernasconi, and M. Molinari. ERAD substrates: Which way out? *Seminars in Cell and Developmental Biology*, 21(5):526–532, 2010.

[214] P. Carvalho, A. M. Stanley, and T. A. Rapoport. Retrotranslocation of a misfolded luminal ER protein by the ubiquitin-ligase hrd1p. *Cell*, 143(4):579–591, 2010.

[215] R. D. Baldridge and T. A. Rapoport. Autoubiquitination of the Hrd1 Ligase Triggers Protein Retrotranslocation in ERAD. *Cell*, 166(2):394–407, 2016.

[216] R. K. Plemper, S. Böhmler, J. Bordallo, T. Sommer, and D. H. Wolf. Mutant analysis links the translocon and BiP to retrograde protein transport for ER degradation. *Nature*, 388(1995):891–895, 1997.

[217] D. C. Scott and R. Schekman. Role of Sec61p in the ER-associated degradation of short-lived transmembrane proteins. *Journal of Cell Biology*, 181(7):1095–1105, 2008.

[218] Y. Ye, Y. Shibata, C. Yun, D. Ron, and T. A. Rapoport. A membrane protein complex mediates retro-translocation from the ER lumen into the cytosol. *Nature*, 429(6994):841–847, 2004.

[219] B. N. Lilley and H. L. Ploegh. A membrane protein required for dislocation of misfolded proteins from the ER. *Nature*, 429(6994):834–840, 2004.

[220] N. Hosokawa, I. Wada, K. Nagasawa, T. Moriyama, K. Okawa, and K. Nagata. Human XTP3-B forms an endoplasmic reticulum quality control scaffold with the HRD1-SEL1L ubiquitin ligase complex and BiP. *Journal of Biological Chemistry*, 283(30):20914–20924, 2008.

[221] R. Bernasconi, T. Pertel, J. Luban, and M. Molinari. A dual task for the Xbp1-responsive OS-9 variants in the mammalian endoplasmic reticulum: Inhibiting secretion of misfolded protein conformers and enhancing their disposal. *Journal of Biological Chemistry*, 283(24):16446–16454, 2008.

[222] J. P. Lu, Y. Wang, D. A. Sliter, M. M. P. Pearce, and R. J. H. Wojcikiewicz. RNF170 protein, an endoplasmic reticulum membrane ubiquitin ligase, mediates inositol 1,4,5-trisphosphate receptor ubiquitination and degradation. *Journal of Biological Chemistry*, 286(27):24426–24433, 2011.

[223] Y. Jo, P. V. Sguigna, and R. A. Debose-Boyd. Membrane-associated ubiquitin ligase complex containing gp78 mediates sterol-accelerated degradation of 3-hydroxy-3-methylglutaryl-coenzyme a reductase. *Journal of Biological Chemistry*, 286(17):15022–15031, 2011.

[224] Y. Ye, H. H. Meyer, and T. a. Rapoport. The AAA ATPase Cdc48/p97 and its partners transport proteins from the ER into the cytosol. *Nature*, 414(6864):652–656, 2001.

[225] E. Rabinovich, A. Kerem, K.-U. Fröhlich, N. Diamant, and S. Bar-Nun. AAA-ATPase p97/Cdc48p, a cytosolic chaperone required for endoplasmic reticulum-associated protein degradation. *Molecular and Cellular Biology*, 22(2):626–34, 2002.

[226] Y. Ye, H. H. Meyer, and T. A. Rapoport. Function of the p97-Ufd1-Npl4 complex in retrotranslocation from the ER to the cytosol: Dual recognition of nonubiquitinated polypeptide segments and polyubiquitin chains. *Journal of Cell Biology*, 162(1):71–84, 2003.

[227] A. Neutzner, M. Neutzner, A. S. Benischke, S. W. Ryu, S. Frank, R. J. Youle, and M. Karbowski. A systematic search for endoplasmic reticulum (ER) membrane-associated RING finger proteins identifies nixin/ZNRF4 as a regulator of calnexin stability and ER homeostasis. *Journal of Biological Chemistry*, 286(10):8633–8643, 2011.

[228] M. Kaneko, I. Iwase, Y. Yamasaki, T. Takai, Y. Wu, S. Kanemoto, K. Matsuhisa, R. Asada, Y. Okuma, T. Watanabe, K. Imaizumi, and Y. Nomura. Genome-wide identification and gene expression profiling of ubiquitin ligases for endoplasmic reticulum protein degradation. *Scientific Reports*, 6:30955, 2016.

[229] M. L. van de Weijer, M. C. Bassik, R. D. Luteijn, C. M. Voorburg, M. A. M. Lohuis, E. Kremmer, R. C. Hoeben, E. M. LeProust, S. Chen, H. Hoelen, M. E. Ressing, W. Patena, J. S. Weissman, M. T. McManus, E. J. H. J. Wiertz, and R. J. Lebbink. A high-coverage shRNA screen identifies TMEM129 as an E3 ligase involved in ER-associated protein degradation. *Nature Communications*, 5(May):3832, 2014.

[230] H. Meyer, M. Bug, and S. Bremer. Emerging functions of the VCP/p97 AAA-ATPase in the ubiquitin system. *Nature Cell Biology*, 14(2):117–23, 2012.

[231] H. H. Meyer, Y. Wang, and G. Warren. Direct binding of ubiquitin conjugates by the mammalian p97 adaptor complexes, p47 and Ufd1-Npl4. *EMBO Journal*, 21(21):5645–5652, 2002.

[232] H. Richly, M. Rape, S. Braun, S. Rumpf, C. Hoege, and S. Jentsch. A series of ubiquitin binding factors connects CDC48/p97 to substrate multiubiquitylation and proteasomal targeting. *Cell*, 120(1):73–84, 2005.

[233] A. Beskow, K. B. Grimberg, L. C. Bott, F. A. Salomons, N. P. Dantuma, and P. Young. A conserved unfoldase activity for the p97 AAA-ATPase in proteasomal degradation. *Journal of Molecular Biology*, 394(4):732–746, 2009.

[234] Q. Wang, Y. Liu, N. Soetandyo, K. Baek, R. Hegde, and Y. Ye. A ubiquitin ligase-associated chaperone holdase maintains polypeptides in soluble states for proteasome degradation. *Molecular Cell*, 42(6):758–770, 2011.

[235] M. Hermansson, K. Hokynar, and P. Somerharju. Mechanisms of glycerophospholipid homeostasis in mammalian cells. *Progress in Lipid Research*, 50(3):240–257, 2011.

[236] F. Gibellini and T. K. Smith. The Kennedy pathway-de novo synthesis of phosphatidylethanolamine and phosphatidylcholine. *IUBMB Life*, 62(6):414–428, 2010.

[237] P. Fagone and S. Jackowski. Membrane phospholipid synthesis and endoplasmic reticulum function. *Journal of Lipid Research*, 50 Suppl:S311–S316, 2009.

[238] D. E. Vance, Z. Li, and R. L. Jacobs. Hepatic phosphatidylethanolamine N-methyltransferase, unexpected roles in animal biochemistry and physiology. *Journal of Biological Chemistry*, 282(46):33237–33241, 2007.

[239] J. E. Vance and R. Steenbergen. Metabolism and functions of phosphatidylserine. *Progress in Lipid Research*, 44(4):207–234, 2005.

[240] S. J. Stone and J. E. Vance. Phosphatidylserine synthase-1 and -2 are localized to mitochondria-associated membranes. *Journal of Biological Chemistry*, 275(44):34534–34540, 2000.

[241] B. Antonsson. Phosphatidylinositol synthase from mammalian tissues, 1997.

[242] Y. J. Kim, M. L. Guzman-Hernandez, and T. Balla. A highly dynamic ER-derived phosphatidylinositol-synthesizing organelle supplies phosphoinositides to cellular membranes. *Developmental Cell*, 21(5):813–824, 2011.

[243] D. Lingwood and K. Simons. Lipid rafts as a membrane-organizing principle. *Science*, 327(5961):46–50, 2010.

[244] V. A. Blaho and T. Hla. Regulation of mammalian physiology, development, and disease by the sphingosine 1-phosphate and lysophosphatidic acid receptors. *Chemical Reviews*, 111(10):6299–6320, 2011.

[245] P. H. Lopez and R. L. Schnaar. Gangliosides in cell recognition and membrane protein regulation. *Current Opinion in Structural Biology*, 19(5):549–557, 2009.

[246] A. H. Futerman and H. Riezman. The ins and outs of sphingolipid synthesis. *Trends in Cell Biology*, 15(6):312–318, 2005.

[247] K. Hanada. Serine palmitoyltransferase, a key enzyme of sphingolipid metabolism. *Biochimica et Biophysica Acta - Molecular and Cell Biology of Lipids*, 1632(1-3):16–30, 2003.

[248] D. K. Breslow. Sphingolipid homeostasis in the endoplasmic reticulum and beyond. *Cold Spring Harbor Perspectives in Biology*, 5(4):a013326, 2013.

[249] A. Jakobsson, R. Westerberg, and A. Jacobsson. Fatty acid elongases in mammals: Their regulation and roles in metabolism. *Progress in Lipid Research*, 45(3):237–249, 2006.

[250] J. T. Hannich, K. Umebayashi, and H. Riezman. Distribution and functions of sterols. *Cold Spring Harbor Laboratory Press*, 3:47–62, 2011.

[251] T. H. Haines. Do sterols reduce proton and sodium leaks through lipid bilayers? *Progress in Lipid Research*, 40(4):299–324, 2001.

[252] R. Emter, A. Heese-Peck, and A. Kralli. ERG6 and PDR5 regulate small lipophilic drug accumulation in yeast cells via distinct mechanisms. *FEBS Letters*, 521(1-3):57–61, 2002.

[253] M. Bramkamp and D. Lopez. Exploring the existence of lipid rafts in bacteria. *Microbiology and Molecular Biology Reviews*, 79(1):81–100, 2015.

[254] T. Li and J. Y. L. Chiang. Bile acids as metabolic regulators. *Current Opinion in Gastroenterology*, 31(2):159–165, 2015.

[255] D. D. Bikle. Vitamin D metabolism, mechanism of action, and clinical applications. *Chemistry and Biology*, 21(3):319–329, 2014.

[256] A. H. Payne and D. B. Hales. Overview of steroidogenic enzymes in the pathway from cholesterol to active steroid hormones. *Endocrine Reviews*, 25(6):947–970, 2004.

[257] P. S. Pannu, S. Allahverdian, and G. A. Francis. Oxysterol generation and liver X receptor-dependent reverse cholesterol transport: Not all roads lead to Rome. *Molecular and Cellular Endocrinology*, 368(1-2):99–107, 2013.

[258] W. D. Nes. Biosynthesis of cholesterol and other sterols. *Chemical Reviews*, 111(10):6423–6451, 2011.

[259] S. L. Sturley. Conservation of eukaryotic sterol homeostasis: New insights from studies in budding yeast. *Biochimica et Biophysica Acta - Molecular and Cell Biology of Lipids*, 1529(1-3):155–163, 2000.

[260] J. a. Tobert. Lovastatin and beyond: the history of the HMG-CoA reductase inhibitors. *Nature reviews. Drug Discovery*, 2(7):517–526, 2003.

[261] L. J. Sharpe, E. C. L. Cook, N. Zelcer, and A. J. Brown. The UPS and downs of cholesterol homeostasis. *Trends in Biochemical Sciences*, 39(11):527–535, 2014.

[262] E. S. Istvan and J. Deisenhofer. The structure of the catalytic portion of human HMG-CoA reductase. *Biochimica et Biophysica Acta - Molecular and Cell Biology of Lipids*, 1529(1-3):9–18, 2000.

[263] L. J. Sharpe and A. J. Brown. Controlling cholesterol synthesis beyond 3-hydroxy-3-methylglutaryl-CoA reductase (HMGCR). *Journal of Biological Chemistry*, 288(26):18707–18715, 2013.

[264] S. Thomas and D. A. Fell. The role of multiple enzyme activation in metabolic flux control. *Advances in Enzyme Regulation*, 38(1):65–85, 1998.

[265] L. Liscum. *Cholesterol biosynthesis*. 2002.

[266] E. S. Radisky and C. D. Poulter. Squalene synthase: steady-state, pre-steady-state, and isotope-trapping studies. *Biochemistry*, 39(7):1748–1760, 2000.

[267] M. Thurnher, G. Gruenbacher, and O. Nussbaumer. Regulation of mevalonate metabolism in cancer and immune cells. *Biochimica et Biophysica Acta - Molecular and Cell Biology of Lipids*, 1831(6):1009–1015, 2013.

[268] N. Xu, N. Shen, X. Wang, S. Jiang, B. Xue, and C. Li. Protein prenylation and human diseases: A balance of protein farnesylation and geranylgeranylation. *Science China Life Sciences*, 58(4):328–335, 2015.

[269] E. M. Paradise, J. Kirby, R. Chan, and J. D. Keasling. Redirection of flux through the FPP branch-point in saccharomyces cerevisiae by down-regulating squalene synthase. *Biotechnology and Bioengineering*, 100(2):371–378, 2008.

[270] L. Henneman, A. G. van Cruchten, W. Kulik, and H. R. Waterham. Inhibition of the isoprenoid biosynthesis pathway; detection of intermediates by UPLCMS/MS. *Biochimica et Biophysica Acta - Molecular and Cell Biology of Lipids*, 1811(4):227–233, 2011.

[271] H. H. Tai and K. Bloch. Squalene epoxidase of rat liver. *Journal of Biological Chemistry*, 247(12):3767–3773, 1972.

[272] T. T. Tchen and K. Bloch. On the conversion of squalene to lanosterol in vitro. *The Journal of Biological Chemistry*, 226:921–930, 1957.

[273] N. Shibata, M. Arita, Y. Misaki, N. Dohmae, K. Takio, T. Ono, K. Inoue, and H. Arai. Supernatant protein factor, which stimulates the conversion of squalene to lanosterol, is

a cytosolic squalene transfer protein and enhances cholesterol biosynthesis. *Proceedings of the National Academy of Sciences of the United States of America*, 98(5):2244–2249, 2001.

[274] J. L. Goldstein and M. S. Brown. Regulation of the mevalonate pathway. *Nature*, 343(6257):425–430, 1990.

[275] M. Wang and P. J. Casey. Protein prenylation: Unique fats make their mark on biology. *Nature Reviews Molecular Cell Biology*, 17(2):110–122, 2016.

[276] S. J. McTaggart. Isoprenylated proteins. *Cellular and Molecular Life Sciences*, 63(3):255–267, 2006.

[277] S. L. Moores, M. D. Schaber, S. D. Mosser, E. Rands, M. B. O'Hara, V. M. Garsky, M. S. Marshall, D. L. Pompliano, and J. B. Gibbs. Sequence dependence of protein isoprenylation. *Journal of Biological Chemistry*, 266(22):14603–14610, 1991.

[278] E. A. Zverina, C. L. Lamphear, E. N. Wright, and C. A. Fierke. Recent advances in protein prenyltransferases: Substrate identification, regulation, and disease interventions. *Current Opinion in Chemical Biology*, 16(5-6):544–552, 2012.

[279] V. L. Boyartchuk, M. N. Ashby, and J. Rine. Modulation of Ras and a-factor function by carboxyl-terminal proteolysis. *Science*, 275(5307):1796–1800, 1997.

[280] C. A. Hrycyna, S. K. Sapperstein, S. Clarke, and S. Michaelis. The Saccharomyces cerevisiae STE14 gene encodes a methyltransferase that mediates C-terminal methylation of a-factor and RAS proteins. *The EMBO Journal*, 1(7):1699–1709, 1991.

[281] J. D. Romano, W. K. Schmidt, and S. Michaelis. The Saccharomyces cerevisiae prenylcysteine carboxyl methyltransferase Ste14p is in the endoplasmic reticulum membrane. *Molecular Biology of the Cell*, 9(8):2231–2247, 1998.

[282] A. M. Winter-Vann and P. J. Casey. Post-prenylation-processing enzymes as new targets in oncogenesis. *Nature Reviews. Cancer*, 5(5):405–412, 2005.

[283] M. S. Brown and J. L. Goldstein. Multivalent feedback regulation of HMG CoA reductase, a control mechanism coordinating isoprenoid synthesis and cell growth. *Journal of Lipid Research*, 21(44):505–517, 1980.

[284] P. Tricarico, S. Crovella, and F. Celsi. Mevalonate pathway blockade, mitochondrial dysfunction and autophagy: A possible link. *International Journal of Molecular Sciences*, 16(7):16067–16084, 2015.

[285] N. Sever, B.-L. Song, D. Yabe, J. L. Goldstein, M. S. Brown, and R. A. DeBose-Boyd. Insig-dependent ubiquitination and degradation of mammalian 3-hydroxy-3-methylglutaryl-CoA reductase stimulated by sterols and geranylgeraniol. *Journal of Biological Chemistry*, 278(52):52479–52490, 2003.

[286] G. S. Leichner, R. Avner, D. Harats, and J. Roitelman. Metabolically regulated endoplasmic reticulum-associated degradation of 3-hydroxy-3-methylglutaryl-CoA reductase: evidence for requirement of a geranylgeranylated protein. *Journal of Biological Chemistry*, 286(37):32150–32161, 2011.

[287] M. M. Schumacher, R. Elsabrouty, J. Seemann, Y. Jo, and R. A. DeBose-Boyd. The prenyltransferase UBIAD1 is the target of geranylgeraniol in degradation of HMG CoA reductase. *eLife*, page 4:e05560, 2015.

[288] P. Tontonoz. Transcriptional and posttranscriptional control of cholesterol homeostasis by liver X receptors. *Cold Spring Harbor Symposia on Quantitative Biology*, 76:129–137, 2011.

[289] J. D. Horton, J. L. Goldstein, and M. S. Brown. SREBPs: Activators of the complete program of cholesterol and fatty acid synthesis in the liver. *Journal of Clinical Investigation*, 109(9):1125–1131, 2002.

[290] J. L. Goldstein, R. A. DeBose-Boyd, and M. S. Brown. Protein sensors for membrane sterols. *Cell*, 124(1):35–36, 2006.

[291] M. S. Brown and J. L. Goldstein. The SREBP pathway: Regulation of cholesterol metabolism by proteolysis of a membrane-bound transcription factor. *Cell*, 89(3):331–340, 1997.

[292] J. T. Pai, O. Guryev, M. S. Brown, and J. L. Goldstein. Differential stimulation of cholesterol and unsaturated fatty acid biosynthesis in cells expressing individual nuclear sterol regulatory element-binding proteins. *Journal of Biological Chemistry*, 273(40):26138–26148, 1998.

[293] J. R. Smith, T. F. Osborne, J. L. Goldstein, and M. S. Brown. Identification of nucleotides responsible for enhancer avtivity of sterol regulatory element in low density lipoportein receptor gene. *The Journal of Biological Chemistry*, 265(4):2306–2310, 1990.

[294] M. S. Brown and J. L. Goldstein. A proteolytic pathway that controls the cholesterol content of membranes, cells, and blood. *Proceedings of the National Academy of Sciences of the United States of America*, 96(20):11041–11048, 1999.

[295] A. Radhakrishnan, J. L. Goldstein, J. G. Mcdonald, and S. Michael. Switch-like control of SREBP-2 transport triggered by small changes in ER cholesterol: a delicate balance. *Cell Metabolism*, 8(6):512–521, 2008.

[296] J. Sakai, A. Nohturfft, D. Cheng, K. Ho, M. S. Brown, L. Joseph, Y. K. Ho, and J. L. Goldstein. Identification of complexes between the COOH-terminal domains of sterol regulatory element-binding proteins (SREBPs) and SREBP cleavage-activating protein. *The Journal of Biological Chemistry*, 272(32):20213–20221, 1997.

[297] A. J. Brown, L. Sun, J. D. Feramisco, M. S. Brown, and J. L. Goldstein. Cholesterol addition to ER membranes alters conformation of SCAP, the SREBP escort protein that regulates cholesterol metabolism. *Molecular Cell*, 10(2):237–245, 2002.

[298] L. P. Sun, L. Li, J. L. Goldstein, and M. S. Brown. Insig required for sterol-mediated inhibition of Scap/SREBP binding to COPII proteins in vitro. *Journal of Biological Chemistry*, 280(28):26483–26490, 2005.

[299] B. A. Janowski, P. J. Willy, T. R. Devi, J. R. Falck, and D. J. Mangelsdorf. An oxysterol signalling pathway mediated by the nuclear receptor LXR alpha, 1996.

[300] J. M. Lehmann, S. A. Kliewer, L. B. Moore, T. A. Smith-Oliver, B. B. Oliver, J. L. Su, S. S. Sundseth, D. a. Winegar, D. E. Blanchard, T. A. Spencer, and T. M. Willson. Activation of the nuclear receptor LXR by oxysterols defines a new hormone response pathway. *The Journal of Biological Chemistry*, 272(6):3137–3140, 1997.

[301] N. Zelcer, C. Hong, R. Boyadjian, and P. Tontonoz. LXR regulates cholesterol uptake through Idol-dependent ubiquitination of the LDL receptor. *Science*, 325(5936):100–104, 2009.

[302] P. Costet, Y. Luo, N. Wang, and A. R. Tall. Sterol-dependent transactivation of the ABC1 promoter by LXR/RXR. *Journal of Biological Chemistry*, 275(36):28240–28245, 2000.

[303] J. J. Repa, S. D. Turley, J. A. Lobaccaro, J. Medina, L. Li, K. Lustig, B. Shan, R. A. Heyman, J. M. Dietschy, and D. J. Mangelsdorf. Regulation of absorption and ABC1-mediated efflux of cholesterol by RXR heterodimers. *Science*, 289(5484):1524–1529, 2000.

[304] A. Venkateswaran, J. J. Repa, J.-m. A. Lobaccaro, A. Bronson, D. J. Mangelsdorf, and P. A. Edwards. Human white/murine ABC8 mRNA levels are highly induced in lipid-loaded macrophages. A transcriptional role for specific oxysterols. *The Journal of Biological Chemistry*, 275(19):14700–14707, 2000.

[305] O. V. Baboshina, R. Crinelli, T. J. Siepmann, and A. L. Haas. N-end Rule Specificity within the Ubiquitin/Proteasome Pathway Is Not an Affinity Effect. *Journal of Biological Chemistry*, 276(42):39438–39447, 2001.

[306] S. L. Sabol, H. B. Brewer, and S. Santamarina-Fojo. The human ABCG1 gene: identification of LXR response elements that modulate expression in macrophages and liver. *Journal of Lipid Research*, 46(10):2151–2167, 2005.

[307] Y. Gong, J. N. Lee, P. C. W. Lee, J. L. Goldstein, M. S. Brown, and J. Ye. Sterol-regulated ubiquitination and degradation of Insig-1 creates a convergent mechanism for feedback control of cholesterol synthesis and uptake. *Cell Metabolism*, 3(1):15–24, 2006.

[308] N. L. Joon, B. Song, R. A. DeBose-Boyd, and J. Ye. Sterol-regulated degradation of insig-1 mediated by the membrane-bound ubiquitin ligase gp78. *Journal of Biological Chemistry*, 281(51):39308–39315, 2006.

[309] Y. Jo, P. C. W. Lee, P. V. Sguigna, and R. A. DeBose-Boyd. Sterol-induced degradation of HMG CoA reductase depends on interplay of two Insigs and two ubiquitin ligases, gp78 and Trc8. *Proceedings of the National Academy of Sciences*, 108(51):20503–20508, 2011.

[310] A. Luong. *Identification of three novel SREBP-activated target genes: acetyl CoA synthetase, 3-β-hydroxysterol dehydrogenase, and CL-6/INSIG1. (PhD Dissertation, University of Texas Southwestern Medical Center at Dallas).* PhD thesis, 2000.

[311] T. Punga, M. T. Bengoechea-Alonso, and J. Ericsson. Phosphorylation and ubiquitination of the transcription factor sterol regulatory element-binding protein-1 in response to DNA binding. *Journal of Biological Chemistry*, 281(35):25278–25286, 2006.

[312] Y. Hirano, M. Yoshida, M. Shimizu, and R. Sato. Direct demonstration of rapid degradation of nuclear sterol regulatory element-binding proteins by the ubiquitin-proteasome pathway. *Journal of Biological Chemistry*, 276(39):36431–36437, 2001.

[313] K. T. Chun, N. S. Bar, and R. D. Simoni. The regulated degradation of 3-hydroxy-3-methylglutaryl CoA reductase requires a short lived protein and occurs in the endoplasmic reticulum. *The Journal of Biological Chemistry*, 265(35):22004–22010, 1990.

[314] T. E. Meigs and R. D. Simoni. Regulated degradation of 3-hydroxy-3-methylglutaryl-coenzyme A reductase in permeabilized cells. *Journal of Biological Chemistry*, 267(19):13547–13552, 1992.

[315] R. Y. Hampton and J. Rine. Regulated degradation of HMG-CoA reductase, an integral membrane protein of the endoplasmic reticulum, in yeast. *Journal of Cell Biology*, 125(2):299–312, 1994.

[316] B. L. Song, N. Sever, and R. A. DeBose-Boyd. Gp78, a membrane-anchored ubiquitin ligase, associates with Insig-1 and couples sterol-regulated ubiquitination to degradation of HMG CoA reductase. *Molecular Cell*, 19(6):829–840, 2005.

[317] Y. Jo, P. C. W. Lee, P. V. Sguigna, and R. A. DeBose-Boyd. Sterol-induced degradation of HMG CoA reductase depends on interplay of two Insigs and two ubiquitin ligases, gp78 and Trc8. *Proceedings of the National Academy of Sciences*, 108(51):20503–20508, 2011.

[318] Y. C. Tsai, G. S. Leichner, M. M. P. Pearce, G. L. Wilson, R. J. H. Wojcikiewicz, J. Roitelman, and A. M. Weissman. Differential regulation of HMG-CoA reductase and Insig-1 by enzymes of the ubiquitin-proteasome system. *Molecular Biology of the Cell*, 23(23):4484–4494, 2012.

[319] N. Zelcer, L. J. Sharpe, A. Loregger, I. Kristiana, E. C. L. Cook, L. Phan, J. Stevenson, and A. J. Brown. The E3 ubiquitin ligase MARCH6 degrades squalene monooxygenase and affects 3-hydroxy-3-methyl-glutaryl coenzyme A reductase and the cholesterol synthesis pathway. *Molecular and Cellular Biology*, 34(7):1262–1270, 2014.

[320] Y. Lange, D. S. Ory, J. Ye, M. H. Lanier, F. F. Hsu, and T. L. Steck. Effectors of rapid homeostatic responses of endoplasmic reticulum cholesterol and 3-hydroxy-3-methylglutaryl-CoA reductase. *Journal of Biological Chemistry*, 283(3):1445–1455, 2008.

[321] V. Howe, N. K. Chua, J. Stevenson, and A. J. Brown. The regulatory domain of squalene monooxygenase contains a re-entrant loop and senses cholesterol via a conformational change. *Journal of Biological Chemistry*, 290(46):27533–27544, 2015.

[322] M. Dieckmann, M. F. Dietrich, and J. Herz. Lipoprotein receptors-an evolutionarily ancient multifunctional receptor family. *Biological Chemistry*, 391(11):1341–1363, 2010.

[323] C. J. Packard and J. Shepherd. Lipoprotein heterogeneity and apolipoprotein B metabolism. *Arteriosclerosis, Thrombosis, and Vascular Biology*, 17(12):3542–3556, 1997.

[324] I. Ramasamy. Recent advances in physiological lipoprotein metabolism. *Clinical Chemistry and Laboratory Medicine*, 52(12):1695–1727, 2014.

[325] G. W. Go and A. Mani. Low-density lipoprotein receptor (LDLR) family orchestrates cholesterol homeostasis. *Yale Journal of Biology and Medicine*, 85(1):19–28, 2012.

[326] P. Durrington. Dyslipidaemia. *Lancet*, 362(9385):717–731, 2003.

[327] M. S. Brown and J. L. Goldstein. Familial hypercholesterolemia: defective binding of lipoproteins to cultured fibroblasts associated with impaired regulation of 3-hydroxy-3-methylglutaryl coenzyme A reductase activity. *Proceedings of the National Academy of Sciences of the United States of America*, 71(3):788–792, 1974.

[328] J. L. Goldstein and M. S. Brown. Binding and degradation of low density lipoproteins by cultured human fibroblasts. *The Journal of Biological Chemistry*, 249(16):5153 – 5162, 1974.

[329] J. G. Wideman. The ubiquitous and ancient ER membrane protein complex (EMC): tether or not? *F1000 Research*, 4(624):doi:10.12688/f1000research.6944.2, 2015.

[330] G.-W. Li, D. Burkhardt, C. Gross, and J. S. Weissman. Quantifying absolute protein synthesis rates reveals principles underlying allocation of cellular resources. *Cell*, 157(3):624–635, apr 2014.

[331] S. Lahiri, J. T. Chao, S. Tavassoli, A. K. O. Wong, V. Choudhary, B. P. Young, C. J. R. Loewen, and W. A. Prinz. A conserved endoplasmic reticulum membrane protein complex (EMC) facilitates phospholipid transfer from the ER to mitochondria. *PLoS Biology*, 12(10):e1001969, oct 2014.

[332] M. Y. Hein, N. C. Hubner, I. Poser, J. Cox, N. Nagaraj, Y. Toyoda, I. A. Gak, I. Weisswange, J. Mansfeld, F. Buchholz, A. A. Hyman, and M. Mann. A human interactome in three quantitative dimensions organized by stoichiometries and abundances. *Cell*, 163(3):712–723, 2015.

[333] A. Goytain and G. A. Quamme. Identification and characterization of a novel family of membrane magnesium transporters, MMgT1 and MMgT2. *American Journal of Physiology. Cell Physiology*, 294(2):C495–C502, feb 2008.

[334] G. Ring, C. M. Khoury, A. J. Solar, Z. Yang, C. A. Mandato, and M. T. Greenwood. Transmembrane protein 85 from both human (TMEM85) and yeast (YGL231c) inhibit hydrogen peroxide mediated cell death in yeast. 2008.

[335] Y. Li, Y. Zhao, J. Hu, J. Xiao, L. Qu, Z. Wang, D. Ma, and Y. Chen. A novel ER-localized transmembrane protein, EMC6, interacts with RAB5A and regulates cell autophagy. *Autophagy*, 9(2):150–163, feb 2013.

[336] M. Richard, T. Boulin, V. J. P. Robert, J. E. Richmond, and J.-L. Bessereau. Biosynthesis of ionotropic acetylcholine receptors requires the evolutionarily conserved ER membrane complex. *Proceedings of the National Academy of Sciences of the United States of America*, 110(11):E1055–E1063, mar 2013.

[337] J. Smirle, C. E. Au, M. Jain, K. Dejgaard, T. Nilsson, and J. Bergeron. Cell biology of the endoplasmic reticulum and the Golgi apparatus through proteomics. *Cold Spring Harbor Perspectives in Biology*, 5(1):a015073, 2013.

[338] K. S. Junes-Gill, T. K. Gallaher, Z. Gluzman-Poltorak, J. D. Miller, C. J. Wheeler, X. Fan, and L. A. Basile. hHSS1: A novel secreted factor and suppressor of glioma growth located at chromosome 19q13.33. *Journal of Neurooncology*, 102(2):197–211, 2011.

[339] S. Ninagawa, T. Okada, Y. Sumitomo, S. Horimoto, T. Sugimoto, T. Ishikawa, S. Takeda, T. Yamamoto, T. Suzuki, Y. Kamiya, K. Kato, and K. Mori. Forcible destruction of severely misfolded mammalian glycoproteins by the non-glycoprotein ERAD pathway. *The Journal of Cell Biology*, 211(4):775–784, 2015.

[340] K. D. Tsirigos, C. Peters, N. Shu, L. Kaell, and A. Elofsson. The TOPCONS web server for consensus prediction of membrane protein topology and signal peptides. *Nucleic Acids Research*, 43(W1):W401–W407, 2015.

[341] R. Chen, X. Jiang, D. Sun, G. Han, F. Wang, M. Ye, L. Wang, and H. Zou. Glycoproteomics analysis of human liver tissue by combination of multiple enzyme digestion and hydrazide chemistry. *Journal of Proteome Research*, 8(2):651–661, 2009.

[342] K. O. Kopec and A. N. Lupas. β-Propeller blades as ancestral peptides in protein evolution. *PloS one*, 8(10):e77074, 2013.

[343] M. Ghosh, C. Anthony, K. Harlos, M. G. Goodwin, and C. Blake. The refined structure of the quinoprotein methanol dehydrogenase from Methylobacterium extorquens at 1.94 A. *Structure*, 3(2):177–187, 1995.

[344] R. S. Sikorski, M. S. Boguski, M. Goebl, and P. Hieter. A repeating amino acid motif in CDC23 defines a family of proteins and a new relationship among genes required for mitosis and RNA synthesis. *Cell*, 60(2):307–317, 1990.

[345] M. Goebl and M. Yanagida. The TPR snap helix: a novel protein repeat motif from mitosis to transcription. *Trends in Biochemical Sciences*, 16:173–177, 1991.

[346] A. K. Das, P. T. W. Cohen, and D. Barford. The structure of the tetratricopeptide repeats of protein phosphatase 5: Implications for TPR-mediated protein-protein interactions. *EMBO Journal*, 17(5):1192–1199, 1998.

[347] G. L. Blatch and M. Laessle. The tetratricopeptide repeat: A structural motif mediating protein-protein interactions. *BioEssays*, 21(11):932–939, 1999.

[348] J. R. Lamb, S. Tugendreich, and P. Hieter. Tetratrico peptide repeat interactions: to TPR or not to TPR? *Trends in Biochemical Sciences*, 20(7):257–259, 1995.

[349] R. D. Finn, P. Coggill, R. Y. Eberhardt, S. R. Eddy, J. Mistry, A. L. Mitchell, S. C. Potter, M. Punta, M. Qureshi, A. Sangrador-Vegas, G. A. Salazar, J. Tate, and A. Bateman. The Pfam protein families database: towards a more sustainable future. *Nucleic Acids Research*, 44(D1):D279–D285, 2015.

[350] M. T. Borowska, P. K. Dominik, S. A. Anghel, A. A. Kossiakoff, and R. J. Keenan. A YidC-like protein in the archaeal plasma membrane. *Structure*, 23(9):1715–1724, 2015.

[351] M. J. Saller, Z. C. Wu, J. De Keyzer, and A. J. M. Driessen. The YidC/Oxa1/Alb3 protein family: Common principles and distinct features. *Biological Chemistry*, 393(11):1279–1290, 2012.

[352] F. Sievers, A. Wilm, D. Dineen, T. J. Gibson, K. Karplus, W. Li, R. Lopez, H. McWilliam, M. Remmert, J. Söding, J. D. Thompson, and D. G. Higgins. Fast, scalable generation of high-quality protein multiple sequence alignments using Clustal Omega. *Molecular Systems Biology*, 7(1):539, 2011.

[353] M. Mitra, H. Kirst, D. Dewez, and A. Melis. Modulation of the light-harvesting chlorophyll antenna size in Chlamydomonas reinhardtii by TLA1 gene over-expression and RNA interference. *Philosophical Transactions of the Royal Society B*, 367(1608):3430–3443, 2012.

[354] T. P. J. Dunkley, S. Hester, I. P. Shadforth, J. Runions, T. Weimar, S. L. Hanton, J. L. Griffin, C. Bessant, F. Brandizzi, C. Hawes, R. B. Watson, P. Dupree, and K. S. Lilley. Mapping the Arabidopsis organelle proteome. *Proceedings of the National Academy of Sciences of the United States of America*, 103(17):6518–6523, 2006.

[355] B. Kuhlman, G. Dantas, G. C. Ireton, G. Varani, B. L. Stoddard, and D. Baker. Design of a novel globular Protein fold with atomic-level accuracy. *Science*, 302(2003):1364–1368, 2003.

[356] M. R. Hoja, C. Wahlestedt, and C. Höög. A visual intracellular classification strategy for uncharacterized human proteins. *Experimental Cell Research*, 259(1):239–246, aug 2000.

[357] T. Satoh, A. Ohba, Z. Liu, T. Inagaki, and A. K. Satoh. dPob/EMC is essential for biosynthesis of rhodopsin and other multi-pass membrane proteins in Drosophila photoreceptors. *eLife*, 4:e06306, 2015.

[358] M. R. Taylor, S. Kikkawa, A. Diez-Juan, V. Ramamurthy, K. Kawakami, P. Carmeliet, and S. E. Brockerhoff. The zebrafish pob gene encodes a novel protein required for survival of red cone photoreceptor cells. *Genetics*, 170(1):263–273, 2005.

[359] M. Dreger, L. Bengtsson, T. Schöneberg, H. Otto, and F. Hucho. Nuclear envelope proteomics: novel integral membrane proteins of the inner nuclear membrane. *Proceedings of the National Academy of Sciences of the United States of America*, 98(21):11943–11948, 2001.

[360] A. Ruggiano, O. Foresti, and P. Carvalho. ER-associated degradation: Protein quality control and beyond. *Journal of Cell Biology*, 204(6):869–879, 2014.

[361] H. Kadowaki, A. Nagai, T. Maruyama, Y. Takami, P. Satrimafitrah, H. Kato, A. Honda, T. Hatta, T. Natsume, T. Sato, H. Kai, H. Ichijo, and H. Nishitoh. Pre-emptive quality control protects the ER from protein overload via the proximity of ERAD components and SRP. *Cell Reports*, 13(5):944–956, 2015.

[362] R. Friedlander, E. Jarosch, J. Urban, C. Volkwein, and T. Sommer. A regulatory link between ER-associated protein degradation and the unfolded-protein response. *Nature Cell Biology*, 2(7):379–384, 2000.

[363] K. J. Travers, C. K. Patil, L. Wodicka, D. J. Lockhart, J. S. Weissman, and P. Walter. Functional and genomic analyses reveal an essential coordination between the unfolded protein response and ER-associated degradation. *Cell*, 101(3):249–258, 2000.

[364] S. Raj, K. Krishnan, D. S. Askew, O. Helynck, P. Suzanne, A. Lesnard, S. Rault, U. Zeidler, C. D'Enfert, J.-P. Latgé, H. Munier-Lehmann, and C. Saveanu. The toxicity of a novel antifungal compound is modulated by endoplasmic reticulum-associated protein degradation components. *Antimicrobial Agents and Chemotherapy*, 60(3):1438–1449, 2015.

[365] D. Swennen, C. Henry, and J. M. Beckerich. Folding proteome of yarrowia lipolytica targeting with uracil permease mutants. *Journal of Proteome Research*, 9(12):6169–6179, 2010.

[366] H. Ma, Y. Dang, Y. Wu, G. Jia, E. Anaya, J. Zhang, S. Abraham, J.-G. Choi, G. Shi, L. Qi, N. Manjunath, and H. Wu. A CRISPR-based screen identifies genes essential for West-Nile-virus-induced cell death. *Cell Reports*, 12(4):673–683, 2015.

[367] M. A. Brinton. Replication cycle and molecular biology of the west nile virus. *Viruses*, 6(1):13–53, 2013.

[368] G. R. Medigeshi, A. M. Lancaster, A. J. Hirsch, T. Briese, W. I. Lipkin, V. Defilippis, K. Früh, P. W. Mason, J. Nikolich-Zugich, and J. A. Nelson. West Nile virus infection activates the unfolded protein response, leading to CHOP induction and apoptosis. *Journal of Virology*, 81(20):10849–10860, 2007.

[369] R. J. Louie, J. Guo, J. W. Rodgers, R. White, N. Shah, S. Pagant, P. Kim, M. Livstone, K. Dolinski, B. A. McKinney, J. Hong, E. J. Sorscher, J. Bryan, E. A. Miller, and J. L. Hartman. A yeast phenomic model for the gene interaction network modulating CFTR-F508 protein biogenesis. *Genome Medicine*, 4(12):103, 2012.

[370] A. Krogh, B. Larsson, G. von Heijne, and E. L. Sonnhammer. Predicting transmembrane protein topology with a hidden Markov model: Application to complete genomes. *Journal of Molecular Biology*, 305:567–580, 2001.

[371] A. Nestler, G. Sponder, K. Rutschmann, L. Mastrototaro, C. Weise, J. Vormann, M. Schweigel-Röntgen, and M. Kolisek. Nature of SLC41A1 complexes: report on the split-ubiquitin yeast two hybrid assay. *Magnesium Research*, 26(2):56–66, jan 2013.

[372] A. Janer, J. Prudent, V. Paupe, S. Fahiminiya, J. Majewski, N. Sgarioto, C. D. Rosiers, A. Forest, Z.-y. Lin, A.-c. Gingras, G. Mitchell, H. M. Mcbride, and E. A. Shoubridge. SLC 25 A 46 is required for mitochondrial lipid homeostasis and cristae maintenance and is responsible for Leigh syndrome. *EMBO Molecular Medicine*, 8(9):1019–1038, 2016.

[373] S. E. Brockerhoff, J. B. Hurley, G. A. Niemi, and J. E. Dowling. A new form of inherited red-blindness identified in zebrafish. *The Journal of Neuroscience*, 17(11):4236–4242, 1997.

[374] P. A. Hargrave. Rhodopsin structure, function, and topography: The Friedenwald lecture. *Investigative Ophthalmology and Visual Science*, 42(1):3–9, 2001.

[375] X. Wang, J. Venable, P. LaPointe, D. M. Hutt, A. V. Koulov, J. Coppinger, C. Gurkan, W. Kellner, J. Matteson, H. Plutner, J. R. Riordan, J. W. Kelly, J. R. Yates, and W. E. Balch. Hsp90 cochaperone Aha1 downregulation rescues misfolding of CFTR in cystic fibrosis. *Cell*, 127(4):803–815, nov 2006.

[376] R. R. Nayak, M. Kearns, R. S. Spielman, and V. G. Cheung. Coexpression network based on natural variation in human gene expression reveals gene interactions and functions. *Genome Research*, 19(11):1953–1962, nov 2009.

[377] P. W. Bircham, D. R. Maass, C. A. Roberts, P. Y. Kiew, Y. S. Low, M. Yegambaram, J. Matthews, C. A. Jack, and P. H. Atkinson. Secretory pathway genes assessed by high-throughput microscopy and synthetic genetic array analysis. *Molecular BioSystems*, 7(9):2589–2598, sep 2011.

[378] S. Willingham, T. F. Outeiro, M. J. DeVit, S. L. Lindquist, and P. J. Muchowski. Yeast genes that enhance the toxicity of a mutant huntingtin fragment or alpha-synuclein. *Science*, 302(5651):1769–1772, 2003.

[379] X. Shen, S. Kan, J. Hu, M. Li, G. Lu, M. Zhang, S. Zhang, Y. Hou, Y. Chen, and Y. Bai. EMC6/TMEM93 suppresses glioblastoma proliferation by modulating autophagy. *Cell Death and Disease*, 7(1):e2043, 2016.

[380] M. N. Krishnan, A. Ng, B. Sukumaran, F. D. Gilfoy, P. D. Uchil, H. Sultana, A. L. Brass, R. Adametz, M. Tsui, F. Qian, R. R. Montgomery, S. Lev, P. W. Mason, R. A. Koski, S. J. Elledge, R. J. Xavier, H. Agaisse, and E. Fikrig. RNA interference screen for human genes associated with West Nile virus infection. *Nature*, 455(7210):242–245, 2008.

[381] C. Le Sommer, N. J. Barrows, S. S. Bradrick, J. L. Pearson, and M. A. Garcia-Blanco. G protein-coupled receptor kinase 2 promotes flaviviridae entry and replication. *PLoS Neglected Tropical Diseases*, 6(9):e1820, 2012.

[382] M. Saeed, R. Suzuki, N. Watanabe, T. Masaki, M. Tomonaga, A. Muhammad, T. Kato, Y. Matsuura, H. Watanabe, T. Wakita, and T. Suzuki. Role of the Endoplasmic Reticulum-associated Degradation (ERAD) pathway in degradation of hepatitis C virus envelope proteins and production of virus particles. *Journal of Biological Chemistry*, 286(43):37264–37273, 2011.

[383] G. Savidis, W. M. Mcdougall, P. Meraner, J. M. Perreira, J. M. Portmann, G. Trincucci, S. P. John, A. M. Aker, N. Renzette, D. R. Robbins, Z. Guo, S. Green, T. F. Kowalik, and A. L. Brass. Identification of Zika virus and dengue Virus dependency factors using functional genomics. *Cell Reports*, 16(1):232–246, 2016.

[384] K. S. Junes-Gill, C. E. Lawrence, C. J. Wheeler, R. Cordner, T. G. Gill, V. Mar, L. Shiri, and L. a. Basile. Human hematopoietic signal peptide-containing secreted 1 (hHSS1) modulates genes and pathways in glioma: implications for the regulation of tumorigenicity and angiogenesis. *BMC Cancer*, 14(1):920, 2014.

[385] T. Harel, G. Yesil, Y. Bayram, Z. Coban-Akdemir, W.-L. Charng, E. Karaca, A. Al Asmari, M. K. Eldomery, J. V. Hunter, S. N. Jhangiani, J. A. Rosenfeld, D. Pehlivan, A. W. El-Hattab, M. A. Saleh, C. A. LeDuc, D. Muzny, E. Boerwinkle, R. A. Gibbs, W. K. Chung, Y. Yang, J. W. Belmont, and J. R. Lupski. Monoallelic and biallelic variants in EMC1 identified in individuals with global developmental delay, hypotonia, scoliosis, and cerebellar atrophy. *The American Journal of Human Genetics*, 98(3):562–570, 2016.

[386] L. Abu-Safieh, M. Alrashed, S. Anazi, H. Alkuraya, A. O. Khan, M. Al-Owain, J. Al-Zahrani, L. Al-Abdi, M. Hashem, S. Al-Tarimi, M.-A. Sebai, A. Shamia, M. D. Ray-Zack, M. Nassan, Z. N. Al-Hassnan, Z. Rahbeeni, S. Waheeb, A. Alkharashi, E. Abboud, S. A. F. Al-Hazzaa, and F. S. Alkuraya. Autozygome-guided exome sequencing in retinal dystrophy patients reveals pathogenetic mutations and novel candidate disease genes. *Genome Research*, 23(2):236–247, feb 2013.

[387] M. Uhlen, B. M. Hallstro m, C. Lindskog, A. Mardinoglu, F. Ponten, and J. Nielsen. Transcriptomics resources of human tissues and organs. *Molecular Systems Biology*, 12(4):862–862, 2016.

[388] Z. C. Gu and C. Enenkel. Proteasome assembly. *Cellular and Molecular Life Sciences*, 71(24):4729–4745, 2014.

[389] F. Fontanesi, I. C. Soto, D. Horn, and A. Barrientos. Assembly of mitochondrial cytochrome c-oxidase, a complicated and highly regulated cellular process. *American Journal of Physiology. Cell Physiology.*, 291(6):C1129–C1147, 2006.

[390] M. Gamerdinger, S. Carra, and C. Behl. Emerging roles of molecular chaperones and co-chaperones in selective autophagy: focus on BAG proteins. *Journal of Molecular Medicine*, 89(12):1175–82, dec 2011.

[391] S. Barth, D. Glick, and K. F. Macleod. Autophagy: Assays and artifacts. *Journal of Pathology*, 221(2):117–124, 2010.

[392] M. Schröder and R. J. Kaufman. The mammalian unfolded protein response. *Annual review of biochemistry*, 74:739–89, jan 2005.

[393] D. Ron and P. Walter. Signal integration in the endoplasmic reticulum unfolded protein response. *Nature reviews. Molecular cell biology*, 8(7):519–29, jul 2007.

[394] N. Borgese, M. Francolini, and E. Snapp. Endoplasmic reticulum architecture: structures in flux. *Current Opinion in Cell Biology*, 18(4):358–364, 2006.

[395] A. R. English and G. K. Voeltz. Endoplasmic reticulum structure and interconnections with other organelles. *Cold Spring Harbor Perspectives in Biology*, 5(4):a013227, 2013.

[396] A. G. Manford, C. J. Stefan, H. L. Yuan, J. A. Macgurn, and S. D. Emr. ER-to-plasma membrane tethering proteins regulate cell signaling and ER morphology. *Developmental Cell*, 23(6):1129–1140, dec 2012.

[397] E. Vance. Phospholipid synthesis in a membrane fraction associated with mitochondria. *Journal of Biological Chemistry*, 265(13):7248–7257, 1990.

[398] S. Fang, M. Ferrone, C. Yang, J. P. Jensen, S. Tiwari, and A. M. Weissman. The tumor autocrine motility factor receptor, gp78, is a ubiquitin protein ligase implicated in degradation from the endoplasmic reticulum. *Proceedings of the National Academy of Sciences of the United States of America*, 98(25):14422–14427, 2001.

[399] M. Mehnert, T. Sommer, and E. Jarosch. ERAD ubiquitin ligases: Multifunctional tools for protein quality control and waste disposal in the endoplasmic reticulum. *Bioessays*, 32(10):905–913, 2010.

[400] B. A. Macher and T.-Y. Yen. Proteins at membrane surfaces-a review of approaches. *Molecular bioSystems*, 3(10):705–713, 2007.

[401] D. Josic and J. G. Clifton. Mammalian plasma membrane proteomics. *Proteomics*, 7(16):3010–3029, 2007.

[402] C. G. Gahmberg and M. Tolvanen. Why mammalian cell surface proteins are glycoproteins. *Trends in biochemical sciences*, 21(8):308–11, 1996.

[403] A. Varki. Glycan-based interactions involving vertebrate sialic-acid-recognizing proteins. *Nature*, 446(7139):1023–9, 2007.

[404] Y. Zeng, T. N. C. Ramya, A. Dirksen, P. E. Dawson, and J. C. Paulson. High-efficiency labeling of sialylated glycoproteins on living cells. *Nature methods*, 6(3):207–9, mar 2009.

[405] W. Cao, J. Cao, J. Huang, L. Zhang, J. Yao, H. Xu, and P. Yang. Enhanced N-glycosylation site exploitation of sialoglycopeptides by peptide IPG-IEF assisted TiO2 chromatography. *Glycoconjugate Journal*, 29(5-6):433–443, 2012.

[406] T. N. C. Ramya, E. Weerapana, B. F. Cravatt, and J. C. Paulson. Glycoproteomics enabled by tagging sialic acid- or galactose-terminated glycans. *Glycobiology*, 23(2):211–21, feb 2013.

[407] R. L. Gundry, K. Raginski, Y. Tarasova, I. Tchernyshyov, D. Bausch-Fluck, S. T. Elliott, K. R. Boheler, J. E. Van Eyk, and B. Wollscheid. The mouse C2C12 myoblast cell surface N-linked glycoproteome: identification, glycosite occupancy, and membrane orientation. *Molecular & cellular proteomics : MCP*, 8(11):2555–69, nov 2009.

[408] R. Schiess, L. N. Mueller, A. Schmidt, M. Mueller, B. Wollscheid, and R. Aebersold. Analysis of cell surface proteome changes via label-free, quantitative mass spectrometry. *Molecular & cellular proteomics : MCP*, 8(4):624–38, apr 2009.

[409] M. Heller, M. Von der Ohe, R. Kleene, M. H. Mohajeri, and M. Schachner. The immunoglobulin-superfamily molecule basigin is a binding protein for oligomannosidic carbohydrates: An anti-idiotypic approach. *Journal of Neurochemistry*, 84(3):557–565, 2003.

[410] T. Muramatsu and T. Miyauchi. Basigin (CD147): a multifunctional transmembrane protein involved in reproduction, neural function, inflammation and tumor invasion. *Histology and histopathology*, 18(3):981–7, jul 2003.

[411] J. M. Fadool and P. J. Linser. Differential glycosylation of the 5A11/HT7 antigen by neural retina and epithelial tissues in the chicken. *Journal of neurochemistry*, 60(4):1354–64, 1993.

[412] W. Tang, S. B. Chang, and M. E. Helmer. Links between CD147 function, glycosylation, and caveolin-1. *Molecular Biology of the Cell*, 15:4043–4050, 2004.

[413] H. Mi, S. Poudel, A. Muruganujan, J. T. Casagrande, and P. D. Thomas. PANTHER version 10: Expanded protein families and functions, and analysis tools. *Nucleic Acids Research*, 44(D1):D336–D342, 2016.

[414] J. Cox and M. Mann. MaxQuant enables high peptide identification rates, individualized p.p.b.-range mass accuracies and proteome-wide protein quantification. *Nature Biotechnology*, 26(12):1367–72, 2008.

[415] J. Cox, I. Matic, M. Hilger, N. Nagaraj, M. Selbach, J. V. Olsen, and M. Mann. A practical guide to the MaxQuant computational platform for SILAC-based quantitative proteomics. *Nature protocols*, 4:698–705, 2009.

[416] G. von Heijne. Membrane-protein topology. *Nature Reviews. Molecular Cell Biology*, 7:909–918, 2006.

[417] S. Tyanova, T. Temu, P. Sinitcyn, A. Carlson, M. Y. Hein, T. Geiger, M. Mann, and J. Cox. The Perseus computational platform for comprehensive analysis of (prote)omics data. *Nature Methods*, 13(9):731–40, 2016.

[418] J. Butler, H. R. Watson, A. G. Lee, H. J. Schuppe, and J. M. East. Retrieval from the ER-golgi intermediate compartment is key to the targeting of c-terminally anchored ER-resident proteins. *Journal of Cellular Biochemistry*, 112(12):3543–3548, 2011.

[419] K. D. Stamellos, J. E. Shackelford, I. Shechter, G. Jiang, D. Conrad, G. A. Keller, and S. K. Krisans. Subcellular localization of squalene synthase in rat hepatic cells. Biochemical and immunochemical evidence. *The Journal of Biological Chemistry*, 268(17):12825–12836, 1993.

[420] P. P. V. Veldhovens and G. P. Mannaerts. Subcellular localization and membrane topology of sphingosine- 1-phosphate lyase in rat liver. *Journal of Biological Chemistry*, 266(19):12502–12507, 1991.

[421] M. Ikeda, A. Kihara, and Y. Igarashi. Sphingosine-1-phosphate lyase SPL is an endoplasmic reticulum-resident, integral membrane protein with the pyridoxal 5'-phosphate binding domain exposed to the cytosol. *Biochemical and Biophysical Research Communications*, 325(1):338–343, 2004.

[422] X. Meng, C. Zhang, J. Chen, S. Peng, Y. Cao, K. Ying, Y. Xie, and Y. Mao. Cloning and identification of a novel cDNA coding thioredoxin-related transmembrane protein 2. *Biochemical Genetics*, 41(3-4):99–106, 2003.

[423] J. G. Van Vranken, U. Na, D. R. Winge, and J. Rutter. Protein-mediated assembly of succinate dehydrogenase and its cofactors. *Critical Reviews in Biochemistry and Molecular Biology*, 50(2):168–180, 2015.

[424] D. Novikov, D. R. Fitzpatrick, M. Vihinen, D. Valle, and J. K. Hiltunen. Delta(3,5)-delta(2,4)-dienoyl-CoA isomerase from rat liver. *The Journal of Biological Chemistry*, 273(1):349–355, 1998.

[425] A. Lapucci, M. Lulli, A. Amedei, L. Papucci, E. Witort, F. Di Gesualdo, F. Bertolini, G. Brewer, A. Nicolin, A. Bevilacqua, N. Schiavone, D. Morello, M. Donnini, and S. Capaccioli. Zeta-Crystallin is a bcl-2 mRNA binding protein involved in bcl-2 overexpression in T-cell acute lymphocytic leukemia. *The FASEB Journal*, 24(6):1852–1865, 2010.

[426] S. Contractor and K. Krakauer. Immunofluorescent localisation of cathepsin D in trophoblastic cells in tissue culture. *Beitraege zur Pathologie*, 158(4):445–449, 1976.

[427] R. Do, R. S. Kiss, D. Gaudet, and J. C. Engert. Squalene synthase: A critical enzyme in the cholesterol biosynthesis pathway. *Clinical Genetics*, 75(1):19–29, 2009.

[428] T. R. Tansey and I. Shechter. Structure and regulation of mammalian squalene synthase. *Biochimica et Biophysica Acta*, 1529(1-3):49–62, 2000.

[429] A. Busquets, V. Keim, M. Closa, A. del Arco, A. Boronat, M. Arró, and A. Ferrer. Arabidopsis thaliana contains a single gene encoding squalene synthase. *Plant Molecular Biology*, 67(1-2):25–36, 2008.

[430] J. Pandit, D. E. Danley, G. K. Schulte, S. Mazzalupo, T. a. Pauly, C. M. Hayward, E. S. Hamanaka, J. F. Thompson, and H. J. Harwood. Crystal structure of human squalene synthase. A key enzyme in cholesterol biosynthesis. *The Journal of Biological Chemistry*, 275(39):30610–30617, 2000.

[431] G. Guan, G. Jiang, R. L. Koch, and I. Shechter. Molecular cloning and functional analysis of the promoter of the human squalene synthase gene. *The Journal of Biological Chemistry*, 270(37):21958–21965, 1995.

[432] G. Guan, P. H. Dai, T. F. Osborne, J. B. Kim, and I. Shechter. Multiple sequence elements are involved in the transcriptional regulation of the human squalene synthase gene. *The Journal of Biological Chemistry*, 272(15):10295–10302, 1997.

[433] R.-i. Tozawa, S. Ishibashi, J.-i. Osuga, H. Yagyu, T. Oka, Z. Chen, K. Ohashi, S. Perrey, F. Shionoiri, N. Yahagi, K. Harada, T. Gotoda, Y. Yazaki, and N. Yamada. Embryonic lethality and defective neural tube closure in mice lacking squalene synthase. *The Journal of Biological Chemisrty*, 274(43):30843–30848, 1999.

[434] K. B. Linscott, T. D. Niehaus, X. Zhuang, S. A. Bell, and J. Chappell. Mapping a kingdom-specific functional domain of squalene synthase. *Biochimica et Biophysica Acta*, 1861(9):1049–1057, 2016.

[435] S. Gill, J. Stevenson, I. Kristiana, and A. J. Brown. Cholesterol-dependent degradation of squalene monooxygenase, a control point in cholesterol synthesis beyond HMG-CoA reductase. *Cell Metabolism*, 13(3):260–273, 2011.

[436] K. Brusselmans, L. Timmermans, T. Van De Sande, P. P. Van Veldhoven, G. Guan, I. Shechter, F. Claessens, G. Verhoeven, and J. V. Swinnen. Squalene synthase, a determinant of raft-associated cholesterol and modulator of cancer cell proliferation. *Journal of Biological Chemistry*, 282(26):18777–18785, 2007.

[437] H. Hiyoshi, M. Yanagimachi, M. Ito, N. Yasuda, T. Okada, H. Ikuta, D. Shinmyo, K. Tanaka, N. Kurusu, I. Yoshida, S. Abe, T. Saeki, and H. Tanaka. Squalene synthase inhibitors suppress triglyceride biosynthesis through the farnesol pathway in rat hepatocytes. *Journal of Lipid Research*, 44(1):128–135, 2003.

[438] D. L. Bradfute, C. J. Silva, and R. D. Simoni. Squalene synthase-deficient mutant of Chinese hamster ovary cells. *Journal of Biological Chemistry*, 267(26):18308–18314, 1992.

[439] G. Gimpl and K. Gehrig-Burger. Cholesterol reporter molecules. *Bioscience Reports*, 27(6):335–358, 2007.

[440] M. Hao, S. X. Lin, O. J. Karylowski, D. W. Stner, T. E. McGraw, and F. R. Maxfield. Vesicular and non-vesicular sterol transport in living cells: The endocytic recycling compartment is a major sterol storage organelle. *Journal of Biological Chemistry*, 277(1):609–617, 2002.

[441] S. Mukherjee, X. Zha, I. Tabas, and F. R. Maxfield. Cholesterol distribution in living cells: fluorescence imaging using dehydroergosterol as a fluorescent cholesterol analog. *Biophysical Journal*, 75(4):1915–1925, 1998.

[442] P. J. Price and E. A. Gregory. Relationship between in vitro growth promotion and biophysical and biochemical properties of the serum supplement. *In Vitro*, 18(6):576–584, jun 1982.

[443] J. Nishijo, S. Moriyama, and S. Shiota. Interactions of cholesterol with cyclodextrins in aqueous solution. *Chemical & Pharmaceutical Bulletin*, 51(11):1253–1257, 2003.

[444] S. Mahammad and I. Parmryd. Cholesterol homeostasis in T cells. Methyl-beta-cyclodextrin treatment results in equal loss of cholesterol from Triton X-100 soluble and insoluble fractions. *Biochimica et Biophysica Acta - Biomembranes*, 1778(5):1251–1258, 2008.

[445] E. Luegmayr, H. Glantschnig, G. A. Wesolowski, M. A. Gentile, J. E. Fisher, G. A. Rodan, and A. A. Reszka. Osteoclast formation, survival and morphology are highly dependent on exogenous cholesterol/lipoproteins. *Cell Death and Differentiation*, 11(Suppl 1):S108–S118, 2004.

[446] Y. C. Li, M. J. Park, S.-K. Ye, C.-W. Kim, and Y.-N. Kim. Elevated levels of cholesterol-rich lipid rafts in cancer cells are correlated with apoptosis sensitivity induced by cholesterol-depleting agents. *The American Journal of Pathology*, 168(4):1107–1118, 2006.

[447] H. Ohvo and J. P. Slotte. Cyclodextrin-mediated removal of sterols from monolayers: Effects of sterol structure and phospholipids on desorption rate. *Biochemistry*, 35(24):8018–8024, 1996.

[448] E. Ottico, A. Prinetti, S. Prioni, C. Giannotta, L. Basso, V. Chigorno, and S. Sonnino. Dynamics of membrane lipid domains in neuronal cells differentiated in culture. *Journal of Lipid Research*, 44(11):2142–2151, 2003.

[449] Y. Ohtani, T. Irie, K. Uekama, K. Fukunaga, and J. Pitha. Differential effects of alpha-, beta- and gamma-cyclodextrins on human erythrocytes. *European Journal of Biochemistry*, 186(1-2):17–22, 1989.

[450] S. Ilangumaran and D. C. Hoessli. Effects of cholesterol depletion by cyclodextrin on the sphingolipid microdomains of the plasma membrane. *The Biochemical Journal*, 335(Pt 2):433–440, 1998.

[451] F. L. Aachmann, D. E. Otzen, K. L. Larsen, and R. Wimmer. Structural background of cyclodextrin-protein interactions. *Protein Engineering*, 16(12):905–912, 2003.

[452] J. D. Bergstrom, M. M. Kurtz, D. J. Rew, A. M. Amend, J. D. Karkas, R. G. Bostedor, V. S. Bansal, C. Dufresne, F. L. VanMiddlesworth, and O. D. Hensens. Zaragozic acids: a family of fungal metabolites that are picomolar competitive inhibitors of squalene synthase. *Proceedings of the National Academy of Sciences of the United States of America*, 90(1):80–84, 1993.

[453] G. Guan, P. Dai, and I. Shechter. Differential transcriptional regulation of the human squalene synthase gene by sterol regulatory element-binding proteins (SREBP) 1a and 2 and involvement of 5' DNA sequence elements in the regulation. *Journal of Biological Chemistry*, 273(20):12526–12535, 1998.

[454] H. Tong, S. A. Holstein, and R. J. Hohl. Simultaneous determination of farnesyl and geranylgeranyl pyrophosphate levels in cultured cells. *Analytical Biochemistry*, 336(1):51–59, 2005.

[455] J. E. Buss, L. A. Quilliam, K. Kato, P. J. Casey, P. A. Solski, G. Wong, R. Clark, F. McCormick, G. M. Bokoch, and C. J. Der. The COOH-terminal domain of the Rap1A (Krev-1) protein is isoprenylated and supports transformation by an H-Ras:Rap1A chimeric protein. *Molecular and Cellular Biology*, 11(3):1523–1530, 1991.

[456] B. Binnington, L. Nguyen, M. Kamani, D. Hossain, D. L. Marks, M. Budani, and C. A. Lingwood. Inhibition of Rab prenylation by statins induces cellular glycosphingolipid remodeling. *Glycobiology*, 26(2):166–180, 2015.

[457] B. Huang, J. Guo, L. Sun, and W. Chen. ERG9 and COQ1 disruption reveals isoprenoids biosynthesis is closely related to mitochondrial function in Saccharomyces cerevisiae. *Integrative Biology: Quantitative Biosciences from Nano to Macro*, 5(10):1282–1296, 2013.

[458] W. Jiang and B.-L. Song. Ubiquitin ligases in cholesterol metabolism. *Diabetes & Metabolism Journal*, 38(3):171–180, 2014.

[459] G. W. Robinson, Y. H. Tsay, B. K. Kienzle, C. A. Smith-Monroy, and R. W. Bishop. Conservation between human and fungal squalene synthetases: similarities in structure, function, and regulation. *Molecular and Cellular Biology*, 13(5):2706–2717, 1993.

[460] M. H. Bengtson and C. a. P. Joazeiro. Role of a ribosome-associated E3 ubiquitin ligase in protein quality control. *Nature*, 467(7314):470–473, 2010.

[461] J. F. Thompson, D. E. Danley, S. Mazzalupo, P. M. Milos, M. E. Lira, and H. J. Harwood. Truncation of human squalene synthase yields active, crystallizable protein. *Archives of Biochemistry and Biophysics*, 350(2):283–290, 1998.

[462] L. H. Cohen, M. Griffioen, C. W. van Roermund, and R. J. Wanders. Subcellular localization of squalene synthase in human hepatoma cell line Hep G2. *Biochimica et Biophysica Acta*, 1126(1):114–118, 1992.

[463] P. K. Kim, F. Janiak-Spens, W. S. Trimble, B. Leber, and D. W. Andrews. Evidence for multiple mechanisms for membrane binding and integration via carboxyl-terminal insertion sequences. *Biochemistry*, 36(29):8873–8882, 1997.

[464] H. Kadowaki, A. Nagai, T. Maruyama, Y. Takami, P. Satrimafitrah, H. Kato, A. Honda, T. Hatta, T. Natsume, T. Sato, H. Kai, H. Ichijo, and H. Nishitoh. Pre-emptive quality

control protects the ER from protein overload via the proximity of ERAD components and SRP. *Cell Reports*, 13(5):944–956, 2015.

[465] N. E. Buchler, U. Gerland, and T. Hwa. Nonlinear protein degradation and the function of genetic circuits. *Proceedings of the National Academy of Sciences*, 102(27):9559–9564, 2005.

[466] G. Asher, N. Reuven, and Y. Shaul. 20S proteasomes and protein degradation by default. *BioEssays*, 28:844–849, 2006.

[467] A. L. Goldberg. Protein degradation and protection against misfolded or damaged proteins. *Nature*, 426(18/25):895–899, 2003.

[468] V. Zickermann, H. Angerer, M. G. Ding, E. Nuebel, and U. Brandt. Small single transmembrane domain (STMD) proteins organize the hydrophobic subunits of large membrane protein complexes. *FEBS Letters*, 584(12):2516–2525, 2010.

[469] V. Guarani, E. M. McNeill, J. A. Paulo, E. L. Huttlin, F. Fröhlich, S. P. Gygi, D. Van Vactor, and J. W. Harper. QIL1 is a novel mitochondrial protein required for MICOS complex stability and cristae morphology. *eLife*, 4:e06265, 2015.

[470] K. von der Malsburg, J. M. Mueller, M. Bohnert, S. Oeljeklaus, P. Kwiatkowska, T. Becker, A. Loniewska-Lwowska, S. Wiese, S. Rao, D. Milenkovic, D. P. Hutu, R. M. Zerbes, A. Schulze-Specking, H. E. Meyer, J. C. Martinou, S. Rospert, P. Rehling, C. Meisinger, M. Veenhuis, B. Warscheid, I. J. van der Klei, N. Pfanner, A. Chacinska, and M. van der Laan. Dual role of mitofilin in mitochondrial membrane organization and protein biogenesis. *Developmental Cell*, 21(4):694–707, 2011.

[471] M. Harner, C. Körner, D. Walther, D. Mokranjac, J. Kaesmacher, U. Welsch, J. Griffith, M. Mann, F. Reggiori, and W. Neupert. The mitochondrial contact site complex, a determinant of mitochondrial architecture. *The EMBO Journal*, 30(21):4356–4370, 2011.

[472] S. Hoppins, S. R. Collins, A. Cassidy-Stone, E. Hummel, R. M. DeVay, L. L. Lackner, B. Westermann, M. Schuldiner, J. S. Weissman, and J. Nunnari. A mitochondrial-focused genetic interaction map reveals a scaffold-like complex required for inner membrane organization in mitochondria. *Journal of Cell Biology*, 195(2):323–340, 2011.

[473] M. A. Huynen, M. Mühlmeister, K. Gotthardt, S. Guerrero-Castillo, and U. Brandt. Evolution and structural organization of the mitochondrial contact site (MICOS) com-

plex and the mitochondrial intermembrane space bridging (MIB) complex. *Biochimica et Biophysica Acta - Molecular Cell Research*, 1863(1):91–101, 2016.

[474] N. Pfanner, M. van der Laan, P. Amati, R. A. Capaldi, A. A. Caudy, A. Chacinska, M. Darshi, M. Deckers, S. Hoppins, T. Icho, S. Jakobs, J. Ji, V. Kozjak-Pavlovic, C. Meisinger, P. R. Odgren, S. K. Park, P. Rehling, A. S. Reichert, M. S. Sheikh, S. S. Taylor, N. Tsuchida, A. M. van der Bliek, I. J. van der Klei, J. S. Weissman, B. Westermann, J. Zha, W. Neupert, and J. Nunnari. Uniform nomenclature for the mitochondrial contact site and cristae organizing system. *Journal of Cell Biology*, 204(7):1083–1086, 2014.

[475] V. Guarani, C. Jardel, D. Chrétien, A. Lombès, P. Bénit, C. Labasse, E. Lacène, A. Bourillon, A. Imbard, J. Benoist, I. Dorboz, M. Gilleron, E. S. Goetzman, P. Gaignard, A. Slama, M. Elmaleh-Bergès, N. B. Romero, P. Rustin, H. Ogier de Baulny, J. A. Paulo, J. W. Harper, and M. Schiff. QIL1 mutation causes MICOS disassembly and early onset fatal mitochondrial encephalopathy with liver disease. *eLife*, 5:e17163, 2016.

[476] C. Ott, E. Dorsch, M. Fraunholz, S. Straub, and V. Kozjak-Pavlovic. Detailed analysis of the human mitochondrial contact site complex indicate a hierarchy of subunits. *PLoS ONE*, 10(3):e0120213, 2015.

[477] B. H. Robinson. Human cytochrome oxidase deficiency. *Pediatric Research*, 48(5):581–585, 2000.

[478] A. Poyau, K. Buchet, M. F. Bouzidi, M. T. Zabot, B. Echenne, J. Yao, E. A. Shoubridge, and C. Godinot. Missense mutations in SURF1 associated with deficient cytochrome c oxidase assembly in Leigh syndrome patients. *Human Genetics*, 106(2):194–205, 2000.

[479] Z. Zhu, J. Yao, T. Johns, K. Fu, I. De Bie, C. Macmillan, A. P. Cuthbert, R. F. Newbold, J. Wang, M. Chevrette, G. K. Brown, R. M. Brown, and E. A. Shoubridge. SURF1, encoding a factor involved in the biogenesis of cytochrome c oxidase, is mutated in Leigh syndrome. *Nature Genetics*, 20(4):337–343, 1998.

[480] A. Kuehn, N. Simon, and G. Pradel. Family members stick together: Multi-protein complexes of malaria parasites. *Medical Microbiology and Immunology*, 199(3):209–226, 2010.

[481] G. Pradel, C. Wagner, C. Mejia, and T. J. Templeton. Plasmodium falciparum: Co-

dependent expression and co-localization of the PfCCp multi-adhesion domain proteins. *Experimental Parasitology*, 112(4):263–268, 2006.

[482] N. Simon, S. M. Scholz, C. K. Moreira, T. J. Templeton, A. Kuehn, M. A. Dude, and G. Pradel. Sexual stage adhesion proteins form multi-protein complexes in the malaria parasite Plasmodium falciparum. *Journal of Biological Chemistry*, 284(21):14537–14546, 2009.

[483] H. E. Trueman, J. D. Raine, L. Florens, J. T. Dessens, J. Mendoza, J. Johnson, C. C. Waller, I. Delrieu, A. A. Holders, J. Langhorne, D. J. Carucci, J. R. Yates, and R. E. Sinden. Functional characterization of an LCCL-lectin domain containing protein family in Plasmodium berghei. *The Journal of Parasitology*, 90(5):1062–1071, 2004.

[484] S. Saeed, A. Z. Tremp, and J. T. Dessens. Conformational co-dependence between Plasmodium berghei LCCL proteins promotes complex formation and stability. *Molecular and Biochemical Parasitology*, 185(2):170–173, 2012.

[485] H. Okazaki, F. Tazoe, S. Okazaki, N. Isoo, K. Tsukamoto, M. Sekiya, N. Yahagi, Y. Iizuka, K. Ohashi, T. Kitamine, R.-I. Tozawa, T. Inaba, H. Yagyu, M. Okazaki, H. Shimano, N. Shibata, H. Arai, R.-Z. Nagai, T. Kadowaki, J.-I. Osuga, and S. Ishibashi. Increased cholesterol biosynthesis and hypercholesterolemia in mice overexpressing squalene synthase in the liver. *Journal of Lipid Research*, 47(9):1950–1958, 2006.

[486] G. Vinci, X. Xia, and R. A. Veitia. Preservation of genes involved in sterol metabolism in cholesterol auxotrophs: Facts and hypotheses. *PLoS ONE*, 3(8):e2883, 2008.

[487] M. Rauthan and M. Pilon. The mevalonate pathway in C. elegans. *Lipids in Health and Disease*, 10:243, 2011.

[488] C. Mo and M. Bard. A systematic study of yeast sterol biosynthetic protein-protein interactions using the split-ubiquitin system. *Biochimica et Biophysica Acta - Molecular and Cell Biology of Lipids*, 1737(2-3):152–160, 2005.

[489] F. Vilardi, H. Lorenz, and B. Dobberstein. WRB is the receptor for TRC40/Asna1-mediated insertion of tail-anchored proteins into the ER membrane. *Journal of Cell Science*, 124(8):1301–1307, 2011.

[490] Y. Yamamoto and T. Sakisaka. The emerging role of calcium-modulating cyclophilin ligand in posttranslational insertion of tail-anchored proteins into the endoplasmic reticulum membrane. *Journal of Biochemistry*, 157(6):419–429, 2015.

[491] D. J. F. Du Plessis, N. Nouwen, and A. J. M. Driessen. Subunit a of cytochrome o oxidase requires both YidC and SecYEG for membrane insertion. *Journal of Biological Chemistry*, 281(18):12248–12252, 2006.

[492] C. E. Price and A. J. M. Driessen. Conserved negative charges in the transmembrane segments of subunit K of the NADH:ubiquinone oxidoreductase determine its dependence on YidC for membrane insertion. *Journal of Biological Chemistry*, 285(6):3575–3581, 2010.

[493] R. E. Dalbey, A. Kuhn, L. Zhu, and D. Kiefer. The membrane insertase YidC. *Biochimica et Biophysica Acta - Molecular Cell Research*, 1843(8):1489–1496, 2014.

[494] A. Saeaef, M. Monne, J. W. DeGier, and G. VonHeijne. Membrane topology of the 60-kDa Oxalp homologue from Escherichia coli. *Journal of Biological Chemistry*, 273(46):30415–30418, 1998.

[495] F. Jiang, M. Chen, L. Yi, J. W. De Gier, A. Kuhn, and R. E. Dalbey. Defining the regions of Escherichia coli YidC that contribute to activity. *Journal of Biological Chemistry*, 278(49):48965–48972, 2003.

[496] S. An, R. Kumar, E. D. Sheets, and S. J. Benkovic. Reversible compartmentalization of de novo purine biosynthetic complexes in living cells. *Science*, 320(5872):103–106, 2008.

[497] R. Narayanaswamy, M. Levy, M. Tsechansky, G. M. Stovall, J. D. O'Connell, J. Mirrielees, A. D. Ellington, and E. M. Marcotte. Widespread reorganization of metabolic enzymes into reversible assemblies upon nutrient starvation. *Proceedings of the National Academy of Sciences of the United States of America*, 106(25):10147–10152, 2009.

[498] R. J. Conrado, J. D. Varner, and M. P. DeLisa. Engineering the spatial organization of metabolic enzymes: mimicking nature's synergy. *Current Opinion in Biotechnology*, 19(5):492–499, 2008.

[499] H. Lee, W. C. DeLoache, and J. E. Dueber. Spatial organization of enzymes for metabolic engineering. *Metabolic Engineering*, 14(3):242–251, 2012.

[500] D. Gachotte, J. Eckstein, R. Barbuch, T. Hughes, C. Roberts, and M. Bard. A novel gene conserved from yeast to humans is involved in sterol biosynthesis. *Journal of Lipid Research*, 42(1):150–154, 2001.

[501] C. Mo, M. Valachovic, S. K. Randall, J. T. Nickels, and M. Bard. Protein-protein interactions among C-4 demethylation enzymes involved in yeast sterol biosynthesis. *Proceedings of the National Academy of Sciences of the United States of America*, 99(15):9739–9744, 2002.

[502] C. Mo, M. Valachovic, and M. Bard. The ERG28-encoded protein, Erg28p, interacts with both the sterol C-4 demethylation enzyme complex as well as the late biosynthetic protein, the C-24 sterol methyltransferase (Erg6p). *Biochimica et Biophysica Acta - Molecular and Cell Biology of Lipids*, 1686(1-2):30–36, 2004.

[503] C. Mo and M. Bard. Erg28p is a key protein in the yeast sterol biosynthetic enzyme complex. *Journal of Lipid Research*, 46(9):1991–1998, 2005.

[504] A. H. Kachroo, J. M. Laurent, C. M. Yellman, A. G. Meyer, C. O. Wilke, and E. M. Marcotte. Systematic humanization of yeast genes reveals conserved functions and genetic modularity. *Science*, 348(6237):921–925, 2015.

[505] R. Kribii, M. Arró, A. Del Arco, V. González, L. Balcells, D. Delourme, A. Ferrer, F. Karst, and A. Boronat. Cloning and characterization of the Arabidopsis thaliana SQS1 gene encoding squalene synthase - involvement of the C-terminal region of the enzyme in the channeling of squalene through the sterol pathway. *European journal of biochemistry / FEBS*, 249(1):61–69, 1997.

[506] S. Norlin, V. S. Parekh, P. Naredi, and H. Edlund. Asna1/TRC40 controls beta cell function and ER homeostasis by ensuring retrograde transport. *Diabetes*, 65(1):110–119, 2015.

[507] J. Binici and J. Koch. BAG-6, a jack of all trades in health and disease. *Cellular and Molecular Life Sciences*, 71(10):1829–1837, 2014.

[508] C. C. Farnsworth, M. C. Seabra, L. H. Ericsson, M. H. Gelb, and J. A. Glomset. Rab geranylgeranyl transferase catalyzes the geranylgeranylation of adjacent cysteines in the small GTPases Rab1A, Rab3A, and Rab5A. *Proceedings of the National Academy of Sciences of the United States of America*, 91(25):11963–11967, 1994.

[509] A. Q. Gomes, B. R. Ali, J. S. Ramalho, R. F. Godfrey, D. C. Barral, A. N. Hume, and M. C. Seabra. Membrane targeting of Rab GTPases is influenced by the prenylation motif. *Molecular Biology of the Cell*, 14(5):1882–1899, 2003.

[510] F. Samuel and D. L. Hynds. RHO GTPase signaling for axon extension: Is prenylation important? *Molecular Neurobiology*, 42(2):133–142, 2010.

[511] Anjaneyulu Kowluru. Protein prenylation in glucose-induced insulin secretion from the pancreatic islet β cell: A perspective. *Journal of Cellular and Molecular Medicine*, 12(1):164–173, 2007.

[512] R. K. Keller. Squalene synthase inhibition alters metabolism of nonsterols in rat liver. *Biochimica et Biophysica Acta - Lipids and Lipid Metabolism*, 1303(3):169–179, 1996.

[513] D. M. Peffley and A. K. Gayen. Inhibition of squalene synthase but not squalene cyclase prevents mevalonate-mediated suppression of 3-hydroxy-3-methylglutaryl coenzyme A reductase synthesis at a posttranscriptional level. *Archives of Biochemistry and Biophysics*, 337(2):251–260, 1997.

[514] M. A. Haeuptle, M. Welti, H. Troxler, A. J. Hülsmeier, T. Imbach, and T. Hennet. Improvement of dolichol-linked oligosaccharide biosynthesis by the squalene synthase inhibitor zaragozic acid. *Journal of Biological Chemistry*, 286(8):6085–6091, 2011.

[515] R. Zidovetzki and I. Levitan. Use of cyclodextrins to manipulate plasma membrane cholesterol content: Evidence, misconceptions and control strategies. *Biochimica et Biophysica Acta - Biomembranes*, 1768(6):1311–1324, 2007.

[516] E. P. C. Kilsdonk, P. G. Yancey, G. W. Stoudt, F. W. Bangerter, W. J. Johnson, M. C. Phillips, and G. H. Rothblat. Cellular cholesterol efflux mediated by cyclodextrins, 1995.

[517] S. K. Rodal, G. Skretting, O. Garred, F. Vilhardt, B. van Deurs, and K. Sandvig. Extraction of cholesterol with methyl-beta-cyclodextrin perturbs formation of clathrin-coated endocytic vesicles. *Molecular Biology of the Cell*, 10(4):961–974, 1999.

[518] Y. C. Li, M. J. Park, S.-K. Ye, C.-W. Kim, and Y.-N. Kim. Elevated levels of cholesterol-rich lipid rafts in cancer cells are correlated with apoptosis sensitivity induced by cholesterol-depleting agents. *The American Journal of Pathology*, 168(4):1107–1118, 2006.

[519] J. Han, D. P. Hajjar, J. M. Tauras, and A. C. Nicholson. Cellular cholesterol regulates expression of the macrophage type B scavenger receptor, CD36. *Journal of Lipid Research*, 40(5):830–838, 1999.

[520] E. M. Park, L. N. Nguyen, Y. S. Lim, and S. B. Hwang. Farnesyl-diphosphate farnesyltransferase 1 regulates hepatitis C virus propagation. *FEBS Letters*, 588(9):1813–1820, 2014.

[521] J. M. Mackenzie, A. A. Khromykh, and R. G. Parton. Cholesterol manipulation by West Nile virus perturbs the cellular immune response. *Cell Host and Microbe*, 2(4):229–239, 2007.

[522] C. Rothwell, A. LeBreton, C. Young Ng, J. Y. H. Lim, W. Liu, S. Vasudevan, M. Labow, F. Gu, and L. A. Gaither. Cholesterol biosynthesis modulation regulates dengue viral replication. *Virology*, 389(1-2):8–19, 2009.

[523] H. Aizaki, K.-J. Lee, V. M.-H. Sung, H. Ishiko, and M. M. C. Lai. Characterization of the hepatitis C virus RNA replication complex associated with lipid rafts. *Virology*, 324(2):450–461, 2004.

[524] G. R. Medigeshi, A. J. Hirsch, D. N. Streblow, J. Nikolich-Zugich, and J. A. Nelson. West Nile virus entry requires cholesterol-rich membrane microdomains and is independent of $\alpha v\beta 3$ integrin. *Journal of Virology*, 82(11):5212–5219, 2008.

[525] R. Soto-Acosta, C. Mosso, M. Cervantes-Salazar, H. Puerta-Guardo, F. Medina, L. Favari, J. E. Ludert, and R. M. Del Angel. The increase in cholesterol levels at early stages after dengue virus infection correlates with an augment in LDL particle uptake and HMG-CoA reductase activity. *Virology*, 442(2):132–147, 2013.

[526] J. Martinez-Botas, A. J. Ferruelo, Y. Suarez, C. Fernandez, D. Gomez-Coronado, and M. A. Lasuncion. Dose-dependent effects of lovastatin on cell cycle progression. Distinct requirement of cholesterol and non-sterol mevalonate derivatives. *Biochimica et Biophysica Acta - Molecular and Cell Biology of Lipids*, 1532(3):185–194, 2001.

[527] C. R. Santos and A. Schulze. Lipid metabolism in cancer. *FEBS Journal*, 279(15):2610–2623, 2012.

[528] U. Fünfschilling, G. Saher, L. Xiao, W. Möbius, and K.-A. Nave. Survival of adult neurons lacking cholesterol synthesis in vivo. *BMC Neuroscience*, 8(1):doi:10.1186/1471–2202–8–1, 2007.

[529] F. Baenke, B. Peck, H. Miess, and A. Schulze. Hooked on fat: the role of lipid synthesis in cancer metabolism and tumour development. *Disease Models & Mechanisms*, 6(6):1353–1363, 2013.

[530] P. K. Kommareddi, T. S. Nair, L. V. Thang, M. M. Galano, E. Babu, V. Ganapathy, T. Kanazawa, J. B. McHugh, and T. E. Carey. Isoforms, expression, glycosylation, and tissue distribution of CTL2/SLC44A2. *The Protein Journal*, 29(6):417–426, 2010.

[531] B. Iwao, M. Yara, N. Hara, Y. Kawai, T. Yamanaka, H. Nishihara, T. Inoue, and M. Inazu. Functional expression of choline transporter like-protein 1 (CTL1) and CTL2 in human brain microvascular endothelial cells. *Neurochemistry International*, 93:40–50, 2016.

[532] T. Akahane, K. Sahara, H. Yashiroda, K. Tanaka, and S. Murata. Involvement of Bag6 and the TRC pathway in proteasome assembly. *Nature Communications*, 4(2234):DOI: 10.1038/ncomms3234, 2013.

[533] Z. Xia, H. Dudek, C. K. Miranti, and M. E. Greenberg. Calcium influx via the NMDA receptor induces immediate early gene transcription by a MAP kinase/ERK-dependent mechanism. *The Journal of Neuroscience*, 16(17):5425–5436, 1996.

[534] F. Glaser, T. Pupko, I. Paz, R. E. Bell, D. Bechor, and E. Martz. ConSurf: identification of functional regions in proteins by surface mapping of phylogenetic information. *Bioinformatics*, 19(1):163–164, 2003.